Application of through-vial impedance spectroscopy as a novel process analytical technology for freeze drying

Muhammad Sohail Arshad

Leicester School of Pharmacy, De Montfort University

Submitted: February 2014

PhD Thesis

In partial fulfilment of the requirements for the degree of

Doctor of Philosophy

Submitted to

De Montfort University

Declaration

I, Muhammad Sohail Arshad, confirm that the content presented within this thesis is of my own work. I confirm that information derived from other sources has been indicated accordingly in this thesis.

Part of this work has been presented or Published

Journal Articles

Smith G., **Arshad M.S.,** Polygalov E., Ermolina, I. , Nazari K., Page T., Taylor J., (2014) Through-Vial Impedance Spectroscopy: A new in-line process analytical technology for freeze-drying. **Pharmaceutical Technology**

Smith G., **Arshad M.S.,** Polygalov E., Ermolina, I (2014) Through-Vial Impedance Spectroscopy of the Mechanisms of Annealing in the Freeze-Drying of Maltodextrin: The Impact of Annealing Hold Time and Temperature on the Primary Drying Rate. **Journal of Pharmaceutical Sciences** online first

Arshad M.S., Smith G., Polygalov E., Ermolina, I (2014) Through-vial impedance spectroscopy of critical events during the freezing stage of the lyophilization cycle: The example of the impact of sucrose on the crystallization of mannitol. **European Journal of Pharmaceutics and Biopharmaceutics**. online first

Smith G., **Arshad M.S.,** Polygalov E., Ermolina, I (2013) Factors Affecting the Use of Impedance Spectroscopy in the Characterisation of the Freezing Stage of the Lyophilisation Process: the Impact of Liquid Fill Height in Relation to Electrode Geometry. **AAPS PharmSciTech**, online first

Smith G., **Arshad M.S**., Polygalov E., Ermolina, I (2013) An application for impedance spectroscopy in the characterisation of the glass transition during the lyophilization cycle: The example of a 10% w/v maltodextrin solution. **European Journal of Pharmaceutics and Biopharmaceutics**, 85**,** 1130-40.

Smith G., Polygalov E., **Arshad M.S**., Page T., Taylor J., Ermolina, I. (2013) An impedance-based process analytical technology for monitoring the lyophilisation process. **International Journal of Pharmaceutics**, 449 (1-2), pp. 72-83

Poster Presentations

Arshad M.S., Ermolina I., Polygalov E., Smith G. (2013) Study on the impact of annealing on the primary drying times using impedance spectroscopy. **UKPharmSci** 2013 Edinburgh, September 2 -4 2013

Arshad M.S., Ermolina I., Polygalov E., Smith G. (2012) LyoDEA™ measurement of the glass transition of sucrose within a freeze-drying vial. **UKPharmSci**, 12th-14th September, 2012

Arshad MS, Ermolina I, Polygalov E, Smith G. (2012) In situ impedance measurement of mannitol crystallization during the lyophilisation cycle using LyoDEA™. **UKPharmSci**, 12th-14th September, 2012

Smith G., **Arshad M.S.,** Ermolina I. Lyosense™. (2011) An evaluation of the impact of electrode design on the freezing onset times in the lyophilisation process. **UKPharmSci** 2011, 31st August- 2nd September 2011.

Abstract

This study aims to validate and develop applications for a novel impedance-based process analytical technology for monitoring the attributes of the product during the entire freeze-drying process (from pre-freezing and annealing to primary and then secondary drying). This measurement approach involves the application of foil electrodes, mounted externally to a conventional glass freeze-drying vial, and coupled to a high-impedance analyser. The location of the electrodes on the outside, rather than the inside of the vial, leads to a description of the technology as a through-vial impedance spectroscopy (TV-IS) technique. The principle observation from this approach is the interfacial-polarization process arising from the composite impedance of the glass wall and product interface. For a conventional glass vial (of wall thickness ~ 1 mm and cross sectional diameter ~ 22 mm) it was shown that the process is manifest within the frequency range 10^1 to 10^6 Hz, as a single, broad band peak which spans 2-3 decades of the imaginary part spectrum. Features of the interfacial-relaxation process, characterised by the peak amplitude, C''_{Peak}, and peak frequency, f_{peak}, of the imaginary capacitance spectra and the equivalent circuit elements that model the impedance spectra (i.e. the solution resistance (R) and solution capacitance (C) were monitored along with the product temperature data during the cycle(s), for a variety of surrogate formulations comprising lactose, sucrose, mannitol or maltodextrin solutions, during the freezing, re-heating, annealing and primary drying stages of freeze drying.

It was shown that the parameters, f_{peak} and R, are strongly coupled to each other and change as a function of the temperature of the solution and its phase state, whereas C''_{Peak} is strongly coupled to the amount of ice that remains during the drying process. Both log f_{peak} and log R have a linear dependence on the temperature of the solution, provided there was no phase change in the solution. The crystallization process (ice onset, solidification and equilibration to shelf temperature) is characterized well by both log f_{peak} and log R, whereas the parameter R demonstrates most clearly the formation of eutectic crystallization during freezing. In contrast it was the parameter C which was most sensitive to the detection of the glass transition during re-heating. During primary drying, it was shown that C''_{peak}, is dependent on the amount of ice remaining and therefore provides a convenient assessment of the rate of drying and primary drying end point.

The impedance changes during annealing provide a mechanistic basis for the modifications in ice structure which result directly in the observed decrease in primary drying times. The principal observation on annealing of a 10% w/v solution of maltodextrin, was the minimal changes in the glass transition (recorded at ~−16 °C) during the re-heating and cooling step (post-annealing). This result alone appears to indicate that a maximum freeze concentration was achieved during first freezing with no further ice being formed on annealing. The phenomenon of devitrification (and the production of more ice, and hence larger ice crystals) was therefore discounted as the mechanism by which annealing impacts the drying time. Having excluded devitrification from the mechanism of annealing enhanced drying, it was then possible to conclude that the decrease in the electrical resistance (that was observed during the annealing hold time) must necessarily result from the simplified structure of the unfrozen fraction and the improved connectivity of ice crystals that may be the consequence of Ostwald ripening.

The application of through vial impedance measurement approach provides a non-invasive, real time monitoring of critical process parameters which subsequently leads to an improved understanding of the mechanisms and effects of different parameters, providing a reliable basis for process optimization, along with improved risk management to ensure optimum quality of the formulation and optimization of the freeze drying process.

Table of Contents

List of Figures

List of Tables

List of Abbreviations

C: Capacitance

C_{eu} : concentration for eutectic crystallization

C_g': solute concentration in maximally freeze concentrated solution

CPE: Constant phase element

CPP: critical process parameters

CQA: critical quality attributes

DAQ: data acquisition card

DSC: differential scanning calorimetry

ER: electrical resistance

FDM: freeze drying microscopy

ICH: International Conference on Harmonization

IVC: current to voltage converter

K_c: thermal coefficient contribution from the conductive mechanisms

K_g: thermal coefficient contribution from the gas convection

K_r: thermal coefficient contribution from the radiative mechanisms

K_v: thermal co-efficient of vial

MTM: manometric temperature measurement

NIRS: near infra-red spectroscopy

ϕ: fill factor in relation to the electrode height

PAT: process analytical technology

P_C: Vapour pressure in the chamber

P_{ice}: Vapour pressure at sublimation interface

QbD: Quality by design

R: resistor

R_p: resistance to vapour flow due to product

R_s: resistance to vapour flow due to stopper

RTD: resistor thermal devices

RTMT: Resistance to mass transfer

T_c: Collapse temperature

TDLAS: tuneable diode laser absorption spectroscopy

T_{eu}: eutectic temperature

T_g: glass transition temperature

T_g': glass transition temperature of maximally freeze concentrated solution

T_m: melting temperature

T_o: Kauzman's temperature

T_p: Product temperature

TPP: target product profile

T_s: Shelf temperature

TVIS: through-vial impedance spectroscopy

VTF: Vogel-Fulcher-Tammann

W^*_{cL} : closed loop transfer function

W^*_{OL} : open loop transfer function

WLF: Williams–Landel–Ferry

WTMS: wireless temperature measurement system

$Z^*_{FB:}$ complex feedback impedance

$\mathbf{Z^*_{IN}}$: complex input impedance

$\mathbf{Z^*_{P}}$: complex parasitic impedance

Acknowledgements

Foremost, I would like to express my sincere gratitude to my supervisors Dr Geoff Smith and Dr Irina Ermolina for the continuous support of my PhD study and research, for their patience, motivation, enthusiasm, and immense knowledge. Their guidance helped me in all the time of research and writing of this thesis. I could not have imagined having a better advisors and mentors for my PhD study.

My sincere thanks to Mr Eugene Polgalov, inventor of the through vial impedance spectroscopy system (LyoDEA) for his admirable dedication and support during the study, expert opinions to characterize the complex data and a great zeal to address the hardware and software related issues.

I would extend a special thanks to the Collaborators of TSB project, in particular, Trevor Page and Julian Taylor from GEA pharma system, Steve Metcalf formerly Astra Zeneca, now consultant at Stem solution, for their valuable contribution in the project, Ahmed al Rasheed from Ametek and Richard Storey for Astra Zeneca for their intellectual input, appreciation and encouragement. A special thanks to Steve for securing support from Astra Zeneca to help with my studies.

I thank Dr Richard Webster and his technical team for their generous support to continue my experimental work.

I thank my fellow lab mates in the Pharmaceutical Technologies Group: Amjad Hussain, Alex Wall, Joseph Darkhwah, Kazem Nazari and Amee Pandya, for the stimulating discussions, motivating and helping gestures to meet deadlines, and for all the fun we have had in the last four years. Also I thank my friends Abid, Ali, Tayyab, Zahid, kashif for their rejoicing and caring company.

I would extend my special thanks to my wife Sadia and daughters Fariah and Samiya for their valuable support which kept me motivated to undertake my research. Last but not the least; I would like to thank my parents for their affection, care and support throughout my career which always make me feel blessed.

Chapter 1

1 Introduction

Lyophilisation or freeze drying is a process in which water or some other solvent is removed from a frozen material by sublimation under hypobaric conditions. The sublimation process involves direct transformation of frozen solvent to its gaseous counterpart without crossing the solid-liquid phase boundary. The resultant product is highly porous, with a very large surface area, and hence possesses a fast dissolution rate (Salvatore A. Velardi, 2008). Given that the majority of water has been removed without raising the product temperature, then the shape, taste, colour and flavour of the product may be readily preserved (Reyes et al., 2010). In the case of biological substrates (for example cells and proteins) the presence of little or no water renders the product metabolically dormant. In all cases, this removal of water ensures extended shelf life in comparison with their liquid counterparts. By removing the water and rendering a light weight solid, this process can also reduce both the costs of carriage and cold storage. As a direct consequence of these beneficial features, freeze drying has found extensive applications in the fields of food preservation, drug delivery, biotechnology and microbiology, among others (Genin et al., 1996, Gan. et al., 2005).

In spite of the significant potential to improve product quality, freeze drying has been limited in application to high value products. This is principally because of the higher processing costs associated with energy intensive and prolonged manufacturing cycles (Barresi et al., 2009). Relatively slow drying rates are usually encountered during lyophilisation which result in long drying times, ranging from few hours to days. Empirical control and the need for conservative process cycles, involving low drying temperatures and prolonged drying times (to ensure optimal product quality), have led to protracted lyophilisation times, increased cost and compromised productivity. Significant interest has therefore developed in optimization strategies to reduce process cycle time. However, further developments in process understanding are required in order to achieve these goals and hence there is a need to further re-evaluate options for process measurements and control.

1.1 An historical overview

During 1813, Sir John Leslie studied the phenomenon of evaporation induced freezing and sublimation and narrated the latter as “ice wasting by continuous and invisible process of evaporation” (Leslie, 1813). Later in 1813, William Wollaston designed an instrument termed

Chapter 1

Cryophorus which results freezing and sublimation under vacuum (Wollaston, 1813). None of the above studies were intended specifically to yield a dry product. An actual freeze drying cycle was developed by Richard Altman during 1890 in Leipzig, Germany. In this experiment, tissue frozen at -15 °C, was dehydrated under vacuum (Altmann, 1890). Later, rabies virus was successfully freeze dried by Vansteenberghe during 1903 (Vansteenberge.M.P., 1903). Bordas and d'Arsonval carried out evacuation of water at low temperature for distillation (F Bordas and d'Arsonval., 1906). During 1906, Leon Shackell preserved venom by vacuum desiccation which can essentially be termed as freeze drying (Shackell, 1909). In 1927, Henry Tivall, a French inventor was issued first patent on drying of the frozen materials under vacuum. William Elser in 1934 upgraded the freeze drier by employing an apparatus with a manifold and a cold trap, which offers a heat input to the product and improved vapour flow from the product respectively, during the sublimation process. This advancement provides the basis of modern freeze drying (Elser et al., 1935). Earl W Flosdorf carried out freeze drying of a variety of materials including human plasma and serum for clinical application (Flosdorf and Mudd, 1935). In their publication, Flosdorf and Mudd introduced the term "Lyophile" which mean "Likes the solvent" to explain great ability of the dried product to rehydrate on subsequent exposure to solvent. During the later years, Flosdorf (Flosdorf. and Stokes., 1940) and Greave (Greaves, 1946) developed large scale freeze driers for the production of plasma during World War II. Sir Ernst Boris Chain carried out freeze drying of mold broth and isolated Penicillin for practical use during 1941 (Bergman, 2008). For his research on penicillin, Chain was awarded Nobel Prize in 1945. Both the freeze dried plasma and penicillin saved countless lives during the World War II. During this era (the mid 40's) substantial efforts were made to improve the process (Flosdorf et al., 1945).

Some of the early scientific attempts to investigate the process were undertaken by Louis Rey, who investigated the freezing process by the application of freezing microscope and electrical resistance at 1 kHz in 1960 (Rey, 1960). Mackenzie developed the freeze drying microscope; an essential tool which is employed for the development of successful freeze drying cycle (Mackenzie, 1964). Differential thermal analysis (DTA) was applied by Luvet et al in the evaluation of thermal instabilities in the frozen solutions of sugars (Luyet and Rasmussen, 1968).The aforementioned methodology for product characterization (by electrical resistance, DTA and freeze drying microscopy) has been adapted by commercial organizations such as

Chapter 1

Biopharma, for product characterization. Differential Scanning Calorimetry (DSC) measurements of the frozen solutions were carried which showed a good agreement with the DTA (Patel and Hurwitz, 1972). During the later years, the application of DSC was increased due to the fact DSC was less error-prone and more sensitive than the conventional counterpart.

The phase behaviour of aqueous solutions, including ice nucleation, eutectic melting and glass transitions phenomenon, were explained in terms of the phase diagrams thereby enabling studies on the impact of the additive on the freezing process during 1970s (MacKenzie et al., 1977, MacKenzie, 1976). Dielectric analysis was then employed in the prediction of collapse temperature termed take off temperature in this publication (Morris et al., 1994). Cryo-environment electron microscopy was used to explore the structural changes during sublimation process (Meredith et al., 1996). Modulated DSC was applied to investigate the collapse temperature defined by the freeze drying microscopy (Knopp et al., 1998). Characterization of the frozen solutions was carried out using X-rays during freezing thawing (Pyne and Suryanarayanan, 2001, Pyne et al., 2002, Sundaramurthi et al., 2010, Varshney et al., 2007, Pyne and Suryanarayanan, 2003). Nail and co-workers applied NMR to investigate the shape and position of sublimation front during the freeze drying(Li and Nail, 2006). Optical coherence microscopy which provides 3D images during the sublimation of solution detected the collapse temperature (Mujat et al., 2012).

Thermocouple probes have been included in the measurement of product and shelf temperature from the early years of freeze drying. Since 1980s research has been dedicated to the field of process analytical technologies (PATs). One of the earlier PATs investigated the application of capacitance manometer to record the chamber pressure during freeze drying (Armstrong, 1980). The gravimetric changes in the formulation following sublimation were studied by Pikal and co-workers in 1983 (Pikal et al., 1983). Later, in 1993 Bardat reported the changes in chamber pressure as a function of product sublimation using a Pirani pressure gauge (Bardat et al., 1993). The application of Manometric temperature measurement in the freeze drying were reported by Milton and co-worker in 1997 (Milton N et al., 1997). The technology has been described to measure the product temperature and end of primary drying. During 2007, Mayresse and co-workers applied a cold plasma ionization device to study the primary drying stage of the freeze drying process(Mayeresse et al., 2007). Sublimation kinetics was also studied using tuneable diode laser absorption spectroscopy during 2010

(Kuu et al., 2010). All these technologies are invariably employed to define the end of primary drying stage, only thermocouple is used to monitor the freezing process, but at best it may only recognize the onset and end of solidification.

1.2 The concept of freeze drying

The freeze drying process generally involves the freezing of the solution or suspension, removal of the frozen water at low temperature under the vacuum and then dehydration of the bound water at higher temperatures leaving a porous dried cake.

Freeze dried products can be readily constituted to the solutions following the addition of water; their tendency to form solutions on exposure to water provides the basis for the synonym ‘lyophilization’. Consequently the formulation is expected to be of acceptable quality, have longer shelf life, stable at room temperature storage.

1.2.1 Freeze drying principle

An understanding of the freeze drying process may be demonstrated by the phase behaviour of water as described in the schematic of Figure 1. The existence of three physical states of water (liquid, solid and vapour) can be explained by the phase boundaries defined by the values of temperature and pressure; evaporation curve, fusion curve and sublimation curve.

At standard pressure (1 atm) and at room temperature, water exists as liquid state (point A in Figure 1) which transforms to ice (point C in Figure 1) if the temperature is decreased below the values defined by fusion curve. Frozen water (ice) can be transformed to vapours if the pressure is decreased below the sublimation curve (point D in Figure 1). The liquid state transforms to vapours if its temperature is increased above the evaporation curve; this process forms the basis of conventional drying.

With the reduction in temperature value to 0.0098 °C and the pressure (6×10^{-3} atm) the phase boundaries merge with each other suggesting the coexistence of liquid solid and vapours. These temperature and pressure values are referred as triple point.

Chapter 1

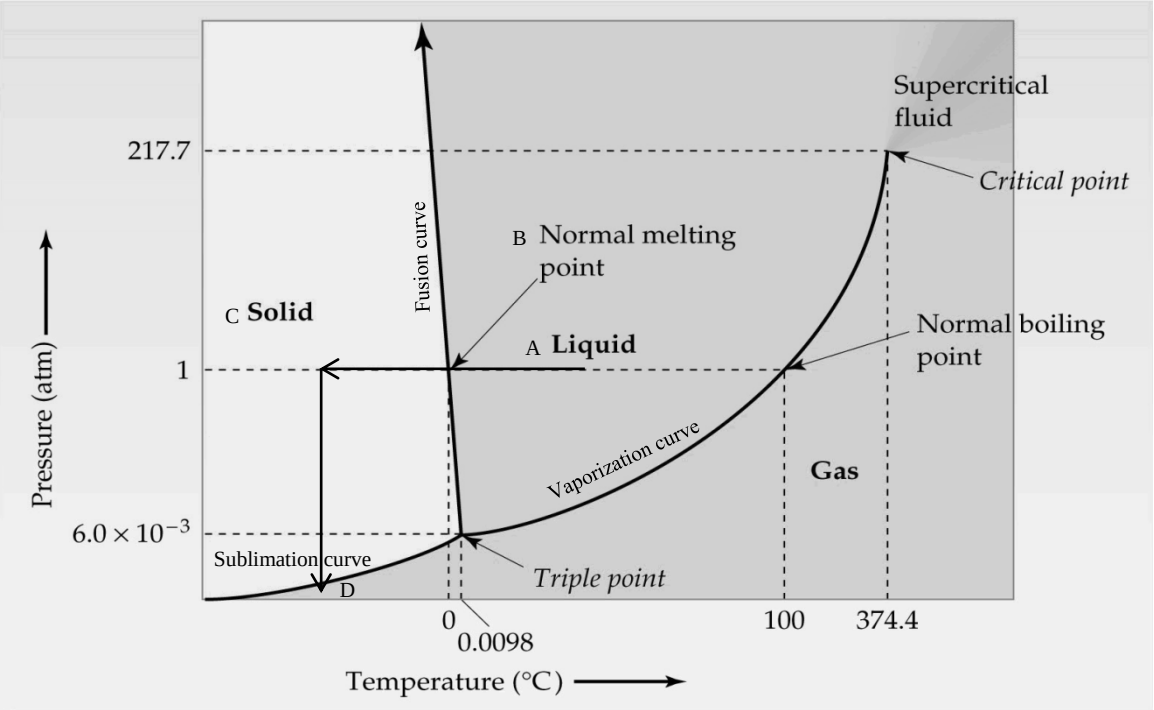

Figure 1 Phase diagram of water (Aulton, 2002)

During the freezing stage of process, the product temperature is set well below the melting point to ensure the complete solidification of the solution. In the second stage, the pressure is decreased to promote sublimation of the frozen water. The vapours find their way to the condenser, which is maintained at temperatures lower than the temperature of the product. This temperature gradient creates the partial pressure which is responsible for the vapour flow. As temperature and pressure values are kept below the triple point, the melting of ice is unlikely during sublimation Figure 1. A greater detail of each step and their implication to the process efficiency are described in the sections below.

1.3 Freeze-drying cycle development: A quality by design (QbD) approach

Lyophilisation process development is increasingly being accomplished in accordance with quality by design principles. This concept was developed by a consensus of expert groups with participants from lead industrial organizations and international regulatory authorities in Europe, the US and Japan and is currently embodied within various Quality Guidelines from the International Conference on Harmonization (ICH).

1.3.1 QbD framework

Quality by design (QbD) is a new development paradigm which is defined as "a systematic approach to development that begins with predefined objectives and emphasizes product and process understanding and process control, based on sound science and quality risk management''(ICH, 2009). The ICH guidelines on QbD are ICH Q8, ICH Q9, ICH Q10 and ICH Q11. ICH Q8 concerns pharmaceutical development, with a primary focus on process understanding and knowledge management. Other guidelines, associated with QbD are the subsequent directives of ICH Q9 on Quality Risk Management, which refer to the structuring of risk based approaches across the product life cycle (ICH, 2005). ICH Q10 addresses pharmaceutical quality systems, and provides a framework to support the assurance of quality and continuous improvement over the product life cycle (ICH, 2010). Finally, ICH Q11 relates to the development and manufacture of drug substances (ICH, 2011).

In brief, the QbD approach involves the following principles: (1) the identification of target product profile (TPP) and critical quality attributes (CQA) that assure product efficacy, (2) a risk analysis and the definition of a product design space to deliver these attributes and (3) a robust control strategy to ensure the reproducibility of the process (Rathore, 2009). Enhanced understanding of the process thereby leads to extended product cycle Figure 2.

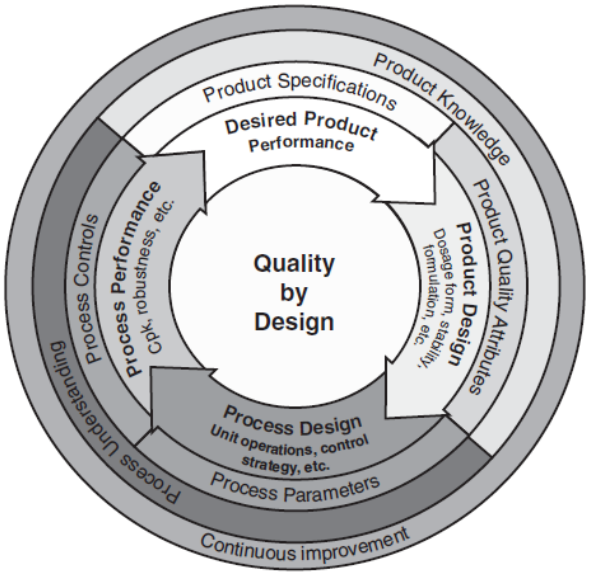

Figure 2 Quality by design model (Winkle, 2007)

An outline of the QbD routine for product development is summarized by a flow diagram displayed in Figure 3.

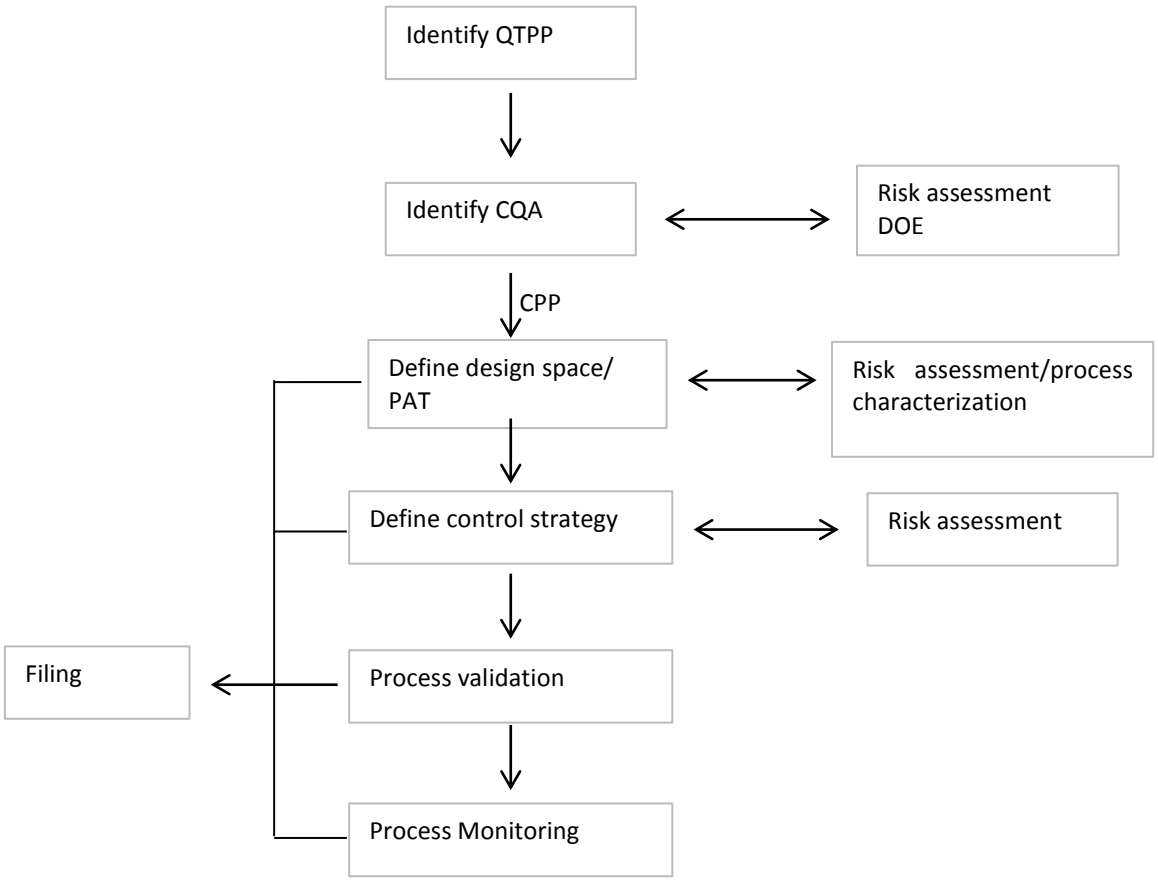

Figure 3 Quality by design methodology (ICH, 2009)

The design space, being an important component of the QbD approach, is defined as "a multidimensional combination and interaction of material attributes and process parameters demonstrated to provide assurance of quality" (ICH, 2009).

In addition raw material management, statistical approaches and process analytical technologies (PAT) are often employed to ensure the designed process viability. PAT, as defined by the ICH, is "a system for designing analysing and controlling the manufacturing through timely measurement (during the process) of critical quality and performance attributes of raw and in-process materials and process with the goal of ensuring final product quality". Furthermore, the application of PAT to the tracking of processes also provides for continuous improvement of the operation (ICH, 2009).

1.3.2 QbD in freeze drying

Critical Quality Attributes (CQA) for freeze drying

A freeze dried formulation must exhibit the following attributes

Appearance of the cake: an intact cake will retain the structure of the frozen matrix. In so doing, a high specific surface and faster dissolution is expected. Compromised cake structures result from suboptimal formulation and process design; these outcomes are termed as cake shrinkage, product collapse and melt-back.

Reconstitution time: provides an empirical estimate of the porosity and surface area of dried cake. The collapsed product reconstitute slowly as the porosity of the dried cake is compromised and low surface area is minimum. Moreover, longer reconstitution times pose marketing challenges (Chang and Patro, 2004). Shorter reconstitution times are desirable as they facilitate dissolution and administration of the lyophilized formulation.

Target moisture content: the presence of residual moisture impacts storage stability of the product. Due to this reason, lower water fractions are recommended (<0.5%). However, for protein pharmaceuticals, the moisture targets are relatively intermediate (~2%) in order to prevent 'over-drying' of the active pharmaceutical ingredient. (Wei, 2000, Tang and Pikal, 2004).

Post-freeze drying concentration of active ingredient: concentration of the API in the final formulation is required to comply with the label specification. A variety of factors including interaction with excipients, freeze concentration, solute crystallization, isomorphic changes and dehydration of both the active ingredients and the excipients are expected to impact the quality of the formulation. Due to the reason optimum formulation and process design is desirable for a successful product cycle.

Shelf life: storage recommendations are required to prevent physical transitions of both the active ingredients and excipients which may affect the product efficacy.

1.4 Different stage of the freeze drying process

Since the implementation of a QbD system requires a broad understanding of the process and product parameters, it may be appropriate to describe the different stage of freeze drying process in more detail with an emphasis on the changes in the physical states of the product.

1.5 Overview of the freeze-drying process

There are a number of discrete stages in a typical lyophilisation process: Freezing (sometimes followed by annealing) transforms the solution to stable frozen matrix, primary drying to remove the ice, and secondary drying to remove residual water from the unfrozen super-cooled liquid domains of the material (Figure 4).

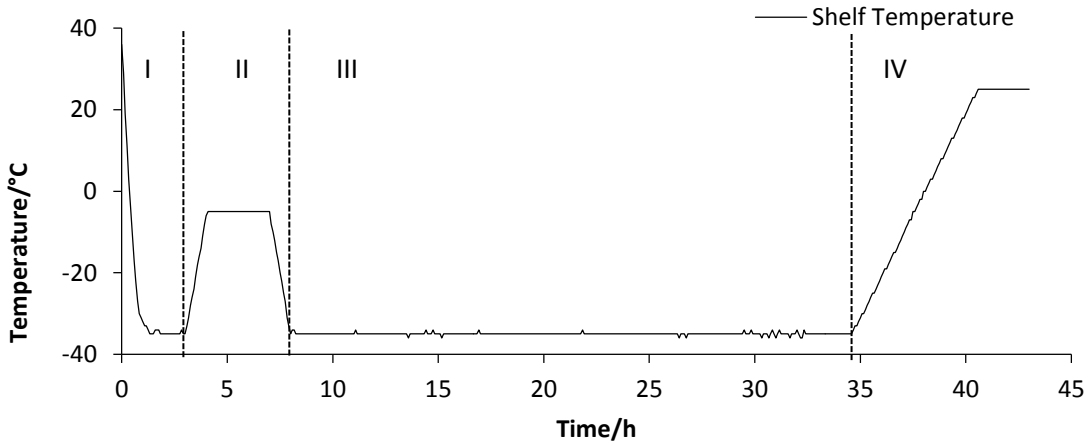

Figure 4 Shelf temperature profile showing different stage of a freeze drying cycle; (I) freezing, (II) annealing, (III) Primary drying, (IV) secondary drying

1.5.1 Freezing

During the freezing stage, the temperature of the product is lowered to some temperature below the melting point of ice and the eutectic/glass transition temperature(s) of any solutes that might exhibit eutectic freezing or glass transition. The amount and structure of the ice that forms, on reducing the temperature, is pivotal to the overall efficiency of the freeze drying process. Attention to the development of an effective freezing strategy is therefore essential to the creation of an efficient cycle. In effect, it is the ice crystal morphology which defines pore shape, pore size and tortuosity of the dried matrix formed by the sublimation of the frozen water in the primary drying stage. Hence, the duration and therefore cost of the freezing drying cycle is largely defined by the characteristics of the freezing events (A.I. Liapis, 1996). A variety of freezing methods are available to assist the tailoring of the ice structure to the requirements of the product. These are, in decreasing order of freezing rate: liquid nitrogen immersion or spraying, reduced pressure ice fog technique, placing the container on a pre-chilled freeze drier shelf or the application of a temperature ramp to the freeze drier shelf after placing the container on the shelf (Patel et al., 2009, Louis

Rey, 2004). The freezing process, in general, is propagated through nucleation and then solidification of the liquid mass, through crystal growth. The crystal morphology that results is dependent upon the degree of super cooling and the freezing rate.

In addition several other factors, such as nature of solute, concentrations of solute, volume of fill, vial geometry and freezing temperatures, may also contribute to the crystal morphology. It is worth noting at this point that an efficient mass transfer rate of water vapours has been reported in the matrices containing homogenously dispersed, large sized, dendritic crystals (A.I. Liapis, 1996). It follows that the control of ice crystal morphology is one of the principal concerns in the development of an efficient process cycle.

Nucleation and Crystal Growth

Nucleation

The phase transition from liquid water to ice proceeds through a series of intermediate steps termed primary nucleation, secondary nucleation and crystal growth (which ultimately leads to solidification). Primary nucleation refers to a spontaneous event involving density changes and molecular rearrangements in the bulk solvent, which originate from fluctuations in the extent of Brownian motions, and leads to the formation of molecular clusters which increase in size and number with decreasing temperature. The probability of nucleation is thought to be directly associated with the lifetime of the molecular clusters (Franks, 2007). This lifetime increases in the presence of surfaces (and foreign particles, in the case of non-filtered liquids) which act as inherent nucleation loci to seed and stabilise, the clustering of solvent molecules. The result is that nucleation begins to seed the formation of ice at temperatures much higher than would be the case if the system were to nucleate through the spontaneous self-association of water molecules alone (a process known as homogeneous nucleation). It has been postulated that secondary nucleation involves the addition of solvent molecules from the bulk phase to the surface of primary nuclei. This progresses at a fairly rapid velocity (called nucleation front velocity) and is of the order of mm/s.

Ice Crystal Growth

Following secondary nucleation, the crystal growth and solidification phases progress either slowly or swiftly, depending on the temperature and therefore viscosity of the liquid.

There are broadly two ways in which solidification can develop in the material. This first is directional solidification from the base of the container. The relatively slow rate of directional solidification is attributed to a hindered transfer of the heat of crystallization from the solidification interface to the shelf via the already solidified layer and the base of the vial (Louis Rey, 2004, James A. Searles, 2001). Elevated thermal gradients and further retardation of the rate of solidification are frequently observed with higher fill volumes and elevated height to diameter ratios of the samples. The second is global solidification, which is the consequence of efficient thermal conductions and diminutive thermal gradients between freezing interface and the shelf. It has been suggested that there is a critical cooling rate below which the sample freezes by global solidifications whereas directional solidification results from cooling above the critical rate (James A. Searles, 2001).

Following ice formation, a significant fraction of the water phase separates out from the solution as ice crystals while the remaining water forms a concentrated solution with the solute; this phenomenon is commonly referred as freeze concentration or cryo-concentration. The frozen matrix resembles a honey comb structure wherein the ‘cells’ are derived from the ice crystals while the ‘walls’ are formed by the viscous solution. With a further decrease in the product temperature, physical changes in the walls of the frozen matrix are observed. As a consequence of these transitions (eutectic crystallization and/or glass transition), the matrix supports its structure after the sublimation of ice.

Eutectic Crystallization

Following ice crystallization, free water decreases in the system (freezing curve Figure 5) while the solute concentration increases. Simultaneously, temperature dependent decrease in solubility limits the interaction between solute and water molecules (solubility curve Figure 5). With the further decrease in temperature the concentration of water and solute approaches to a critical level which favours the eutectic crystallization of solute and water molecule. (The concentration at which crystallization occurs is termed eutectic crystallization C_{eu}). The temperature associated with the onset of eutectic crystallization is recorded as the eutectic temperature or T_{eu} (Point C in Figure 5).

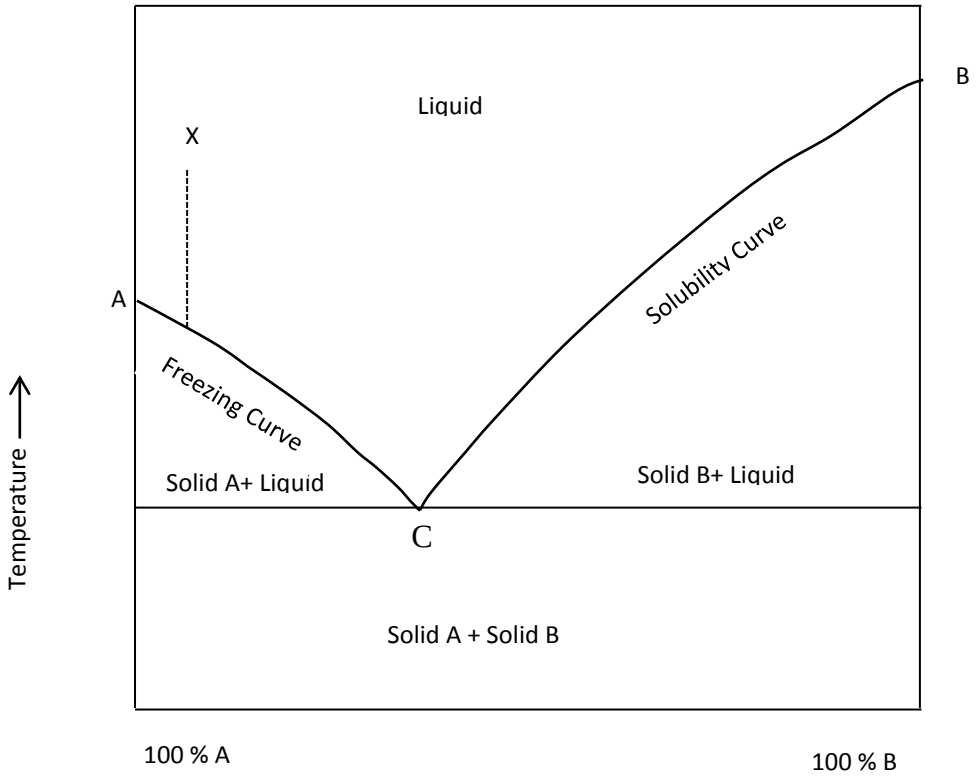

Figure 5 Phase diagram of eutectic crystallization (A water; B solute; C eutectic point)

The phase diagram suggests that no liquid remains in the system at temperatures below the eutectic point; this ideal situation is rarely observed. In practice, different physical states may exist within a frozen solution, i.e. ice, liquid water, crystallized/ non-crystallized solute and the eutectic mixture. In practice, the term eutectic crystallization is frequently used in the context of freeze drying where the solute crystallized in the solution without necessarily forming a eutectic mix.

Glass transition

For a solution of non-crystallizing solute (e.g. sucrose), the ice formation is accomplished with (i) an increase the product temperature close equilibrium melting temperature (point B to C Figure 6), and (ii) freeze concentration of the solute which continues with further decrease in product temperature resulting in an increased viscosity within the 'walls' of the frozen matrix. The viscous solution transform from liquid to rubber and then glass state as the viscosity increases to ~10^{14} poise. The temperature associated with this transition is called glass transition temperature T_g and the corresponding solute concentration is denoted as C_g (Figure 6).

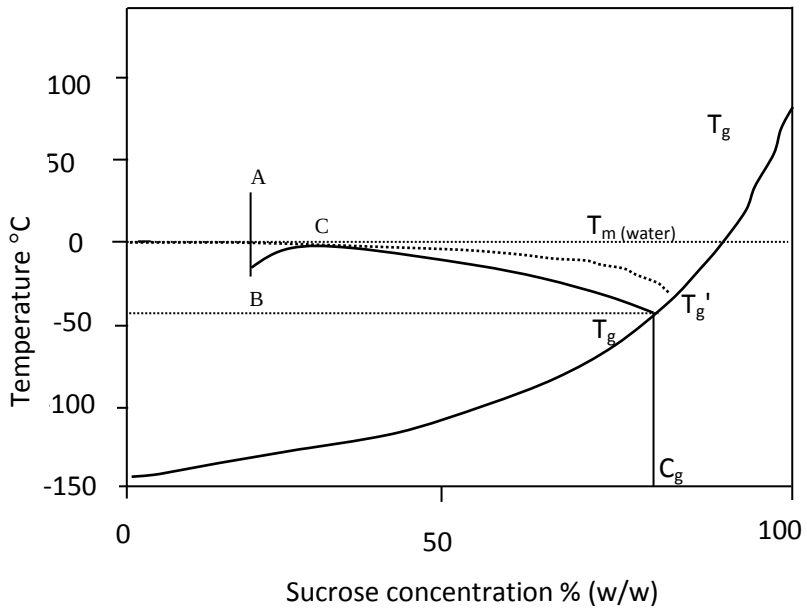

Figure 6 State diagram of sucrose; Point A ambient temperature, B demonstrate super cooling C is equilibrium freezing

At higher cooling rates a low degree of freeze concentration is expected due to the fact water molecule remains entrapped in the frozen matrix which may reflect a low Tg. At low degree of cooling one may achieve a maximal freeze concentration relating to T_g'.

Phase transitions during freeze drying are explained by the energy/free volume diagram (Figure 7). The enthalpy or free volume of the liquid decreases with the temperature at a constant gradient as long as the physical state is not changed.

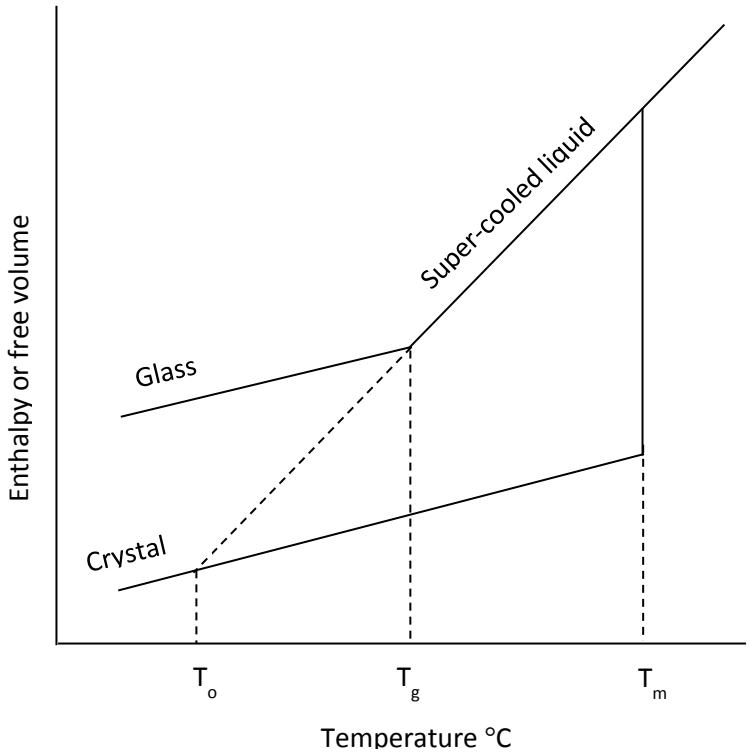

Figure 7 Thermodynamics relationship between liquid glass and solid state (T_m is melting temperature, T_g denotes glass transition temperature and T_o is Kauzmann's temperature) (Franks, 2007)

The gradient of enthalpy change decreases after the glass formation due to loss of co-operative motions within the molecules. The enthalpy change after crystallization is greater than that of the glass (Debenedetti and Stillinger, 2001, Kauzmann, 1948); lower entropy is ascribed with the ceased transition translational motion as well as the molecular rotation.

The techniques employed to monitor these thermodynamic transition provide a rationale for the set-up of shelf temperature during the freezing drying cycle which will ensure a desired physical state of the solute within the frozen matrix i.e. crystalline or glass. Nevertheless, the rate of sublimation is impacted by the size and shape of ice crystals which is required to be optimized for faster drying rates.

Manipulation of the Freezing Process

There are a number of opportunities for controlling the characteristics of the frozen product such that the subsequent primary drying stage might be optimised (i.e. reduced). These involve the manipulation of the freezing rate, the use of a range of approaches to control the nucleation stage, and annealing.

Chapter 1

Freezing Rate

The freezing methods providing rapid cooling rates, lead to smaller ice crystals and therefore a more tortuous path for the ice sublimation which, in turn, results in prolonged subsequent primary drying time compared with their counterparts produced from slow freezing rates. It has also been reported that the velocity of the secondary nucleation front is dependent on the degree of super cooling, and directly contributes to the resultant crystal morphology. The degree of super cooling is defined as the temperature difference between the equilibrium ice formation temperature and the actual temperature at which ice formation begins, and is usually between 10 and 20 ^{o}C. The actual value varies with cooling rate and other factors such as heat flow, formulation viscosity, etc. (Tang and Pikal, 2004). It has been demonstrated that a low degree of super cooling generates dendritic crystals whereas a higher degree of super cooling generates crystal filaments (Figure 8) (James A. Searles, 2001, Kochs et al., 1993). The greatest degree of super-cooling is observed with liquid nitrogen based freezing methods while the pre-cooled shelf loading method delivers the lowest degree of super cooling. However, the heterogeneity in temperature distribution across the shelf can mean that the pre-cooled shelf loading method is undesirable. Alternatively the shelf ramp method (for example at a rate of 0.5^{o}C/min) is preferred as it lacks the extreme super cooling associated with pre-cooled shelf freezing method (Tang and Pikal, 2004). The impact of freezing rate on process efficiency can be quantified as follows: For each 1^{o}C increase in the degree of super cooling there is an increase in the primary drying time by approximately 1-4% (James A. Searles, 2001, Roy ML, 1989).

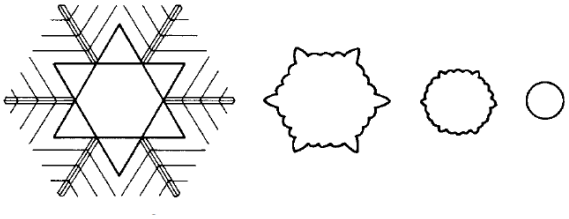

Figure 8 Ice crystal sizes with increasing degree of super cooling (Oetjen, 2007)

Controlled nucleation

A variety of techniques have been investigated to achieve controlled nucleation and deliver predictable rates of sublimation. These include sono-crystallization, electro freezing, vacuum induced surface freezing, and the ice fog technique.

Sono-crystallization. A technique using ultrasound in the activation and control of the nucleation step, has been reported to be an efficient intervention in the lyophilisation process (Chow et al., 2003). Nucleation through this technique is accomplished by positioning the filled vials on aluminium plates which are in turn are stationed over the heat exchanger and in proximity to the horn of an ultrasound transducer. Ultrasound mediated nucleation of the sample was shown to be triggered at different time points, which depend upon the degree of super cooling, and hence can be controlled with a good degree of repeatability (Kyuya Nakagawa, 2006).

Electro freezing is another approach adapted to initiate nucleation and crystallization at sub melting temperatures. The materials to be freeze-dried are introduced into a pre-designed chamber provided with platinum electrodes and a temperature control system. As the temperature drops below the melting point of a particular aqueous solution (−4 to −14^{o}C) an electric pulse U=1 kV/s is applied and the nucleation time recorded using a temperature data acquisition system. This technique has been reported to be statistically viable in terms of the reproducibility of cooling rate and nucleation temperatures (Petersen et al., 2006).

The **vacuum induced surface freezing technique** has been reported to preclude unnecessary under cooling of the solution while promoting a high yield large dendritic ice crystals. The ice crystallization starts on the solution surface as the chamber pressure approaches ~1 mbar at a shelf temperature +10^{o}C. The underlying mechanism of this phase transition is the reduction in surface temperature which results from the heat transfer associated with the enthalpy of

vaporization ΔH_v as moisture evaporates from the surface of the liquid. As the ice layer advances to 1-3 mm in thickness (within 5 minutes) the pressure is rapidly increased to atmospheric pressure, in order to prevent the liquid from boiling. Simultaneously, the shelf temperature is reduced to 4−5^{o}C below the melting point, in order to prevent melt back of the ice layer. The growth of coarse crystal morphologies is then accomplished as the shelf is maintained at this low level of super cooling (1 hour). Subsequently, the shelf temperature is reduced to the set freezing temperature value via a moderate freezing rate (2 ^{o}C /min) (Kramer et al., 2002). Although crystal morphologies obtained with this technique are optimal, the underlying risk of boiling the unfrozen solution, the heterogeneities in ice morphologies and blowing up of the frozen surface layer outweighs its application to real world manufacturing (Kasper and Friess, 2011). A modification to the surface freezing technique entails holding the shelf temperature at -10^{o}C, pulling a vacuum at 600 mTorr and subsequently dropping the temperature to −45^{o}C at a rapid freezing rate (> 1^{o}C/min) (Liu et al., 2005).

The **Ice Fog technique** involves lowering the shelf temperature to provide the nucleation temperature of the solution followed by the introduction of liquid nitrogen vapours to the chamber, under a high pressure of 10 psig, which transforms the atmospheric moisture to ice crystals; which subsequently provide nuclei for the subsequent solidification of the solution (Rambhatla et al., 2004). Variations in the solute concentration, the degree of super-cooling, the liquid nitrogen pressure and the humidity of the chamber may be used to modulate the rate of nucleation. The reduced pressure ice fog technique has been reported to provide fairly rapid (< 1 minute) nucleation compared to vacuum induced surface freezing (> 5min) (Patel et al., 2009).

Hold temperature and time

After the apparent completion of the freezing process, the product should be held for a further period (below the T_g' for amorphous substances and below T_{eu} for crystalline materials) to ensure the complete solidification of the whole solution. The hold temperature for a particular material is usually 2 $^{\circ}$C below the T_g' whereas the hold time depends on the fill volume. The situation is often complicated by compromised heat transfer profiles through the frozen matrix and base of the glass vial, which delay the dissipation of heat of crystallization from the interior of the frozen solution. Therefore a holding period is required to ensure complete freezing. This holding time is directly related to the filled depth of the liquid. As a

general rule, for each centimetre of the filled volume, one hour of hold time is suggested. However, it has been recommended in at least one publication that a fill depth in excess of 2 cm should be avoided where possible (Tang and Pikal, 2004).

After the initial freezing stage, there remains a further opportunity to influence the state of the frozen matrix, prior to the initiation of the first drying phase. This is achieved through the process known as annealing.

1.5.2 Annealing

Annealing refers to a process step, during the freezing stage, whereby the temperature of the substance is raised to a sub-freezing point for a defined period of time. The primary purpose is to change the ice crystal morphology (Abdelwahed et al., 2006) while promoting further crystallization of ice (through de-vitrification and recrystallization). Secondary to this, but possibly of equal importance, is the crystallization of the active pharmaceutical ingredients and certain excipients of the formulation (e.g. mannitol and glycine) (Carpenter et al., 1997, Lu and Pikal, 2004).

By raising the temperature of the product during the annealing stage, one can promote the growth of ice crystals through the enhanced diffusion towards the ice front (de-vitrification) and Ostwald ripening of ice structures (recrystallization); with the result being larger crystal morphologies and improved ice networking which facilitate primary drying and reduce the overall cycle time.

Ostwald ripening (recrystallization) is the phenomenon whereby crystals, smaller than a critical size, decrease in number as those larger than the critical size grow. At temperatures above Tg', the smaller crystals melt preferentially owing to higher chemical potentials associated with their smaller radii of curvature, leading to either diffusion or surface-attachment limited recrystallization.

Ostwald ripening of non-ionic molecules is controlled by bulk diffusion and is described by the Equation 1:

$$dr/dt = D\boldsymbol{v}/\boldsymbol{r}[(\boldsymbol{c} - \boldsymbol{c}*) - 2v\gamma c*/RTr\boldsymbol{]} \qquad \text{Equation 1}$$

where dr/dt is the rate of crystal growth, r is the radii of the crystal, D is the diffusion coefficient of water through amorphous phase, υ is the molecular volume, and c and c* are the concentration of the amorphous bulk phase water at current time and equilibrium time respectively. Actual growth in the ice crystal size from the sucrose solution is shown in Figure 9.

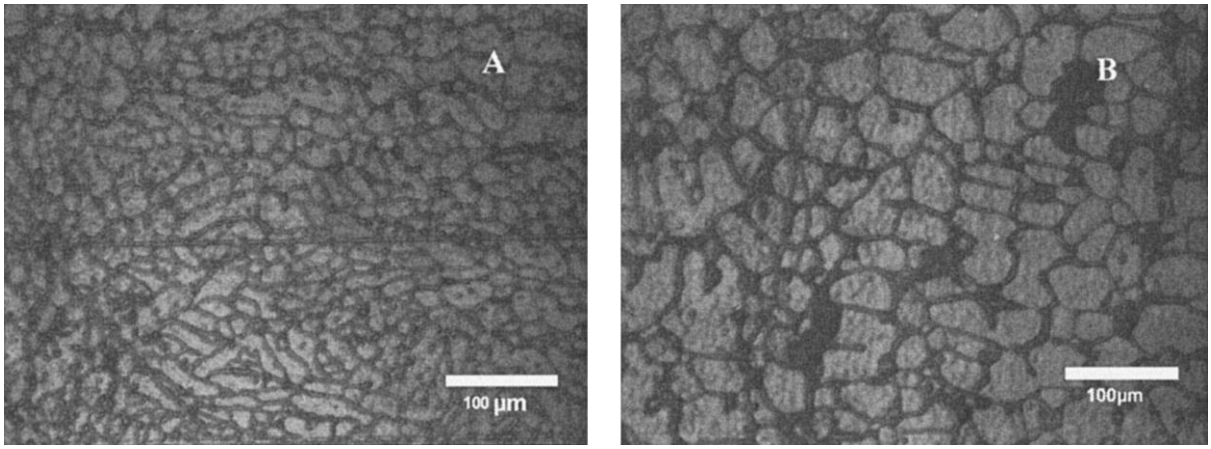

Figure 9 Ice crystal sizes measured before and after annealing at -10 °C (Chouvenc et al., 2006)

Devitrification is another significant feature of annealing (above Tg') which helps to overcome imperfections of freeze concentration associated with suboptimal freezing rates (Ablett et al., 1992). Herein the water molecules relocate from the amorphous phase containing unfrozen solute and amorphous water (bound water) to the predominant ice form (free water) resulting in a higher degree of freeze concentration.

The relationship between recrystallization rate and temperature has been indicated to follow William-Landel-Ferry equation (Equation 2).

$$In\ k/k_o = K\ (T - T_o)/(T - T_\infty) \qquad \text{Equation 2}$$

Where k and k_o are the rates of recrystallization at T and T_o respectively, K is a constant and T_∞ is reference temperature having a k value equal to 0. Although the equation depicts a linear relationship between the temperature gradient and recrystallization, an annealing temperature of 10^oC above T_g' but well below the T_{eu} is suggested for an optimal output of freeze dried biopharmaceuticals (Byeong S. Chang, 2004).

It follows from the above discussion that the time required to correct the heterogeneities in particle size distribution depends ultimately on the parameters affecting recrystallization.

From a practical point of view this correction time may be considered to lie within the broad range of 0.5 to 10 h.

In concluding the discussion of the application of annealing to the attainment of the desired state, with respect to ice formation, one might consider the impact of post annealing re-cooling rates. There is evidence to suggest that the re-cooling rate has little effect on the particle size distribution and primary drying time; probably the large crystals serve as nuclei for the additional growth and no fine crystals are re-produced (James A. Searles, 2000). Consequently, sufficient post annealing refreezing hold time, as aforementioned, is suggested to ensure the temperature equilibration of the entire all samples.

The **secondary purpose of annealing** is to promote the crystallization of the API and other solutes. In this case, the rational for annealing is that a frozen mass, containing excipients with incomplete crystallizations, often carry a significant potential to depress T_g' hence necessitating a further reduction in the primary drying temperature. Moreover, the presence of 'dissolved' solid presents a potential instability hazard on storage, since the recrystallization of these components might in turn impact reconstitution behaviour and time (Hawe and Friess, 2006, Lueckel et al., 1998). However, some care must be exercised, as the crystallization of these bulking agents (which can also occur in primary drying) may result in vial breakage especially with high fill volumes. Although this can be avoided by using low sublimation temperatures (e.g. $<-25\ ^{o}C$ for mannitol) it might be considered, on balance, that annealing presents as the preferred, economical choice (Pyne et al., 2002). Annealing is also intended to reduce vial to vial heterogeneities of ice crystal size by regularizing the particle size distribution in the frozen matrix (Hawe and Frieß, 2006). Matrices with homogenous particle size are reported to sublimate up to 3 times faster than the non-annealed counterparts owing to efficient mass transfer rates during the primary drying which ensue from uniform pore structures and minimal dead ends (James A. Searles, 2001, James A. Searles, 2000).

In spite of the dramatic reduction the primary drying times, annealing is also associated with lower specific surface area of the matrices, which leads to elevated resistance to desorption and hence proportionally elongated secondary drying times (Mousavi et al., 2005, Pikal et al., 1990).

1.5.3 Primary Drying

Primary drying (otherwise known as the sublimation stage) results in the removal of greater than 90 per cent of water from the substance being freeze-dried. Typically, this stage involves a reduction in the chamber pressure to within the range 50-150 mTorr and the elevation of the frozen product temperature to a level that will provide sufficient energy to drive the sublimation process (Tang and Pikal, 2004).

Primary drying is recognized as the longest, most significant, expensive and risky phase of the lyophilisation cycle (Giordano et al., 2011). Over the past decades, extensive investigations have been carried out to elucidate both the theoretical and practical aspects of this central stage. The sublimation rate and length of primary drying are reported to be linked with the properties and features of the equipment (heat transfer, pressure regulation), the container (wall thickness, thermal conductivity, curvature of the bottom) and the product formulation (height of fill volume, dry layer resistance to mass transfer) (Chen et al., 2008). Economic drivers to optimize primary drying have directed formulation and process development scientists to investigate the critical parameters impacting mass transfer, namely, heat transfer rate, product temperature, product dry layer resistance and chamber pressure.

The heat and mass transfer mechanism summarised in Figure 10 describe that the heat inflow to the formulation (through conduction, convection and radiation) results in ice sublimation which raises the vapour pressure at ice sublimation interface than the chamber. Later, the water vapours flow to the chamber with a consequent product cooling which is manifested with a reduction in the product temperature. Finally, with the opening of the separation valve, the drying chamber connects to the condenser (maintained at temperature lower than the former), water vapours get trapped on the condenser surface. This pressure gradient maintains the vapour drive from the sublimation interface until the ice sublimation is completed.

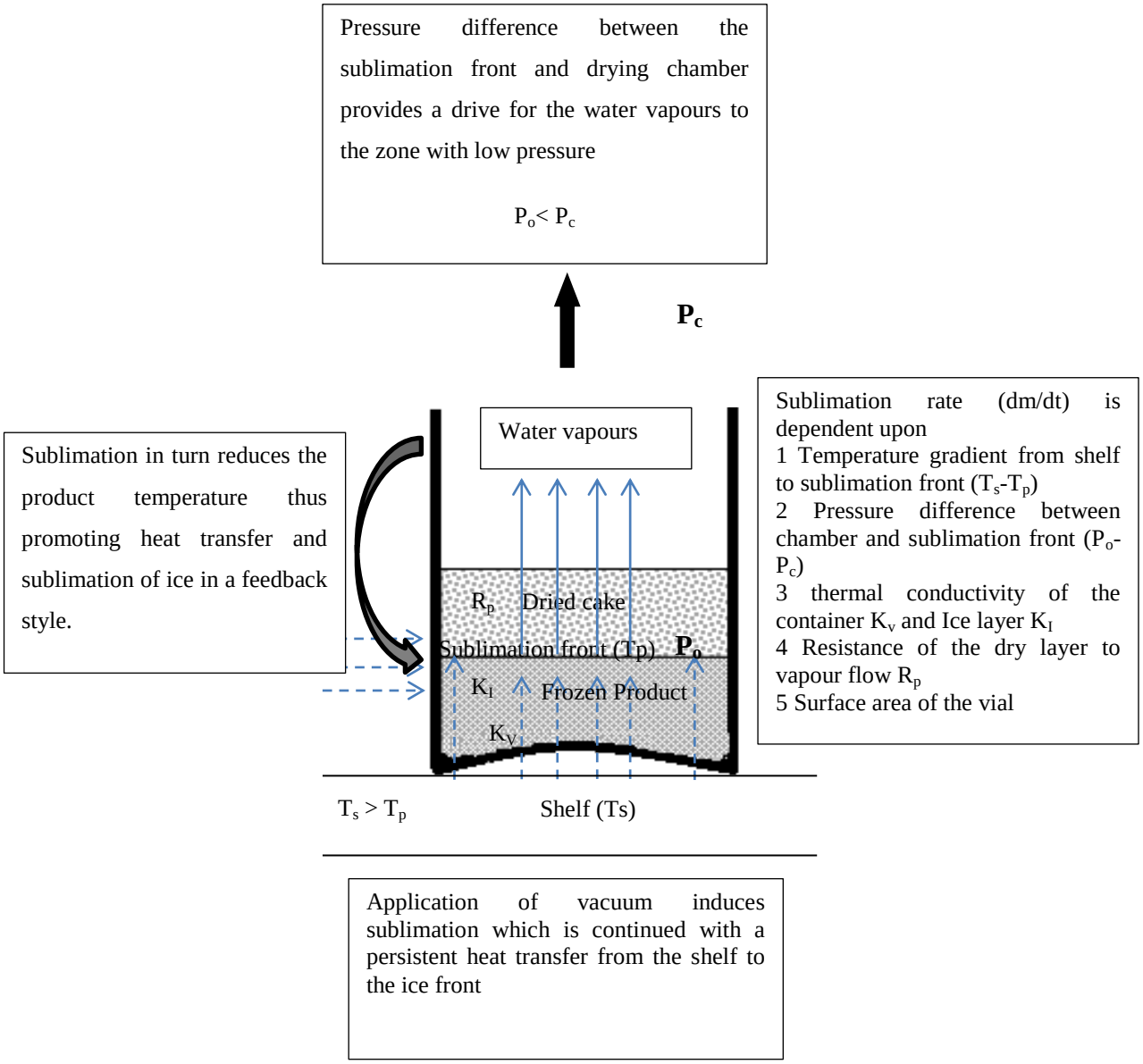

Figure 10 Overview of heat and mass transfer mechanism during primary drying

These are discussion, in turn, below:

The **heat transfer rate** to a vial has been calculated using the Equation 3

$$dQ/dt = 3600.A_v.K_v.(T_s - T_b) \quad \text{Equation 3}$$

Where dQ/dt is the heat transfer rate between the vial and the shelf (J/s.per vial), A_v is the outer area of the base of the vial (m^2), K_v is the heat transfer coefficient (J/s m^2K), T_b-T_s is the temperature difference between the product container bottom surface and the shelf respectively, and 3600 is the value obtained from the conversion of cal/sec per vial to cal/ h per vial.

The vial heat transfer coefficient K_v is calculated from the summation of three primary contributing mechanisms Equation 4

$$K_v = K_c + K_r + K_g \quad \text{Equation 4}$$

Where K_c is thermal co-efficient contribution arising from conduction, K_r is input from radiative mechanism and K_g is the contribution from gas convection between the shelf and the bottom of the vial. Two of the heat flow coefficients namely K_c and K_r are independent of the chamber pressure while the K_g increases with the chamber pressure, which can be expressed by Equation 5

$$K_g = \frac{\alpha \Lambda o P}{1 + l(\alpha \Lambda o/\lambda o)P} \quad \text{Equation 5}$$

Where Λo is the free molecular conductivity of gas at 0 °C, λo is the heat conductivity at ambient pressure; l is the distance between the shelf surface and the vial base α is energy accommodation coefficient (Pikal, 1985).

Radiative heat transfer is progressed through the vial base and to the top of the vial which can be explained with Equation 6.

$$K_r = 4\,(es + ev)\,\kappa T^3 \quad \text{Equation 6}$$

Where e_s Emissivity of the shelf surface, e_v emissivity of the vial, T is average temperature, κ is Stefan-Boltzman constant (Pikal et al., 1984).

Mass transfer

During the steady state of primary drying as the product temperature is largely constant, the heat transfer rate can be explained with the mass transfer rate and the heat of sublimation of water/solvent Equation 7.

$$\frac{dQ}{dt} = \Delta H_s \frac{dm}{dt} \qquad \text{Equation 7}$$

By substituting the value of dQ/dt from Equation 3 the value for K_v can be calculated provided other parameters of the Equation 8 are known

$$A_v . K_v . (T_s - T_b) = \Delta H_s \frac{dm}{dt} \qquad \text{Equation 8}$$

In addition to the heat inputs, the mass transfer from a frozen matrix is also explained with an additional driving force for the water vapours i.e. pressure gradient across the sublimation front and the drying chamber in combination with the barrier effect contributed by the dry layer. The ice sublimation at a defined temperature is (i) directly proportional to the pressure gradient between the vapour pressure at ice surface and partial pressure contributed by water vapours in the chamber and (ii) inversely proportional to the sum of resistances in vapour flow conferred by dry product layer and the stopper. This can be shown mathematically by Equation 9;

$$dm/dt=(P_{ice}-P_c)/(R_p+R_s) \qquad \text{Equation 9}$$

where dm/dt is the sublimation rate of ice (g/hour per vial), P_{ice} is the vapour pressure of ice at sublimation interface (Torr) P_c is the chamber pressure, R_p and R_s are the resistance in vapour flow imparted by dry layer of the product and stopper respectively. Theoretically, the attainment of the lowest possible pressure will generate the highest ice sublimation rates. But in practice very low chamber pressures (< 50 mTorr) are linked with contamination of the product with pump oil or volatile stopper components and low heat transfers owing to increased density of gas between the shelf and vial bottom (Zhai et al., 2005). Similarly, insignificant mass transfer is evident at chamber pressures above 200 mTorr (Tang and Pikal, 2004, Nail, 1980).

The **Resistance to mass transfer** (RTMT) is another determinant of the sublimation rate and therefore drying time. The RTMT has been attributed to sample geometry; filled volume depths, diameter of the samples, nature of the solutes crystal morphology, porosity and tortousity of the dried layer and stopper dimensions (Liu et al., 2005). Pikal et al demonstrated that $R_p >> R_s$ especially for high fill volume sample (Rambhatla et al., 2006, Patel et al., 2004). Therefore an accurate prediction of vapour flow resistance profile of the product can result a reproducible drying rates.

As sublimation proceeds, the mass transfer of the water vapours from the ice interface to the surface of sample has been documented to follow the modified Fick's law of diffusion Equation 10

$$N = -D_k \, \Delta P / \Delta x \qquad \text{Equation 10}$$

where N is the vapour flux (Kg m^{-2} s^{-1}), D_k is the effective diffusion coefficient (m^{-2} s^{-1}), and ΔP and Δx is the pressure gradient (Torr) and distance between the amorphous surface of the sample and sublimation interface (m). In turn the magnitude of D_k is directly proportional to the channel diameter, as shown in the Knudsen diffusion Equation 11

$$D_k = d/3\sqrt{8RT/\pi M} \qquad \text{Equation 11}$$

Where d is the channel radius (m), R is the gas constant (m^2kg $kmol^{-1}K^{-1}$ s^{-2}) M is the molecular weight (kg $kmol^{-1}$) (Kochs et al., 1993). Although the heat transfer from the shelf surface to the sublimation front is improved, as the latter recedes during primary drying, the mass transfer rates do not increase proportionately owing to the increased thickness of the dried layer and the associated extension to the diffusion path length for vapours to exit the sample (Zhai et al., 2005). In addition the literature supports the evidence that the crystal morphologies in vicinity of the bottom of the vial are spherical rather than dendritic on the top regions which may also significantly slow down the sublimation rates (Kyuya Nakagawa, 2006).

Risk assessment for Freeze drying cycle development

The combination of input parameters (formulation composition and process parameters i.e. shelf temperature and chamber pressure) is likely to endanger the quality of the finished product. This, proactive approach, requires identification of potential risks to the critical

quality attributes of the formulation when a proposed formulation and/or process design will be practiced. An Ishikawa diagram is helpful in demonstrating the impact of input parameters on the product attributes (Figure 11).

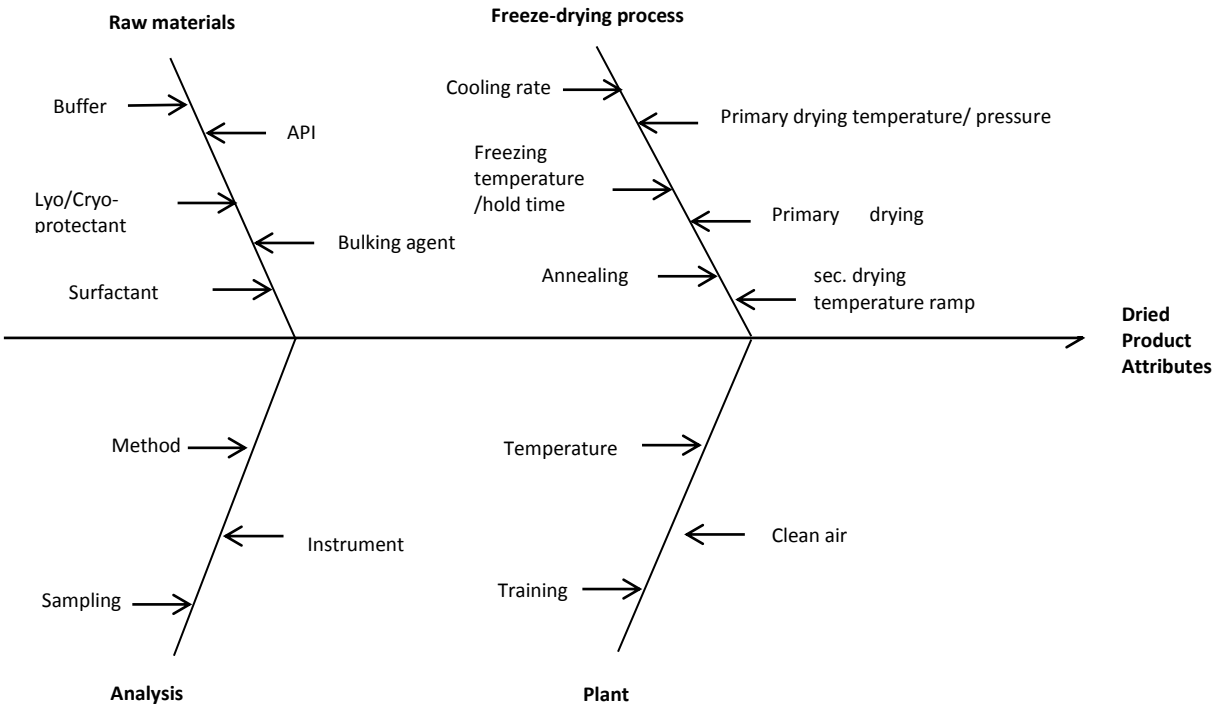

Figure 11 Ishikawa diagram for freeze drying process development

For a particular attribute the risk factor can be calculated from the Equation 12

$$\text{Risk factor} = \text{severity} \times \text{likelihood of occurrence} \qquad \text{Equation 12}$$

The severity is related to safety and efficacy of the product while the occurrence is related to process/product knowledge and control (Lotlikar, 2013). The risk factor from each attribute, calculated from the multiplication of pre-set scale for each contributor (severity and occurrence) is described either by risk priority numbers or by standard colour codes (whereby red denotes a high risk factor requiring certain precautions in order to reduce the risk, yellow represents an intermediate risk which requires close monitoring, while green colour is for risk factor with low degree of harm, i.e. safe). Table 1 describes the risk assessment of a typical biopharmaceutical formulation.

Table 1 Risk assessment of a freeze dried biopharmaceutical formulation

CQA	Formulation	Freezing	Primary Drying	Secondary Drying
Moisture Content				
Stability				
Appearance				
Activity				
Reconstitution Time				

The risk assessment is based on prior knowledge, initial experimental data and a failure mode and effects analysis (FMEA) approach (Rathore and Winkle, 2009, ICH, 2009). FMEA involves the manufacture of a series of trial batches under processing (drying) conditions with increasing order of severity until the failure mode is approached. The failure modes in the case of a freeze-dried product include collapse (amorphous), eutectic melting (crystalline) and/or loss of solids, in case of formulations having low solid contents dissolved in the co-solvent system. These are often recorded through systematic elevation of either the chamber pressure or product temperatures.

Design space for Freeze drying cycle

For a particular formulation the design space for process parameters of product temperature and chamber pressure, can be extracted from an FMEA study (Figure 12).

The upper limit of the design space is defined by the highest product temperature which results in an acceptable product quality. This is in effect, the collapse temperature of the product (i.e. dashed line at $-25^{o}C$ in Figure 12), as determined off-line by freeze drying microscopy. Whereas, the lower limit of the design space is defined from the choked flow of water vapours due to low chamber pressures. The choke point, a determinant of the equipment capabilities, is estimated by evacuating the ice slab filled system to a low chamber pressure and heating the shelf to a level whereby the chamber pressure is no longer regulated by the system containing ice slab. The boundary of the design space relating the choked flow is shown in as solid line in Figure 12.

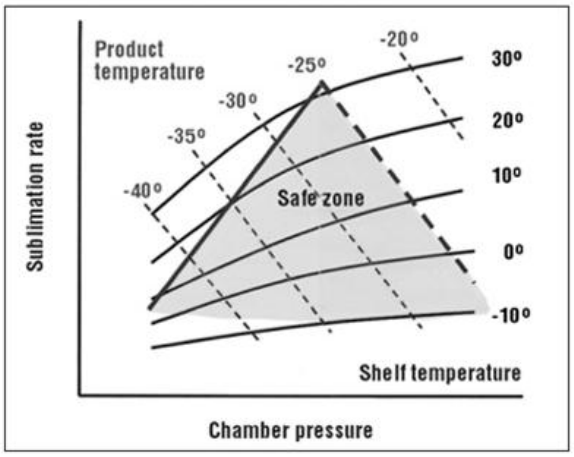

Figure 12 A schematic presentation of design space with boundary limits imposed by the product (dashed line describing the product temperature) and equipment (i.e. the solid line describing the shelf temperature) (Steven L. Nail, 2008)

In summary, the design space is bounded on the right side (dotted line on the right of Figure 12) with the temperature isotherm which defines the failure mode known as product collapse, and on the left side, by the solid line relating to the failure mode known as choke flow. Although any process operating in the design space is acceptable, the process operating near the apex of these two boundaries, being more efficient, is hence more desirable (Steven L. Nail, 2008).

It is also necessary to account for the equipment related boundaries which impact the sublimation rate; In particular the electrical power that heats the silicon oil, the design of the internal flow channel within the shelves, and the heat transfer fluid type and flow rate.

Control space

Although the application of QbD approaches to freeze drying cycle development requires the identification of the operational window (known as the design space) that will routinely produce products of acceptable quality, the wide boundaries of the design space are often suboptimal in terms of time and energy consumption. Within the design space of a formulation, a refined adjustment of the process input parameters (i.e. shelf temperature, chamber pressure) is made which ensures an optimum output of product with CQAs, this is called control space (Figure 13).

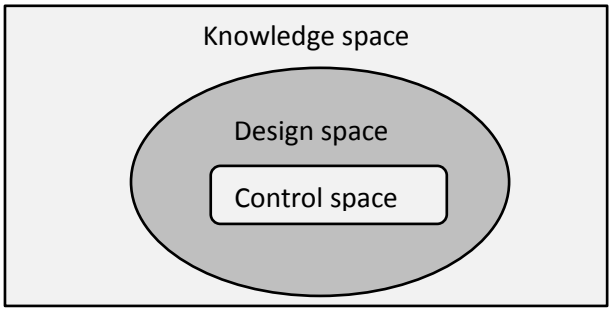

Figure 13 the concept of design space

Efficient monitoring and control of both the product and instrument related process variables necessitate the application of certain approaches using process analytical technologies (PAT).

Set up of shelf temperature

The product temperature is principally defined by the shelf temperature, provided the chamber pressure is maintained at the level of 1000 mbar. However, if the chamber pressure is reduced such that the product crosses the phase boundary between ice and vapour then the ice will begin to sublime and draw the energy of sublimation from the local environment. Given that the heat transfer between the product and the shelf is limited by the thermal conductivity of the glass vial then one can find that the product temperature begins to drop below that of the shelf temperature. For example, thermocouple temperature measurement data has shown that a reduction in pressure to 0.1mbar, during primary drying, decreases the product temperature by 5−7 ^{o}C with reference to shelf temperature. The actual temperature gradient, in each specific case, is related to the inequality between the rate of consumption of energy (which depends on the rate of mass transfer/sublimation) and the rate of heat supplied (which occurs through the base of the vial and from thermal radiation through the walls of the vial, and depends on the thermal transfer coefficient of the glass container).

Whereas the mass transfer rate is dependent on the difference in partial pressures of water vapour at the ice front and water vapour at the surface of the condenser, the heat transfer rate depends on the temperature gradient that develops between the shelf and the product such that the heat transfer rate will inevitably increase as the temperature gradient develops. As the two rates of energy transfer equalise one ends up with the equilibrium temperature gradient that is sustained during the time that the sublimation rate remains constant.

whereas the latter is dependent on the dry cake layer thickness and porosity which may change as the ice front recedes through the material. Once the ice is removed the rate of sublimation decreases and the product temperature starts to equalise with that of the shelf.

There are additional temperature gradients within the product itself and across the freeze-drier. For example, the temperature measurements obtained from the bottom position (the usual position of the thermocouple in the vial) differs from the temperature values at sublimation front.

Thermal mapping of the freeze drying shelf has also confirmed that spatial heterogeneities exist, unsurprisingly, within the freeze-drier; Higher temperatures were recorded in the samples positioned in close proximity with the chamber door and walls, owing to additional radiation heat transfer, compared to the interior of the shelf (Gan. et al., 2005). The thermal heterogeneities that originate close to chamber door and within the edge vials can be minimized by the use of thermal / radiation shields such as aluminium foils placed on the inner side of the door or by employing empty vials around the sample vials (Rambhatla and Pikal, 2003). The impact of hot and cold spots, identified on the shelf surface of different freeze driers, on the primary drying time revealed that the front vials in the laboratory scale lyophilizer received 1.8 times more heat than the manufacturing scale counterparts operating at shelf temperature −25^{o}C and chamber pressure 150 mTorr (Rambhatla et al., 2006).

During primary drying, the product temperature (measured by thermocouple) must be kept several degrees below its collapse temperature (T_c) to avoid unintended loss in structure of the cake. The temperature difference between product temperature and T_c is often referred to as the safety margin temperature. While one might think, at first, that a high safety margin temperature would be desirable to ensure that the product is far from the edge of failure, one must also recognise that that every 1^{o}C increase in this safety margin temperature leads to ~13% prolongation of the primary drying time (Pikal, 1990). It follows that there is an optimal safety margin which (i) should be neither too high to protract the freeze drying cycles nor too low to endanger product collapse, and (ii) should be maintained throughout the entire cycle (Tang and Pikal, 2004). The difficulty is that the product temperature can seldom be controlled directly during primary drying owing to its dependence upon a variety of parameters, namely shelf temperature, formulation/composition, container system and chamber pressure. However, for practical purposes it has been suggested that the safety margin of 2, 5 and 3^{o}C should be selected respectively, for long (>2 days), short (10 hours) and intermediate duration (10 hours-2days) lyophilisation cycles (Tang and Pikal, 2004).

Once the target product temperature has been defined, it is then possible (at least theoretically) to use this value as a ***process control set point*** to ensure an optimum output from the process. The literature shows that the product temperature can be estimated using a variety of techniques including, thermocouples, resistance thermal detectors; RTD, temperature remote interrogation system; TempRIS and manometric temperature measurements; MTM (Schneid and Gieseler, 2008).

Setting up the chamber pressure

An optimum chamber pressure value is in fact a compromise between low pressure driven high sublimation rate and elevated pressure linked heat transfer rates. Table 2 shows the vapour pressure at the surface of ice.

Table 2 vapour pressure at the ice surface (Oetjen, 2007)

ice crystals to be sublimed Temp	Vapor Pressure	ice crystals to be sublimed Temp	Vapor Pressure
°C	mBar	°C	mBar
0	6.11148	-50	0.03933
-2	5.176893	-52	0.03066
-4	4.374295	-54	0.02387
-6	3.686353	-56	0.0184
-8	3.099737	-58	0.01413
-10	2.598446	-60	0.0108
-12	2.173149	-62	0.00821
-14	1.811846	-64	0.00621
-16	1.506539	-66	0.00468
-18	1.24896	-68	0.00351
-20	1.032446	-70	0.00261
-22	0.850861	-72	0.00193
-24	0.699007	-74	0.00141
-26	0.572485	-76	0.00104
-28	0.467294	-78	0.00076
-30	0.380101	-80	0.00055
-32	0.30824	-82	0.00039
-34	0.249045	-84	0.00028
-36	0.200383	-86	0.0002
-38	0.160786	-88	0.00013
-40	0.128389	-90	9.6E-05
-42	0.102258	-92	6.5E-05
-44	0.08106	-94	4.5E-05
-46	0.063995	-96	3.1E-05
-48	0.050262	-98	0.00002

As a general rule the chamber is set one third of the vapour pressure at ice surface in order to provide an optimum gradient for the ice vapour during primary drying.

Optimal chamber pressure (Pc) can also be calculated from Equation 13.by using the target product temperature (Tp) (Tang and Pikal, 2004).

$$Pc = 0.29 * 10\text{^}(0.019 * Tp) \qquad \text{Equation 13}$$

The units for chamber pressure are Torr and the product temperature is °C.[1]

[1] 1Bar = 750.06 Torr=10^5 Pascal

1.5.4 Secondary drying

The secondary drying phase targets the removal of 'sorbed' (absorbed and/or adsorbed) water which remains unfrozen during the freezing step, and therefore does not sublime. Following primary drying, an amorphous product will contain a reasonable level (about 5-20%) of residual water, which if not removed will have detrimental effect on product stability. In secondary drying, the product temperature is raised above $0^{o}C$ to overcome the physic-chemical interactions between the water molecules and the other components of the formulation. At the same time, the chamber pressure is kept low to facilitate the prompt removal of the released water vapours (Tang and Pikal, 2004).

The secondary drying temperature should be approached at a slower rate in order to avoid product collapse; an event which is more probable for amorphous products. This results from the fact that the high residual moisture content, during the early phase of secondary drying, supresses the glass transition temperature of the amorphous products thereby creating greater potential for collapse. Slow temperature ramps (0.1-0.15 ^{o}C/min) are suggested for these products in order to create time for the moisture to leave the sample, before the product is allowed to heat up to ambient temperature. Such precautions are seldom recommended for crystalline product as they carry little risk of collapse. Rather higher temperature ramp rates (0.3-0.4^{o}C/min) are prescribed for these formulations (Tang and Pikal, 2004).

The studies relating to desorption kinetics depict that the drying rate is highly sensitive to the product temperature, and, vice versa for the chamber pressure. However the drying temperature should in no case exceed the denaturation temperatures, in the case of proteins, or the decomposition temperature, in the case of other thermo-sensitive compounds. The water contents of the product drops at faster rates during the early hours of secondary drying, leading to a plateau level which exceeds the equilibrium water contents calculated from desorption isotherm reflected. This plateau level decreases with the increase in product temperature. The (secondary) drying rates are proportional to the product specific surface at a given temperature (Pikal et al., 1990). At higher solute concentrations (>10%) the dried mass will possess low specific surface and hence requires longer drying time as well as an elevated drying temperature (Tang and Pikal, 2004).

1.6 Freeze-drying process control

The quality by design framework requires identification and control of critical process parameters in order to ensure the critical quality attributes in a product. A brief description of the critical process parameters for freeze drying along with the techniques employed to identify and control is given below:

1.6.1 Off-line formulation characterization for the development of freeze drying cycle

The development of an appropriate formulation and an optimized process cycle for freeze drying of drug products is based on the determination of a set of customized process conditions which take in account the specific temperatures that define the physical state(s) of the drug formulation (Tang and Pikal, 2004). For solutions containing glass-forming solutes, the critical temperature is the glass transition temperature (Tg′), whereas for solutions containing crystallizing solutes, the critical temperature is the eutectic temperature (T_{eu}) (Kett., 2010, Ward and Matejtschuk, 2010). The measurement of these events requires the physical characterization of the solution during freezing and re-heating through a specific temperature range (Her and Nail, 1994).

Freezing of a solution invariably induces the separation of the ice phase from the solute phase; a phenomenon known as freeze concentration or cryo-concentration. For formulations with non-crystallizing solutes, the solution phase is transformed progressively into a viscous liquid, followed by a rubbery mass and then a rigid glass with the continuous decrease in the solution temperature. The transition from rubber to rigid glass corresponds to the solution viscosity changing from 10^{11}-10^{13} Poise to as high as ~10^{14} Poise (Champion et al., 2000).

The high viscosity of the glassy state is a desirable feature of a solution to be freeze-dried, as it provides sufficient strength to support the matrix structure once the ice is sublimed. Temperatures close to this transition (the glass transition temperature or Tg′) are meant to define the upper temperature limit for the mixture during primary drying. Above these temperatures, the solution viscosity is often insufficient for the unfrozen matrix to support its own weight. Invariably this results in the collapse of the product as the temperature is increased further. The temperature, at which collapse occurs, is known as collapse temperature (Tc) and is now routinely assessed through the use of a freeze-drying microscope. Whilst this technology is ideal for that specific purpose it fails to provide any additional

information concerning the structural properties of the glass forming liquid, including the strength of the glass and the concentration of water in the unfrozen fraction.

Heating the solution through the glass transition results in enhanced molecular dynamics (with significant changes in the degrees of freedom associated with vibrational, translational and rotational motions). These degrees of freedom are manifest in changes to the rheological, thermal, electrical and mechanical properties of the solution (Liu et al., 2006). It is interesting to note that the temperature dependence of the molecular relaxation times in the glassy state is Arrhenius; whereas, at temperatures above the glass transition the temperature dependence of the relaxation times conforms to VTF behaviour. The reason for this change in the temperature response is due to the fact that the degree of co-operativity increases as the temperature is increased through T_g.

Off-line techniques for process development

The techniques that are invariably used for the measurement of the glass transition temperature are differential scanning calorimetry (DSC) (Angell, 2002) and electrical impedance measurements (Kilmartin et al., 2000, Ward and Matejtschuk, 2010).

Differential Scanning Calorimetry (DSC)

Despite its widespread application in the materials characterization, there are certain drawbacks with this technique: (i) Tg' is often difficult to characterize for dilute solutions; (ii) Sometimes the glass transition is coupled with a relaxation endotherm and hence the solution has to be cycled through Tg to release this entrapped energy and thereby observe the glass transition more clearly; and (iii) Multiple endothermic discontinuities can be potentially misleading. However the main disadvantage of DSC is that estimates for Tg' may not replicate those experienced by the solution in the process of freeze-drying, owing to the fact that the amount of ice that forms on freezing (and hence the concentration of solute in the unfrozen fraction) is impacted by the inequity in freezing rates associated with the different container geometry and product fill heights, compared with the relatively small volumes used in DSC analysis.

Electrical Resistance

The application of electrical impedance measurements, to characterize the freezing behaviour of solutions, dates back to the 1960s (Rey, 1960). Electrical resistance measurements were used principally in the 1960s whereas studies of the electrical impedance were introduced later because it was observed empirically that it provided much a greater resolution of the physical state of solution of both ionic and non-ionic species (principally as a result of the impact of the electrode polarization impedance). In the majority of cases the solution impedance was measured at a fixed frequency (e.g. 1 kHz) by means of a pair of pin electrodes placed securely in a cryostat measurement cell containing the solution. Changes in the mobility of delocalised charges (ions) in the frozen solution are reflected in the electrical impedance of the sample as the solution is heated through the glass transition temperature. However, given that the electrodes are in direct contact with the frozen solution then this may alter the ice nucleation sites during the freezing stage, which could easily impact the rate of freezing and the amount of ice which forms (Ward and Matejtschuk, 2010). This would in turn impact the concentration of solute in the unfrozen super-cooled liquid phase and hence alter the glass transition temperature experienced by the product.

Freeze drying microscopy

Freeze drying microscopy records the microscopic images of the formulation during simulated freeze drying conditions. For the purpose it includes temperature controlled stage coupled with vacuum pump. The temperature controller precisely maintains the product temperature by means of Liquid Nitrogen and electric heating source while the vacuum pump maintains the low pressure (~50Pa) in the sample compartment. The formulations (one droplet) are frozen under low temperature and then temperature is ramped up slowly under reduced pressure, and photographic images of the product are captured with the digital camera. At low temperature the drying front progresses slowly (from the edges of the droplet to inward direction) with the product initially dried at its periphery, while at higher temperature, the drying front proceeds inward leaving behind the distinct zones of collapsed product. This temperature is termed as collapse temperature and is used to define the product temperature during freeze drying cycle (Meister and Gieseler, 2009, S. Zhai et al., 2003). Similarly this technique has been utilized to observe eutectic melting temperatures in the formulations containing crystalline materials (Ward and Matejtschuk, 2010).

However the results from freeze drying microscopy are adapted with small safety margins due to the fact

- Vial freeze drying has different thermal contact.
- The latter does not evidence sublimation cooling due to thin layer of formulation.
- FDM Does not take into account the convection mechanism of heat transfer.

Nevertheless, the freeze-drying microscopy is designed to measure intrinsic T_c which is adapted to vial freeze drying with some safety margins in terms of temperature and pressure.

1.7 Process analytical technologies (PAT)

ICH defines a process analytical technology as "A system for designing, analysing and controlling the manufacturing through timely measurement (during the process) of critical quality and performance attributes of raw and in-process materials and process with the goal of ensuring final product quality."

Depending upon their utility in the processes, PATs have been classified as

- In-line PAT: involves the measurement of product attributes during the process without removal
- At-line PAT: requires removal of the product from the process stream, analysis for a particular attribute(s) and return to process
- On-line: requires removal of the product from the process stream and may be returned to the process stream (FDA, 2004).

Various process analytical technologies (PAT) have been developed over the years in order to assess the critical stages of the manufacturing process, during the development of the freeze-drying process rather than by assessing the post-manufacture quality of product (Patel et al., 2010). PATs in conjunction with the off-line process development tools are practiced for the development and monitoring and control a freeze drying cycle. A brief description of these tools is included in the section below.

1.7.1 PATs for freeze drying

The currently available PATs, intended for freeze drying, can be divided into two categories namely; single vial measurement tools and batch measurement techniques.

Single vial measurement process analytical technologies

These techniques record critical events in a limited number of selected samples as the process progress. Give an overview of the range and types available viz. Thermocouple, TempRIS, microbalance, heat and mass transfer measurement system, photographic imaging, heat flux transducer, near infrared spectroscopy, and Raman spectroscopy.

Thermocouples

By convention, the sublimation end point is established invariably using the product temperature profiles collected by placing thermocouple or resistance temperature detectors into a limited number test vials. The end point is then defined as the time at which the product temperature reverts back to the shelf temperature. However the estimations based on thermocouple data are not considered to be representative of the entire batch because these devices, on introduction to the product, are considered to provide additional nucleation sites, while providing a further source of heat transfer which collectively can reduce the degree of super-cooling, and in turn produce larger crystal sizes, more rapid sublimation rates and hence shorter primary drying times (Roy ML, 1989). Furthermore these sensors are inserted to the vials in the front row close to the chamber door which show even higher rates of drying, owing to radiation effects, compared to samples positioned in the interior localities of the vial array (Rambhatla and Pikal, 2003). In laboratory scale freeze driers, thermocouple containing vials were reported to exhibit nucleation temperatures 1.4^{o}C higher than the controls. This difference could increase to 10^{o}C in the manufacturing scale lyophilizers (Roy ML, 1989). Thermocouples being invasive are also found to be inappropriate for automatic loading. A soak period or safety margin hold times (about 10-30% of primary drying times estimated from thermocouple containing vials data) have been recommended to ensure the complete primary drying in remaining vials without thermocouples (Tang and Pikal, 2004). These ‘catch-up’ times often vary depending upon thermal coefficients, volume fill depth and crystal morphologies.

Chapter 1

TempRIS device

TempRIS, a recently developed technique, has been shown to record temperature changes efficiently in different areas of the arrays over the entire lyophilisation process. This system, which is often referred to as a wireless temperature remote interrogation system, consists of (i) a number of battery-free wireless sensors that are positioned within individual vials (Figure 14), (ii) a transmitter usually stationed outside the freeze dryer and (iii) software to record the temperature data. The sensors receive energy from the excitation of a passive transponder, using an amplitude modulated electromagnetic signal from the internationally available 2.4 GHz ISM band.

Figure 14 Vial containing temperature sensor for Tempris (Schneid, 2009)

The temperature measurements obtained with this technique using different fill volumes, concentration of the solutes and compositions of the freeze dried materials were in good agreement with thermocouple and manometric temperature measurements (Schneid and Gieseler, 2008). TempRIS offers a number of advantages over the thermocouple, such as compatibility with automatic loading mechanisms and flexibility in its placement in different vials. However, being an invasive technique, there is significant potential for the sensor to bias the freezing process (Rambhatla and Pikal, 2003), to alter the geometry of the product, while requiring a specified orientation of the sensor in the bottom-centre of the vial in order to produce an acceptable output. Therefore it has been stated that the drying profiles displayed by Tempris loaded vials are not representative of the entire batch (Patel and Pikal, 2009).

Chapter 1

Microbalance

The gravimetric methods involving weight measurements of the samples using the vacuum microbalance technique has been intended to evaluate the sublimation kinetics at different drying temperatures and pressure levels (Pikal et al., 1983, Xiang et al., 2004). A modified vacuum microbalance, provided with a holding arm, capable of lifting the test vial (Figure 15) for a short time (10s) and placing it back to shelf, has been rated as appropriate for the gravimetric measurement of primary drying (Roth et al., 2001). The microbalance approach provides a direct measure of the cumulative water loss and momentary drying rate which can assist in the development of the product formulation and the freeze-drying process. Many of the previously discussed relationships between atmospheric determinants and mass transfer rates have been confirmed with this analytical tool.

Figure 15 Microbalance with vial positioned in holding arm (Schneid, 2009)

Studies by Xiang and co-workers (Xiang et al., 2004), using a vacuum microbalance, showed that moderate increases in chamber temperatures had the greatest impact on the sublimation rate, whereas the elevation in chamber pressure (30mTorr to 1000 mTorr) at subzero temperature (-35^{o}C) was shown to suppress sublimation owing to lower pressure gradients between the sublimation front and the bulk space (Xiang et al., 2004). On the contrary, the annealing step was shown by this technique to suppress the sublimation rates which is in general disagreement with previous studies (James A. Searles, 2000). This unexpected behaviour was explained by the dissimilar heat transfer pattern in different freeze drying equipment. The vials loaded onto the shelves of the conventional freeze drier transfer most heat through the conduction between the bottom of the vial and the upper surface of the shelf, yielding a bottom to top crystallization direction. However for the microbalance

measurements it requires the vials to be suspended above the shelf, so that convection and radiation were probably the dominant modes of heat transfer, which in turn would then lead to different crystal morphologies. The annealing step in this set-up was believed to favour the formation of pore geometries which inevitably retard the rate of sublimation (Xiang et al., 2004).

The principal disadvantages are that:

- This technique permits the investigation of only one freeze-drying vial from the whole batch (unless of course multiple microbalances are installed within the freeze-drier)
- The sample volumes/weight is restricted to 50 g.
- There is an impact on the heat transfer pattern in microbalance loaded vials compared to the counterpart in conventional freeze drier shelf which can result in different cake structures in each of the drying stations under observation (Xiang et al., 2004).
- The microbalance loaded vial cannot be positioned within the normal hexagonal arrangement/array in which the rest of the batch is invariably disposed and hence the microbalance vial experiences further non-representative heat transfer profiles.

Although, the modified vacuum microbalance provide shorter lifting time and positioning of vials back to the shelf which provide a drying profile broadly similar to the conventional edge vials, nonetheless 'the edge effect', non-representative arrangement and misleading assumptions relating to scale up remained some of the major drawbacks associated with this technique (Patel and Pikal, 2009).

Heat and Mass transfer measurement system

More recently, a new measurement system has been developed which comprises wireless temperature measurement system (WTMS) coupled with a microbalance. The thermal response of the product is recorded by placing thermocouples linked to a wireless device in the drying chamber which transmit the signals to the data processor through a transmitter coil and data reader. Mass transfer rates are calculated by periodically weighing these samples using a specifically designed balance which lifts up the vials periodically for a short time and place them back for effective heat transfer. A prototype measurement system has been reported to document the temperature range -40^{o}C to +40^{o}C and weight measurement up to 200 ± 0.1g (Vallan, 2007) over the entire process. This system has been shown to measure

thermal responses in the individual samples without requiring communication wires from the drying chamber to data acquisition system. However, thermocouple related perturbation of heat transfer profiles, in conjunction with disturbed sublimation kinetics associated with weighing process, remain the major disadvantages. Nevertheless, this system may be of value for the estimation of heat and mass transfer rates in the lyophilisation process development phase but its utilization in automated processes is yet to be evaluated.

Photographic data

Visual observations of the sublimation front using photographic technique have been incorporated with other measurement approaches to confirm primary drying endpoints. Frequently this technique involves photography of the vials in a time lapse fashion and estimation of the height of sublimation interface from the vial bottom Figure 16. The sublimation rates of pure ice calculated from photographic data were found in good agreement with the simulation profiles predicted through a two dimensional unsteady state axisymmetric model developed for the purpose (Zhai et al., 2005). Although the sublimation kinetics evident from the photographic measurements of the vials at different positions of the shelf confirm the values derived from simulation model, in some cases, the ice sublimation leads to a geometrically undefined mass resulting in miscalculations of the height of sublimation interface. Variations in the sublimation profiles of different products with that of pure ice also render this method of only a limited application.

Photographic observations have also been used to calculate the sublimation rates in lactose and sucrose solutions (5% and 10% w/w) and further correlate the sublimation kinetics with the heat flux from shelf to product (Chen et al., 2008). Sublimation front data has been advocated to address the imperfections in positioning of the thermocouples; the photographic data suggested residual ice even after the temperature elevations evident from thermocouple probe data in cases where the probes were inserted above the bottom centre of the vials. Although this imprecision associated with thermocouples is accommodated in the recommended ‘soak period’ ranging up to 45% of the primary drying time, the economic impact of extended holding of the products at energy consuming conditions necessitate an accurate alternate approach. In spite of the documented benefits, visual observations are least significant in the conditions where the sublimation front loses its planner geometry at the

terminal stage of primary drying. Another drawback of this technique is its inappropriateness for pilot or production scale freeze dryers (Patel and Pikal, 2009).

Figure 16 Photographic image showing sublimation front during primary drying of a sucrose solution (Chen et al., 2008)

Heat Flux transducer

The heat flux transducer, comprising a rectangular array of paired thermocouples, is fixed between the upper surface of the freeze drier shelf and the bottom surface of the vial through adhesive tape of known heat conductivity (in order to ensure appropriate thermal contact) (Chen et al., 2008). The temperature gradients between two surfaces of the sensing device, detected as voltage, provide an estimation of the magnitude and direction of heat flow rates (Patel and Pikal, 2009). Heat flux data reported from the sublimation of lactose and sucrose (5% and 10% w/w) reflected a fairly constant heat transfer rates even when a steep elevation in the product temperature was evident from thermocouple data. However with the depletion of ice in the product as confirmed by visual observation a sharp decrease in heat flux was recorded which may better be regarded as an endpoint of the primary drying step of lyophilisation cycle. Furthermore the sublimation rates calculated though the heat transfer data of the transducer were in general agreement with the same parameter estimated through manometric temperature measurements (MTM) and visual observations (Patel and Pikal, 2009).

Smaller geometric dimensions, minimal thermal inputs, robust appearance and non-invasive measurement of the individual vials make this device an advantageous tool for the estimation of primary drying profiles in various segments of the cluster array.

The limitations associated with the use of these devices include;

- Altered heat flow to the vial; as the device is positioned between the heat flow path between the vial and shelf
- Potentially error prone; particularly if the device does not make an intimate contact between the surfaces is inappropriate and
- Poor adaptability to automatic loading procedures.

Due to the reason this instrument may find some applications in the process development but it utility as a process analytical technique is uncertain.

Near Infrared spectroscopy

Over the recent years, near infrared spectroscopy has gained popularity as online / at-line process control tool for a variety of pharmaceutical procedures, such as blending (Berntsson et al., 2002), granulation (Frake et al., 1997) and film coating (Kirsch and Drennen, 1996). This technique has been used for many years for the off-line determination of moisture content in lyophilized products, given the non-destructive, non-invasive and rapid method of analysis (Kamat et al., 1989). The development of fibre optic reflectance probes for NIR spectroscopy has extended application profile of this tool, to in situ monitoring of lyophilisation process. The Probes are equipped with two fine fibres, each of which is 500 µm in thickness. One acts as source of the IR signal while the other receives the signals after reflection from the glass bottom (Figure 17). These are frequently positioned at the bottom of the sample where the sublimation front reaches at the end of sublimation. The data described a shifting in the absorption peaks at 1450 and 1920 nm to 1490 and 2080 nm respectively during ice formation. The end point of sublimation is characterized by an exponential drop in the intensity of absorption peaks relating to water. Furthermore a good agreement of NIR spectral changes with the product temperature data signifies its validity in monitoring of freeze drying cycle (Brülls et al., 2003) .

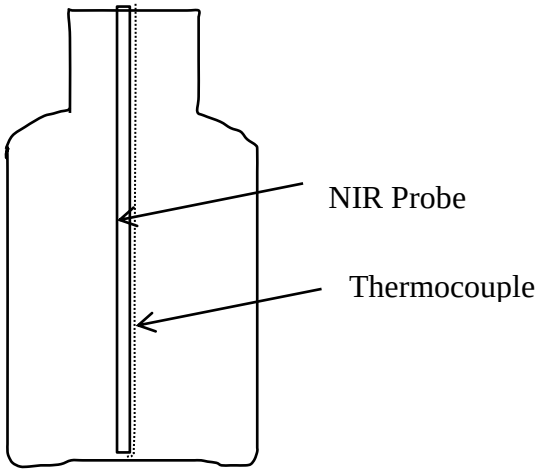

Figure 17 Schematic representation of glass vial with NIR probe (Brülls et al., 2003)

This technique also offers an opportunity to measure residual moisture contents after primary drying as one can compare the IR spectrum during secondary drying with a dried reference. The NIR data remained in agreement with the temperature data during initial phase of secondary drying that is until the product temperature reached the steady state. During secondary drying temperature hold step, the NIR spectra showed steady state water content with a time delay which points to effective desorption period.

The limitations associated with the NIRS technique include invasive mode of analysis, single vial measurement, and altered ice crystallization profiles by providing additional nucleation sites. Although valuable information regarding the essential milestone of the process, such as ice crystallization, endpoint of primary drying and residual moisture contents in the product (Brülls et al., 2003) however, intra vial real time variation in sublimation kinetics were not evident from this technique (De Beer et al., 2009). In addition certain excipients can absorb in spectral regions designated for water thereby carry the potential to affect the quantification of water (Grohganz et al., 2009).

Raman spectroscopy

Raman spectroscopy is based on the principal of light scattering wherein the incident beam of photons with particular wavelength is scattered in-elastically by the target molecules. Under normal irradiation, most of the incident photons are either absorbed or elastically scattered (Rayleigh scatter). The remaining small fraction of radiation is modified owing to coupling between the photon and electron cloud of the molecule. Wavelength-sifts of the scattered light

can be ‘stokes’ (to a longer wavelengths) or ‘anti-stokes’ (to shorter wavelength) (De Beer et al., 2010). A good correlation between the signal intensity and concentration of the material provides the basis for its utilization in product mapping (Ryder et al., 2000). Fibre optic probe assisted Raman spectroscopy has been utilized for the characterization of fluidized bed drying, tablet manufacturing (Hausman et al., 2005) and freeze drying (Romero-Torres et al., 2007). The literature evidences (Romero-Torres et al., 2007, De Beer et al., 2007) suggest that this technique provides valuable information pertaining to the ice crystallization, polymorphism of the excipients and onset of ice sublimation in non-invasive, non-destructive and swift style; however its efficiency in measurement of sublimation rate is obscure due to very weak spectral peaks of the water and ice in the Raman band. Owing to the difficulties related with the installation of Raman spectroscopic probe in the industrial freeze driers, single vial measurement approach (non-representative of the entire batch) and poor description of the drying progression, Raman spectroscopy caries no significant potential as PAT for the freeze drying process (Patel and Pikal, 2009).

LyoRx Lyocontrol-sensor

LyoRx measures electrical resistivity of the formulation within the glass vial by means of two metal pin electrodes contacting the product. A PT100 RTD probe is located between the metal pin electrodes to track the changes in the product temperature Figure 18.

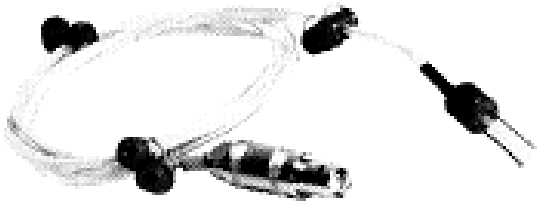

Figure 18 LyoRx lyocontrol sensor

During freezing stage, the electrical resistivity of the formulation increases from 5% to 90% following the phase transition from liquid to frozen solid respectively. Simultaneous temperature measurement characterizes the temperature dependence of the electrical responses of the formulations. This technique resembles to off-line electrical resistance measurement approach as both measures electrical resistivity at a fixed frequency (1 kHz). Due to the reason lyoRx may also find applications in recording the ice formation and eutectic

crystallization, however, due to its invasive nature the probes are expected to provide nucleation sites thereby impacting the onset of these critical events; making the precision somewhat questionable.

The LyoRx sensor is of limited use in recording the sublimation rates and the measurement of drying end points. Since the individual vial is introduced with three probe system, these measurement pins are expected to provide additional path for the vapour flow during primary drying, resulting in drying rates higher than the vial without such perturbations.

Batch measurement tools

The techniques listed under this category are applicable for monitoring the entire batch, and at all levels of scale from the laboratory through to manufacturing operations. However, it is essential to state that the values of process parameters like product temperature, resistance of the dried product and water vapour concentrations that are evident from these tools are determined as a batch average rather than a distribution of individual vial measurements.

Manometric temperature measurement (MTM)

MTM is a procedure intended for the measurement of the product temperature, at sublimation interface, without having to insert temperature sensors into any of the vials (Tang et al., 2006a). This technique involves the pre-installation of a valve between the chamber and condenser of the lyophilizer. Closure of the value, momentarily for a short period of ~ 25 s after each 0.5-1 h during primary drying (Patel et al., 2010) isolates the drying chamber from the condenser causing *the chamber pressure to rise* Figure 19. With the depletion of ice, the pressure rise decreases; suggests the application of this technique in the measurement of end of primary drying. Moreover, the pressure rise time also provide basis for the calculation of product temperature at the sublimation interface.

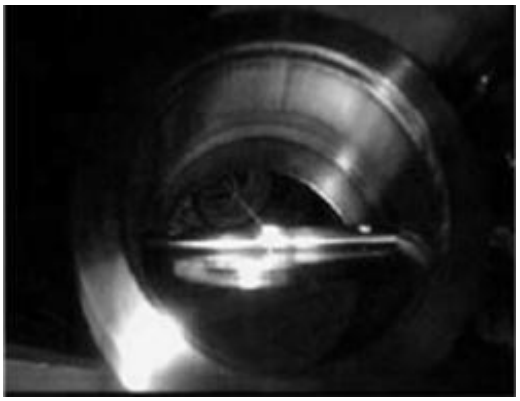

Figure 19 MTM valve for the measurement of pressure rise during primary drying (Schneid, 2009)

The experimental transient pressure rise was found to be in agreement with that estimated from a mathematical algorithm based on the following contributory mechanisms; direct ice sublimation through the dried matrix at constant temperature, temperature elevation at the sublimation front due to diminution of the temperature gradient across frozen layer, and the increase in the ice temperature due to continued heating and pressure leak within the chamber. The mathematical model estimates that the product temperature at the sublimation front should be approximately 2^{o}C lower than thermocouple measured product temperature (Milton N et al., 1997). The principle drawback is that the manometric temperature measurement technique displays only one temperature value for the entire batch and does not take into account the inter-vial heterogeneities in different locations of the shelf, which are evidenced through individual temperature sensing devices. Generally, the product temperature values obtained from the MTM technique are believed to be related with the colder region of the shelf that is non-edge or centre of the array. Moreover this tool has been shown to record the product temperature as low as −45^{o}C during primary drying (Tang et al., 2006a). End point of primary drying is characterized by a sharp drop in vapour pressure of ice. MTM being non-invasive, adaptable to scale up, representing the entire batch has been advocated as an effective PAT (Tang et al., 2006b). Recently ‘Smart’ freeze drier has been designed commercially on the principal of MTM which offers an efficient means to measure and analyse the vapour pressure at sublimation interface and mass transfer resistance, therefore assist in optimization of the freeze drying recipes (Gieseler et al., 2007b, Tang et al., 2005).

MTM lead product temperature measurement has been fairly representative with first 2/3rd of the primary drying time however after this time heterogeneities in the rates of ice sublimation amongst vials located at different position in the shelf are predominant (Gieseler et al., 2007b). Therefore the system lead product temperature after this point of time may be non-representative of the actual product temperature (Gieseler et al., 2007b, Patel and Pikal, 2009). Furthermore the heat transfer rates were misleading when lyophilisation cycles were performed at very low temperatures and low pressure (Tang et al., 2006c) using low solid contents (Tang et al., 2006a). A minimum sublimation area of 150 cm^2 is required for an accurate MTM product temperature measurement. Lyophilisation of the formulations with high amorphous solid contents were measured inaccurately with MTM especially in the early phase of primary drying a high drying temperatures due to re adsorption of vapours in the dried layer due to pressure rise (Patel and Pikal, 2009, Johnson et al., 2009). Lastly, the closure of MTM valve hinders the sublimation process owing to slowed self-cooling which may sequence to collapse if the freeze drying cycle is operated at temperatures close enough to collapse temperature (Patel and Pikal, 2009).

Tuneable diode laser absorption spectroscopy (TDLAS)

Tuneable diode laser absorption spectroscopy (TDLAS) is intended as monitoring and control tool for various processes including freeze drying over the recent years.

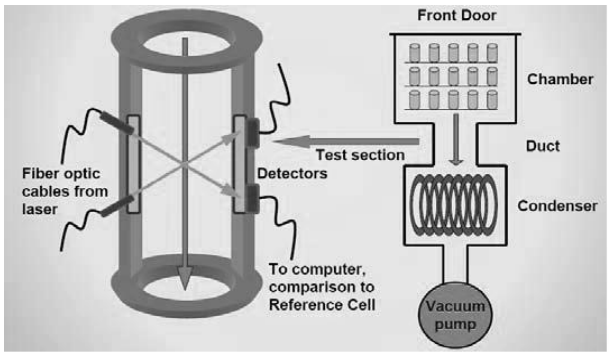

Figure 20 Schematic view of tuneable diode laser absorption spectroscopic probes installed in the spool (Schneid, 2009)

Principally this technique continuously measures trace gas concentrations using the absorption of near infrared laser beam similar to other spectroscopic approaches (Gieseler et al., 2007a). TDLAS sensors are installed in the spool / duct (Figure 20) connecting the freeze drying chamber and the condenser where in the laser beam corresponding to the absorption

frequencies of the target molecules is tuned and transmitted across the area of interest, containing trace gas vapours. The absorption of light as a function of wavelength provides a quantitative estimation of the target vapours (molecules/cm^3) across the passage (Gieseler et al., 2007a) in agreement with the Beer Lambert Law (Patel and Pikal, 2009, Gieseler et al., 2007a). Furthermore, Doppler shift in the wavelengths of the incident beam compared to reference gas sample with zero velocity reveals the gas flow velocity (u), which on multiplication with density of the vapours (ρ) and area of the duct (A) yields the sublimation rate (dm/dt) Equation 14 (Patel and Pikal, 2009, Gieseler et al., 2007a).

$$\frac{dm}{dt} = u * \rho * A \qquad \text{Equation 14}$$

Owing to its promising capabilities regarding accurate measurement of critical process parameters like vapour concentration, gas velocity and sublimation rates TDLAS offers a great potential for the determination of end point of primary drying step of lyophilisation cycle. A sharp drop in water vapour concentration serves as a bench mark for the endpoint of primary drying (Patel and Pikal, 2009). The onset in drop of vapour pressure signifies about 40% of the residual moisture in the amorphous product (Patel and Pikal, 2009) conversely, midpoint of the slope referring to drop in vapour pressure entails only 10% of the moisture contents in both amorphous and crystalline products (Patel et al., 2010); the latter provides a more reliable determinant of sublimation endpoint (Patel and Pikal, 2009).

Recently, vial heat transfer coefficients across the different positions of the shelf; calculated using an algorithm which gathers inputs from TDLAS data, have been found to be in good agreement with the traditional gravimetric approaches. Similarly, TDLAS has been used to predict the product temperatures in various localities of the shelf at varying sample loads, from partial to full loading of the shelf. The temperature data measured by TDLAS during the steady state was in (1-2^oC) agreement with thermocouple data for the ‘centre vials’(Schneid et al., 2009) (Kuu et al., 2010) reported another utility of TDLAS regarding the calculation of the product mass transfer resistance during freeze drying, thereby providing a diverse characterisation over the propagation of complex drying process.

A wide range of advantages linked to TDLAS are non-invasive batch measurement approach, accurate prediction of process parameters like water vapour concentration, gas flow rate, heat transfer coefficients, sublimation rate, product temperature, and quantification of edge vial

(Gieseler et al., 2007a, Schneid et al., 2009, Kuu et al., 2010) effect promise is application as effective PAT for freeze drying process. LyoFlux^{TM} technology, based on the TDLAS principal has been developed to obtain the aforementioned benefits. However this technique is applicable to the freeze driers with sufficient length of spool that ensure absorption measurements at an angle to the gas flow velocity vector (Gieseler et al., 2007a). Vapour flow dynamics varies significantly in equipments having different length to diameter ratios of the spool (Patel and Pikal, 2009).

Cold Plasma ionization device

The cold plasma ionization device has been developed for in-situ measurement of moisture content in the lyophilisation chamber. This technique is based on the principal of inductive coupled plasma/optical emission spectroscopy. The device comprises a quartz tube that directly contacts the lyophilisation chamber and a low power radio frequency source which ionizes the gas in the quartz tube thereby generating plasma. The light emitted by the plasma is collected through an optical fibre and is diffracted by optical spectrometer. The analysis of spectra is performed with plasma sensor software which relates the radiation wavelength to the gas component; with the humidity levels in the camber being displayed in real time (Mayeresse et al., 2007). The drying rates evident from plasma ionization device were successfully calibrated with the microbalance technique. This technique offers the advantages of robustness, ability to withstand the sterilization stress and effectiveness at scale up from laboratory to pilot scale freeze drier. However a slight modification in the signal was reported when installed in industrial level freeze drier. This may suggest altered vapour flow kinetics in scale up. At present Lyotrack, a PAT, based on this principle, has been marketed by Adixen for measurement and control of moisture content during the freeze drying process.

Heterogeneities in the signal response were also recorded as the position of the device was changed from the drying chamber to spool; the duct connecting the drying chamber to condenser. Former evidenced higher response than the latter (Mayeresse et al., 2007).

The device placed in the drying chamber measured sublimation time longer than that in the spool. Nevertheless, formation of free radicals ensuing from ionization of the chamber gas carries a potential risk of product instability during and following the freeze drying. The probability of such consequences remains high with the freeze driers installed with ionization device within the drying chamber.

The signal quality was also responsive to the chamber pressure. As long as the chamber pressure was regulated by nitrogen injection, the gas contents changed sensitively, therefore the plasma response may be affected in the freeze dryers where chamber pressure is regulated by alternate methods.

Furthermore, the calibration of the device in a manufacturing scale freeze drier requires complex equipment that yield vapour-saturated chamber under vacuum which adds cost and skill. The chamber gas profile measured by cold plasma ionization device assimilates that provided by Pirani pressure gauge data, therefore it offers no further advantages over the latter, yet carries higher cost (Patel and Pikal, 2009).

Pirani pressure gauge

Principally, the Pirani gauge measures thermal conductivity of the gas present in the freeze drying compartment as an indicator of chamber pressure. This in turn explains the concentration to the water vapours in the chamber and determines sublimation kinetics.

It comprises two platinum filaments (of low thermal emissivity 0.03-0.1), one of which is present in the gauge tube which opens out to the drying chamber while the second one is fixed into a reference tube containing a reference gas, nitrogen (Figure 21). It has been assumed that heat transfer from the platinum wire under this condition is primarily affected through conduction rather than radiation (Patel and Pikal, 2009). Small elevations in chamber pressure under vacuum increase effective collisions of the gas molecules with the filament resulting in its heating which thereby drops the resistance this change in the current flow in comparison with the reference provide the basis for chamber pressure measurement. The Pirani gauge works satisfactorily at chamber pressures of 10^{3}-10^{-4} mBar.

The reliable application of the Pirani gauge in the calculation of freeze drying chamber pressure requires further manipulations to avoid inaccuracies. Higher thermal conductivity of the water vapour in the gauge tube as compared to the counterpart in reference tube, i.e. pure nitrogen (thermal conductivity of water vapour ~1.6 times higher than nitrogen (Patel et al., 2010) necessitate further calculations to accurately predict the gas contents (Hottot et al., 2009). Due to the fact, Pirani gauge reads chamber pressure 60 % higher than the capacitance manometer during primary drying when all of the chamber gas is essentially water vapour. Furthermore the end point of primary drying is identified by the Pirani pressure gauge as a

sharp decrease (onset) in the pressure readings. Some of the key advantages linked with Pirani gauge include; low cost, ability to withstand steam sterilization and easy installation without modification to existing dryer (Patel et al., 2010).

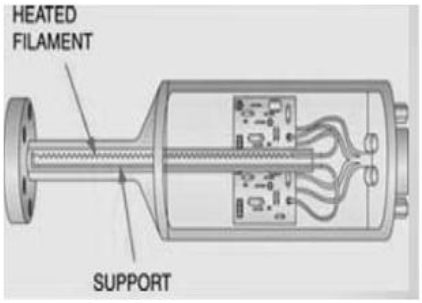

Figure 21 Pirani pressure gauge with heated filament which contact gas molecules from the drying chamber (Lesker, 1996)

However there are several limitations which preclude this device as an ideal PAT. The emissivity of the platinum filament increases upon continuous use owing to oxidation leading to a significant heat transfer via radiation thereby misleading output. At the end of sublimation step, gas composition is changed from water vapour to nitrogen; the energy exchange rates are shifted to lower levels which display inaccurate pressure measurements (Patel and Pikal, 2009).

Micro-Pirani gauges are the recent advancement in the Pirani gauges having single wire (Pt, Ni) for pressure sensing. The two ends of the metal wire are bonded to a pad of ceramic structure with a cavity for micro system to furnish the electric circuit which can effectively sense the chamber pressure from 1 Pa to 100 Pa (Yunsong et al., 2009).

Capacitance manometer

The capacitance sensor measures the change in electric capacitance ensuing from the movement of the sensing diaphragm in relation with the fixed capacitance electrodes. It comprises of a chamber partitioned through a tensioned inconel diaphragm which separate reference cavity having standard vacuum ($<10^{-7}$ Torr), equipped with capacitance electrodes from the measurement compartment with unknown pressure (Figure 22). As the vacuum pressure exceeds from the reference cavity it simply pull the diaphragm away from the capacitance electrode resulting in a change in the output of voltage applied. Unlike Pirani gauge sensors, capacitance manometer directly measures the chamber pressure without taking

in account its gas composition. This device has been shown to measure a wide range of chamber pressure (0-760 Torr) with an acceptable accuracy (±1 mTorr). Another feature of withstanding steam sterilization conditions renders it a method of choice for freeze drying chamber pressure control (Patel and Pikal, 2009). Frequently, the Pirani is used in combination with the capacitance manometer to make a reliable measurement of the primary drying endpoint.

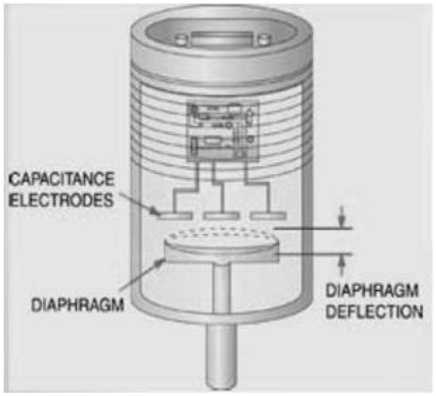

Figure 22 Capacitance manometer showing diaphragm deflection in response to chamber pressure (Lesker, 1996)

Dew point

This electronic moisture sensor measures partial pressure of water vapours in the freeze drying chamber which is utilized for the estimation of saturation temperature (dew point) and sublimation end points (Zhou et al., 2009, Roy and Pikal, 1989). Water vapour adsorption mediated changes in the capacitance of thin Alumina film provide the basis for an accurate estimation of moisture content in the chamber (Genin et al., 1996). The measured capacitance is later translated to voltage which depicts dew point or partial vapour pressure (Roy and Pikal, 1989). The end point of primary drying is characterized by 'onset of drop in the dew point curve'(Patel et al., 2010). Although suited for batch measurement, it can also operate in satisfactory fashion at partial loads (as low as 0.3 % with residual ice). The sensitivity of electronic moisture sensor was consistent with the weighing method (Zhou et al., 2009). In comparison with Pirani gauge, moisture sensor has been rated as more sensitive tool for the determination of primary and secondary drying end point at full loads (Bardat et al., 1993). Moreover it allows an easy scale up in the industrial freeze driers.

Nonetheless moisture sensors available at present cannot withstand steam sterilization. This situation has been successfully addressed by the development of a sterilizing filter and a valve which separates the sensor from the drying chamber of clinical-scale freeze drier during sterilization (Patel and Pikal, 2009).

Residual Gas Analyzer

The residual gas analyzer comprises of a quadrupole mass spectrometer which after installation in the vacuum line connecting the freeze drying chamber and condenser effectively sorts the ionic entities of residual gas molecules based on their mass to charge ratios, thereby enumerate water vapour contents of the drying chamber over entire cycle (Patel and Pikal, 2009, Michael Wiggenhorn, 2005). The end point of sublimation is characterized by a sharp decline in the water vapour contents of the chamber (Connelly and Welch, 1993) which essentially equates the Pirani pressure gauge measurements (Patel and Pikal, 2009). Residual gas analysis profiles were also significantly sensitive to desorption phase of the lyophilisation cycle. Elevated shelf temperatures of the secondary drying lead a second water vapour peak, relating to diffusion of water vapours from the dry cake, which subsets to baseline with moisture contents 1-2%. This practically refers to the end point of freeze drying cycle (Michael Wiggenhorn, 2005). Pikal et al suggested that the establishment of the calibration curves relating partial pressure of the water vapours in the chamber to residual water, over the entire drying cycle, for each of the candidate formulation potentially promises the end points of both primary and secondary drying phases (Patel and Pikal, 2009).

Soft sensors (Observers)

Numerous observers based on fundamental mass and energy balance equations have been proposed to predict the real time modelling and optimization of the freeze drying process (Edinara Adelaide Boss, 2004). The improvements in the development of these simulation models were made in parallel with the understanding of the process dynamics. Some of the key considerations are needed for the design of an observer include: product temperature, shelf temperature, chamber pressure, heat transfer coefficient between shelf and bottom of the glass vial, evolution of sublimation interface and mass diffusivity of the dried matrix (Velardi et al., 2010, Edinara Adelaide Boss, 2004). The incorporation of these input variables to the designed algorithms result in transport coefficient for process control and optimization. Fissore et al described a sensor that predicts optimum chamber pressure relating to a

particular shelf temperature that ensures minimum drying time. Moreover, a varying temperature scheme is predicted by the soft sensor that ensure maximum allowable product temperature hence a shorter primary drying (Fissore et al., 2008).

Dynamic process estimation (DPE) approach permits collection of the parameter without a probe. DPE based software furnish optimal shelf temperature values ensuring the shortest primary drying time (Barresi. et al., 2009, Pisano et al., 2010). Another observer termed as High Gain (HG) observer capable of estimating the product temperature along with the position of moving sublimation front over the entire primary drying. This sensor also successfully estimates heat and mass transfer coefficients in a relative swift mode owing to fewer input parameters and shorter algorithm as compared to kalman filter (Salvatore A. Velardi, 2009), a previously documented sensor which operate DPE with longer algorithms. However its sensitivity to predict the position of sublimation front is rather obscure especially with noisy signals of input parameters (Velardi et al., 2010).

Strategies for the use of PAT in freeze drying

In defining a strategy for the use of PAT in freeze-drying process development, it is first necessary to recognise that freeze drying is not a single process but rather a combination of multi-event processes, each with a range of onset times/temperatures and durations which are dependent on number of process parameters. These process parameters include the shelf temperature, the partial pressure in the chamber, the characteristics of the container (wall thickness and base profile) and the location and packing of the containers within the freeze-drier. It therefore seems appropriate to consider a combination of sensors, each with its own suitability for any particular stage of the process. Full and detailed assessment of the variations in critical process parameters across each batch might then allow for the design of an efficient cycle which accommodates the variability in individual product processing times while minimizing the overall cycle time. Ideally, the PAT should continuously measure the critical process and product parameters of all containers to ensure a strict compliance within the control space. However, in freeze-drying this is considered to be highly impractical owing to restricted access to individual vials (which are invariably clustered in high numbers across multiple shelves within a large chamber) and high risk to the product quality. Nonetheless, acceptable product attributes can be achieved through minimal invasion of the process. One could imagine a scenario whereby spot measurements on individual vials at critical positions within the drier may be used to define set points (e.g. temperatures) and capture end points

(e.g. end of primary drying) and would be sufficient in defining a well-controlled process. However, the same issues of restricted access and a required a prior knowledge of these critical positions makes this untenable.

The development of a rational (structured) approach is imperative for the effective implementation of process monitoring and/or control technologies. The primary objectives for the application of PAT vary from screening of the excipients and product/process characterization at the product development stage to reproducibility and determination of end of primary drying at production scale.

The formulation and process development phase requires in-line measurements of the individual products in order to establish process / product components profiles at different spatial configurations and processing conditions. Although the PATs intended for the measurement of individual vials (thermal sensors, microbalance) do not comply with GMP requirements (given that they perturb different stages of the freeze drying cycle, they do not withstand sterilization and do not provide process feedback) their application in the thermal mapping of the shelf, inter vial and intra vial variations in the drying rates are some of the valuable information that can be advantageous in the process control. A brief comparison of these techniques is shown in Table 3.

Table 3 Comparison of the process analytical techniques for Individual vial measurement

	Thermocouple	**Tempris**	**Microbalance**	**NIRS**	**Heat flux transducer**	**Photographic imaging**
Measurement Approach	Thermo	Thermo	Gravi	Spectroscop	Thermometric	visual
Ice Nucleation	yes	yes	no	yes	no	yes
Freezing progression	yes	yes	no	yes	no	no
Critical temp for PD	no	no	no	no	no	no
End of sublimation	yes	yes	yes	yes	yes	Potentially Misleading
Desorption	-	-	-	yes	-	no
Feedback	no	no	no	no	no	no
Shelf mapping	yes	yes	no	no	-	no
Sterilization	yes	-	-	no	-no	yes
Support Automation	no	yes	no	no	-	yes
Product invasive	yes	yes	no	yes	no	no
Impact on the process	high	high	medium	medium	medium	no
cost	low	$>10^4$	10^4	$>10^4$	$>10^4$	10^3

The end of primary drying, as measured by NIRS and temperature measurement probes, depends upon their position in the vial; the time at which the sublimation interface recedes through the sensing region of the probe is taken as end of sublimation. Moreover inadequate information on sublimation rates is obtained through these single point individual vial measurement techniques.

Techniques that enable the shelf temperature to be mapped, either indirectly or directly, require multiple point measurements, in which each measurement point is invariably associated with an individual vial. Only those technologies that permit simultaneous measurement on multiple vials have any remote possibility to determine the spatial map of temperature across the shelf. The exceptions are the microbalance technique, and optical measurements such as NIR and Raman, which by virtue of the size of sensing element do not allow for measurements on clusters of vials that are representative of the manufacturing process.

Technologies that are considered to be product invasive are those in which the sensing element is immersed directly within the substance being freeze-dried. This is not to say that only such technologies have an impact on the process rather some other techniques for instance heat flux transducer also bear some impact on the process. Moreover the microbalance operation associated lifting of the sample carries potential to affect sublimation profile and hence feedback profile.

Application of different PATs which complement each other, for example microbalance, for the development of a freeze drying cycle will enable formulation scientist to determine end of sublimation, heterogeneities in the sublimation rates arising from product (product fill volume, and container-closure system) and process variables (position in the shelve, cooling rates, chamber pressure and shelf temperatures).

The stringent GMP requirements restrict process analytical technologies intended for the measurement of full batches to be non-invasive, withstand sterilization, no impact on the process and reproducible. Therefore the PATs are either positioned in the duct connecting the condenser and the drying chamber or in proximity with the condenser. The technologies (Pirani, Dew point analyzer and residual gas analyzer) which cannot withstand sterilization

conditions often requires an aperture which isolates the PAT from drying chamber to permit asepsis of the chamber. Moreover the PAT associated changes in chamber gas composition reported with MTM, Cold plasma ionization mass spectrometry interrupts both the process and the product.

Given the large scale of manufacturing freeze-driers, one might imagine that an effective process control strategy is more likely to be assured if single vial measurements are coupled to an appropriate batch measurement technology. It is therefore not surprising to see industry controlling the freeze-drying process through a combination of Tempris sensor within individual vials, coupled to MTM measurements.

1.8 GAP in the knowledge/summary

It follows from the literature that the batch measurement techniques provide 'average measurements' from the entire fill load and are of little value in recording the actual vials formulations located at different positions on the shelf. Although this issue is addressed in part by the single vial measurement techniques, these systems are also attributed to product invasion by the measurement probe, modified ice structure, perturbed heat flow, probes inaccessible to vials in the core of hexagonal arrays (thermocouple) and/or the technologies do not permit hexagonal arrangement of the vials on the shelf (freeze drying microbalance).

Although, the existing process analytical technologies provide useful formation of the primary drying profile. However, these are of limited value in pre-characterization of the formulation. For the purpose, one has to rely largely on the off-line formulation characterization techniques for the measurement of glass transition temperature (T_g'), eutectic temperature (T_{eu}) and collapse temperature (T_c). The critical temperatures measured by off-line techniques may not represent the actual vial conditions as the latter differs in terms of container geometry, fill depth, thermal co-efficient and heating rates. In practice, these off-line critical temperature measurements are employed in the development of freeze drying cycles with some safety limits which result in suboptimal drying profiles.

It is also true that annealing mechanisms are poorly explained with the current in-line tools. The impact of annealing is often studied retrospectively either by microscopic investigation of the freeze dried matrix or by mass transfer resistance during the primary drying. In both cases, optimization of the ice structure remains the subject of trial and error which requires

multiple experimental runs and seldom provides information regarding the growth of ice crystals or changes in the fragility of the glassy matrix during the annealing phase of a freeze drying cycle.

Changes in the electrical impedance of the frozen solutions are expected to provide real-time information as to whether the ice structure is optimally conditioned to progress through the primary drying. Current in-vial impedance measurement systems employ an electrode system, placed internal to the vial, which comprises two straight pins necessarily requires a rather bulky adapter (to maintain the parallel geometry of the pins) which can only be located over the neck of the vial, and therefore inevitably impedes the efflux of vapours during primary drying; making this technology inappropriate for the study of primary drying. The impedance measured by the internal electrodes is significantly impacted by the contributions from the cables which vary with the position on or above the shelf.

Chapter 2

2 Aim

The present work aims to study the application of impedance spectroscopy as a minimally-invasive process analytical technology for freeze drying. “Through-vial impedance spectroscopy” was employed to investigate changes in electrical impedance of the product during different stages of the lyophilization process, in particular for the study of (i) ice formation, eutectic crystallization and glass transition during freezing and re-heating step, (ii) sublimation rates and primary drying endpoint during the primary drying and (iii) the impact of annealing hold time and temperatures on the primary drying profiles.

Chapter 2

2.1 Objectives

Objective I

The first objective was to provide a brief description of theoretical aspect of impedance spectroscopy and an overview of the through vial impedance measurement system in order to provide an insight to the technology. A brief description of the impedance response from the vial and the methodologies applied to characterize the impedance spectrum are also included.

Objective II

To demonstrate the use of through vial impedance spectroscopy in the characterization of the freezing stage of lyophilisation process and to establish the universality of the measurement by fixed electrode system for different fill volumes. For this purpose the impedance profiles from a 3% w/v solution of sucrose were investigated to identify the different stages of freezing process; the onset of ice formation, progression of ice formation and equilibration with the shelf. Freezing profiles were also recorded at different fill height in relation to electrode dimension in order to define the general application of fixed electrode geometries.

Objective III

Third objective was to characterize the eutectic crystallization of the solute in a solution of mannitol during freezing step by using through-vial impedance spectroscopy. The changes in the crystallization profile with respect to the initial concentration of the solute were also explained. The impact of added non-crystallizing solute (sucrose) was also studied on the crystallization of mannitol.

Objective IV

To measure the glass to liquid transition of a surrogate formulation comprising 10% w/v maltodextrin, during shelf freezing in the glass tubing vials by using through vial impedance spectroscopy. The non-linearity in the impedance response (f_{peak} and R) during the glass transition was also characterized by Vogel-Fulcher-Tammann equation to determine the fragility of the frozen glassy matrix.

Chapter 2

Objective V

To develop a methodology to determine the primary drying end point from the impedance profile. For this purpose, the different features of the interfacial relaxation process (f_{peak}, C''_{peak}, C''_{1kHz}) were employed to provide an insight into the changes in the frozen matrix following the application of vacuum.

Objective VI

To explore the mechanistic basis of annealing which result in reduced primary drying times of maltodextrin 10% w/v solution using impedance spectroscopy. The changes R and C values were employed to (i) explain the changes in the ice structure and (ii) differentiate between two possible mechanisms, i.e. devitrification and/or recrystallization during the annealing. An application of through-vial impedance spectroscopy to optimize the annealing step was also investigated.

3 Rationale for the selection of excipients

The disaccharide sugars including sucrose, lactose and trehalose were selected for the study of freezing and primary drying stages of freeze-drying process. These compounds, having empirical formula $C_{12}H_{22}O_{11}$, are frequently included in the lyophilised formulations as bulking agents and /or lyoprotectants (Wang, 2000, Liao et al., 2007). Although they possess collapse temperatures within a narrow range of-27 °C to -31 °C, their freeze drying behaviour varies; lactose solution can form a skin during freezing which results in slow drying rate during the stage of primary drying. The application of impedance measurement system in the characterization of freezing stage of the lyophilization process will describe the versatility of this minimally invasive process analytical technique to study different formulations.

Mannitol is used in formulations as bulking agent and a potential lyoprotectants depending upon the product cooling rates and its concentration in the formulation. Following fast freezing rate the mannitol remains amorphous which provides lyoprotectant effect, in contrast, with slow cooling rates or annealing at -20 °C , mannitol crystallize to elegant cake structure after the ice sublimation. The former requires no crystallization while the latter necessitates predominant crystallization of the excipient i.e mannitol (Liao et al., 2007, Meyer et al., 2009). The freezing profiles of mannitol solution were investigated to register the application of impedance spectroscopy in the formulations.

Maltodextrins are partially hydrolysed starches prepared by acid and/or enzyme hydrolysis of the substrates, comprising monosaccharides, disaccharide and oligosaccharides. These are included in the pharmaceutical formulations for a variety of roles including the study of glass transition, stabiliser and viscosity modifier. The rationale for the use of maltodextrin as a model formulation includes (i) its previous application as a lyoprotectant in protein freeze drying, (ii) previous measurements of the glass transition process (Corveleyn and Remon, 1996, Elnaggar et al., 2010) and (iii) the fact that the glass transition of the DE16-19.5 grade (T_g = -17 °C) is midway in the temperature range achievable for the freeze-drier used for this study (0 to -35 °C).

A list of excipients used in the present study is described in Table 4

Table 4 Summary of excipient used

No.	Material	Study	Section
1	Sucrose	Freezing, Primary drying	5, 8
2	Mannitol	Eutectic crystallization	6
3	Maltodextrin DE 16-19.5	Glass transition, Mechanism of annealing	7,9

Chapter 4

4 An Overview of Impedance spectroscopy

4.1 Objectives

This section provides an overview of the theory of impedance spectroscopy followed by a brief description of the through-vial impedance measurement system. A brief description the interfacial polarization peak, impedance response, arising from the interfacial polarization of the glass wall-solution interface and methodologies applied to characterize the impedance spectrum is also outlined.

4.2 Impedance Spectroscopy

Impedance spectroscopy (IS) concerns the response of a material to an applied electric field. The response may range from the delocalised charge phenomenon of ionic conduction, through localised space charge polarization (e.g. interfacial polarization of the boundaries between two phases) to true dielectric phenomenon such as dipole re-orientation. The majority of applications for IS are for the analysis of materials in which ionic conduction predominates (e.g. solid and liquid electrolytes), for example in the study of fuel cells, rechargeable batteries, and corrosion. There are fewer, but equally important, applications for impedance spectroscopy in the study of dielectric materials (i.e. solid or liquid non-conductors whose electrical characteristics involve dipolar rotation, e.g. glasses and polymers) and for those materials whose mechanism of conduction is predominantly electronic (e.g. single-crystal or amorphous semiconductors) (Macdonald. and Johnson, 2005). Invariably the term dielectric spectroscopy is adopted in preference to IS for the latter types of materials, as the main focus for investigation is the thermally damped relaxation of molecular dipoles. However, many materials do not fall into one category or another, and so IS often finds uses in more complex situations, such as a partly conducting dielectric material with some ionic conductivity. Pharmaceutical materials are a good example of this latter type of material, with even the driest of materials (e.g. powders and granules) exhibiting protonic conduction processes which percolate through the hydration surface of a powder (Suherman and Smith, 2003, Petrovsky et al., 2012), whilst displaying pronounced dielectric relaxation phenomena associated with dipole reorientation (Ermolina and Smith, 2011). Despite numerous scientific studies on a wide range of material types, the application for IS for industrial process control

is much less prevalent, with the most well-known being the monitoring of the fermentation process in the brewing industry (Soley et al., 2005, Olmi et al., 2007).

4.2.1 Impedance

The term impedance refers to the opposition to the flow of electrons or the current. In direct current this effect is rendered by the resistor. However in alternate current other circuit elements capacitor and inductor also obstruct the current flow. The impedance is a vector quantity, expressed as complex number, consisting of real component related to resistance while the imaginary component is evident from capacitance and inductor. The total impedance in the circuit is a combined effect of the circuit elements including resistor, capacitor and inductor. The impedance like resistance is measured in ohm (Ω).

For circuit element in series

$$Z_{total} = Z_1 + Z_2 \qquad \text{Equation 15}$$

It may be worth saying that the real components of the elements in series combination are added together and the vice versa.

$$Z_{total} = Z'_{total} + Z''_{total} = (Z'_1 + Z'_2) + (Z''_1 + Z''_2) \qquad \text{Equation 16}$$

For circuit elements in parallel, the admittance values (inverse of impedance) are added to obtain the total obstruction in the current flow (Instruments, 2010).

$$\frac{1}{Z_{total}} = \frac{1}{z'} + \frac{1}{z''} \qquad \text{Equation 17}$$

The impedance contributions from the circuit elements resistor, capacitor and inductor are termed as resistance, capacitive reactance and the inductive reactance. The impedance of a resistor lacks imaginary component while the reactance is devoid of real components (Macdonald. and Johnson, 2005).

4.2.2 Resistance

The impedance of a resistor lacks the imaginary components. Both the current and the voltage propagate in same phase; no phase shift is observed with the resistors. Both the

current and the impedance are independent of the frequency. Impedance of a resistor is expressed by the following equation

$$Z = R + 0i \qquad \text{Equation 18}$$

4.2.3 Capacitive reactance

The opposition in the flow or AC current (impedance) contributed from the capacitor is termed as capacitive reactance (X_c). The measurement of the reactance is made by the expression

$$X_c = -i/2\pi fC \qquad \text{Equation 19}$$

Where f is the frequency of the electrical signal passing through the signal and C is the capacitance. For a capacitor element, the reactance will be high at low frequency values and vice versa. The capacitive reactance causes a phase shift between the current and voltage.

4.2.4 Inductive reactance

In contrast the inductive reactance (X_L), the perturbation in current flow due to inductor, is calculated by the expression

$$X_L = +i2\pi fL \qquad \text{Equation 20}$$

Where X_L is inductive reactance, f is the frequency in Hz and L is inductance in Henry. X_L is small at low frequencies and large at higher frequencies. The total reactance of the circuit is calculated as the difference between inductive capacitance and the capacitive reactance.

$$X = X_L - X_C \qquad \text{Equation 21}$$

The resistance and the reactance cannot be added simply to give the resultant impedance, rather a vector sum of the resistance and reactance at 90 degrees to the former yields an effective representation of total impedance (Research, Macdonald. and Johnson, 2005, Hewes, 2011).

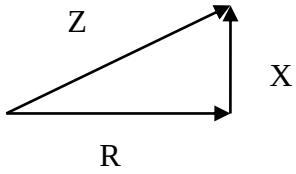

Figure 23 Direction of Impedance parameters

$$Z = \sqrt{R^2 + X^2} \qquad \text{Equation 22}$$

4.2.5 Capacitance

Capacitance (C), another determinant of dielectric responses of the materials, measures the amount of charge (Q) stored onto the capacitor plates over an applied voltage (V). The capacitance can be considered as a proportionality constant between the charge and voltage from the coulombs law (Craig, 2005).

$$Q = CV \qquad \text{Equation 23}$$

$$C = Q/V \qquad \text{Equation 24}$$

The charge storage capacity is in turn dependent on the geometric configuration of the capacitor namely the area (A) of the plates that directly overlap and distance (D) between the plates. This relationship between the capacitance and the geometric dimensions is expressed by following equation

$$C \propto A/d \qquad \text{Equation 25}$$

$$C = \varepsilon A/d \qquad \text{Equation 26}$$

The capacitance of a capacitor (air filled parallel plate capacitor) in response to DC current is calculated from the following expression

$$C_o = \varepsilon_0 A/d \qquad \text{Equation 27}$$

The capacitance of the parallel plate capacitor increases following the introduction of dielectric material into the capacitor plates. Dielectrics act by neutralizing the charges at the

electrode which would contribute to the external field. The resultant capacitance is calculated by the formula

$$C = \varepsilon'_{r}.C_{o} \quad \text{Equation 28}$$

$$\varepsilon'_{r} = \varepsilon'/\varepsilon'_{o} \quad \text{Equation 29}$$

The capacitor response to an AC voltage can be effectively expressed by its capacitance and the impedance, capacitive reactance (Craig, 2005).

4.2.6 Charging of a capacitor

The charging of the capacitor in a circuit comprising of resistor and capacitor in series is accomplished through a supply voltage V_s with the current passing through the resistor (Hewes, 2011). Initially the voltage across the capacitor V_c is zero but it approaches to V_s as the capacitor is fully charged. The charging current (I) is determined by voltage across the resistor (V_s-V_c).

$$I = (V_s - V_c)/R \quad \text{Equation 30}$$

The value of V_c follows the course; V_c=0→V_s

As the charge at the capacitor is accumulated, Vc is increased, as a consequence the voltage across the resistor is reduced and therefore the charging current is decreased. This means that the rate of charging becomes progressively slower. The rate of charging of the capacitor is measured in terms of time constant or Tau (τ).

$$\text{Time constant } (\tau) = R * C \quad \text{Equation 31}$$

Where τ is time constant in seconds, R is resistance in Ohm and C capacitance in Farads. A large time constant reflects slow charging of the capacitor.

The time constant is the time taken for the charging (or discharging) current (I) to fall to $^{1}/e$ of its initial value (Io).

$$\text{Time constant } (\tau) = I_o e^{-1} \quad \text{Equation 32}$$

Where 'e' is the base of natural logarithms, e = 2.71828. After each time constant the current falls by $^{1}/e$ (about $^{1}/_{3}$). After 5 time constants (5RC) the current has fallen to less than 1% of its initial value (Hewes, 2011).

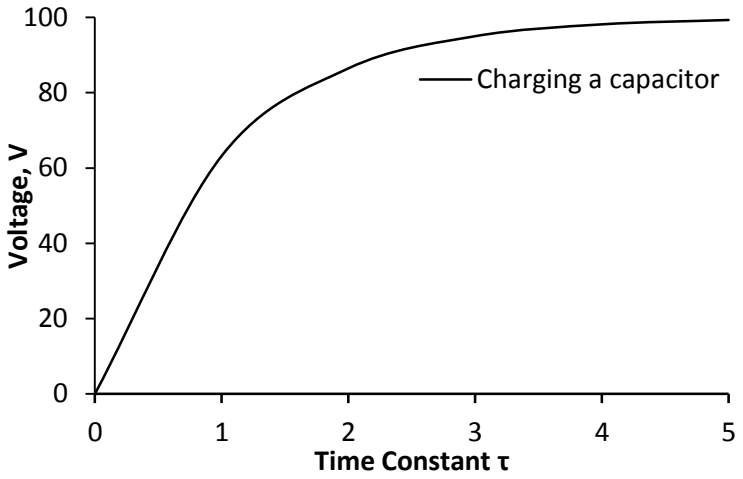

Figure 24 charging of a capacitor

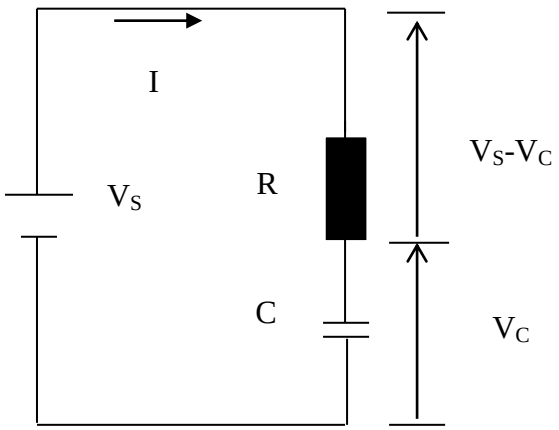

Figure 25 Equivalent circuit comprising of resistor and capacitor (Hewes, 2011)

Subsequently the pharmaceutical materials are modelled as combination of the capacitor and resistor. The time constant of the capacitors (dielectric materials) changes as the composition of the material is altered. This forms the basis of its potential application to the stability evaluation of pharmaceutical ingredients.

4.3 Description of through-vial Impedance Spectroscopy instrument

The technology measures the electrical impedance of the product, contained within a standard freeze-drying vial that has been modified with electrodes placed on the outside of the glass wall. The impedance measurement system comprises of (i) impedance measurement vials (ii) a junction box within the freeze-drier chamber (mounted close to the shelf on which the vials are located) (iii) a pass through for cables (iv) a high precision impedance analyser (v) a NI connector box (vi) a computer system containing data acquisition card within the and a control software. The arrangement of these components is shown as a block diagram in Figure 26.

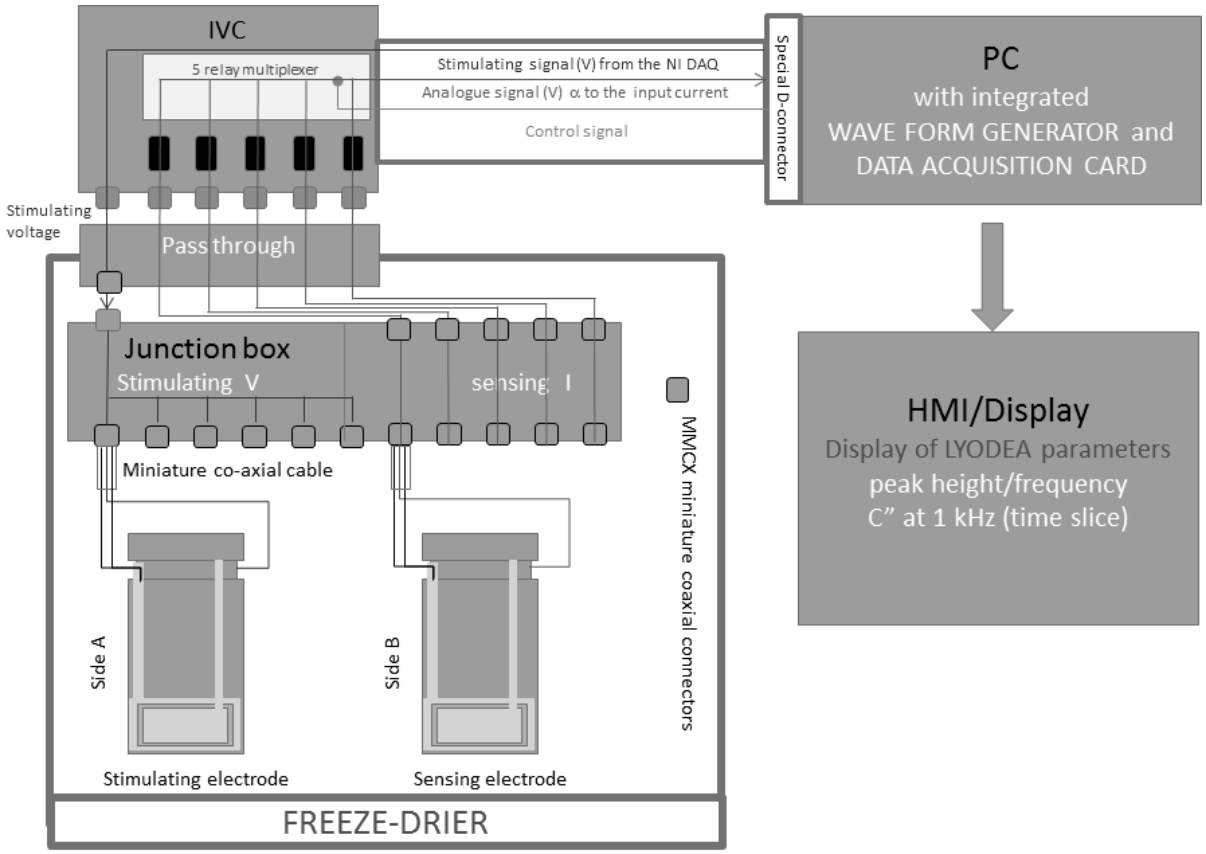

Figure 26 Block diagram of the impedance measurement system. Sides A and B are of the same vial.

The high precision impedance analyser designed and manufactured for this study comprises 5 channels which convert the electrical current to voltage (hence the name IVC) in order to estimate the impedance of the system. An electrical circuit for the IVC, its precision at

useable bandwidth of 10 Hz to 1 MHz along with a flow chart diagram for data acquisition system (including the calibration routine and primary data treatment software) is described in Figure 27 a, b and c respectively.

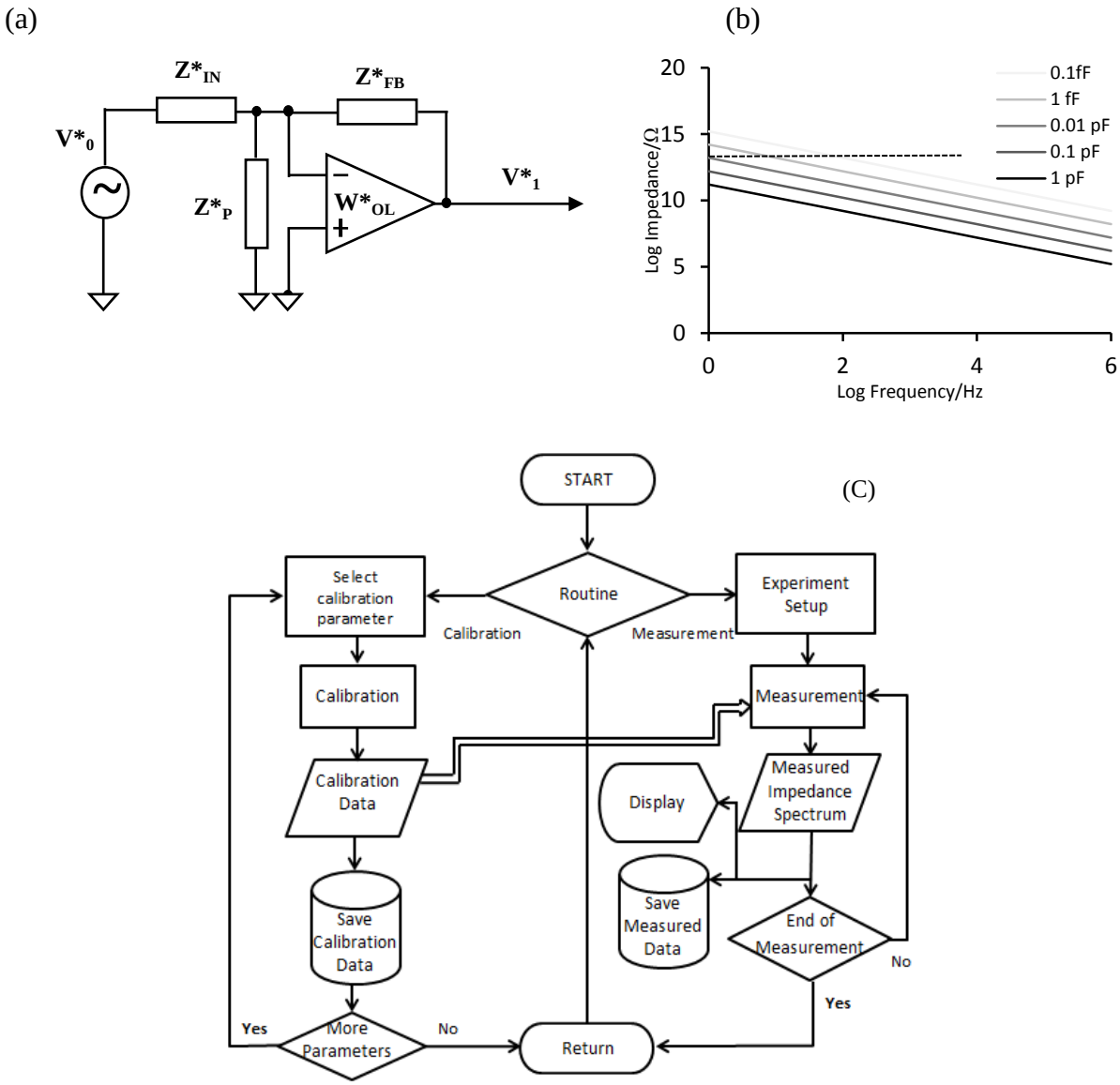

Figure 27 (a) Simplified circuit diagram of the IVC (b) Impedance profiles of different capacitors to demonstrate the approximate magnitude of the impedance and band width which is theoretically achievable in measurements terms (c) Flowchart for control and data acquisition and calibration software.

The operation of IVC requires a sophisticated calibration based on expression (Equation 33) that is obtained as a solution of system of equations mathematically describing the IVC operation. This equation has been worked out by Eugene Polygalov, the inventor of this technology for the particular configuration of the IVC, using Kirchhoff's rules and Ohm's law, as well as data sheet for operational amplifier used for constructing the IVC

$$W^*_{CL} = \frac{V^*_1}{V^*_0} = \frac{W^*_{OL} Z^*_{FB} Z^*_P}{Z^*_{FB} Z^*_P + Z^*_{IN} Z^*_P + Z^*_{IN} Z^*_{FB} - W^*_{OL} Z^*_{IN} Z^*_P} \qquad \text{Equation 33}$$

where W^*_{CL} is a closed loop complex transfer function, W^*_{OL} is an open loop transfer function of the operational amplifier, and Z^*_{IN}, Z^*_{FB} and Z^*_P are complex impedances of a reference object (for that purpose a 1 pF (Pico Farad; 10^{-12} F) capacitor with air dielectric was used), feedback circuitry and parasitic input impedance, respectively, of the operational amplifier and connecting cable respectively (asterisk in superscripts denotes complex values). During the calibration routine ((Figure 27 a, LHS), the complex spectra of W^*_{OL} and the complex spectra of Z^*_{FB} are recorded during the calibration routine, for each channel and stored in a calibration file. Separately, the value of parasitic impedance is measured for each channel and again stored in the calibration.

Then by resolving Equation 33 with respect to Z^*_{IN}, the working formulae (Equation 34) is obtained, which is used subsequently to calculate the complex impedance of an object under test (in this case the measurement vial and its contents).

$$Z^*_{IN} = \frac{\left(W^*_{OL} Z^*_{FB} Z^*P\right)}{\left(V^*_1 / V^*_0\right)} - Z^*_{FB} Z^*_p \Big/ \left(Z^*_{FB} + Z^*_P - W^*_{OL} Z^*_P\right) \qquad \text{Equation 34}$$

Though the calibration routine is rather complex and time consuming (24 h), once been done it yields exceptional accuracy, sensitivity and resolution of the IVC, as listed here: Measurement range up to 10^{14} Ω (Ohm) (impedance magnitude) with a phase angle resolution of ~0.001° or, in terms of minimal measurable capacitance, the designed IVC has a resolution of 0.1 fF (Femto Farad; 10^{-15}F) in the frequency range from 10 Hz to 1MHz (Figure 27 b). This measurement resolution is sufficient to measure changes in the capacitance of the test

system, which typically range from 0.6 pF (for the liquid filled vial at the start of the process) to 0.1 pF (for the dried product, at the end of the process), across the frequency range of 10 Hz to 1 MHz with a precision of 0.1%.

The **measurement vial** (Figure 28) is a standard 10 ml, type I clear glass, tubing vial (Schott) with an added electrode system, which consists of an identical set of stimulating/sensing electrodes (18 x 5 mm), each with a surrounding grounded guard electrode which prevents electrical current leak between stimulating and sensing electrodes over the outer surface of the vial. The cables are attached to the vial via permanent soldering. The electrode system was manufactured from adhesive copper foil and affixed on opposite sides of the external surface of a vial, just above the bottom curvature in order to avoid electrical contact (and hence grounding) with the shelf. The height of the electrodes was fixed at 1 cm from the bottom of the vial, and electrical impedance profiles were recorded for a fill volume of 3 ml which provides a fill depth of 1 cm and fill factor (ϕ) of 1 (ratio of sample height to the height of the top of the guard electrode). It was possible to demonstrate that the freezing onset temperature would be unaffected by the location of the electrodes on the outside of the vial provided the additional thermal mass was kept below a critical limit of ~1% approx. of the vial weight.

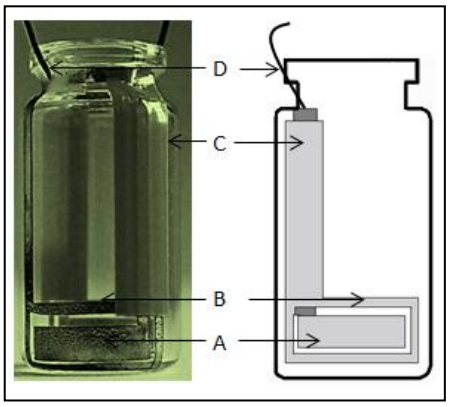

Figure 28 Schematic view of the measurement vial. A stimulating electrode, B guard electrode, C denotes the plastic strip covering copper foils which connect the electrode to coaxial cable, and D coaxial cable.

The decision to locate the electrode system on the external surface of the vial was based on a number of considerations: (i) The low thermal mass of a foil electrode, compared with a pin electrode of sufficient mechanical strength to prevent its flexing, reduces the heat flow to/from the sample, (ii) Having the electrodes external to the vial would not contaminate the sample, while reducing the impact on the crystallization dynamics by not introducing further

nucleation sites from the presence of a foreign body within the liquid, (iii) The impedance measured by external electrodes will be significantly higher than that measured by internal electrodes; It therefore follows that the influence of the cables impedance on the overall measurement will be insignificant, thereby reducing the potential for artefacts being introduced, e.g. from the effect of spatial temperature gradients in relation to the positioning of the cables, (iv) an electrode system placed internal to the vial, which comprises two straight pins necessarily requires a rather bulky adapter (to maintain the parallel geometry of the pins) which can only be located over the neck of the vial, and therefore inevitably impedes the efflux of vapours during primary drying; It is therefore difficult to imagine that such a system may be used in the primary drying stage without significantly impacting the drying rate. The bulky connectors would also preclude the deployment of an automatic vial stoppering mechanism. The last but by far the most important consideration is that the external electrodes do not give rise to a fractal electrode polarisation, which is inevitable when metal electrodes are in direct contact with a sample (Schwan, 1968, Cirkel et al., 1997). This makes the interpretation of spectral data much simpler and straightforward; and this feature enables the extraction of actual values for both the sample resistance and sample capacitance.

The spectral information from the analyser is transmitted to the measurement control software, which in turn displays the measured response in graphical as well as text file formats. The control software also permits the user to define the impedance scanning protocol in terms of (i) the frequency range (the band width of the system is 10 Hz to 1 MHz, but the useful frequency range is typically 100 Hz to 250 kHz), (ii) the stimulating voltage (typically 2V), (iii) the scanning interval, i.e. the time between the measurement sequence on all 5 test vials (typically 5 min), (iv) the number of integration cycles per spectrum (typically n = 4), and (v) the length of the cycle (typically 40-50 h). A Freeze drier (Model FD8, Heto, Denmark) with installed the measurement system, was used for the investigation of the drying process.

4.4 Electrical impedance measurements of formulation vial electrode assembly

4.4.1 Impedance (Z) spectrum

The impedance measurements system records the electrical impedance of the object under test, i.e. formulation vial electrode assembly, which as a characteristic of the physical state of the formulation changes during the process. Figure 29 a and b illustrate the impact of

freezing on the real and imaginary impedance spectra. The real part impedance spectrum gives the first indication that the solution resistance increases by a factor of ~ 500 on freezing; The arrow marked FS indicates the approximate value for the solution resistance in the frozen state (~ 500 MΩ) whereas the arrow marked LS indicates the approximate value for the solution resistance (~ 1 MΩ) in the liquid state. A comparison of the real and imaginary parts of an impedance sprectrum (Figure 29d, double ended arrow) shows that the imaginary impedance is as much as 10 times greater than the real part impedance, over much of the spectral range. The phase angle between the real and imaginary impedance (being in the range 50º to 90 º) (Figure 29c) also confirms that the overall impedance is dominated by the imaginary impedance.

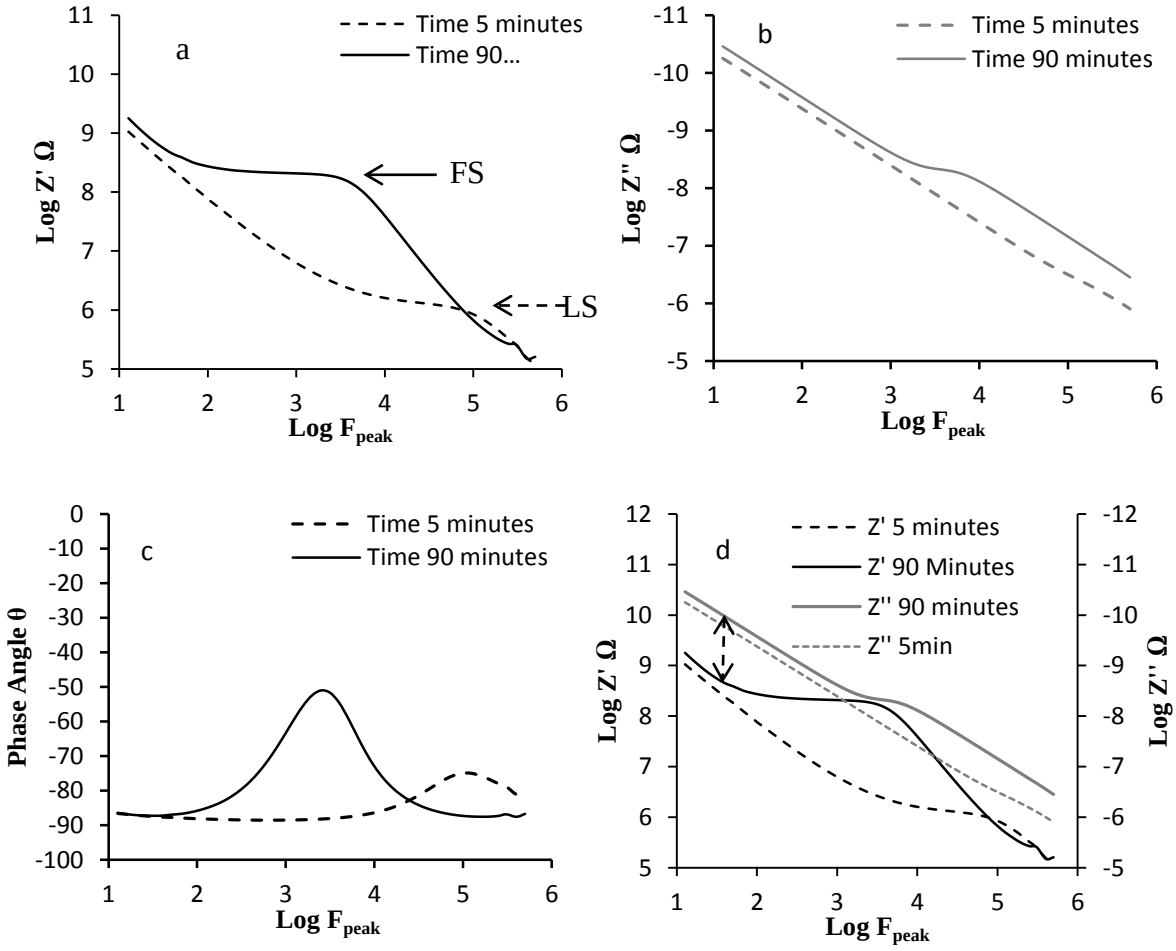

Figure 29 Impedance spectrum of 2.5% sucrose solution during freezing, the dotted line (- - -) denotes the liquid phase while the solid line (——) denotes the frozen (solidified) sample. (a) impedance real part (Z′) (b) impedance imaginary part (Z″) (c) Phase angle θ plot (d) comparison of real and imaginary impedance spectrum; Black colour represents real part (Z′) while the grey colour emphasises imaginary part of impedance (Z″).

This plot provides the first indication that the impedance of the test object (i.e. the formulation/vial/electrode assembly) has a direct correlation with the temperature and physical state of the formulation within the vial. However, the transitions of phase (from liquid to ice) and the impact of temperature on the response surface are more easily determined if the complex impedance (Z(ω))

$$Z(\omega) = Z'(\omega) + i\,Z''(\omega) \qquad \text{Equation 35}$$

is displayed as a complex capacitance (C(ω))

$$C(\omega) = C'(\omega) + iC''(\omega) \qquad \text{Equation 36}$$

where

$$C(\omega) = 1/i\,\omega\,Z\,(\omega) \qquad \text{Equation 37}$$

The formulae deriving real and imaginary capacitances are given in Equation 38 and Equation 39 respectively

$$C'(\omega) = -Z''(\omega) / \omega(Z'(\omega)^2 + Z''(\omega)^2) \qquad \text{Equation 38}$$

$$C''(\omega) = -Z'(\omega) / \omega(Z'(\omega)^2 + Z''(\omega)^2) \qquad \text{Equation 39}$$

Objects that behave like capacitors have a negative imaginary impedance, and therefore by definition the imaginary capacitance of these objects is also negative.

4.4.2 Capacitance spectrum

At a fill factor [2] of ϕ=1 the capacitance spectrum of the material under test (i.e. glass vial and the 30 mg/ml sucrose solution) displayed a step-like decrease in capacitance as the frequency is increased through the critical frequency which corresponds to the relaxation time constant for the sample ($f = 1/2\pi\tau$) (Figure 30 I). There is a corresponding peak in the associated imaginary capacitance (dielectric loss) spectrum as the material under test starts to conduct electricity through the phase lag between the response of the sample and the applied electric field (Figure 30 II).

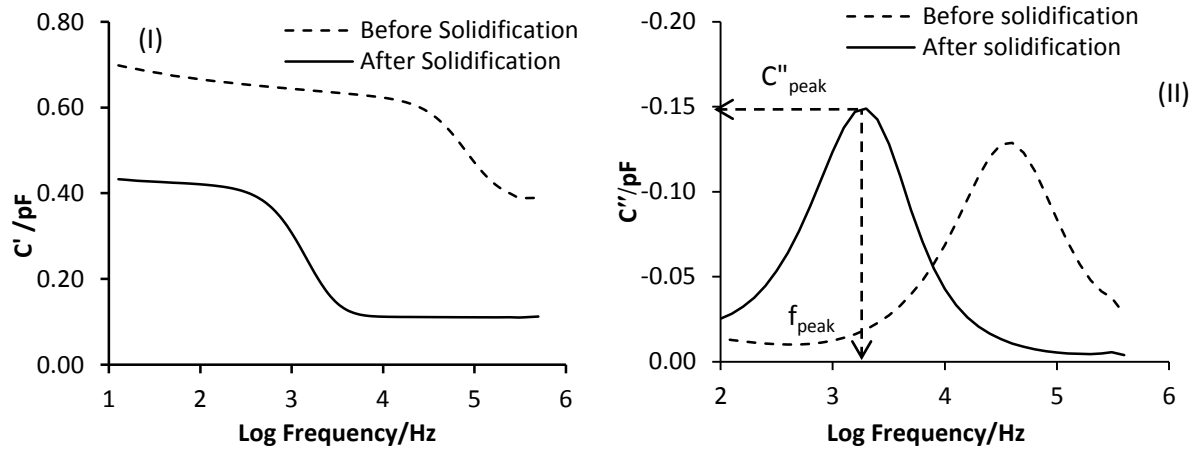

Figure 30 Capacitance plots capacitance for sucrose solution (3% w/v) during freezing (I) Real (C′) and (II) Imaginary (C″) The dotted line represents liquid state and the solid line denotes frozen state.

The manifestation of the step in the real part capacitance and the peak in the imaginary capacitance is known as a pseudo-relaxation process, as it has the appearance of a real relaxation process within a material (i.e. one that has a frequency dependent to its dielectric properties owing to some molecular relaxation or some form of interfacial charging within the material). This response resembles that of a classic Debye relaxation process within a dielectric material (Debye, 1929). In reality the dielectric properties of the material within the vial may be static i.e. invariant with frequency, and one is simply measuring the accumulation of charge at the glass surface as ions migrate through the liquid (or solid) contained within the glass vial. A more appropriate description of the pseudo-relaxation process is therefore 'an interfacial polarization process'.

[2] ratio of sample height to the height of the top of the guard electrode

It is the characteristics of the interfacial polarization process that are used to ‘follow’ the progression of the freeze-drying cycle. Of the real and imaginary capacitances, it was the imaginary capacitance that was used to demonstrate changes to the physical properties of the system.

4.4.3 Electrical circuit model

An equivalent electrical circuit model was used to fit the capacitance spectra in order to derive a more direct understanding of the relationships between the impedance response (i.e. the interfacial polarization process) and the physical characteristics of the solution. This equivalent circuit comprises three physical elements: a constant phase element (CPE), a resistor (R) and a capacitor (C) (Figure 31); the interfacial impedance between the solution and the glass wall is defined by CPE while R and C describe the physical state of the solution (in terms of the conductivity and dielectric permittivity). An example fit result using this equivalent circuit model is shown in (Figure 32 a, b). A brief methodology for the development of an equivalent circuit model is described in appendix iv.

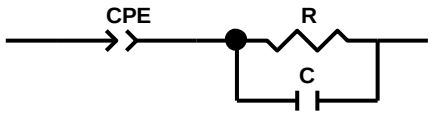

Figure 31 Equivalent circuit model representing the impedance response from the glass vial containing a conductive solution

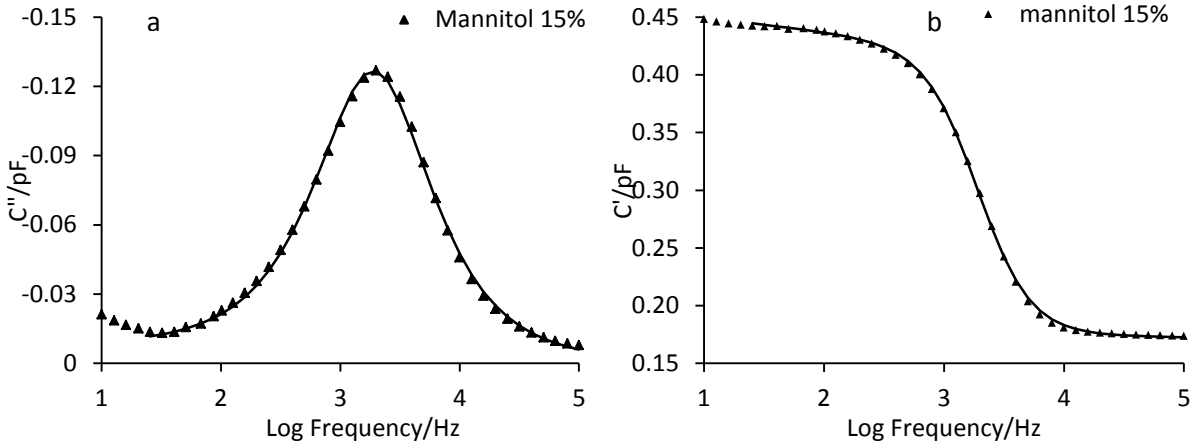

Figure 32 An Impedance spectrum from mannitol solution with fit result using an equivalent electrical circuit model a) Imaginary part b) real part of capacitance

Given that two methods are being presented to characterise the interfacial polarization process of the object under test, it is helpful to define the inter-relationships between the two methods: From the peak frequency one can calculate a time constant ($\tau = 1/2\pi f$) which characterises the rate of charging of the interfacial impedance of the glass wall of the vial. The rate of charging is related to 1) the diffusivity of charges to the interface between the soluiton and the glass wall and 2) the amount of charge that may accumulate at the interface. The former is reflected in the solution resistance and the latter is reflected in the magnitude of the interfacial capacitance between the frozen solution and the glass wall (|CPE|). The time constant is simply derived from the product of the solution resistance (R) and the capacitance of the constant phase element (|CPE|), i.e. $\tau = R.\ |CPE|$. So by assuming that |CPE| remains constant during the re-heating phase, it follows that there will be a direct relationship between R and f_{peak}, i.e. $f_{peak}\ \alpha\ 1/R$.

5 Characterization of the freezing process by TVIS

Measurement of the freezing profile of a sucrose 3% w/v formulations using impedance spectroscopy

5.1 Objectives

The objectives of this chapter are to characterize 1) the freezing stage by through-vial impedance spectroscopy and 2) the impact of the liquid fill height in relation to electrode geometries on the impedance spectrum. These were achieved by an experimental study on conventional 10 mL vial (Schott) with a fill volume ranging from 1.5 to 5 mL, corresponding to a fill height of 0.5 to 1.7 cm. The height of the electrodes was fixed at 1 cm from the bottom of the vial, and electrical impedance profiles were recorded for a fill volume of 3 ml which provides a fill depth of 1 cm and fill factor (ϕ) of 1 (ratio of sample height to the height of the top of the guard electrode). In practice, the fill depth may increase up to 2 cm (equivalent to 2ϕ (6ml)). The measurements of electrical responses at these fill heights will define the potential of impedance spectroscopy in monitoring of the freeze-drying process at variable fill volumes. Fill heights > 2 cm should be avoided where possible as it may result in high intra-vial variability and poor cake appearance due to altered heat flow during freezing and primary drying (Liu et al., 2005).

5.2 Materials

Sucrose, purchased from Sigma Aldrich UK, was used as supplied.

5.3 Methods

A 3 % w/v sucrose solution was prepared in single distilled water obtained from all glass apparatus. Aliquots of the sucrose solution were transferred to impedance measurement vials (N=5) via a 0.2 micron micro filter (Minisart, Germany).

The impedance spectrum was recorded by scanning the frequency range 10^1-10^6 Hz. The acquisition time for each spectrum was 27s and an interval between all five measurements of 3 min. A detailed methodology for data acquisition is described in appendices III and IV. The

product temperature was recorded by means of type K thermocouple placed in the glass vials, arranged in a line on the shelf, using temperature data logger OctTemp 2000 (Madgetech USA).

The fill volume was increased successively from 1.5 to 5 ml. Each freezing experiment was repeated to provide ten measurements at each fill volume. The corresponding solution fill height ranged from ~ 4.6 mm (1.5ml) which sits below the electrode foil height of 10.5 mm, to 17.5 mm (5.0 ml), which sits above the top of the electrodes. These solution fill heights correspond to a fill factor (ϕ) increasing from 0.5 to 1.6 (Figure 33).

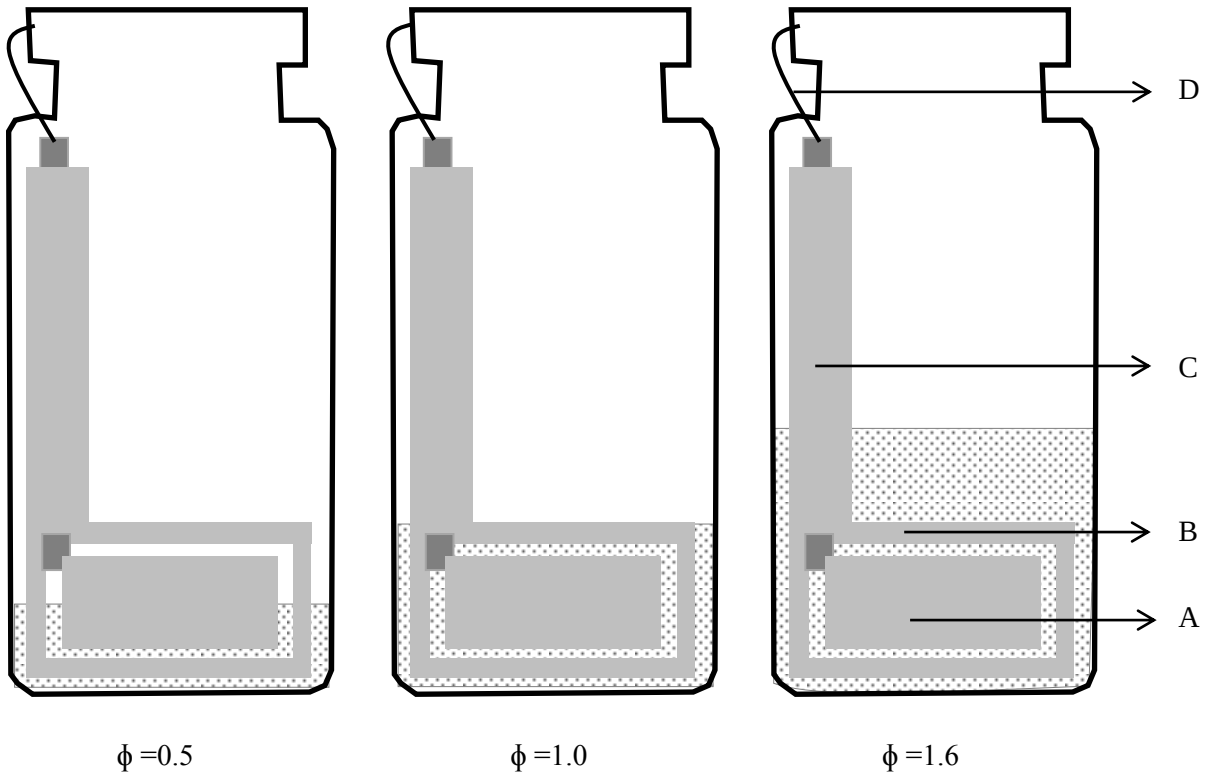

Figure 33 Electrodes attached to the outside of a freeze-drying vial. A is the active electrode, B is the guard electrode, C is the connector strip from the elecrode to the neck of the vial, D is the miniature co-axial wire connecting the electrode to the measuring system (where the outer braiding of the coaxial cable attaches to the guard electrode and the inner conductor attaches either to the stimulating or current sensing electrode (ϕ is the ratio of liquid fill height to the height of the top of the guard electrode)

The freezing cycle comprised the following steps: (1) Temperature ramp to 25 °C, over 10 min; (2) Hold temperature at 25 °C for 20 min; (3) Temperature ramp to -30 °C, over 60 minutes; (4) Hold temperature at -30 °C for 120 min.

Chapter 5

5.4 Results and Discussion

The basic characteristics of the freezing process are described first for a fill factor of ϕ=1 while the impact of fill height is evaluated in the next section.

5.4.1 Freezing Characteristics at fill factor, ϕ=1

The features of the interfacial relaxation process as a function of time were characterized in terms of the amplitude (C''_{peak}) and frequency position (f_{peak}) of the peak in the imaginary capacitance spectrum (Figure 30 II) using data analysis software Lyoview^{TM} (operating procedure of Lyoview^{TM} is described appendix V). The time profile of log f_{peak} (Figure 34 I) is remarkably similar to that recorded by the thermocouple (Figure 34 III) and identifies various phases in the freezing cycle: the pre-cooling phase (A to B), the onset of ice formation (point B), the solidification phase of the product (i.e. the ice growth phase) (B to D) and the subsequent equilibration of the product temperature with the shelf temperature (D to E) (Kasper and Friess, 2011, Nakagawa et al., 2007, Rahman et al., 2002). In contrast the time profile of C''_{peak} (Figure 34 II) is quite different and somewhat scattered, up to the point of complete solidification (point D) suggesting a limited application of this parameter in the characterization of ice formation.

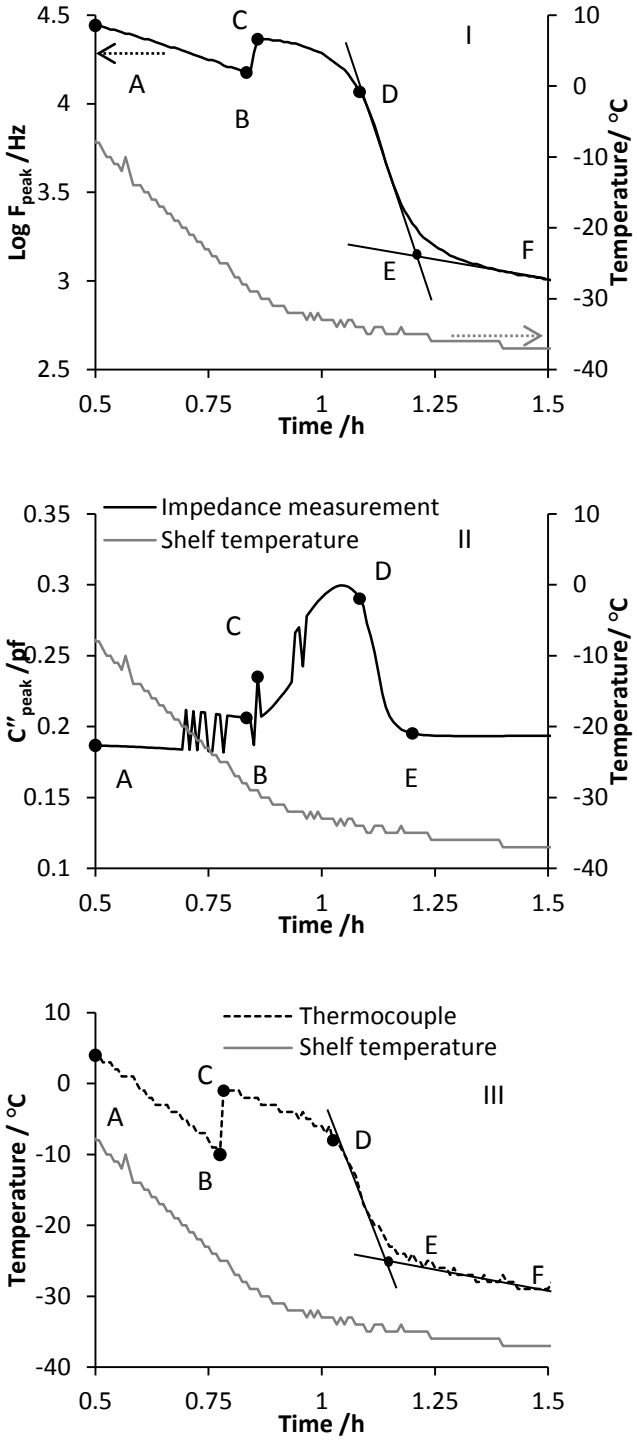

Figure 34 Time profile of (I) the peak frequency (f_{peak}), II) the peak amplitude (C''_{peak}) and III) product temperature of sucrose 3% w/v during freezing. Plots I and III clearly identify critical steps relating to product freezing; A to B is product cooling (pre-ice formation), B is the onset of ice formation, C describes the maximum increase in product temperature following exothermic heat dissipation during ice formation. From these transitions one can define B-D as the ice solidification phase, D-E as the equilibration phase, E-F is product cooling II (post ice formation). C''_{peak} appears noisy during the freezing but delineates precisely the end point of the equilibration phase (point E). Note that time zero is taken from the end of the equilibration phase after the vial and contents have been maintained at 25 °C for 10 min.

Further explanation of each phase is given below:

Cooling Phase (A to B) The magnitude of log f_{peak} decreases linearly with the time because of the temperature dependent decrease in the electrical resistance of the sucrose solution. This behaviour continues until the ice nucleation point is reached (point B).

Ice Nucleation (point B) The onset of freezing or ice nucleation is identified by an abrupt increase in the magnitude of f_{peak} which results from the elevation in temperature, following the release of the heat of ice crystallization (an exothermic process). The time corresponding to this transition was recorded as the nucleation time.

Solidification Phase (B-D) As the ice onset phase (nucleation) progresses to the growth of ice crystals, it is the rate of ice formation that defines the rate of energy release into the product and hence the rate of the temperature rise. However, in parallel with the increase in temperature from ice formation, there is also an increase in the rate of heat dissipation through the walls of the vial. At some point, the rate of ice formation slows down, such that the rate of heat dissipation then exceeds the rate of heat release and the temperature then starts to decrease. This defines the point C. Thereafter, the heat dissipation rate dominates the energy balance in the system and the temperature begins to return to equilibrium with the shelf (point E). However, before equilibrium is reached there comes a point when no more ice forms in the system and energy dissipation alone defines the energy balance in the system. The time period from point B to point D is therefore defined as the solidification time, during which the ice crystallization process is complete, whereas the time period from **D to E** defines the **equilibration phase**.

Cooling Phase II (E-F) Following the equilibration phase, the contents of the vial continue to cool at rate defined by the cooling rate of the shelf; Though the thermal exchange between the vial contents and the surroundings means that the temperature within the vial stabilize 1-2 °C above the shelf temperature.

The end of the equilibration phase (E) was estimated from the point where the tangent of the line through the data from the solidification phase intersects with the tangent of the line through the data from cooling phase II (post ice formation). The **freezing time** is then defined

as the time difference from point B to E. The time duration of each phase was also estimated from the product temperature profile recorded by the thermocouple (Figure 34 II).

5.4.2 Freezing characteristics of sucrose 30 mg/ml at different fill factors (ϕ=0.5 to1.6)

The features of interfacial relaxation process were also assessed at two other fill factors (ϕ= 0.5 and ϕ= 1.6). Both log f_{peak} and temperature profiles show that by increasing the fill volume (so that the fill factor changes from 0.5 to 1.6) results in the prolongation of the freezing process (Figure 35). The analysis of these profiles, along the lines described earlier, provides a range of estimates for the ice nucleation time, the freezing time, the solidification time and the equilibration time. In each plot, the cumulative standard deviation takes in account the variability in freezing times associated with the position of vials on the self in relation to the walls of the drier, and the small differences in vial geometry.

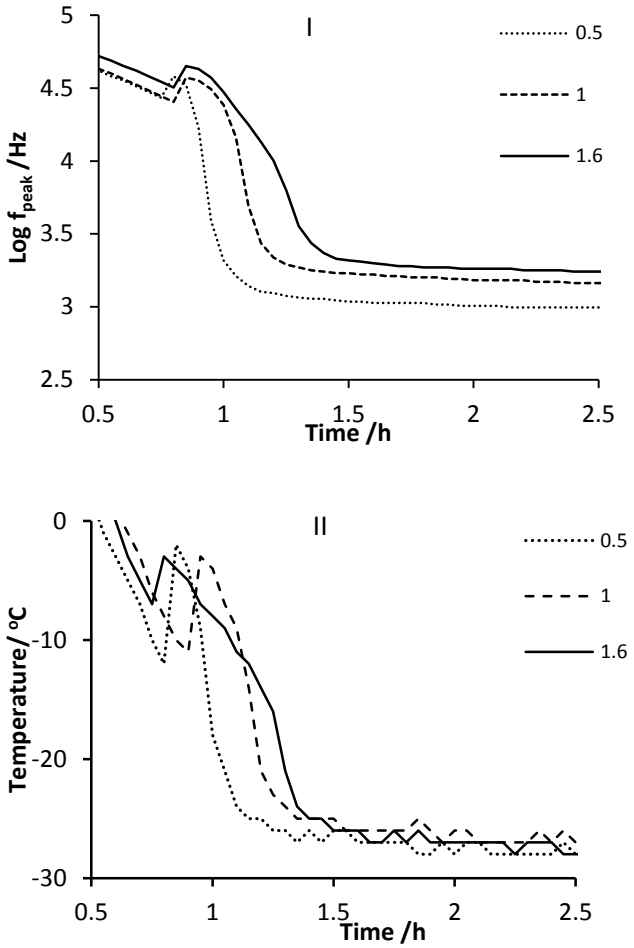

Figure 35 Time profiles of (I) fpeak and (II) temperature for 3 % w/v sucrose during freezing at different fill factors (ϕ =0.5, 1 and 1.6). (n = 10) Note that time zero is taken from the end of the equilibration phase after the vial and contents have been equilibrated at 25 °C for 10 min.

The results from the perspective of ice nucleation time suggest that there appears to be little influence of fill height on the onset time. This observation is consistent with the fact that freezing starts from the base of the vial, and so the fill height has little bearing on when the inititation of the ice nucleation event occurs. Although one could argue that, the greater the fill volume, the longer it will take to cool the product to the nucleation temperature. However, the overlapping standard deviation values preclude the drawing of any definitive conclusion.

The results from ice nucleation time might also suggest an earlier ice nucleation in the impedance spectroscopy measured vials compared to thermocouple TC, however these observation remain inconclusive due to a high degree of variation in the onset of formation signified by the overlapping standard deviation values.

The scatter in the ice nucleation (Figure 36) for any particular fill volume confirms the stochastic nature of the ice nucleation process (Nakagawa et al., 2007) (%COVs range from 12.4 to 8.8 for the thermocouple data and 7.2 to 4.1 for the IS data). This inherent variability in the onset of ice formation could result in differences in the degree of super-cooling and hence different ice morphologies in the frozen matrix. The fact that the scatter in the onset is greater for the TC data than the IS data may be due to the fact that the TC measurement is more sensitive to its position in the vial in relation to the spatial seeding of the ice layer.

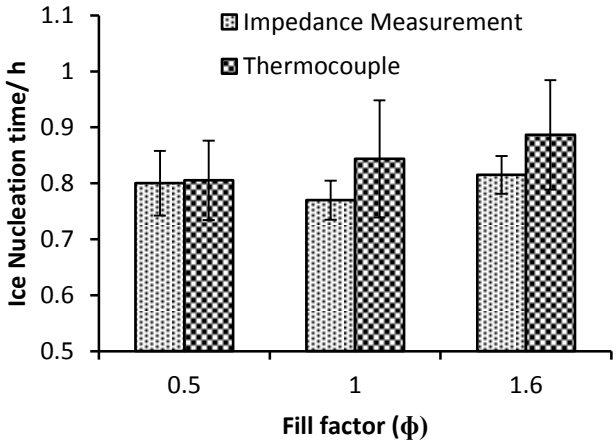

Figure 36 Ice nucleation time for sucrose 3% w/v at different fill factors. Time zero is taken from the end of the equilibration phase after the vial and contents have been equilibrated at 25 °C for 10 min. The nucleation time is then calculated from the time point B (Figure 34)

By plotting the freezing time, the solidification time and the equilibration time (from both the f_{peak} derived-estimates and thermocouple derived-estimates) shows that the duration of each phase has a broadly linear dependance on fill factor (Figure 37). The solidification time almost doubles with a doubling of the fill factor as one might expect. However,the equilibration time is much less dependent on the fill factor. The fact that the equilibration time is almost constant might mean that this time equates to the time required for the excess heat to pass through the base of the vial and to some extent through the walls of the vial. As the volume of the frozen mass increases there is a small increase in the contribution from the vial, which is associated with the increased wall volume that is adjacent to the liquid fill. The intercept on the y-axis can then be considered as the time constant for heat flux through the base and the gradient of the line is the time constant for heat flux through unit area of the side walls of the vial.

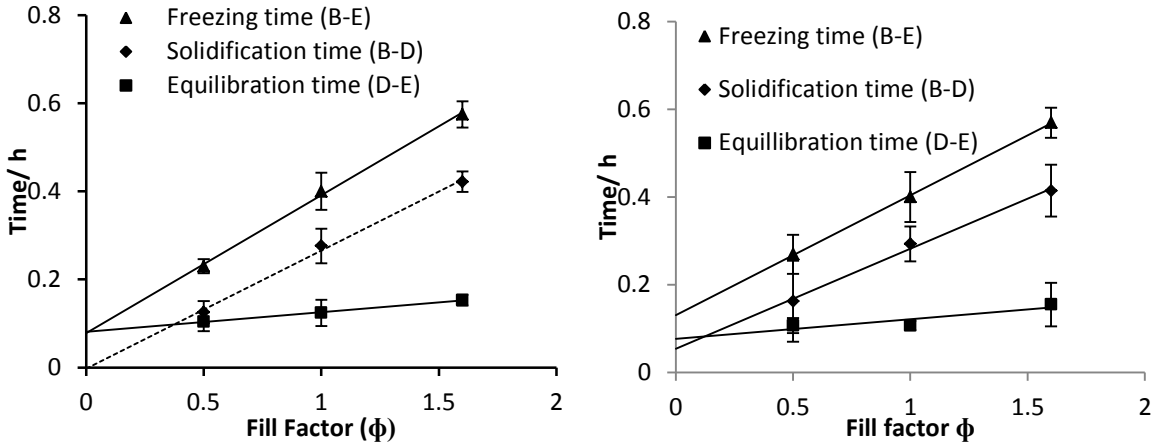

Figure 37 Freezing time, solidification time and equilibration time for 3% w/v sucrose solution at different fill factors (n = 10), (LEFT) Impedance measurement (RIGHT) Thermocouple measurement.

The line of best fit to the TVIS derived solidification time extrapolates back to zero whereas the line of best fit for the TC derived solidification time does not extrapolate to zero. This observation suggests a potential limitation of the point measurement systems, whereby the position of the thermocouple in relation to the fill volume and the walls of the vial will impact the time point at which any one particular phase is deemed to have completed.

In contrast, the improved linearity between the time duration of the solidification phase and the fill volume, as derived from the log fpeak values, is a consequence of the fact that the impedance measurement is sensing the entire fill volume (Given that the guard electrode surrounds the measurement electrodes then this will force the field lines through the contents of the vial and hence the impedance measurements sense the entire contents of the vial).

From this study, it is becoming clear that the through-vial impedance spectroscopy technique may have a role to play in the development of lyophilization processes and formulations. In particular it may find a useful role in defining the *in situ* characteristics of the freezing process, especially in regard to the manefestation of first and second order transitions such as eutectic crystallation and the glass transition (data not presented) and the impact of various process conditions (set temperatures and ramp rates) including those which define the process of annealing. Further development of the technology to establish a non-contact measurement may even allow for the technique to be used more extensively in the processes of scale up.

A major advantage over other single vial measurement techniques (such as NIR, and the freeze-drying microbalance) is that vials may be clustered in the usual hexagonal array (which

is employed when the shelf is fully loaded) as a consequence of the minimal physical space taken up by the electrode system. The major disadvantage (as with all single vial measurements) is that only a limited number of vials may be characterised which makes extrapolation to the whole batch somewhat difficult. However, further development of the technology to establish a non-contact measurement may allow for multiple vials to be assessed within domains of the freeze-drier. Such a development would then render the technique more applicable to scale up and process verification in GMP freeze-driers.

5.5 Summary

The time profile of f_{peak} during the freezing process recorded the various phases of (i) cooling, (ii) ice nucleation and growth leading to the solidification of the product, and (iii) the equilibration of the frozen solution with the shelf temperature. A linear relationship between the duration of the solidification phase and fill volume suggests that fixed electrode geometries may be used to investigate a range of fill volumes. The extension of these studies to lower temperatures (i.e. temperatures below T_g and T_c for sucrose and other materials), so that the technique might be used to track the primary drying stage, would be useful.

Chapter 6

6 Characterization of Eutectic crystallization by TVIS

Measurement of Eutectic temperature of a formulation (Mannitol 15% w/v) during shelf freezing

6.1 Objectives

The objectives of this chapter are to investigate the application of through-vial impedance spectroscopy in the identification of critical product parameters including ice formation and solute crystallization (eutectic formation) as well as the impact of non-crystallizing components on the solute crystallization in a complex formulation. For the purpose impedance profile of surrogate formulation containing different concentrations mannitol (5, 10 and 15% w/v) were recorded over the freezing cycles. The spectral data were analysed to identify additional exothermic event during the freezing. In addition the impact of sucrose (non-crystallizing component) is recorded on the eutectic crystallization of mannitol during the freezing.

6.2 Materials

Mannitol and sucrose were purchased from Sigma-Aldrich UK and used as supplied in the preparation of a number of surrogate formulations.

6.3 Methods

Surrogate formulations were prepared from materials having different physical characteristics, i.e. those which crystallize and those which form amorphous solids: Mannitol in concentration of 5, 10 and 15% w/v and mannitol 5% with sucrose 5% w/v. Aliquots of 3.0 ml were introduced to the impedance measurement vials (N=5) and impedance measurements were performed over a frequency range 10^1-10^6 Hz with the scan interval 1.5 minutes. Temperature measurements were recorded using type K thermocouple at time intervals concurrent with the impedance measurements. The freeze-thaw cycle followed the regime: Hold the shelf at 25 °C for 30 minutes; Temperature ramp to -35 °C within 1 hour; Hold freezing temperature 3 hours.

DSC was also performed by measuring each surrogate formulations over a temperature range of -60 °C to 20 °C at 2 °C min^{-1} using a Perkin Elmer Jade DSC (Germany).

6.4 Results and discussion

6.4.1 Differential Scanning Calorimetry (DSC)

The DSC thermogram of the 5% w/v mannitol solution demonstrates an endothermic step in heat flow, with an onset temperature close to -32 °C. This was registered as the glass transition temperature of the formulation. Subsequently, an exothermic peak was recorded at -22 °C, indicative of the crystallization of the solute (mannitol) and an endothermic peak with an onset temperature of ~ -2 °C indicating the melting of the ice fractions within the solution (Figure 38). Crystallization exotherm and glass transitions were recorded also in the solutions containing 10% and 15% mannitol (thermograms not shown).

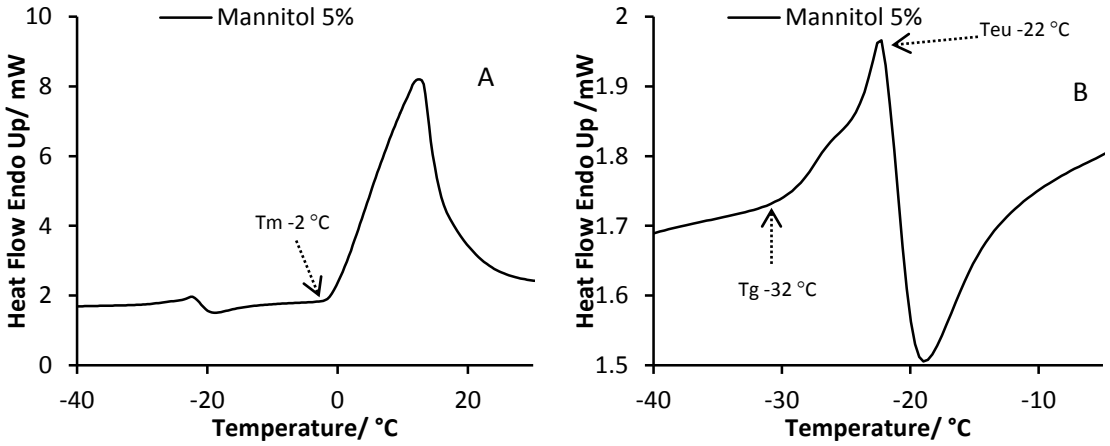

Figure 38 DSC results from the re-heating of mannitol 5% w/v frozen solution A complete scan B magnified view

The co-existence of both amorphous and the crystalline states are evident at intermediate scanning rates of 5 °C and 10 °C, however the proportion of each form within the frozen solution is impacted by the actual choice of cooling rate, with the latter being diminished at the higher cooling rates and seldom observed at 20 °C min^{-1} (Cavatur et al., 2002). Due to this reason, one may expect a different crystalline and glassy state within the glass vial may wherein the cooling rates are close 1 °C min^{-1}.

6.4.2 Through-Vial Impedance Spectroscopy

Response surface: The position and amplitude of interfacial relaxation peak, recorded from the imaginary part of the capacitance spectrum, change with product cooling, ice formation

and solute crystallization (Figure 39). The changes in electrical impedance of the formulation are summarized in the response surface plot showing a relatively small shift in f_{peak} following product cooling (A) followed by a significant drop in the relaxation frequency referring to ice crystallization (B) and the another step like decrease in the f_{peak} (as a small bulb) pointing to second crystallization within the system (C) before stabilizing to the freezing temperature (D).

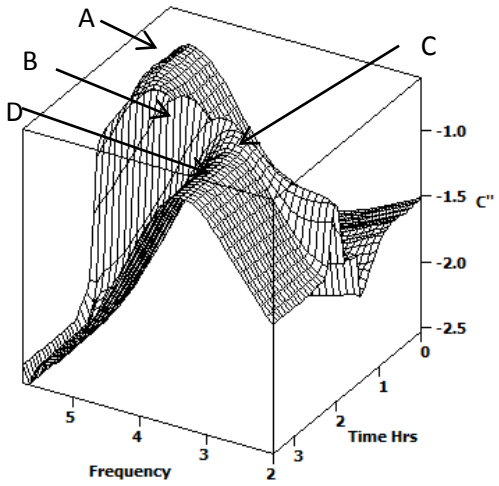

Figure 39 Response surface plot of imaginary capacitance of mannitol 5% w/v solution during freezing.

Product cooling from 20 to -10 °C was associated with a ~ 7% and ~ 8% decrease in the magnitude of log f_{peak} and C''_{peak}, respectively, over 1h (Figure 40). This trend, in the decrease of f_{peak} and C''_{peak} with the temperature, was similar to that recorded for sucrose (chapter 5) (Smith et al., 2013). Moreover, the specific correlation of f_{peak} with the solution temperature during the cooling stage may be used to create a calibration curve for the product temperature in the liquid state. In so doing, one can estimate the cooling rate and degree of super cooling without having to place a temperature probe within the vial.

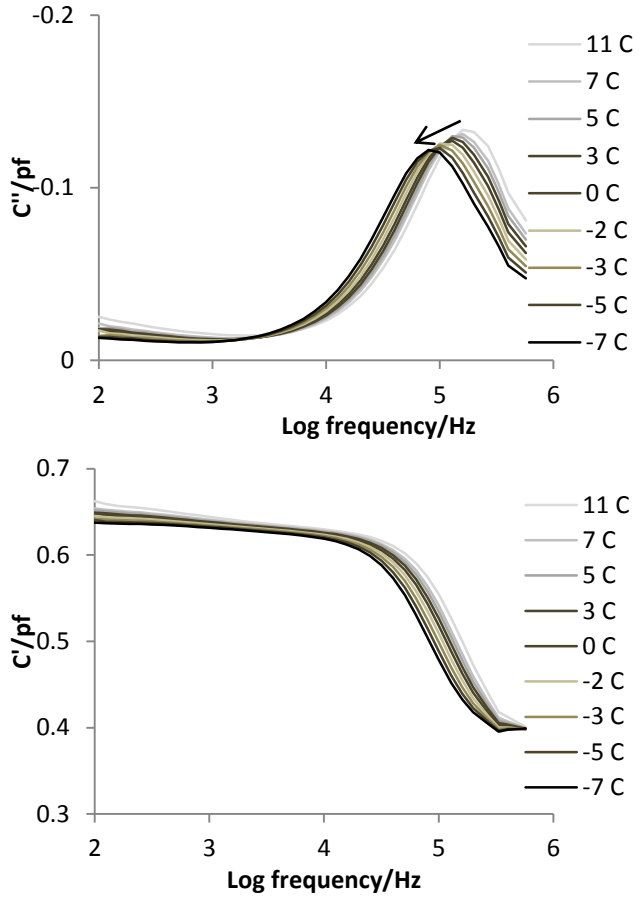

Figure 40 Spectrum profile of mannitol 5% w/v solution during cooling

Ice formation is characterized by a shift in f_{peak} to lower frequencies (by approximately one order of magnitude). In contrast, the peak amplitude (C''_{peak}) increased by approximately 50% during the crystallization of ice.

Spectral time profiles: The features of the interfacial polarization peak (i.e f_{peak} and C''_{peak}) and the values of equivalent circuit elements (R, C and CPE) were plotted against the cycle time in order to describe the different stages of product freezing. The temperature profile was also included in order to identify the occurrence of different events and to relate the electrical impedance changes with those recorded with the DSC.

A detailed description of the changes in impedance characteristics during freezing is given in chapter 4 and 5. A brief summary of this correlation, with an emphasis on the equivalent circuit element response, is described here. Figure 41 shows the dependencies of each of the parameters that characterise the interfacial-polarization process, f_{peak}, and R. The time profiles for both log f_{peak} and -log R are very similar. This is not surprising given that

f_{peak} is strongly coupled (i.e. dependent) on the solution resistance R through the relationship: $f = 1 / R.|CPE|$, where $|CPE|$ is the effective capacitance of the glass wall-solution interface. Of the two parameters (R and $|CPE|$) it is R that changes significantly with the freezing process, whereas $|CPE|$ remains relatively constant. If follows that log f_{peak} is proportional to –log R. This is borne out by the observation that a linear decrease in the product temperature, during the product cooling step (A-B), was reflected by a similar decrease in the gradients of the f_{peak} and -log R. The precise responsiveness of these parameters can be explained by the temperature dependence of the relaxation time constant (τ) of interfacial polarization process of the object under test, in the liquid state. Following ice nucleation, both the product temperature and f_{peak} and –log R increase to the equilibrium freezing point (0°C for pure water and lesser for the solution due to freezing point depression) and remains close to this (equilibrium freezing) value until the heat dissipation due to exothermic crystallization exceeds the heat absorption through the vial base (solidification). Following ice formation, the product temperature decreases rapidly to equilibrate with the shelf temperature while the impedance parameters (f_{peak} and -log R) demonstrate an additional intermediate step like decrease in their time profiles originating at 1.95 h which corresponds to -24 °C after an initial rapid decline. The onset temperature of this second discontinuity in the product impedance was in good correlation with the exothermic response attributed to mannitol crystallization during re-heating. The observation that the second step like decrease in the f_{peak} relates to the crystallization of mannitol is confirmed by the fact that this step-like increments in the f_{peak} were not observed in the freezing profiles of sucrose 3 % w/v solution, as reported in the chapter 5.

R as a means to determining the eutectic: Time profiles for the electrical resistance, plotted on the linear scale, shows a ‘two step’ increase in the product resistance, which is indicative of ice formation and solute crystallization, respectively (Figure 41). The increase in the electrical resistance, following crystallization, is an obvious consequence of the decreased mobility of the ions/protons at the freezing temperature, which is further increased by the decreased fluidity in the system, with the latter being a consequence of the separation of water molecules as ice and the mannitol solute in its crystalline form (Zhao et al., 2011, Chin et al., 2007).

Although, the other parameters used to characterize the impedance spectrum (C''_{peak}, circuit elements C and CPE) also identify the different stages of freezing (i.e. product cooling, ice

nucleation, solidification, equilibration with the shelf temperature, and solute crystallization) as changes in the their gradients at the time points in agreement with those described for f_{peak} and R, their values changed over a smaller range making them less significant in recording the freezing behaviour.

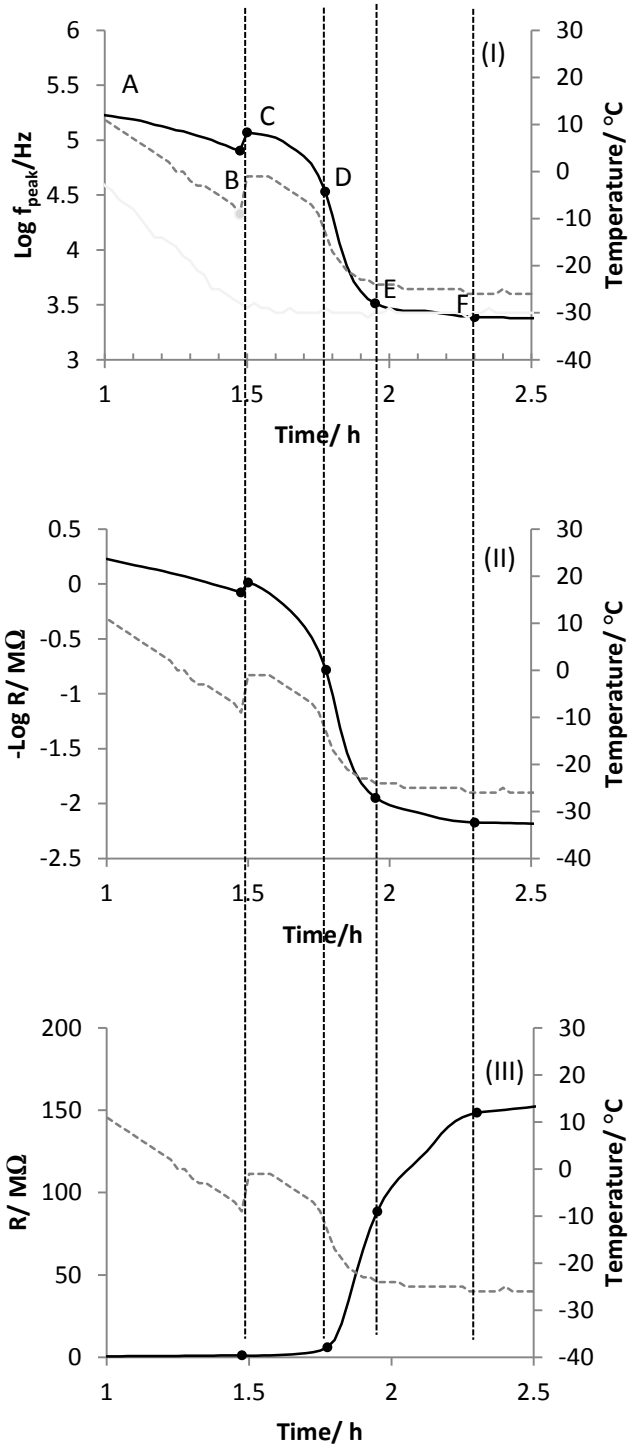

Figure 41 Impedance profile of mannitol 5% w/v solution during freezing (I) F_{peak} (II) -log R and (III) R. The figure demonstrates the pronounced sensitivity of the R parameter to both the ice temperature equilibration phase (post ice formation, i.e. phase D-E) and the crystallization of the solute (mannitol), i.e. phase E-F (solid line describes the impedance profile while dashed line shows temperature profile).

The increase in the magnitude of R, during freezing, was fitted with a sigmoidal function (Equation 40) in order to characterize the two step changes in the product resistance resulting from ice formation and eutectic crystallization.

$$R(t) = R_0 + \Delta R_1/(1+10^{(t1-t)\,h1)}) + \Delta R_2/(1+10^{(t2-t)\,h2}) \qquad \text{Equation 40}$$

R_0 is the resistance before freezing, ΔR_1 and ΔR_2 represent the changes in resistance associated with the two step changes; t_1 and t_2 are the mid-point in time for each step, and h_1 and h_2 are the slope factor of each step.

The sigmoidal function models the increments in the electrical resistance during the tail end of the solidification (I to II) and equilibration stages, wherein the product temperature approaches that of the shelf temperature. In the absence of additional heat dissipative mechanisms (such as the crystallization of mannitol), the latter part of the curve (II to IV) is expected to increase in an exponential fashion, to complete the latter part of a single sigmoid function (see Figure 42 dotted line). In effect, however, the secondary exothermic response, due to solute crystallization, introduces a discontinuity in the quasi-exponential rise in R during the temperature equilibration stage; this is manifested as an additional step in the resistance profile (III to V) which means that the end of ice solidification and the equilibration phase can be described by biphasic sigmoidal function (Figure 42 A, solid line). From the difference between the two sigmoidal curves, (i.e. mono and biphasic) one can identify the relative delay in the increase in R due to solute crystallization.

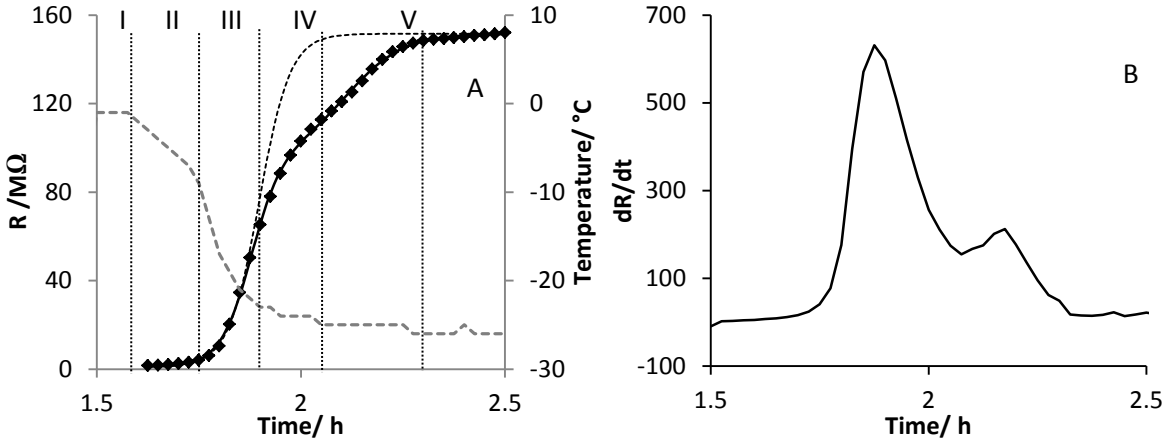

Figure 42 The electrical resistance (R) profile during freezing of a 5% w/v mannitol solution: A) resistance plot with two step sigmoidal function, B) time derivative of R plot.

The time derivative of the resistance data were also calculated in order to identify the maximum gradient during different stages of the product freezing (Figure 42 B). Two distinct peaks confirm the biphasic increase in the solution resistance; the primary peak was recorded at 1.87 h which corresponds to a sample temperature of -17 °C the while the secondary peak was recorded at 2.17 h cycle time and corresponds to a sample temperature of -25 °C.

The mid-point temperature for mannitol crystallization was characterized by taking the second peak in the time derivative profile and determining the temperature of the solution from the adjacent thermocouple containing vial. A value of -24 °C was determined which is within 2 °C of that measured by DSC. These through-vial impedance measurements may be of more relevance in process development as it measures the physical response from the solution placed on the shelf (where the cooling rates are generally lower than those recorded from DSC during the freezing stage). The additional advantage of measuring the physical transition in the actual container (vial) is that it obviates the necessity for any temperature/time adjustments which are usually required when off-line measurements are applied to the in-process scenario.

Impact of mannitol concentration on crystallization: The freezing profile of the higher concentrations of mannitol solutions (10%, 15% w/v) (Figure 43) was also characterized by the biphasic sigmoidal fit function (Equation 40) and the time derivative of the electrical resistance R of the formulations during freezing.

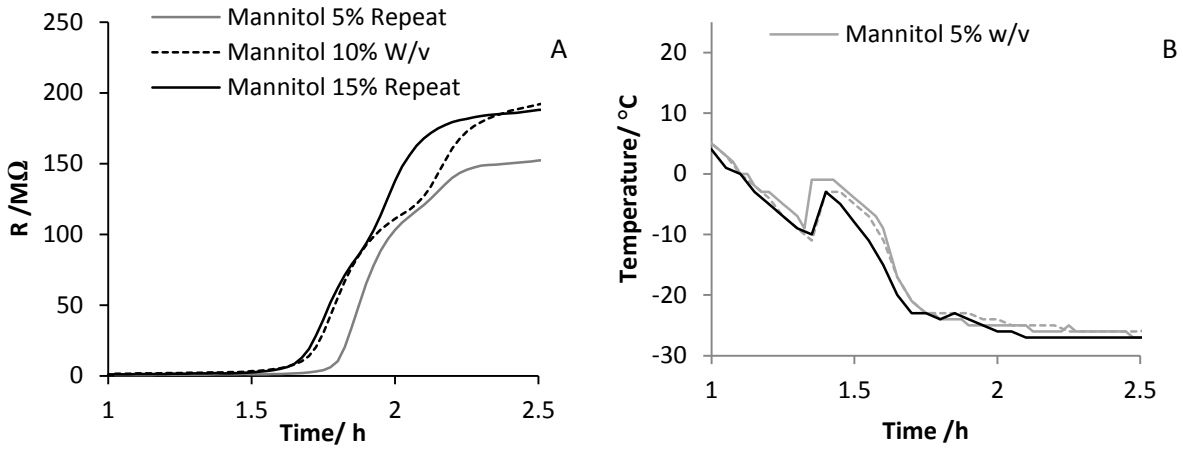

Figure 43 Freezing profile of mannitol solution: (A) resistance vs time profile (B) temperature vs time profile.

The fit results for all concentrations are given in Table 5.

Table 5 Results from two-step sigmoid equation fit from the resistance profile of 5% to 15% w/v mannitol solutions during freezing

	Mannitol 5% w/v		Mannitol 10% w/v		Mannitol 15% w/v	
	Value	±SD	Value	±SD	Value	±SD
R_o	1.45	0.24	3.14	0.78	2.59	1.04
t_1	2.64	0.45	2.68	0.45	1.74	0.01
t_2	3.15	0.53	3.19	0.53	2.01	0.03
h_1	16.12	2.74	13.77	2.42	11.08	0.99
h_2	6.61	1.78	12.94	2.63	6.26	0.66
ΔR_1	95.09	2.71	113.66	10.14	83.50	18.84
ΔR_2	57.48	3.62	82.82	2.38	110.76	10.82

Of these fit results, only the parameter ΔR_2 shows a linear increase as the solute concentrations was increased in the solution (Figure 44). The maximum values of the second peak in the time derivative of R profile (relating to mannitol crystallization) also follow a linear trend (Figure 44). The broad agreement in the profile of ΔR_2 (from the fit results) and the time derivative confirms the application of both parameters in the estimation of extent of solute crystallization during the freezing.

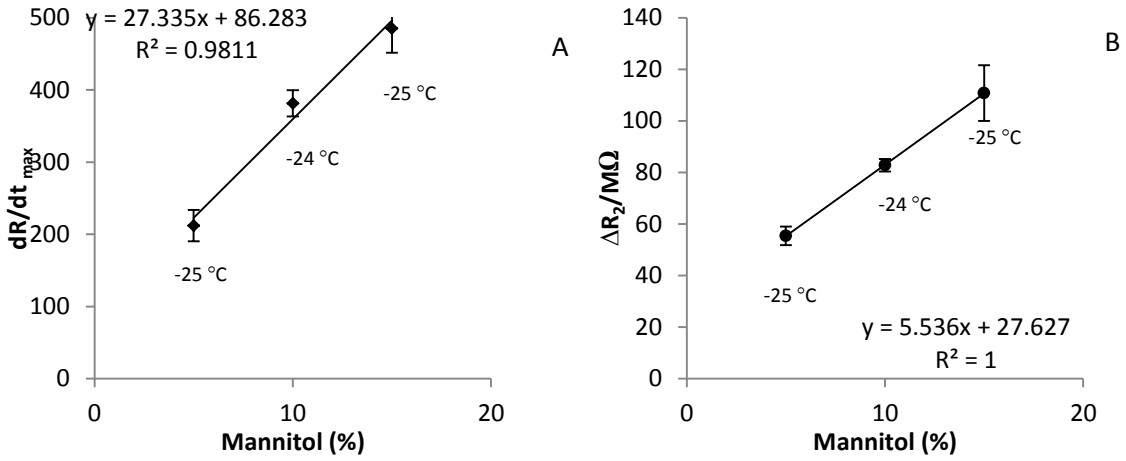

Figure 44 Electrical resistance response of mannitol solutions during solute crystallization: (A) dR/dtmax and B) ΔR2 vs. solute concentration plot for mannitol crystallization (n 4, error bars = one SD).

Impact of added sucrose on the crystallization of mannitol: The crystallization of mannitol is frequently reported to be impacted by additional solutes that are included in the formulation, for example polyvinylpyrrolidone and buffer salts (Cavatur et al., 2002). In the present study, the freezing profile for the electrical resistance of different solutions (mannitol 5% w/v, sucrose 5% w/v and sucrose 5% mannitol 5% w/v solution) were compared to evaluate the thermo-physical changes in the formulation as they approaches the freezing temperature (Figure 45). As described in the section above, changes in the product resistance identifies the various stages of freezing namely; product cooling, ice nucleation, solidification and temperature equilibration. Of note, is that the secondary post-ice formation step-like decrease in the R profile (represented as peak in the time derivative), which is indicative of solute crystallization, was not observed in the impedance profiles of the sucrose solution. This suggests that the solute in the latter solution exists primarily in the amorphous phase, following ice formation. In addition, the formulation containing both mannitol and sucrose (which exists as crystalline and amorphous state in the frozen solution respectively, when frozen as separate solutions) does not show the crystallization process that one would expect from the mannitol fraction alone. This observation of inhibition of mannitol crystallization due to the non-crystallizing co-solute (sucrose) is in agreement with the results reported from DSC measurements (Liao et al., 2005).

It is evident from the above results that the physical state of one component (i.e. mannitol) in a binary solution is influenced by the other accompanying solutes (i.e. sucrose). In such cases, the development of the freeze drying cycle will require the assessment of the glass transition

temperature of the mixture or the primary component of the formulation (another critical event ensuring the production of a stable freeze-dried solid) and then setting up the primary drying temperature below this temperature limit.

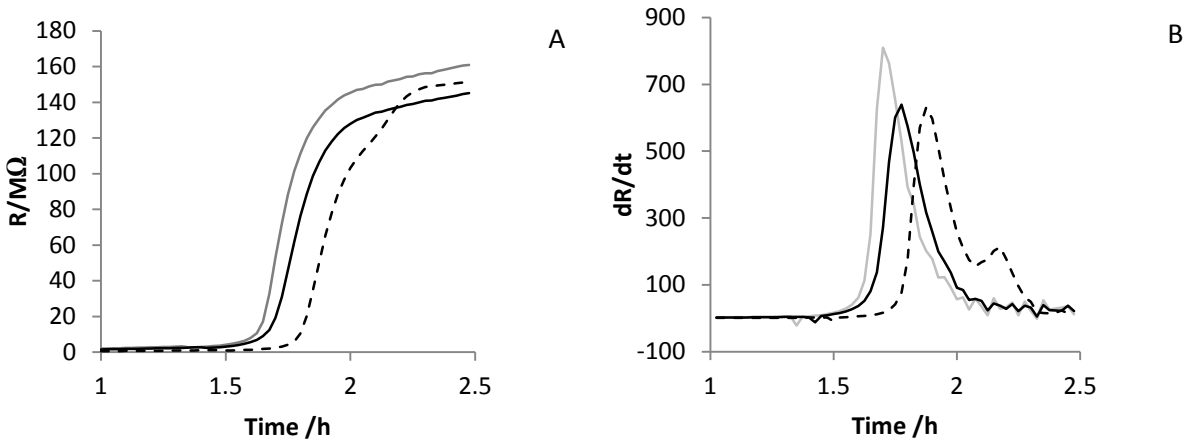

Figure 45 Resistance (A) and time derivative of resistance (B) profiles of Mannitol solution 5% w/v (-----), Sucrose solution 5% w/v (——) and mixture of mannitol 5% w/v and sucrose 5% w/v (——)solutions during freezing

6.5 Discussion

The impedance spectrum arising from the polarization of the solution-electrode interface was characterized by an equivalent electrical circuit model comprising of CPE R and C (Figure 31). Among the fit parameters, the element R exhibits a pronounced sensitivity in recording the different physical states of the solution, with ice formation and solute crystallization being evidenced by a two-step sigmoidal increase in the electrical resistance. While the latter is more prominent for high concentrations of mannitol (Figure 43) the time for eutectic crystallization was independent of the mannitol concentrations, suggesting that the crystallization occurred at a specific temperature during freezing.

In practice, solute crystallization is accomplished by adjusting the shelf temperature to a level that ensures the product temperature reaches the eutectic temperatures, as defined previously by an off-line technique such as DSC. Frequently, this requires the inclusion of an extended ‘safety’ temperature limit to accommodate any shelf to vial temperature differences, the thermal input arising from the thermocouple and the spatial distribution of temperatures across the shelf.

Here, through-vial impedance spectroscopy has been applied for the first time to observe directly the crystallization of the solute from mannitol solutions during shelf freezing. A good agreement between the mannitol crystallization temperatures recorded by the DSC instrument and the through-vial impedance measurement suggests the possible substitution of the off-line technique with the new in-line technique, while obviating the need for the temperature margin. Also, since the measurement probe does not make any physical contact with the contents of the formulation (as would be the case with a thermocouple probe) then the nucleation process is not perturbed.

Frequently, excipients which form amorphous structures are included with crystalizing excipients in order to benefit from the lyoprotection afforded by the amorphous excipient as well elegant cake structure provided by the crystallizing excipient. It follows that by monitoring performance of the formulation in-situ, during the real conditions of a freeze-drier, can provide information on the physical states of the excipients and their respective contribution towards the desired state. In this work it was demonstrated that the crystallization of mannitol was inhibited by the addition of sucrose though no further work was undertaken to examine the impact of this inhibition of crystallization on the cake structure. However, it is clear that the suppression of mannitol crystallization means that primary drying should now be undertaken at drying temperatures that are below the glass transition of the mixture (i.e. someway between T_g of sucrose, at – 34 °C (Hsu et al., 2003) and mannitol, at – 32 °C (Cavatur et al., 2002)). On the other hand, the inclusion of an excipient which inhibits the crystallization of the mannitol can be of value in exploring the cryo-protectant role of mannitol by promoting its amorphous state (Izutsu and Kojima, 2002). The micro-collapse of a non-crystallizing solute is sometimes permissible in a formulation containing higher proportion of crystalline bulking agent given that the crystallization of latter will prevent macro-collapse (Tang and Pikal, 2004). In so doing, the application of impedance measurement is expected to be helpful in the optimization of the formulation as well for cycle development.

6.6 Summary

It has been shown that the feature of the interfacial polarization process (i.e. peak position and amplitude) provide a satisfactory description of the changes in the physical state of a solution during the freeze-drying process, viz. ice formation and eutectic crystallization, and that impedance measurement can be applied to measure the impact of additional excipients on the eutectic crystallization of the product contained in the glass vial without impacting the freezing process. This provides the rationale for development of freeze drying cycles without unnecessary safety temperature margins as one would take in account with the results from off-line techniques.

7 Characterization of the Glass Transition by TVIS

Measurement of glass transition temperature of a formulation (Maltodextrin 10% w/v) during shelf freezing

7.1 Objective

The objective of this chapter is to study the application of that TVIS technology to the in situ measurement of the glass to liquid transition during shelf freezing in the glass tubing vials. For this purpose, impedance measurements were recorded from a surrogate product formulation comprising 10% w/v maltodextrin (DE 16-19.5) during freezing and re-heating. Comparison with off-line technique (DSC) was also made to establish the application of impedance spectroscopy. Enthalpic changes, evident from the in-vial impedance response were also characterized by the Vogel Fulcher-Tammann equation (VTF) to evaluate the strength of frozen mass.

7.2 Methods

Maltodextrin DE 16-19 was purchased from Sigma-Aldrich (UK) and used as supplied in the preparation of the solution. Distilled water was obtained from all-glass apparatus.

A surrogate solution containing 10% w/v maltodextrin was prepared by dissolving the solute (maltodextrin) in distilled water. Aliquots of 3.0 ml were introduced to the impedance measurement vials (N=2) using a syringe and 0.2 micron pore size micro filter Minisart®, Germany. One measurement vial (vial 1 Figure 46) was connected to a high precision impedance analyser and impedance measurements taken during the entire freeze-thaw cycle, over a frequency range 10^1-10^6 Hz with the scan interval of 3 min.[3]

[3] Scan interval defines the time between the start points of each frequency sweep.

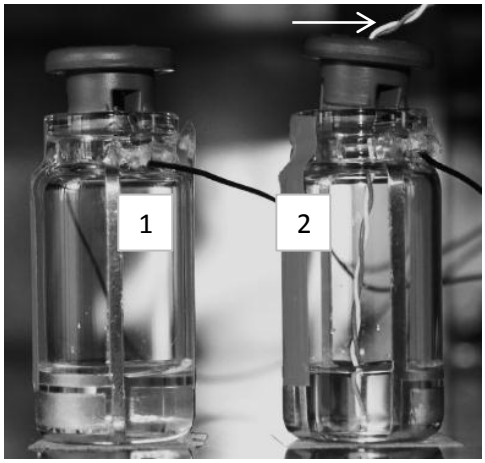

Figure 46 Linear Arrangement of the impedance measurement vials on the freeze drier shelf

Temperature measurements were recorded using a type K thermocouple, inserted in the second impedance measurement vial (vial 2, Figure 46), at time intervals concurrent with the frequency of the impedance measurements. Provided there was no change in the physical state in the solution then it was possible to equate the solution temperature, measured in the neighbouring vial to that within the impedance measurement vial to within a limit of ± 0.15 °C (Nazari, 2012). The reason why the impedance measurements were not recorded in the vial containing the thermocouple was that the presence of the non-grounded thermocouple perturbs the signal and disturbs the spectrum [4]. A cooling/re-heating cycle was then implemented according to protocol described in Table 6.

Table 6 details of the cooling/re-heating cycle

Stage	Temperature (°C)	Time (h)	Cummulative cycle time (h)
Freezing temperature ramp	-35	1	1
Freezing temperature hold	-35	5	6
Thawing temperature ramp	-5	2	8
Hold time	-5	4	12

DSC analysis was also performed by scanning the maltodextrin solution (10% w/v) over a temperature range of -60 to 20 °C at rate of 10 C min^{-1}, using a Jade DSC (Perkin Elmer, USA).

[4] This perturbation is more evident in the liquid state rather than the solid state.

7.3 Results and discussion

7.3.1 Differential Scanning Calorimetry

Thermograms of the maltodextrin solution 10% w/v (n = 3) indicate an endothermic transition which can be described as a peak in the time derivative of heat flow, with an onset temperature of −17 (± 0.5)°C, a mid-glass transition temperature of -15.6 (± 0.5)°C and an end temperature of -13.5 (± 0.3)°C. One such thermogram is shown in Figure 47. The glass transition temperature (T_g) was in agreement with the value given by (Biliaderis et al., 1999).

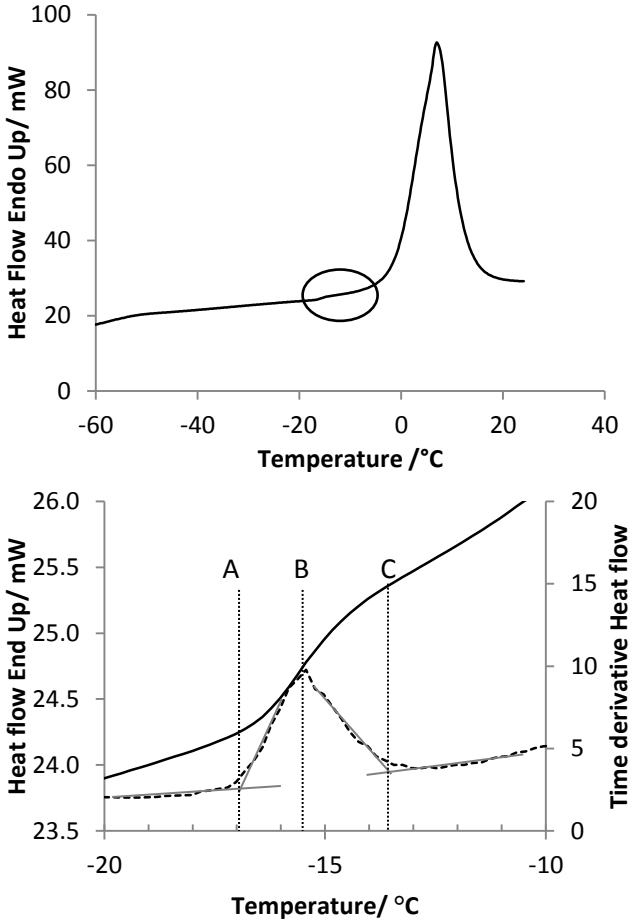

Figure 47 DSC results of Maltodextrin10% w/v solution. Top: Complete thermogram (area circled shows the approximate location of the glass transition). Bottom: Expansion of scale to show the glass transition as a step in the heat flow curve (solid line) and a peak in the derivative curve (dotted line). Point A, B and C shows the onset, midpoint and end set of the glass transition.

7.3.2 Impedance Measurements

The TVIS impedance measurement system records the physical changes of the solution in terms of the composite impedance of the electrode-vial- solution assembly. This composite impedance is responsible for the apparent interfacial relaxation process which is observed in experimental frequency window of 10^1 to 10^6 Hz as a step in the real capacitance (C') spectrum and as a peak in imaginary capacitance (C″) spectrum (Figure 48 A, B).

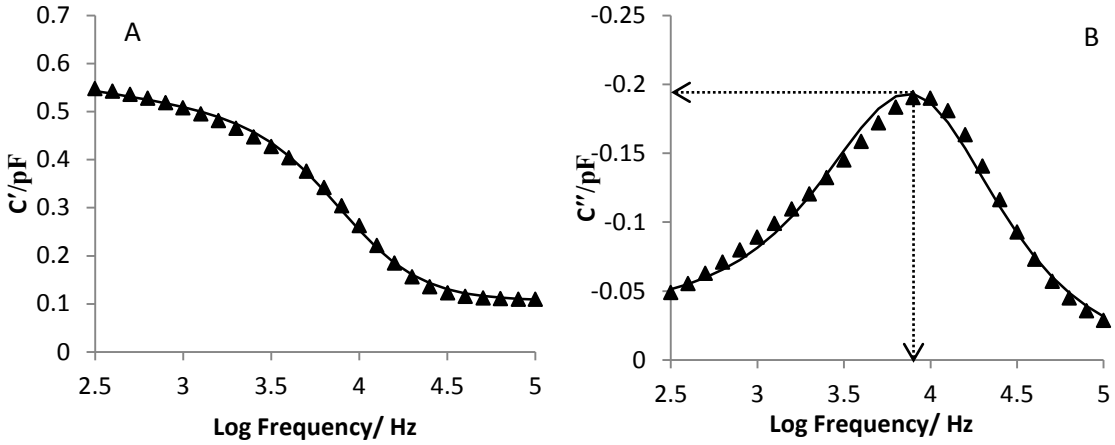

Figure 48 Capacitance spectrum of maltodextrin (10% w/v) at 270 min, when the solution had sufficient time to freeze solid. LEFT hand spectrum shows the real part (C') and the RIGHT hand spectrum shows imaginary part (C″). The triangle mark (▲) show the experimental data. Solid lines (——) describe the fit results to the data using the impedance model described in Figure 31

Changes in the interfacial relaxation process can be monitored empirically by assessing the changes in the peak amplitude (C''_{peak}) and peak frequency (f_{peak}) in the imaginary capacitance spectrum. Figure 48 illustrates how the frequency position, f_{peak}, and peak amplitude, C''_{peak} are derived from the imaginary capacitance spectrum. It has been demonstrated (chapter 4 and 5) that the characteristics of this interfacial-relaxation process are dependent on the electrical conductivity of the formulation, which is in turn dependent on the product temperature and physical state of the formulation (i.e. whether the solution is in the frozen/solid state or the liquid state). Furthermore, the features of the peak (the frequency position, f_{peak}, and peak amplitude, C''_{peak}) describe different stages of freeze drying process, i.e. temperature changes during the cooling of the solution, ice formation and sublimation (chapters 5,6 and 8).

Having defined these relationships, it is then possible to explain the changes in the peak frequency position in terms of the physical changes to the solution during the freezing and re-heating phases of the cycle. Figure 49 shows the temperature profile of the near-neighbour

vial (Figure 46; vial 1) and demonstrates the four phases of super-cooling (A to B); freezing (B to C), temperature equilibration with the shelf (C to D), and the re-heating or annealing phase (D to E). The corresponding changes that one can observe for the capacitance spectra are shown in Figure 50.

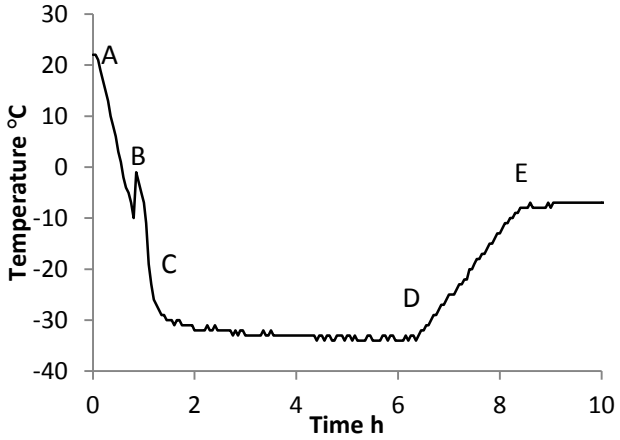

Figure 49 Temperature profile of maltodextrin 10% w/v during cooling and re-heating

In the super-cooling phase (Figure 49 region A-B) the interfacial polarization peak of the maltodextrin solution remains outside (i.e. the right of) the measurement frequency range (Figure 50 A, B) primarily because of the high solution conductivity (high conductivity translates to a low resistance, a fast time constant and therefore a high peak frequency). It was therefore not possible to document the frequency position, f_{peak}, and peak amplitude, C''_{peak} for this formulation in the unfrozen state. However, in the ice formation stage, the solution viscosity increases dramatically and so does the electrical resistance of the solution. The peak frequency then decreases and brings the interfacial-relaxation peak within the experimental frequency range (Figure 50 C, D). In the ice nucleation and growth region (Figure 49 region B-C), the precipitation of ice concentrates the unfrozen fraction (containing maltodextrin), the viscosity of the system increases and the number of mobile charge carriers decreases. The overall result is a rapid increase in solution resistance and a shift in the interfacial-relaxation frequency so that it appears in the experimental frequency range (Figure 50 C and D). Finally, during the re-heating of the solution (Figure 49 region D-E) the increase in temperature decreases the electrical resistance of the solution and the interfacial-relaxation process shifts to higher frequencies (Figure 50 E and F).

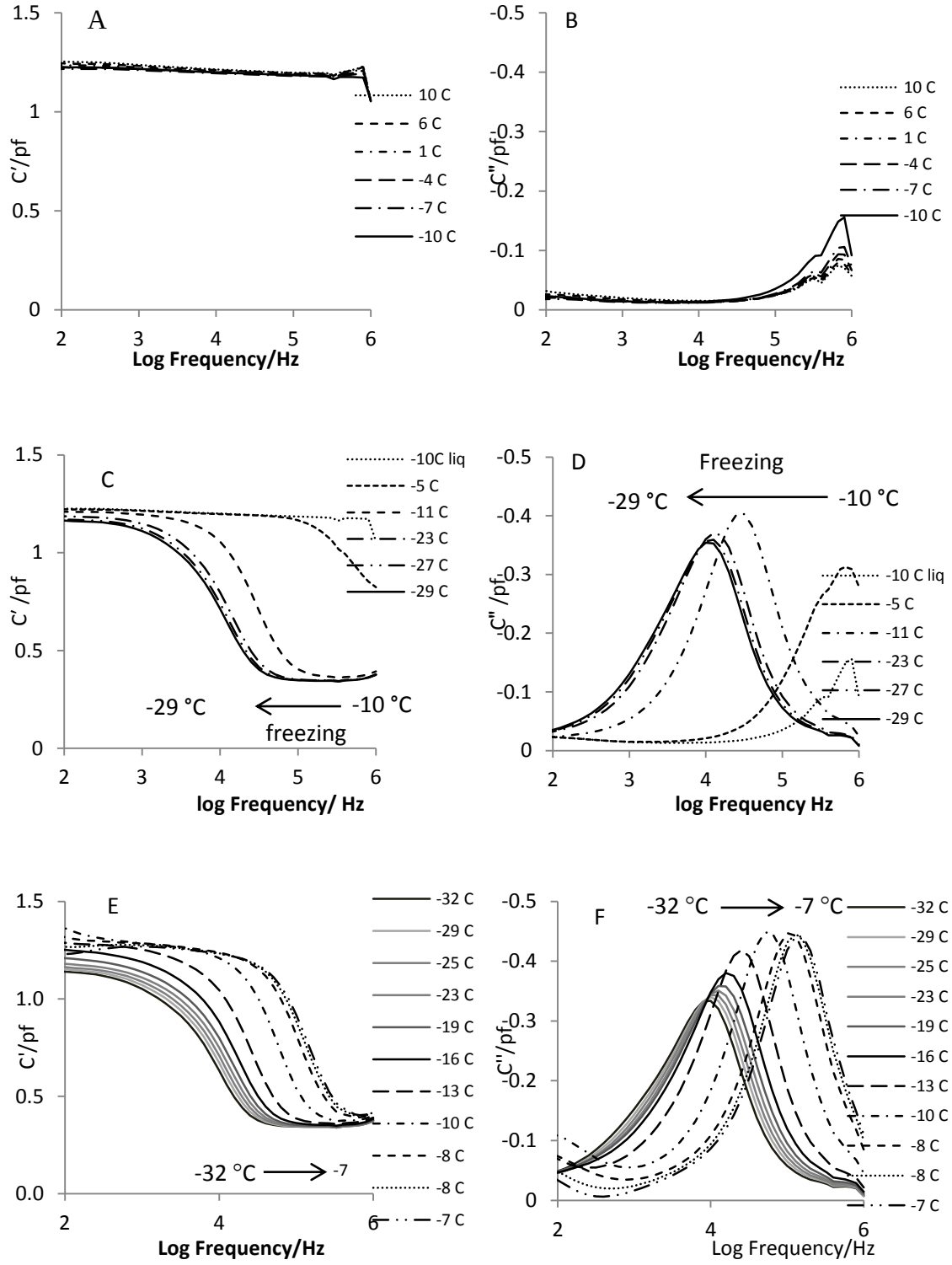

Figure 50 Capacitance spectrum of maltodextrin (10% w/v) in liquid state (Left side shows the real part capacitance and the right side shows the imaginary part capacitance); The interfacial-relaxation peak exist above the measurement range, and frozen states (c, real part and d, imaginary part); the interfacial relaxation peak were recorded during thawing of the frozen solution from -32 °C to -7 °C (e, real part and f, imaginary part).

Determination of the glass transition temperature

The objective of this part of the study is to establish which of the four parameters derived from the impedance response of the freeze-drying vial, containing a solution of glass forming solute (i.e. the peak frequency, f_{peak}, and peak amplitude, C''_{peak}, from the imaginary capacitance plot, and the estimates for the solution resistance and solution capacitance, R and C, respectively) provides the clearest assessment of the glass transition temperature.

Three approaches to the registration of the glass transition, or more precisely the glass to liquid transition (GLT), are described. The first is the manifestation of the GLT in the time profiles for the four parameters of interest (i.e. the f_{peak}, C''_{peak}, R and C); the second is the manifestation of the GLT in the temperature profile of the same four parameters (i.e. where each parameter, as determined from the impedance response of vial 2, is plotted against the temperature recorded in vial 1); and the third is the manifestation of the GLT in the time derivative of each of the four parameters, plotted against the temperature recorded in the neighbouring vial.

In all three approaches, each of the four parameters (f_{peak}, C''_{peak}, R and C) demonstrated an inflection in the profile, which is taken to be the glass transition of the solution. In general terms, the inflection in each parameter may be explained by the increased mobility of the molecules/ions following the second order phase transition from the glassy state to viscous rubber and liquid. For each approach, a simple method of 'intersecting straight lines' was used to extract a 'definitive' assessment of T_g from the four parameters. This method assumes (rightly or wrongly) that the data above and below the transition can be taken as linear. The data was partitioned into two sets (i.e. data above and data below the transition temperature) based on the visual assessment of the apparent transition temperature; and the lines of best fit to each data set calculated by linear regression. By equating each line of best fit to one another it was then possible to estimate the transition temperature.

The change in the gradient of each best fit line was then used as an index of the potential discrimination that each parameter has for observing the glass transition. In other words the greater the % change in the gradient the more likely it is that the parameter in question would be able to observe the glass transitions.

Time Profiles for f_{peak}, C''_{peak}, C and R The parameters derived from the peak analysis (f_{peak} and C''_{peak}) and impedance modelling (R and C), and the temperature recorded by the thermocouple, are show in Figure 51 as a function of time elapsed through the freezing cycle. The first observation to note is that while the temperature rise is linear with time as the product temperature was raised from -32 to -7 °C, all the parameters from the interfacial relaxation process show discontinuities in the time profile at the ~ 8h which correspond to the temperature passing through the range -14 to -17 °C (Table 7).

Both the f_{peak} and C''_{peak} parameters have an inflection point at 7.9 h whereas the impedance modelling parameters R and C have an inflection point at 7.75 h, which correspond to the temperatures -14 °C and -16 °C respectively (Figure 51 a, b, c and d respectively). Estimate for the GLT R and C were therefore in closer agreement with the DSC results than f_{peak} and C''_{peak}.

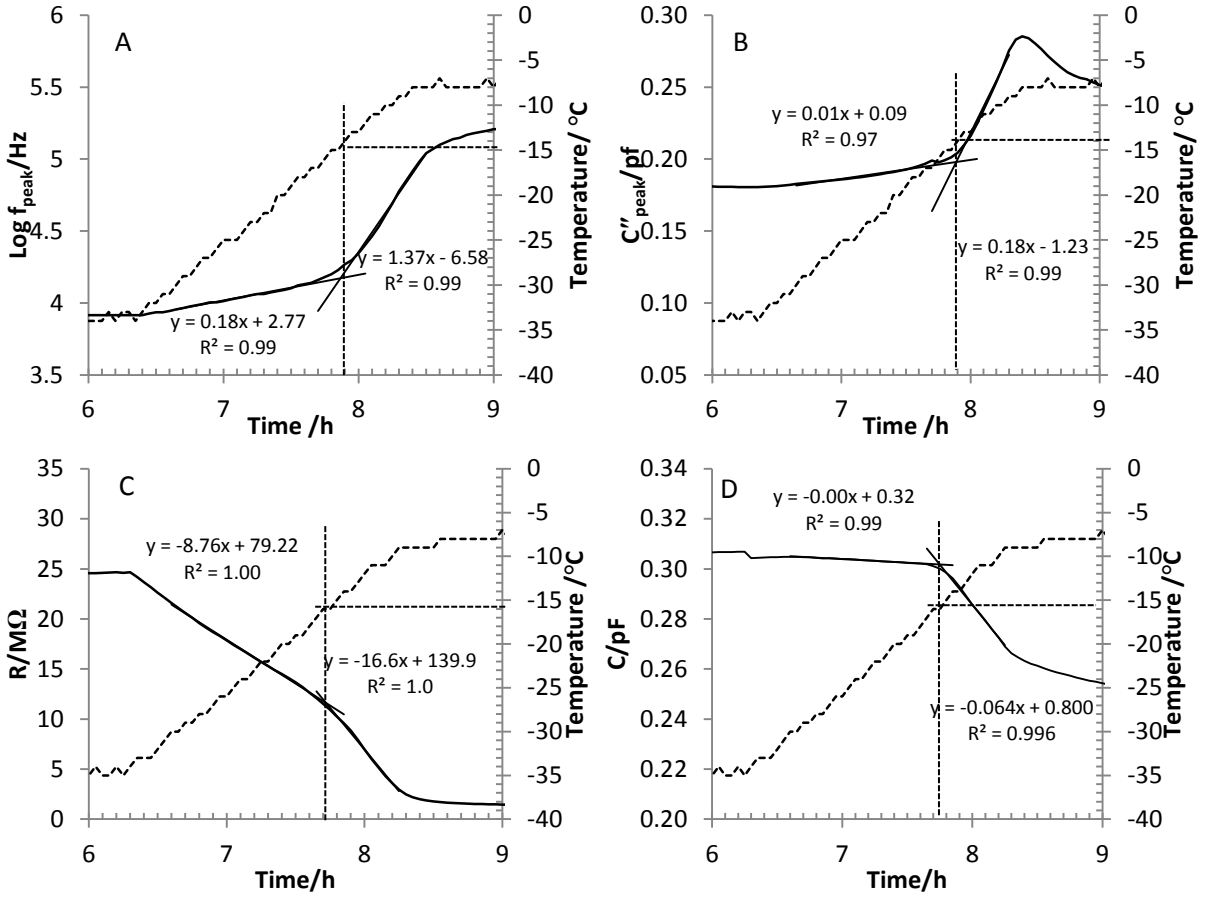

Figure 51 Time profiles of parameters (A) f_{peak} (B), C''_{peak}(C), R and (D) C from spectral analysis of a 10%w/v aqueous solution of maltodextrin during re-heating the solution from -32 °C to -7 °C

Table 7 Regression line parameters for the lines of best fit to the time dependencies of the spectral peak analysis and impedance modelling parameters, at temperatures below and above Tg

	Inflection Time (h)	Below T_g			Above T_g		
		slope	intercept	R2	slope	intercept	R2
f_{peak}	7.9	0.178	2.772	0.9928	1.367	6.578	0.994
C''_{peak}	7.9	0.013	0.095	0.966	0.181	-1.227	0.990
R	7.75	-8.757	79.220	0.999	-16.623	139.950	0.997
C	7.75	-0.003	0.324	0.985	-0.064	0.800	0.996

Temperature Profiles for f_{peak}, C''_{peak}, C and R In order to be clearer about the specific temperature at which the apparent glass transition is observed, the parameters derived from peak analysis (f_{peak} and C''_{peak}) and impedance modelling (R and C) where then plotted as a function of the temperature recorded by the thermocouple in the 1st vial (Figure 52). As with the time profiles, all parameters show a discontinuity in the rate of change at some temperature in the range -14 to -16 °C (Table 8) which again corresponds to the glass transition as measured by DSC.

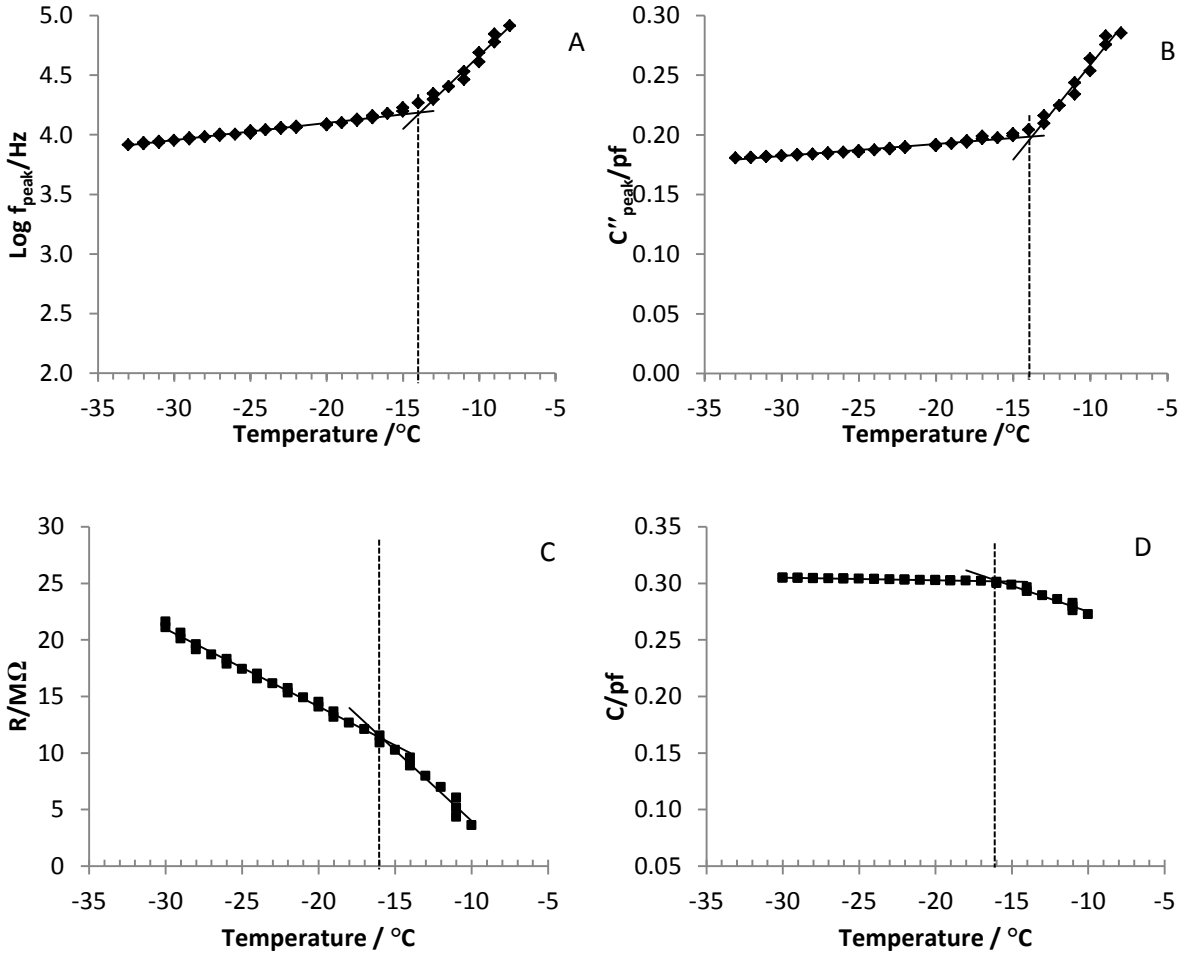

Figure 52 Temperature profiles of parameters (A) f_{peak} (B), C''_{peak}(C), R and (D) C from spectral analysis of a 10%w/v aqueous solution of maltodextrin during re-heating the solution from -32 °C to -7 °C

Table 8 Regression line parameters for the lines of best fit to the temperature dependencies of the spectral peak analysis and impedance modelling parameters, at temperatures below and above Tg

Parameter	Inflection temperature (°C)	Below Tg			Above Tg		
		slope	intercept	R2	slope	intercept	R2
f_{peak}	-13.9	0.0145	4.3883	0.9865	0.1228	5.8893	0.9618
C''_{peak}	-13.8	0.001	0.2126	0.9568	0.0159	0.4172	0.9623
R	-16.0	-0.687	0.3682	0.9916	-1.2482	-8.4818	0.9655
C	-15.8	-0.0002	0.2992	0.9833	-0.0046	0.2291	0.9528

The derivative profiles of f_{peak}, C''_{peak}, C and R The time derivatives of the impedance parameters $F_{peak,}$ $C''_{peak,}$ and the impedance modelling parameters C and R were calculated from the slope of the time dependent response over a period of 0.5h. This routine was continued through the entire cycle. As above, the temperature values corresponding to glass transition were estimated from the intersection between the line of best fit, above and below the inflection points. What is interesting to note is that the gradient above T_g continues to change with temperature, which means that the temperature profiles for each parameter above T_g are not linear, as assumed in the analysis above. This may explain why the inter-section of the two lines of best fit provide an estimate for T_g which are, in general, lower than that determined by DSC.

The glass transition temperature derived from time derivative data are summarized in

Table 9. The T_g value calculated from time derivative of C''_{peak}, f_{peak} and element C were ~-17 °C whereas that from element R was ~ -19 °C (Figure 53) (Table 8). Therefore, of the three approaches to the determination of the glass transition, it was the third method using the plot of the derivative of the inerfacial-relaxation parameters (C''_{peak}, f_{peak}, R, C) that provided the closest estimates to that determined by DSC.

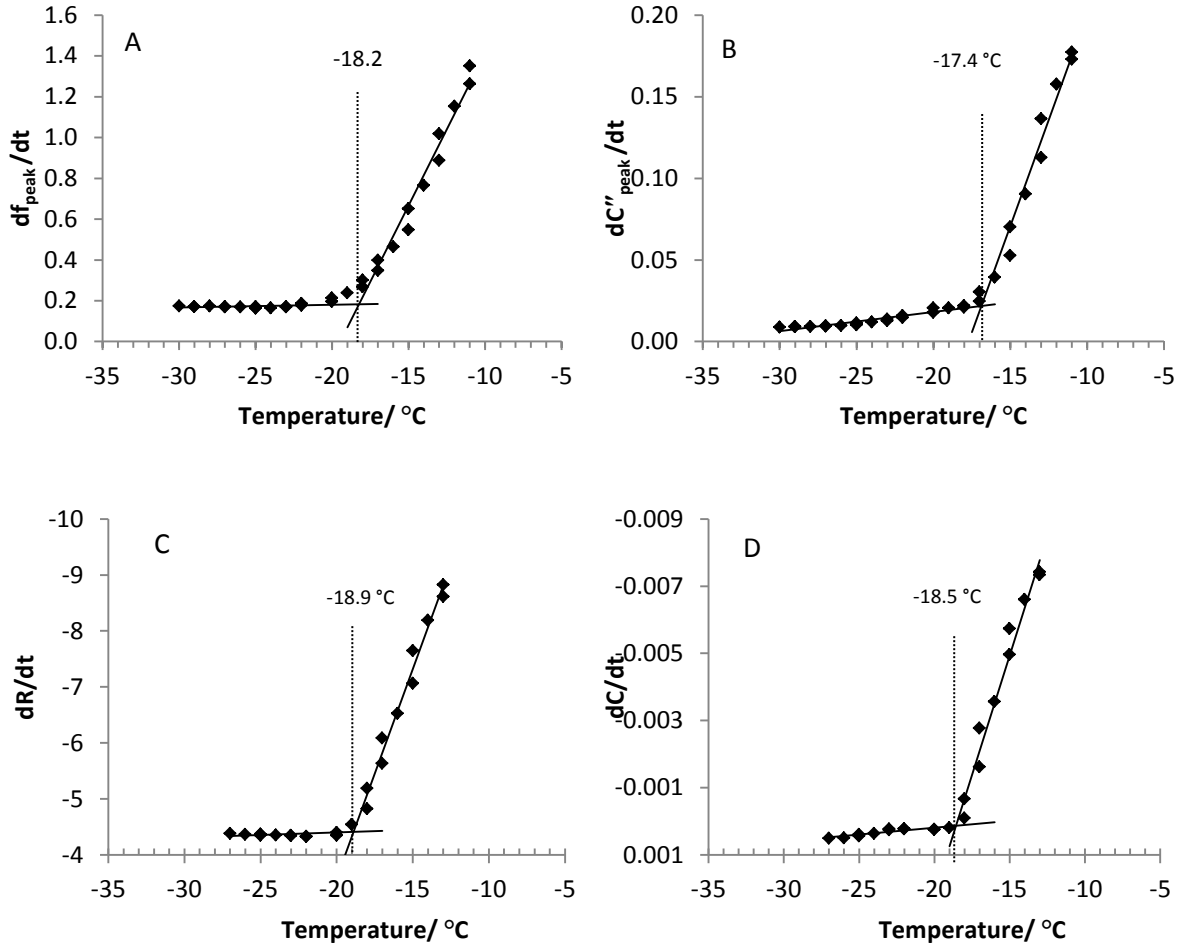

Figure 53Time derivative profiles of parameters (A) f_{peak} (B), C''_{peak} (C), R and (D) C from spectral analysis of a 10%w/v aqueous solution of maltodextrin during re-heating the solution from -32 °C to -7 °C

Table 9 Regression line parameters for the lines of best fit to the time derivative of the spectral peak analysis and impedance modelling parameters, at temperatures below and above Tg

Parameter	Inflection temperature (°C)	Below Tg			Above Tg		
		slope	intercept	R	Slope	intercept	R
$dlogf_{peak}/dt$	-18.2	0.0014	0.2075	0.2342	0.1492	2.9046	0.9721
$dC''_{peak}(pF)/dt$	-17.4	0.0012	0.0416	0.9078	0.026	0.4611	0.972
dR/dt	-18.9	-0.0089	-4.5773	0.1596	-0.07479	-18.579	0.9777
dC/dt	-18.5	-0.00004	-0.0006	0.8172	-0.0014	-0.0262	0.9698

Having established that the derivative plots provide estimates for T_g which are closer to those determined by DSC, the question remaining is which parameter (dF_{peak}/dt, dC''_{peak}/dt,, dC/dt,

or dR/dt) provides the most reliable assessment of the glass transition temperature. Two ways of making this judgment were proposed: The first was to assess the % change in the gradient between the line of best fit above T_g and the line of best fit below T_g, whereby the denominator in this equation was taken from line with the largest gradient. In all cases this was the gradient from the line of best fit to the data above the glass transition T_g (Equation 41).

$$\% \text{ change} = 100 \times (\text{gradient above } T_g - \text{gradient below } T_g) / \text{ gradient above } T_g \quad \text{Equation 41}$$

The percentage change in the gradient of regression line can be considered as one indication of the sensitivity of that parameter to the glass transition and hence the potential resolution afforded.

The second approach was to use the root mean squared error for each line to determine the uncertainty in the estimate for T_g. In this method the upper limit for the uncertainty in T_g was calculated by adding the RMS error to the value of the intercept for the sub T_g line and subtracting it from the line of best fit for the intercept for the supra- T_g line (Figure 54 B). The lower limit was calculated in an analogous way.

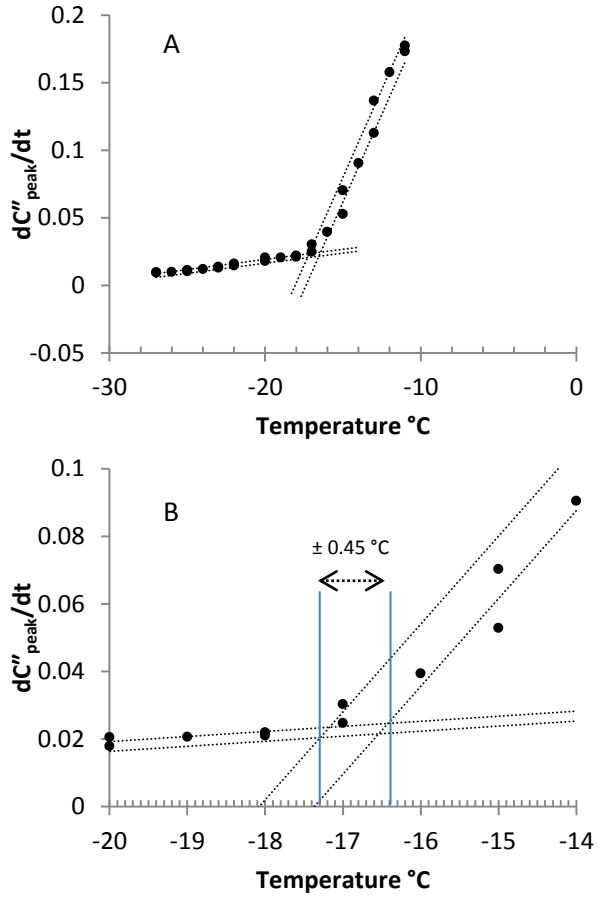

Figure 54 Temperature profile of dC''_{peak}/dt to illustrate the methodology for calculating the uncertainty in Tg from RSM errors. (A) full data set; (B) reduced data set close to T_g. Dotted lines show the RMS error between the line f best fit and the experimental data

This assessment of the degree of uncertainty can be taken as a measure of the precision of the estimate of glass transition.

The rank order of parameters for % change in the gradient following the glass transition was observed as $f_{peak} \sim C \sim C''_{peak} > R$, whereas the rank order of parameters for the uncertainty in the inflection temperature was $C \sim R < C''_{peak} < f_{peak}$ (Table 10).

Table 10 Percentage increment in the slope of regression line of time derivatives of parameters fpeak, C″peak, R and C following glass transition

Parameter	% increment in slope	(Inflection temperature, T_g; °C)	Uncertainty in the inflection temperature (±°C)
dlogf_{peak}/dt	99	-18.2	0.5
dC″$_{peak}$(pF)/dt	95	-17.4	0.45
dR/dt	88	-18.9	0.3
dC/dt	97	-18.5	0.3

7.3.3 Characterization of the glass forming liquid, above and below Tg

Of the four parameters that model the impedance response, it is the product resistance (R) which reflects the charge transfer processes through the frozen solution. The origin of the charge, in a frozen aqueous solution are likely the protons which are liberated from water and then hop from one hydrogen bond to another (Cukierman, 2006).

As, explained earlier, there is a direct relationship between R and f_{peak} (i.e. $f_{peak} \alpha 1/R$) and so the parameter f_{peak} may also be used to track changes in the physical state of the frozen solution. However, this is predicated on the requirement for |CPE| to remain constant during the annealing phase. Figure 55 shows the temperture dependency of |CPE| during the annealing phase. The change in |CPE| over the VTF temperature range is ~ 9 %, thereby questioning whether this parameter may be considered as a constant over the range of temperatures investigated .

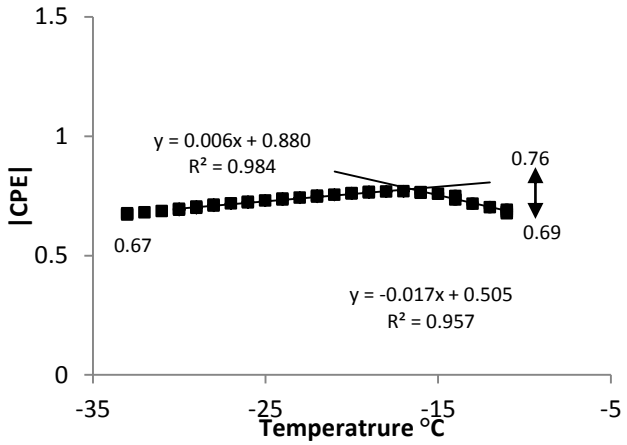

Figure 55 Temperature profile of impedance modelling element CPE

Changes to both R and $1/f_{peak}$, over the temperature ranges either side of the glass transition temperature, were then characterized by the mathematical expression for Arrhenius behaviour and the simplified expression for Vogel Futcher Tammann (VTF) behaviour, (Equation 42and Equation 43 respectively) in order to understand the physical behavior of the solution in both the glassy and liquid states (Figure 56).

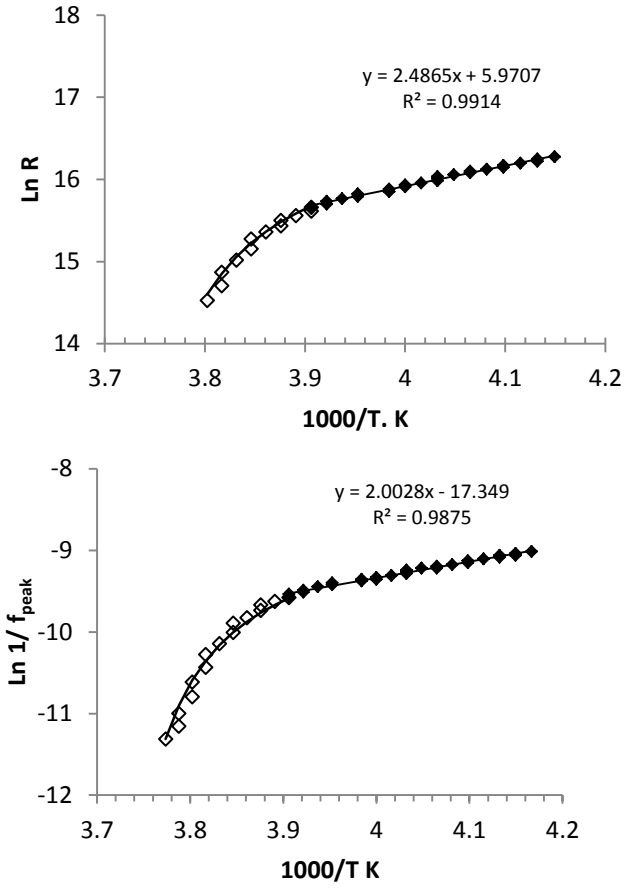

Figure 56 Arrhenius plot showing the temperature dependence of the resistance element R and the peak frequency (f_{peak}) for 10% w/v maltodextrin

$$\ln A = \ln Ao - Ea/RT \qquad \text{Equation 42}$$

In Equation 42, Ao is pre exponetial value, Ea is energy of activation (Joule.mol^{-1}), R is the gas constant (8.314 J.K^{-1}.mol^{-1}), and T is the temperature in Kelvin.

$$\ln A = \ln A_{\infty} + B/(T - T_o) \qquad \text{Equation 43}$$

In Equation 43, A_{∞} refers to the pre-exponential values of the product resistance and f_{peak} at low temperature, B is the constant relating to the diffusivity of molecules (or charge carriers in the present case) and T_o is a constant known as the Vogel temperature. In effect the VTF function is modelling the non-linearity in the Arrhenius plots for resistance (R) and peak frequency (f_{peak}) above T_g.

From the Arrhenius plots of f_{peak} and R, the energy of activation below T_g was found to be 17±1 and 22±1 kJ mol^{-1} respectively (Figure 56). The latter was in close agreement with the activation energy reported for maltodextrin solutions using electron spin resonance (ESR) spectroscopy (Orlien et al., 2004). The activation energy in the sub-Tg region has been ascribed previously to hydrogen bond dissociation (Chaplin, 2007) and can be considered as the average strength of a hydrogen bond in the unfrozen fraction. The fact that f_{peak} provides a slightly lower estimate for activation energy might suggest that the earlier assumption of CPE remaining constant over the measured temperature range may not be strictly accurate.

The fit parameters for the VTF function are given in Table 11. Close agreement between the estimates for B and T_o suggest that either method could be used to characterise the unfrozen fraction above the glass transition temperature.

Table 11 VTF fit results of Maltodextrin 10% w/v solution

parameter	Ln A_∞	B	T_o (K)
R	16.88	-0.265	271.2
$1/f_{peak}$	-8.5	-0.235	271.0

The fragility index (I_f) was defined by the Equation 44

$$I_f = T_o / T_g \approx 1 - \mathrm{B.R}/E_a \qquad \text{Equation 44}$$

Where B is VTF fit parameter, R is universal gas constant and E_a is the energy of activation from the Arrhenius fit results. The index suggest value of $I_f = 0$ for strong glasses while > 0.6 describe fragile glasses. For maltodextrin solution, the I_f value was ~ 0.9, which suggests a fragile nature of the frozen glassy solution (Rault, 2000).

Another empirical approach for estimating the fragility parameter above the glass transition is to calculate the slope (m) of Ln R (Equation 45) and f_{peak} between T_g to $T_g/2$ (Figure 57)

$$\text{Slope (m)} = \text{d Ln R}/\text{d}(\text{T}/T_g) \qquad \text{Equation 45}$$

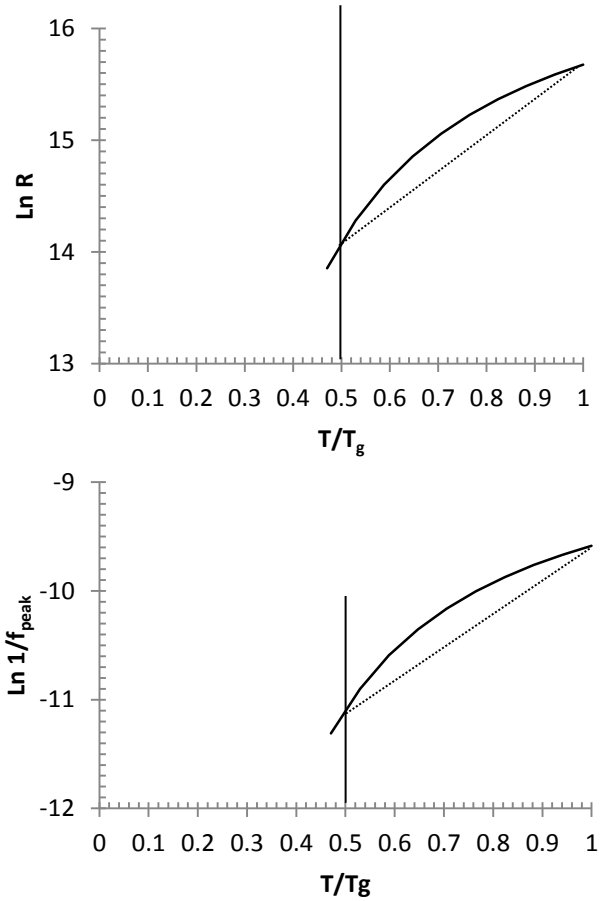

Figure 57 VTF fit line above Tg for 10% w/v maltodextrin

The slope (m) for both parameters R and $1/f_{peak}$ was recorded as 0.75.

7.4 Discussion

Different methodologies are described for analysing the interfacial-relaxation peak arising from the composite impedance of the solution-glass-wall assembly of a liquid filled freeze-drying vial, with a view to defining the glass to liquid transition of a 10% solution of malto-dextrin. The derivative of the time profile of a number of parameters (f_{peak}, C''_{peak} R and C) were found to give the closest estimate to the DSC value (-17 °C) with a precision of (± 0.5 °C). The exploitation of this understanding will become most relevant when the in-vial impedance measurement approach is extended to the determination of the glass transition in

more dilute solutions. Although not reported here, it has been demonstrated that the same methodology may be used to characterise glass forming solutions of poly vinyl pyrrolidone (PVP) and lactose.

The in-situ impedance measurement described in this chapter may be more suitable than a number of off-line techniques, e.g. DSC and electrical impedance, as the latter are expected to measure a T_g' which is different to that experienced by a solution frozen in the vial, due to the fact the former freezes at a comparatively high rates and that the container geometry and sample volume are very different. These features of the off-line techniques could provide a greater degree of super cooling and result in a lower concentration in the unfrozen fraction and therefore a lower glass transition temperature.

The accurate determination of T_g' on the production line may have some relevance to process control strategies in that it may enable the operator to drive the primary drying stage at a higher temperature than is permitted by convention. By convention, the shelf temperature during the freezing stage is usually set at 2-3 °C < T_g' in order to allow for the thermal loss associated with glass vial base. And since a thermocouple probe does not evidence any visible change in the temperature profile following a second order transition (such as the glass transition) then these probes are simply employed to register with the previously measured temperatures (off-line tools) corresponding to the glass-liquid transition of the solution.

This margin in temperature is also applied to real freeze-drying processes because one cannot be sure about the spatial distribution of temperature in the drier, given that there is a thermal lag between the shelf and the vial contents due to the poor thermal contact between the shelf and the vial base. The advantage of a single vial measurement technique, such as that provided by the impedance technology proposed here, is that it may be used to monitor critical domains within the drier where hot and cold spots define the extremes of temperature experienced by the whole population of vials across the drier. A multi-channel approach to the proposed impedance measurement system could analyse a number of vials simultaneously and, hence it could be employed to record the glass transition at different spatial position across the shelf. This would provide a realistic soak time required to ensure the entire formulation units have approached glass transition.

The time derivative of the in situ impedance measurement could then be used to signal that all vials have passed through the glass transition temperature and that it is safe to continue from pre-freezing to primary drying. This would also deliver process efficiencies as it would enable the operator to drive the primary drying stage at a higher temperature than might be permissible if a safety margin of a few degrees in temperature had to be applied. Rather than controlling the process on the basis of temperature (with the safety margin applied) one could instead control the process based on a set point, one which is defined by the observation as to whether the population of vials have their contents in the desired physical state. In this case the desired state is that the solution is in the high viscosity state of a rigid glass.

The physical properties of frozen glassy solution are explained in terms of the unfrozen fraction of the water, the freeze concentration of the solute and the size distribution of ice crystals. Below-T_g, the observed Arrhenius behaviour suggests that a proton hoping phenomenon under pins the charge transport processes. Above T_g, a good correlation with the VTF function suggests a cooperativity in the motions of molecules following an increased free volume.

Various approaches were taken to determine the fragility parameter of the unfrozen fraction above T_g'. All provide reasonable estimates which are similar to those found in the literature for aqueous solution of polymers (Borde et al., 2002). The fragility parameter may have direct relevance to process development, especially in regard to the impact of annealing on the concentration of water remaining in the unfrozen fraction. A decrease in the slope factor (i.e. a tendency to become more linear) following annealing, may point to an increased strength of the glass (i.e. reduced fragility). The significance of the fragility to freeze-drying method development is that it may provide a useful index for the concentration of water in the unfrozen fraction, given that fragility is known to increase with increasing water fraction. Indeed water itself shows the highest fragility. The transformation of water from the unfrozen to frozen state may lower the risk of melt back or collapse during the drying stages. In addition, a conditioned (i.e. annealed) frozen product formulation may therefore dry quicker (in the secondary drying stage) than a non-annealed formulation. This may also have further implications for the lyophilisation of biopharmaceuticals whereby the concentration of protein in the unfrozen fraction could have a bearing on the destabilization of the protein through phenomena such as aggregation.

A more in-depth and mechanistic interpretation as to the impact of composition on the fragility of the glass forming materials have been proposed previously (Coslovich and Pastore, 2009) which suggests that the phenomenon may be linked to the local heterogeneity in the dynamics of fragile glass formers. In binary systems, such as a super-cooled solution of maltodextrin, this might even suggest slow and fast regions which are either polymer rich or water rich respectively. It is outside the scope of this study to expand further on such possible interpretations.

The relevance of the glass transition to maintaining a high solution viscosity and the avoidance of the collapse was highlighted in section 1. However, the problem with the measurement of collapse (whether it is by off-line freeze-drying microscopy or by an on-line technique such as extra-vial impedance measurements) is that there is no prior indication that collapse is about to occur. In other words, there is no inflection in any measureable physical parameter which might signify a pre-collapse microstate has been reached. In addition the thermal inertia of the freeze-drying process means that it would be almost impossible to reverse a temperature ramp that projected the frozen solution to a state of collapse. Instead, what may be possible is that there is a link between the fragility determined by the in situ impedance measurement and the propensity for a super-cooled matrix to collapse. This possibility will form the basis of future articles using impedance spectroscopy.

It has been shown that impedance measurements can be applied to measure the glass transition of the product contained in the glass vial without impacting the freezing process. This provides the rationale for the development of freeze drying cycles without the necessity of a safety temperature margin which makes allowance for the variation in thermal conditions across the shelf. By probing the spatial map of the thermal characteristics across the shelf using impedance measurements at critical positions, e.g. corners and centre of each shelf, one may be able to determine whether the batch has collectively passed through the glass transition during freezing. That would then enable one to set appropriate annealing conditions (set temperatures and holding times) which could then lead to the optimization of the process. This work has also demonstrated the use of in-situ measurement in characterizing the strength of glass forming solution above T_g and highlights the potential application in both formulation and process development for biopharmaceuticals in particular.

As the impedance measurement defines both the glass transition and primary drying end point, it follows that this technological approach may be employed in a multi-functional and non-invasive way: First to establish the freezing and primary drying temperatures, then secondly to investigate the optimum annealing temperature and to study its consequences in term of primary drying time in the real process conditions. In comparison with the conventional methodologies practiced for freeze drying method development/optimization (i.e. product characterization by off-line tools and product temperature measurement by invasive thermocouple probes), the impedance measurement technology offers a reliable measurement of the critical product and process parameters and is therefore expected to reduce the number of trial runs commonly performed during the development of a freeze drying cycle.

7.5 Summary

The characteristics of a glass forming solution (10% w/v maltodextrin) have been observed for the first time by in situ measurements of the electrical properties of the solution, with the electrodes attached to the external surface of the freeze-drying vial. The time derivatives of all four parameters studied (F_{peak}, C''_{peak}, R and C) provided a glass transition for the malto-dextrin solution in close agreement with DSC measurements (−17 °C) and to a precision of +/- 0.5 °C. The fact such measurements may be taken on clusters of vials, without impacting the hexagonal spatial arrangement that one normally expects to have in a production scale drier, suggests an opportunity for using such measurements in the development and monitoring of the freeze-drying cycle, in a way that could not be achieved with currently available techniques. It was also demonstrated that an impedance measurement with external electrodes could be used to characterise the glass forming properties of the solution. The first notable observation was that energy of activation energy below T_g was of an approximate magnitude to that of the hydrogen bond (ΔH ~20 kJ mol^{-1}) and suggests that the charge transport mechanism under-pinning the electrical conductivity of the frozen solution was proton hopping. Finally, the fragility index (I_f = 0.9) of the glass forming liquid, above T_g, was calculated from the VTF function. The significance of this parameter to the freeze-concentration and stability of biopharmaceuticals, in particular, was then highlighted.

8 Primary Drying Rate and Primary Drying End Point Determination by TVIS

Impedance measurement during the complete freeze drying cycle; Measurement of primary drying end point of a Sucrose 2.5% w/v formulation

8.1 Objective

The objective of this chapter is to study the application of TVIS technology in the characterization of the primary drying stage of the lyophilisation process. For this purpose the impedance measurements were recorded from a surrogate formulation containing 2.5% w/v sucrose in deionised water over a complete freeze drying cycle. The main focus of this section is the determination of the end point of the primary drying stage. The results from impedance spectroscopy were compared with the temperature profiles recorded with thermocouple (a conventional process analytical technique) to confirm the relevance of the former in recording product response.

8.2 Methods

A 2.5% w/v sucrose solution was prepared in distilled water. Aliquots (3.0 ml) were introduced to the measurement vials using a 5 ml syringe and a micro filter Minisart® NML, 0.2µm pore size (Sartorius, Germany), to ensure particulate free transfer of the liquid. The measurement vials were arranged in a straight line (position 1-5 from Left to-Right) behind the Perspex door to facilitate photographic imaging (Figure 58).

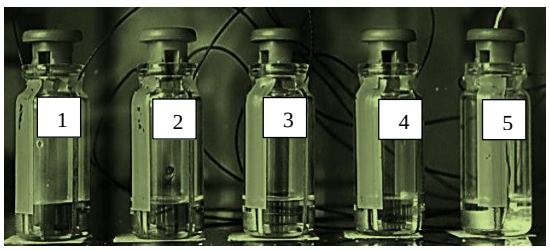

Figure 58 A linear arrangement of the measurement vials on the freeze drier shelf

The vial at position 5 also contained a type-K thermocouple in order to assess what might be a representative product temperature.

The shelf temperature was set below the glass transition temperature (T_g') of sucrose (-34 °C). T_g' was determined by differential scanning calorimetry of the sucrose solution over a temperature range -50 to 30 °C at 10 °C min^{-1} using a Jade DSC (Perkin Elmer, USA). The chamber was set at a pressure of 0.1 mbar, which corresponds to approximately half of the water vapour pressure at the ice surface (0.22 mbar (Oetjen, 2007). The freeze-drying protocol is described in Table 12.

Table 12 Freeze drying protocol

Step	Temperature °C	Duration (h)	Time (h)	Vacuum mBar	Ramp/Hold	Stage
I	-35	1.0	1.0	1000	Ramp	Ramp to freezing temperature
II	-35	2	3.0	1000	Hold	Hold at freezing temperature
III	-15	1	4.0	1000	Ramp	Ramp to annealing temperature
IV	-15	3.5	7.5	1000	Hold	Hold at annealing temperature
V	-35	1	8.5	1000	Ramp	Ramp to freezing temperature
VI	-35	1	9.5	0.1	Vacuum	Vacuum application
VII	-35	25	34.5	0.1	Hold	Hold at primary drying temperature
VIII	+25	6	40.5	0.1	Ramp	Ramp to secondary drying temperature
IX	+25	2	42.5	0.1	Hold	Hold at secondary drying temperature

Impedance measurements were recorded over the entire lyophilisation cycle. The duration of each frequency sweep (10 Hz – 1 MHz) per test vial, was 45 s, resulting in a scan time of 3 min 45 s for the set of 5 test vials. The total interval from the start of one measurement sequence (i.e. a set of sequential measurements on the series of 5 test vials) to another was set at 5 min.

Freezing related phase changes were also documented using a Canon D450 SLR camera in time lapse photographic mode. Images were recorded at an interval of 2 min and the onset time for ice formation documented for each vial. Special note was made of the onset time of the thermocouple containing vial in relation to the others.

8.3 Results and discussion

Changes in phase (e.g. ice formation), the completion of freezing, and the end-points of primary drying are all detected by this method through changes in the composite impedance of the formulation-vial-electrode assembly.

Figure 59 a and b show the response surfaces for the imaginary and real capacitance. In the frozen state (up to 9.5 h, and prior to starting the primary drying phase) the response surface is characterised by a step-like transition in the real part capacitance and a peak in the imaginary part capacitance, as the frequency is increased from 100 Hz to 250 kHz.

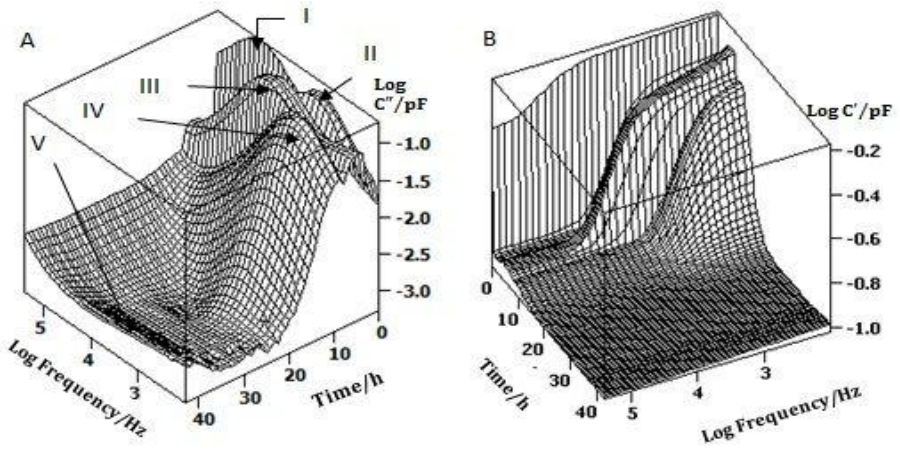

Figure 59 Three dimensional surface plots of (a) imaginary capacitance and (b) real capacitance against time for sucrose 2.5% w/v solution. The imaginary capacitance plot shows the change in peak position resulting from different stages of the process: I. Liquid; II. Solidified product; III. Annealing; IV. Primary drying; V. Secondary drying temperature ramp

These characteristic changes in the interfacial-relaxation peak are more clearly demonstrated by overlaying the imaginary capacitance spectra from individual time points associated with each stage of the process. This was demonstrated for the freezing, annealing and primary drying stages. However, once primary drying is complete, the interfacial-relaxation peak has diminished to zero and therefore may not be used to follow the progress of the cycle. At that point, however, one can still see changes in the impedance response of the sample through changes in the value of C′ or C″ at some representative frequency (e.g. 1 kHz). Given the low

mass (and hence dielectric constant of the product) then the lower limit of capacitance is in effect that of the empty vial.

8.4 Impedance Spectrum Profiles

8.4.1 Spectrum profiles during cooling (phase I)

Product cooling (from 17 to -7 °C) resulted in a small decrease in the interfacial-relaxation frequency (f_{peak}) of ~6% of the initial value (where the initial value is 90 kHz at 18 °C) and an even smaller decrease in the peak amplitude (C''_{peak}) of ~2% of the initial value (0.93 pF at 17 °C) (Figure 60).

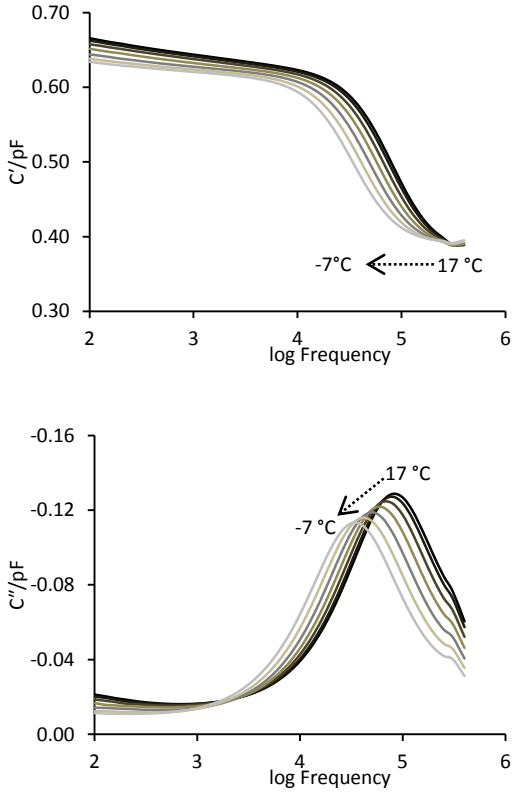

Figure 60 Real (top) and Imaginary (bottom) capacitance spectra as a function of temperature for sucrose solution (2.5 %w/v) in the liquid state. The arrow shows the direction of temperature, as the material is cooled from 17 to −7 °C (in 5 °C decrements) over the first 30 min the freezing cycle

The decrease in the relaxation frequency is consistent with that predicted from an approximation for the time constant of the process ($f = 1/2\pi RC$). As stated previously, R is the resistance of the material within the freeze-drying vial and C is an approximation for the constant phase element (CPE). The approximation works owing to the fact that the phase angle for the interfacial impedance (represented by the constant phase element, CPE) is close

to 90 (e.g. 89.2° when the sample is in the liquid state). Given that the resistance of an aqueous solution (in the liquid state) has negative temperature dependence and the capacitance of a solid (such as glass) also has negative temperature dependence (albeit much smaller than that for the resistance of the liquid) then the overall result is that the relaxation time increases and the corresponding relaxation frequency decreases with a decrease in temperature. The specific dependence of the interfacial-relaxation peak on the product temperature, during cooling, is explained further following the analysis of spectral peak data using peak finding software.

8.4.2 Spectrum profiles during freezing (phase I to II)

The phase transition from liquid to solid state is demonstrated by changes to both the peak frequency (f_{peak}) and peak amplitude (C''_{peak}) of the interfacial relaxation process: In contrast to the relatively small changes that are manifest on cooling through ~20 °C (Figure 60), the interfacial relaxation peak undergoes a more dramatic transition as the product solidifies: The peak frequency (f_{peak}) shifts to the lower frequencies by a factor of 30-100 (i.e. approximately 1.5-2 decades) while the peak amplitude (C''_{peak}) increased by a factor of 0.3, i.e. 30% (Figure 61).

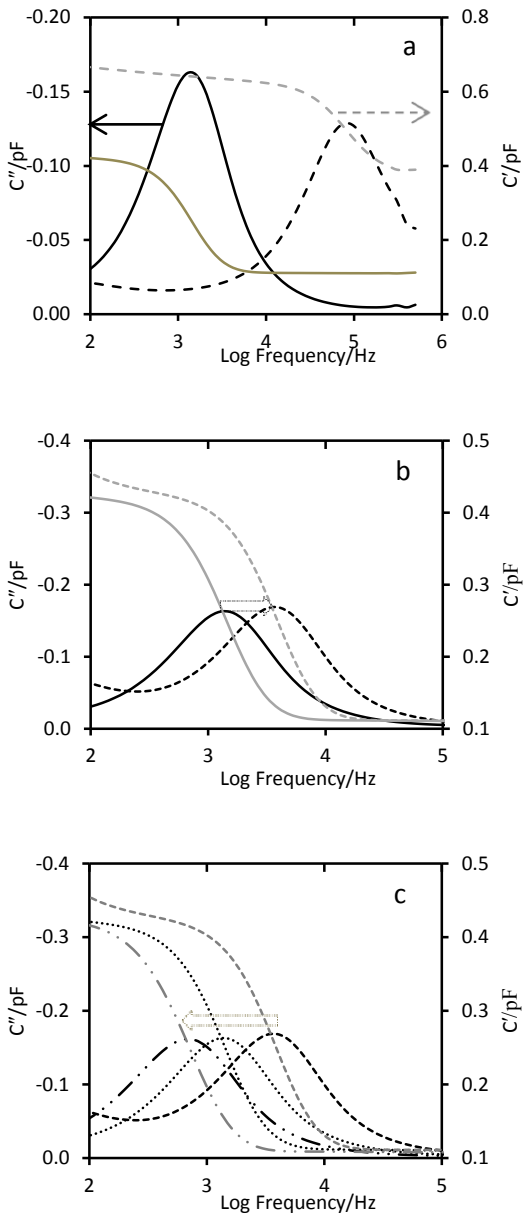

Figure 61 Capacitance (real and imaginary) spectrum of 2.5% sucrose solution during freezing, annealing and onset of primary drying. Black colour represents imaginary part whiles the grey colour emphasises real part of capacitance (a) Capacitance (real and imaginary) spectrum of 2.5% sucrose solution during freezing , the dotted line (- - -) denotes the liquid phase while the solid line (——) denotes the frozen (solidified) sample.. (b) Capacitance spectrum of sucrose 2.5 % w/v solution during annealing. The dotted line (- - -) denotes the annealed (-15 °C) while the solid line (——) denotes the frozen (solidified) sample (-30 °C). (c) Capacitance spectrum of 2.5% sucrose solution during onset of primary drying; the dotted line (-----) denotes the annealed product (at -15 °C) while the solid line (·····) describes the frozen state (-30 °C) and (—···) displays the onset of primary drying (-35 °C)

The shift in relaxation frequency by almost 2 decades is consistent with the fact that the solution resistance increases by almost 100 fold on freezing, as liquid water is converted to ice (Chin et al., 2007). The increase in the peak amplitude (C''_{peak}) may be rationalised if one

considers the dielectric constant of the interfacial region between the glass wall and the sample. Given that the dielectric constant of ice (ε ~ 100) is greater than that of liquid water (by a factor of ~ 25%) then the increase in peak height of 30% is consistent with the high dielectric constant of a frozen aqueous solution relative to its liquid counterpart. Figure 61a shows the shift in interfacial polarization peak following the liquid to solid phase transition. A comparison with the thermocouple responses in a neighbouring vial is shown in Figure 63b and confirms that the two time points illustrated in Figure 61a (5 min and 90 min) correspond to the liquid and frozen states of the sucrose solution.

8.4.3 Spectrum profiles during Annealing (Phase II to III)

During annealing, a 13 °C increase in the product temperature resulted in ~13% increase in the logarithm of the interfacial relaxation peak frequency (Log f_{peak}) (Figure 61 b). These results suggest a greater sensitivity to temperature changes when the solution is in the frozen state compared to the liquid counterpart (in which log f_{peak} decreases by 6% when the temperature was decreased by ~ 25 °C). Similar results were reported by Bettelli et al, who reported a strong correlation of relaxation frequency with the temperature of the ice; whereby the relaxation frequency increases with the increase in temperature of the previously frozen ice (Bittelli et al., 2004). This relationship defines the potential application of impedance measurements in the analysis of the product temperature (especially in the frozen state) without insertion of a thermocouple into the object.

8.4.4 Spectrum profiles during primary drying (III to IV)

The primary drying stage starts by lowering the chamber pressure (to 0.1 mBar) over a period of 15 min. A reduction in the product temperature (~5 °C) over this period confirms the onset of primary drying following the application of vacuum (Figure 61 c). Simultaneously, log f_{peak} decreased by 9%, which is consistent with the temperature dependence of peak frequency as observed above (at stage II). The gradient in the log f_{peak} under the applied vacuum appears to be twice that of observed on heating the product during the annealing phase.

After, the initial drop in temperature, the amplitude of the interfacial-relaxation peak (log C''_{peak}) continuously decreases with the progression of the sublimation process. This observation is a natural consequence of a reduction in the interfacial area between the ice and

the glass wall (as the ice front recedes down the inside of the vial) which in effect defines the magnitude of the interfacial capacitance (or more specifically the magnitude of the constant phase element) through the well-known relationship, $C \propto \varepsilon.a/d$ (where ε and d are the dielectric constant and thickness of the interfacial layer, respectively and a is the area of interfacial layer). In contrast, the peak frequency (like the temperature as measured by the thermocouple) remained relatively stable during the primary drying phase (Figure 62). This phenomenon is explained further in section 8.5.2.

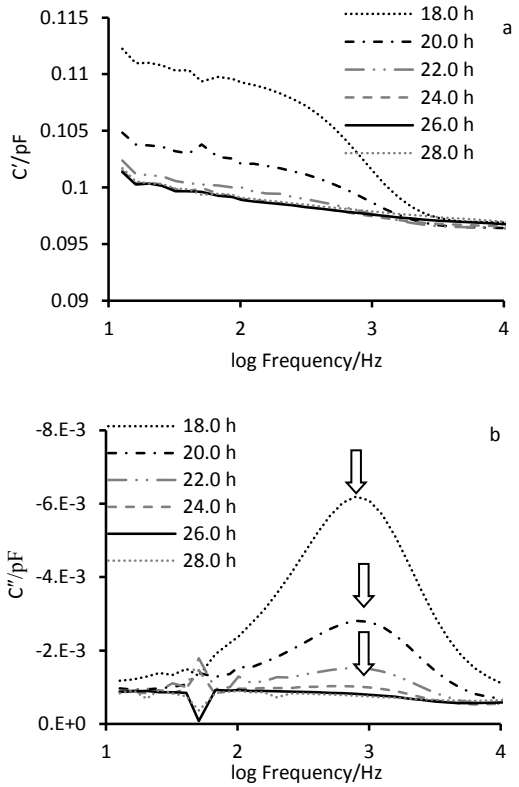

Figure 62 Imaginary capacitance spectrum of 2.5% sucrose solution during of sucrose 2.5% w/v over the later stage of primary drying stage a) real capacitance, and b) imaginary capacitance

At 24 h (Figure 62b) the peak becomes less clear, which has consequences for the determination of the end point of the drying cycle (as explained later). Therefore, in the context of sublimation, the magnitude of the peak i.e. the imaginary capacitance can be termed as an index of the product ice content. However, after ~22h of freeze drying cycle time, the interfacial-relaxation peak becomes rather small, and the peak not so well defined as the low frequency side becomes impacted by the measurement uncertainties.

8.5 Peak profiles

Data files acquired by the control software were subjected to data treatment software which uses a peak finding logic to display the data in a time slice of the peak amplitude (C''_{peak}) and/or peak frequency (f_{peak}) (Figure 63a and b, respectively). Alternatively, one can simply select a time slice of the real and imaginary capacitances at a specific user-defined frequency, e.g. 1 kHz. Using the example of 1 kHz, the displayed parameters would then be termed C' (1 kHz) and C'' (1 kHz), respectively (Figure 63c and d). The derivatives of any of the output parameters where then estimated separately using Microsoft Excel.

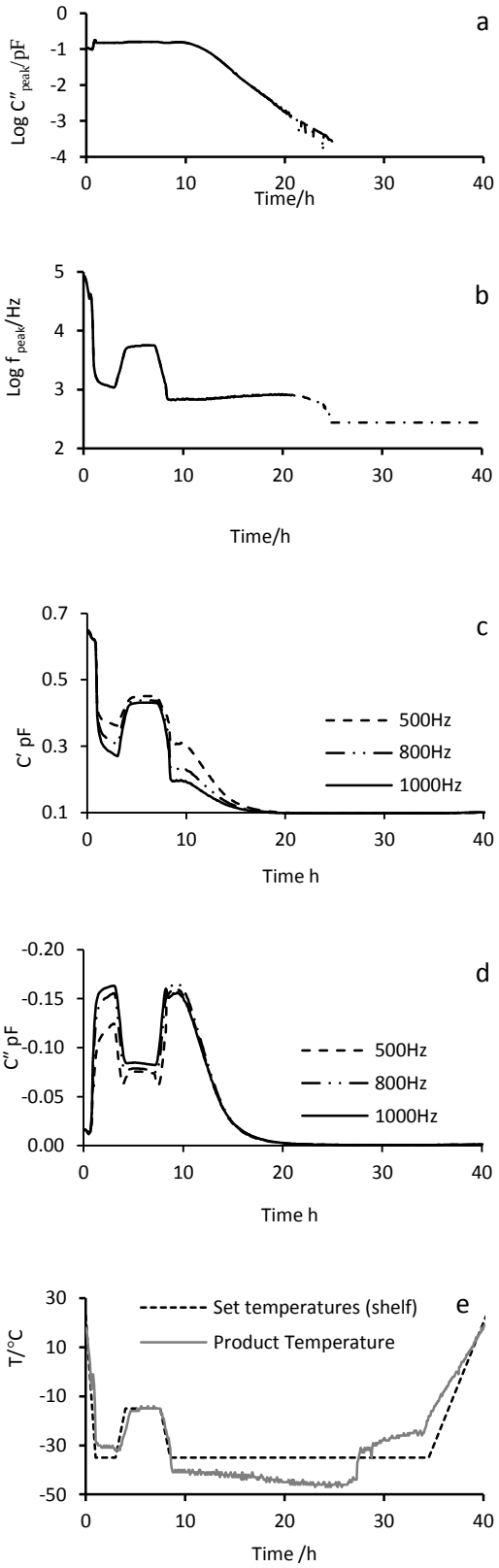

Figure 63 Characteristics of the interfacial relaxation peak for sucrose 2.5% w/v over the entire freeze-drying cycle; time slices of log C''_{peak} (a), log F_{peak} (b), $C'_{frequency}$ (c) and $C''_{frequency}$ (d) compared with the product temperature (e).

8.5.1 Peak Profiles during cooling freezing and annealing stage (I-III)

Over the freezing stage (i.e. the first 9 hours) of the cycle, the measurement system records dramatic changes in the peak frequency and peak amplitude (Figure 64a and b respectively). Primarily these relate to the phase change from liquid to solid, though it can also be said that the temperature in either state also has a significant impact on the measurement parameters.

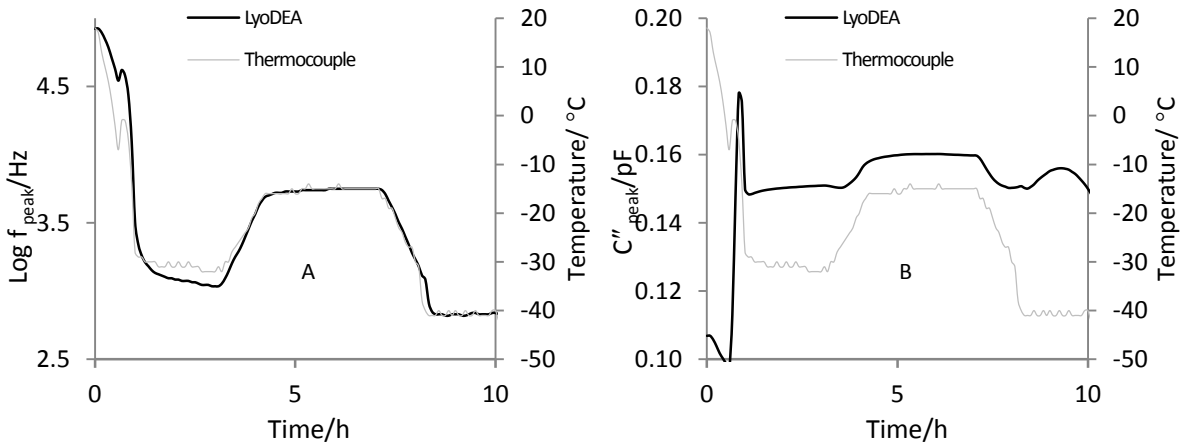

Figure 64 Characteristics of the interfacial relaxation peak of sucrose 2.5% w/v, during the freezing stage, in comparison with thermocouple data. Plot (a) describes the f_{peak} profile and plot (b) shows the C''_{peak} profile.

The temperature hold stage of the annealing period resulted in the stabilization of the interfacial relaxation peak within a narrow frequency range. There is some evidence (though not conclusive at this stage) that the values from the thermocouple stabilise before those measurements from the impedance measurement system. This might point to the fact that the completion of the recrystallization phenomenon (Ostwald ripening) may occur after the system has reached thermal equilibrium.

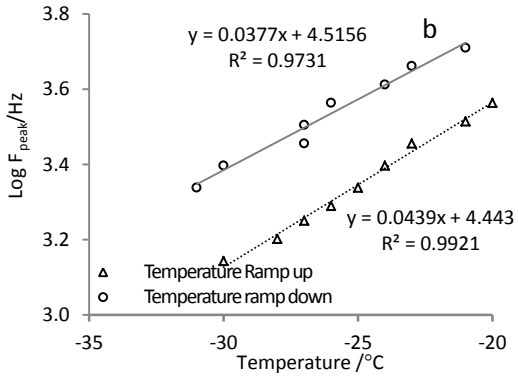

Figure 65 Log F_{peak} and product temperature data during annealing of sucrose 2.5% w/v.

More definitive evidence to suggest that the system has changed following the temperature ramp of the annealing stage comes from the temperature gradients in the log F_{peak} vs temperature plots, in that the slope factor for the temperature ramp 'up' was found to be ~ 15% higher than the annealing temperature ramp 'down' (Figure 65); There is also an apparent increase in Log F_{peak} values on the ramp down phase compared to the ramp up phase. Both phenomena require further investigation as to its significance in terms of the structure of the frozen matrix.

8.5.2 Peak Profiles during primary drying (III to IV)

The impedance profiles (both the C''_{peak} and f_{peak}) changed significantly during the primary drying (Figure 66). The amplitude of the interfacial relaxation peak decreases by a factor of ~100 during primary drying. Following a lag of approximately 2 h, from the onset of primary drying, the values for log C''_{peak} begin to decline in a linear fashion (Figure 66 b). This is a probable consequence of the drying front dropping below the top level of the measurement electrodes.

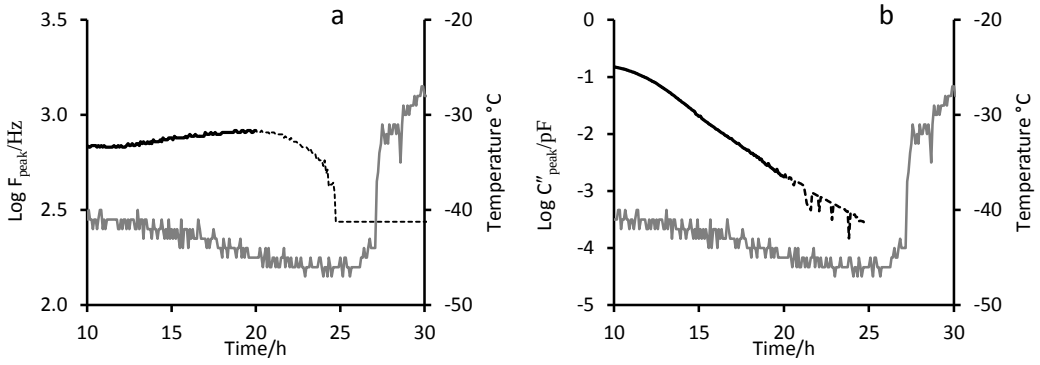

Figure 66 Characteristics of the interfacial relaxation peak of sucrose 2.5% w/v, during the primary drying stage. The black line denotes the frequency and peak imaginary capacitance of the interfacial relaxation frequency, and the grey line represents the temperature profile. Uncertainties in the estimated values for f_{peak} (a) and C''_{peak} (b) following imprecise analysis of the peak by the LyoView software are shown as a dashed line after 20h.

In contrast to C''_{peak}, there are minimal changes in the peak frequency (and hence time constant, τ) during primary drying (Figure 66 a). These observations can be explained in terms of the height of the ice layer across the sensing zone between the electrodes during primary drying. Both the dry layer and the ice layer are modelled as two separate series RC circuits in parallel with each other (Figure 67). Given the higher dielectric constant and lower resistivity of the ice layer, then the impedance of the two layers can be considered simply in terms of the impedance of the ice layer. In effect, the dry layer impedance can be ignored. The interfacial capacitance of the ice layer/glass interface is proportional to its effective area contacting the electrode (CPE ∝ A), whereas the resistance of the ice layer (R) is inversely proportional to the contact area. It follows that as the height (h) of the ice layer decreases then the resistance of the layer decreases as a function of 1/h whereas the interfacial capacitance decreases in proportion to h. The time constant (τ=RC), and hence f_{peak}, remains approximately constant over the entire primary drying, but the amplitude of the peak decreases in proportion to the height of the ice layer (h).

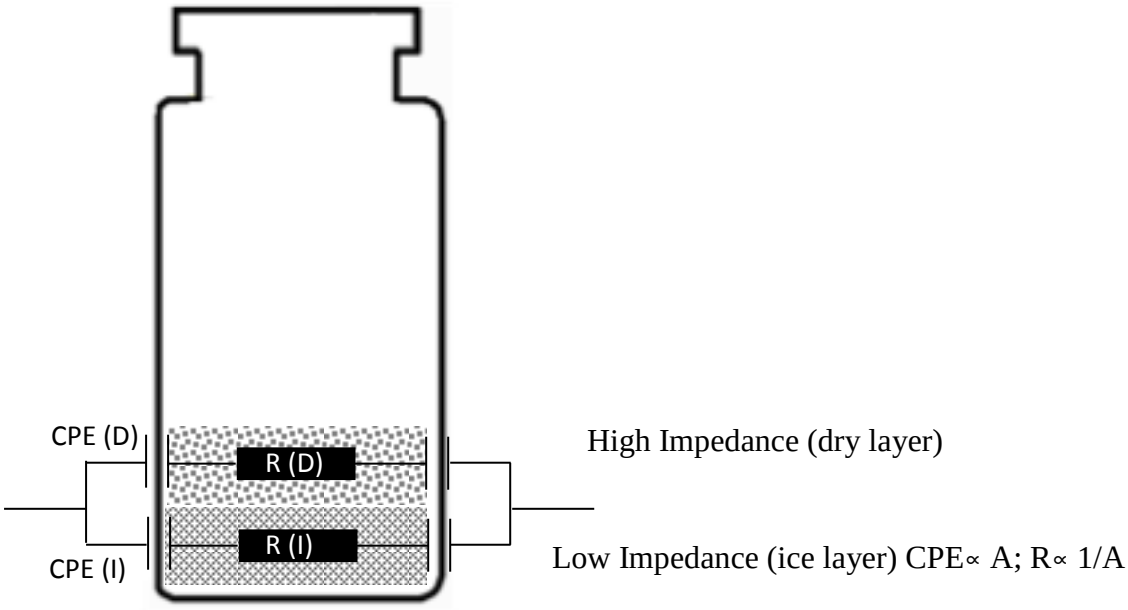

Figure 67 An equivalent circuit model representing the frozen layer (bottom) and dried layer (top) during primary drying. The equivalent circuit elements are as follows: CPE (D) & CPE (I) are the interfacial capacitance at the dry layer/glass interface and ice layer/glass interface, respectively; R(D) & R(I) are the electrical resistances of the dry layer and ice layer, respectively

However, during the terminal stage of primary drying the interfacial relaxation peak appears to be flat and wide. This may be seen in the 23h time point spectrum (Figure 62) and in the 3-D surface plot (Figure 59 a) whereby some low frequency noise results in the apparent broadening of the spectrum on the low frequency side of the peak.

At this point (> 20 h) the data analysis software begins to 'mislocate' the peak at a progressively lower frequency, hence the apparent decrease in the Log f_{peak} vs time profile (see dotted line on Figure 66a). The low frequency noise also disturbs the estimation of the peak magnitude such that the Log C''_{peak} vs time profile becomes noisy at time points beyond 20h (see dotted line on Figure 66b). These uncertainties preclude the use of the interfacial relaxation peak in determining the end point of the primary drying phase.

It may be concluded that, while the peak vs time profiles are of value in the measurement of temperature changes and in characterising the various stages of the freezing step, an alternative approach is required for the determination of the end point of primary drying.

8.6 Time Slice Profiles at Fixed Frequencies

An alternative approach may be realised by use of time slices of the imaginary capacitance at some discrete frequency in the range 500-1000 Hz (i.e. the predominant location of the

interfacial relaxation peak during the primary drying stage). Figure 68a shows time slices at three frequencies of 500, 800 and 1000Hz. The time slice profiles for C′ showed a reduction of only ~ 2% over the 7h period (20-27h) prior to the product-temperature-indicating end point. In addition there was no clear plateau at the end of primary drying rather a minimum in C′ was observed at ~23 h (Figure 68 b). In contrast, the magnitude of C″ (1 kHz) decreased by 70% (-0.00278 to -0.00075 pF) over the time period of 20-27h (Figure 68 b), leading to an asymptotic value which suggests the complete depletion of ice and the end point of primary drying.

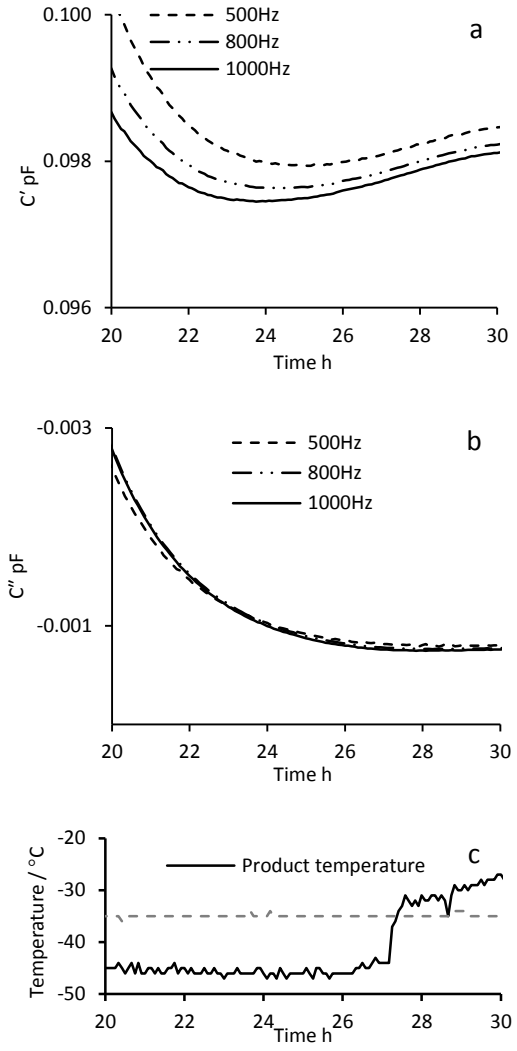

Figure 68 Time slices of capacitance real (a) and imaginary (b) profile of sucrose 2.5% w/v at discrete frequencies in comparison with the thermocouple data (c).

Of the three frequencies profiled, a frequency of 1 kHz was considered to be optimal as it is well above that region where the low frequency noise impacts the signal quality Figure 68b. The asymptote in C" at 1 kHz was comparable to the time point at which the product temperature starts to approach that of the shelf temperature (Figure 68 c).

Whilst it was anticipated that the values of C″ would approach a zero value as the primary drying cycle completed, it was not obvious as to how the exact end point could be defined. In order to arrive at a magnitude independent parameter for the determination of the end of primary drying, values for the derivative of the real and imaginary capacitance were then calculated as a function of time, i.e. dC'_{1kHz}/dt and dC''_{1kHz}/dt. Log values of each derivative displayed a constant slope during the initial phases of primary drying, followed by a sharp decline at some time point (Figure 69). In the case of the log of the derivative of the real part capacitance, this transition point was observed at ~23.5 h (Figure 69a), whereas the transition point for the corresponding parameter for the imaginary capacitance (log dC''_{1kHz}/dt) showed a sharp decline at ~27.5 h (Figure 69b). In each case the transition point was estimated by measuring the intercept of the straight lines extrapolated from the slopes either side.

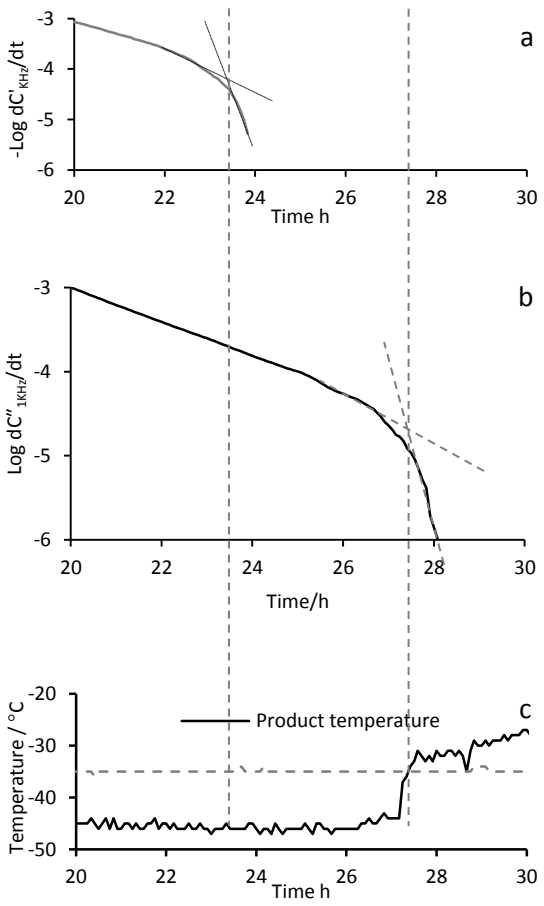

Figure 69 Log dC1kHz/dt vs. time of sucrose 2.5% w/v. (a) Log dC′$_{1kHz}$/dt vs. time, (b) Log dC″$_{1kHz}$/dt vs. time and (c) product temperature profile.

Of the two transition points, it was that for log dC″$_{1KHz}$/dt (27.5 h) which agreed with the thermocouple defined end of primary drying (at 27.2 h), i.e. the time at which product temperature increases above the shelf temperature (Figure 69c). The reason why the imaginary capacitance has an end point which more closely mirrors the end point determined by the thermocouple is that it is sensitive to the electrical conductivity of the system. The shunt conductance provided by the ice layer dominates the response, so while there is still a layer of ice at the base of the vial then the imaginary capacitance will continue to change as the ice layer shrinks to a negligible thickness. The real capacitance, by contrast, is simply the sum of the contributions from the electrical capacitance of the ice layer and the dry layer. And while the capacitance of ice is approx. 50-100 times that of the dry layer, the conductivity of the ice layer compared to the dry layer is likely to be orders of magnitude higher. However, this preliminary result demands further study.

A further consideration is that the time point at which the product temperature reaches that of the shelf temperature actually occurs some minutes prior to the true endpoint. This is a

consequence of the insertion of the thermocouple into the product which results in the shortening of the primary drying time relative to the control. There can be a number of reasons for this, including the possibility of larger ice morphology (from the elevated temperature at which ice growth is seeded) and the associated facilitation of vapour flow, in addition to the additional thermal input from the physical location of the probe in the frozen mass. It is for this reason that the endpoint of the cycle is often defined by the temperature endpoint plus 30 minutes. Further studies using microbalance are required in order to validate the endpoint.

8.7 Discussion

It has been observed that the log of the interfacial relaxation frequency has a linear correlation with the product temperature, provided that there is no product phase change over the temperature range of interest, and that there are different gradients for the pre-freezing and solidified stages of the freezing cycle. It may be possible therefore, to calibrate the impedance measurement system to provide a non-product-invasive temperature sensor. The specific calibration coefficients of the sensor are likely to depend on the composition of the product; in particular, the concentration of any electrolyte or the nature and concentration of the counter ion of a salt form of a drug. These factors are likely to have a significant impact on the conductivity of both the frozen and unfrozen solutions, which in turn will define the magnitude of the interfacial relaxation frequency. Other components within the product, especially those which impact the viscosity of the solution and those which influence the extent of ice formation and the structure of the frozen matrix will in turn affect the conductivity and hence the relaxation frequency. Having recognized this dependence, it is also possible that certain process parameters, the freezing rate in particular, could additionally impact the structure of the ice matrix and therefore the conductivity of the frozen matrix. Whilst it remains to be seen whether general rules can be developed for the creation of formulation-specific calibration routines (which are independent of the process variable) or even without calibration, it’s clear that the use of impedance measurements could be applied for the measurement of hot and cold spots across the shelf, through measurements taken on discrete vials across an individual shelf.

Chapter 8

The main purpose of this research study, however, was to establish the (i) utility of impedance spectroscopy in determining the characteristics of the freezing process, (ii) the end point of primary drying.

On freezing, it was shown that the measurement of impedance faithfully reproduces the observations made by a thermocouple, in terms of the onset time for ice formation, the duration of both solidification phase and the equilibration phase when the product temperature equals that of the shelf temperature. Experience has shown that there can be a wide range of freezing onset times within a freeze drier that contains a full load meaning there can be as much as 30 minutes difference between the ice formation in the first and last vial to undergo the freezing process. With the current study using the impedance system, where there were only five vials placed in close proximity to one another, one might expect less difference in ice onset time. However, one may expect to see differences that result from the insertion of the thermocouple within the product, as it is known to provide additional nucleation sites, with an anticipated impact on the ice onset time. Visual observations by time lapse photography indicated that the thermocouple-containing vial nucleates and form ices approximately 120 s earlier than the four other vials. This time frame is within the 5 minute measurement cycle time to complete the scan on all five vials and therefore such differences between thermocouple containing vial and the impedance measurement vial are not picked up by this technique.

An accurate estimation of the end point of primary drying, the most critical step, has been a primary objective of the process development scientists. Conventionally, the endpoint of the primary drying has been predicted using thermocouple data as the time point at which product temperature raise back to the set shelf temperature. In this study the conventional end point measurement was used as a way of defining which of the transitions in the derivative of the imaginary capacitance time plot may be used as an end point indicator.

So far, it has been shown that the impedance measurement system gives analogous data to that of a thermocouple. However, the principle advantage of the impedance measurement system, over a simple thermocouple measurement, is that it can provide information on the rate of drying (as well as to highlighting the endpoint) of primary drying. Decrease in C''_{peak} during primary drying may suggest a potential application of the technology in defining of sublimation rate. A calibration with the gravimetric techniques will confirm this observation.

Such information is not provided by the thermocouple since the temperature of the product stays largely constant during primary drying. In addition, the potential variations in the shape of the drying front (from planar to convex) can lead to inaccuracies in the measurement of sublimation endpoints, especially if the probe is positioned near the glass wall (Song et al., 2005). The benefit of the impedance measurement system is that it's possible to more precisely locate the electrode assembly on the outside of the vial than it is to locate the thermocouple in the exact same location each time, in each vial. Also the thermocouple is a point sending device and therefore impacted more by position. Impedance measurement probes the entire contents of the vial and is therefore mush less sensitive to positioning effects. In contrast it is evident that the magnitude of imaginary capacitance (for example at a discrete frequency of 1 kHz) has a pronounced dependency on the extent of sublimation from the entire volume occupied by the product, with the potential to yield a definitive end of primary drying, free from probe related errors. So if one understand the relationships between the magnitude of imaginary capacitance and the composition of the product, in terms of the weight fraction of the residual ice, it might be possible then to predict the end point of the cycle well in advance of the actual endpoint. This is a consequence of the nature of the electrode system (of low thermal mass and negligible physical size (with cables attached at the neck of the vials) which means that it is physically possible to cluster the vials within the usual hexagonal array. However, all the experiments in this particular study have been undertaken with the vials in a row at the front of one of the shelves. This was deemed necessary in order to 'view' the physical state of the product, including the onset of ice formation and the extent of the dry layer during primary drying. Further work is required to investigate the physical clustering on the thermodynamics and kinetics of the drying process. This would provide significant advantage to the process scientist who could then interrupt a cycle in advance of the cycle end point, thereby reducing the waiting time to assess the actual duration of the primary drying stage. This would then accelerate the development process, by increasing the throughput of experiments within the Quality by Design approach to product and process development.

8.8 Summary

It has been demonstrated that the frequency of the interfacial relaxation peak (f_{peak}) is strongly coupled to the temperature of the product (through the interdependency of the product temperature on the electrical resistance of the product) whereas the amplitude of the

interfacial relaxation peak (C''_{peak}) is dependent on the phase behavior and the extent to which ice has sublimed from the product, during the early phase of primary drying. It follows that the magnitude of C''_{peak} may be used to define a drying rate. However, if the end point of primary drying is required then one must switch to the characterization of the log of the derivative of the magnitude of the imaginary capacitance at some fixed frequency close to that of the interfacial relaxation peak frequency, e.g. 1 kHz. The end point is then defined in terms of the inflection in the gradient of the time profile.

It is anticipated that the impedance measurement system described in this chapter may be employed as one part of a process control system, in which the freezing rate, the shelf temperature and/or a termination of the lyophilization process or a sub-stage of the lyophilization process can be controlled in response to the product parameters measured by the system.

9 The impact of Annealing on primary drying rates

The impact of annealing hold time, annealing temperature and no. of annealing cycles on the primary drying profile of a formulation (Maltodextrin 10% w/v).

9.1 Objectives

This chapter targets to study an effect of the annealing step on the crystallization process during freeze-drying cycle in maltodextrin solution using through-vial impedance spectroscopy. Specifically the chapter will focus on the a) effect of the annealing time and duration on the primary drying rates and primary drying times of the maltodextrin solution, and b) exploration of the changes in electrical impedance as a way of investigating the mechanisms of annealing c) the changes in glass transition following annealing. Two mechanisms affected the of ice structure alterations during annealing are discussed in the chapter: (i) through either a growth of the ice phase (devitrification) and/or (ii) the recrystallization (Ostwald ripening) of ice crystal structures.

9.2 Materials and Methods

Maltodextrin DE 16-19 was purchased from Sigma Aldrich and used as received for the preparation of a 10% w/v solution in distilled water. Aliquots of 3ml were introduced into four impedance measurement vials and the impedance measurements were taken across the frequency range 10-10^6 Hz, over a scan interval of 3 minutes, throughout the entire freeze drying cycle. One of the measurement vials was supplied with a thermocouple type-K place at the bottom centre of the liquid to provide a representative temperature for all four vials. The freeze drying cycles used in this study are described in the Table 13.

Table 13 Details of the freeze drying cycle

Step	Temperature ^{o}C	Duration (h)	Time (h)	Vacuum mBar	Ramp/Hold	Stage
I	-35	1.0	1.0	1000	Ramp	Ramp to freezing temperature
II	-35	5	6	1000	Hold	Hold at freezing temperature
III	-5,-10 and -15	2	8	1000	Ramp	Ramp to annealing temperature
IV	-5,-10 and -15	5	13	1000	Hold	Hold at annealing temperature
V	-35	2	15	1000	Ramp	Ramp to freezing temperature
VI	-20	1	16	0.1	Vacuum	Vacuum application
VII	-20	20	36	0.1	Hold	Hold at primary drying temperature
VIII	+25	6	42	0.1	Ramp	Ramp to secondary drying temperature
IX	+25	4	46	0.1	Hold	Hold at secondary drying temperature

In a separate set of experiments, at the end of primary drying stage, the cycle was interrupted and weight loss at this stage calculated in both the annealed (annealing temperature -10 °C, hold time 5 h) and non-annealed formulations to determine the weight of additional ice formed in the former.

9.3 Results and discussion

The impedance spectrum of the electrode-vial-solution assembly reveals an interfacial-relaxation process, arising from the polarization of the solution–glass vial interface, as a step in the real part capacitance (C′) and a peak in the imaginary part of the capacitance (C″) (Figure 70).

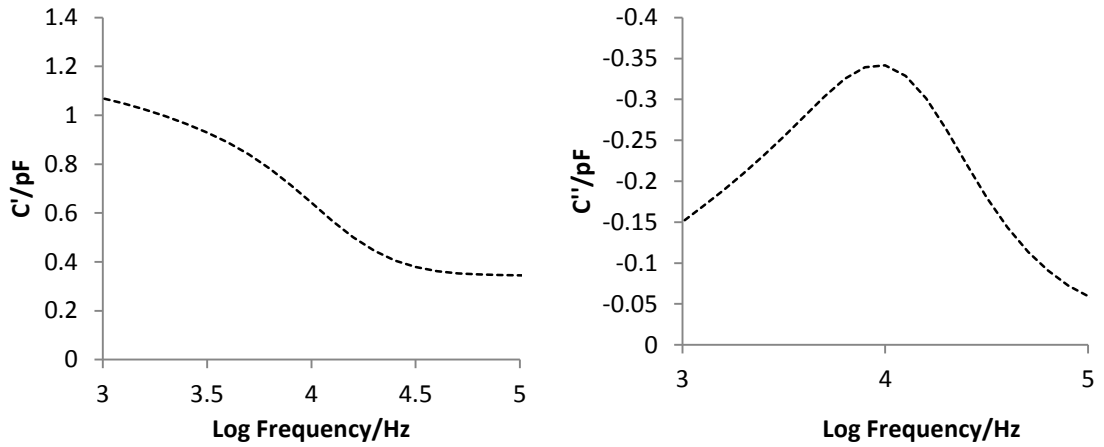

Figure 70 Real and imaginary capacitance spectra showing the interfacial relaxation process. The example spectrum shown here is taken at 3 h when the solution is in the frozen state (-35 °C). The peak frequency in the imaginary capacitance when the solution is in this condition is located at 10 kHz

The features of the interfacial polarization peak in the imaginary part spectrum (i.e. peak position, f_{peak} and peak amplitude, C''_{peak}) are used to characterize different stages of the freeze drying process, viz. product cooling, ice nucleation, freezing and primary drying (section 5,8).

Here, the changes in spectral profile during the entire freeze drying cycle are first visualised in the response surface plot (Figure 71A). Then through an examination of individual spectra one can see how the process of ice formation (solidification) results in a shift in the peak frequency but little change in the peak height, whereas the process of primary drying results in a dramatic reduction in peak height but very little change in peak frequency (Figure 71B and C, respectively). The first part of this chapter focuses on the interpretation and exploitation of the peak amplitude (C''_{peak}) during the primary drying stage to provide information on the impact of the annealing conditions (i.e. time and/or temperature) on the drying rates and drying times. Whereas, the second part examines the freezing/annealing

stage and develops an equivalent electrical circuit model for the physical characteristics of the ice structure that forms on freezing and then altered subsequently by the process of annealing. With the exploration of the freezing stage, an assessment of how the glass transition may be recorded during the ramp up and ramp down stage of the annealing process is also under taken.

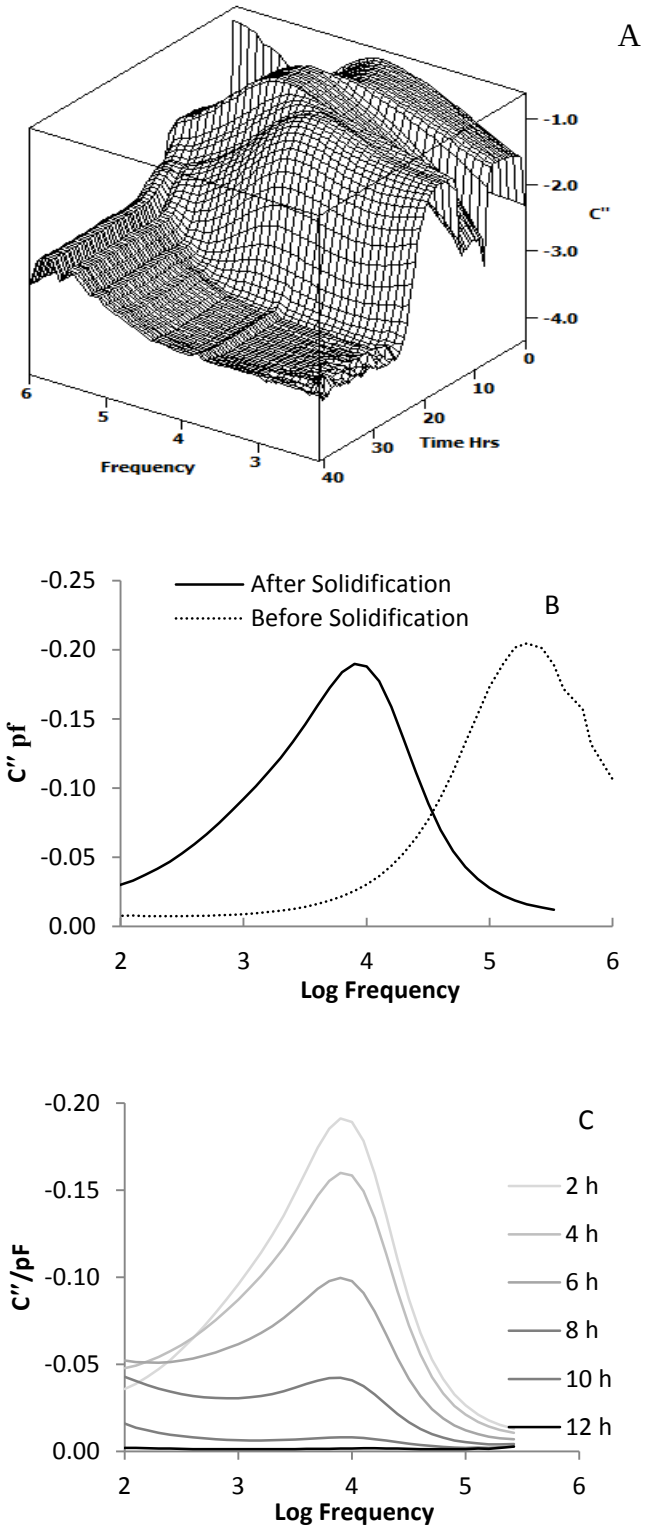

Figure 71 A) 3D spectrum as a function of frequency and time B) 2 spectra before (0.7h) and after (3h) ice solidification Capacitance spectra during primary drying maltodextrin 10% w/v during primary drying

9.3.1 Measurement of relative primary drying rate

Primary drying rates (ice sublimation) are difficult to determine directly from through-vial impedance measurements, without calibration of the spectrum against the volume of ice remaining. However, given that there is a relationship between the magnitude of the interfacial polarization process and the height of the remaining ice layer, it should be possible to determine relative changes in the rate of drying by assessing the derivative of the capacitance at the peak frequency of the relaxation process. In chapter 8, the log of the derivative of the imaginary capacitance (at ~ 1 kHz for a 3% sucrose solution) was used to determine the end point of the primary drying stage. Here we explore the use of the derivative of the peak capacitance as an indicator of the rate of drying. Figure 72a shows a step-like decrease in the imaginary capacitance (at 10 kHz) as ice sublimes from the vial and the ice layer height decreases through the sensing region of the external electrode pair. The maximum in the *surrogate drying rate* (in units of pF min^{-1}) were then calculated from the time point corresponding to the maximum slope. Two methods were used: one taking a moving average of the gradient over 15 data points (equivalent to a time of 45 min, Figure 71B) and the other using the line of best fit through the linear region of the curve (Figure 72A). Figure 72C then shows the methodology for estimating for the primary drying end point.

9.3.2 Measurement of Primary Drying Time

Time profiles of C″ at 10 kHz (the predominant position of interfacial polarization peak during primary drying stage of lyophilisation cycle of 10% maltodextrin) were employed to calculate the primary drying end point from the inflection in the gradients of the log $dC''_{(10\ kHz)}/dt$ profile plotted against the cycle time (Smith et al., 2013). The primary drying time was then calculated as the time difference between the end of primary drying as determined from the inflection and the onset of primary drying. This onset may also be determined from the interfacial relaxation process by an abrupt decrease in the both the position and amplitude of interfacial polarization peak.

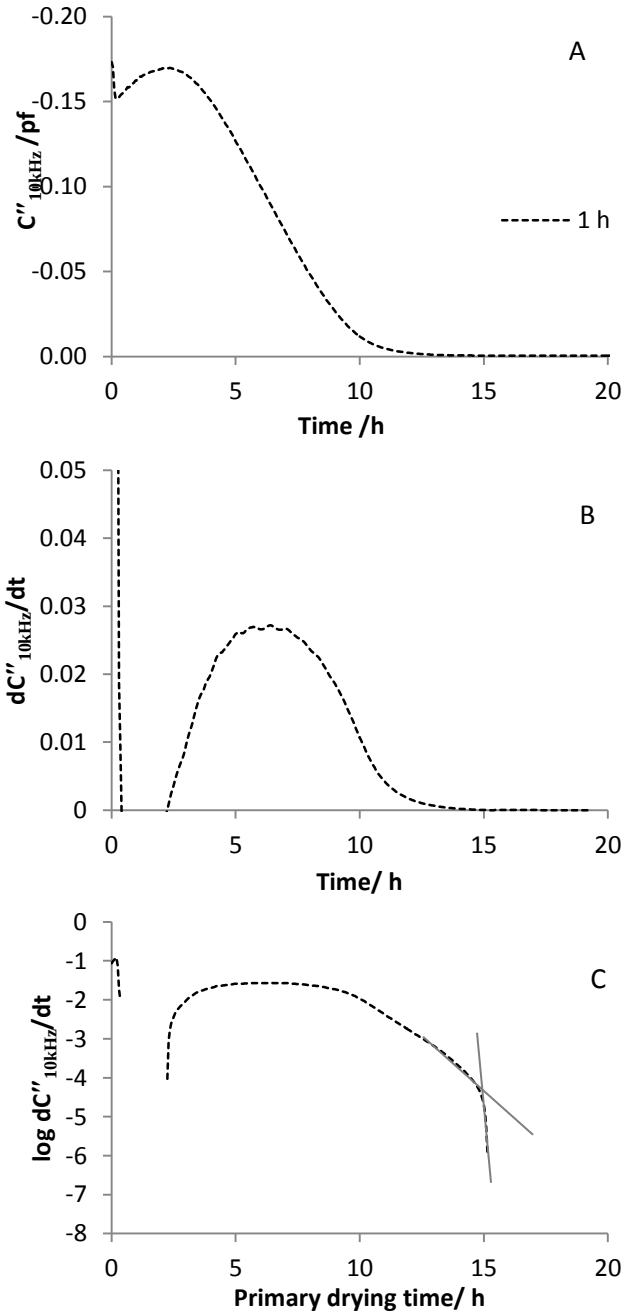

Figure 72 Capacitance vs. time profiles during the primary drying of a frozen 10% w/v maltodextrin solution: (A) magnitude of capacitance at 10 kHz; (B) time derivative of the capacitance at 10 kHz; (C) time derivative of capacitance at 10 kHz in logarithmic scale

9.3.3 Impact of annealing hold time on the primary drying rate and primary drying

This section examines the impact of the annealing hold time on the reduction in primary drying time and provides a first opportunity to demonstrate the use impedance measurements to assess the kinetics of ice formation (recrystallization and/or partial devitrification) at the chosen annealing temperature of -10 °C.

The derivative of the imaginary capacitance (dC″/dt) against time (Figure 73A) shows that the time to reach maximum drying rate occurs at a progressively earlier time point as the annealing hold time is increased. The maximum drying rate increases as the annealing hold time was increased from 1h to 3h. Thereafter the rate dC″/dt remains approximately constant. These relationships are seen more clearly in the plot of maximum drying rate against annealing hold time for the two methods used to calculate the rate (Figure 73B, C). Figure 73D also shows that there is a decrease in the duration of primary drying as the annealing hold time was increased from 1 to 3h. The results (Figure 73E) indicate a significant decrease (~23% i.e. 3-7h) in the duration of primary drying time as the annealing hold time was raised from 1h to 3h. A further increase in the annealing time of 2 h (3h to 5h) only produces an additional 3% (0.7h) reduction in the primary drying time. This infers that the hold time of 3 h was an appropriate annealing hold time for the present freeze drying cycle; the hold time beyond 3 h may be adding unnecessary cycle time without significantly reducing the duration of the primary drying stage. A linear slope between the sublimation rate and the 1° drying time points to a correlation between the two process parameters (Figure 73F).

The observation that the drying time is proportional to the drying rate suggests that both are impacted by the inclusion of an annealing step. The fact that the drying time is seen to correlate well with the drying rate might at first glance appear obvious. The capacitance of the object under test is defined by the material contained in the electrodes which is largely frozen water along with small fraction of unfrozen viscous solution. During primary drying, the ice is replaced with air (a substance with capacitance values 100 times lower than the former). A broad correlation between the capacitance and the amount of ice provides the basis for the application of the impedance spectroscopy in estimation of sublimation rate. The use of dC″/dt as a relative measure of drying rate was not known for certain. These observations, demonstrating the correlation between this measurement of drying rate and the drying time, therefore go some way towards validating the assumption that the time derivative is indeed a reliable measure of the drying rate.

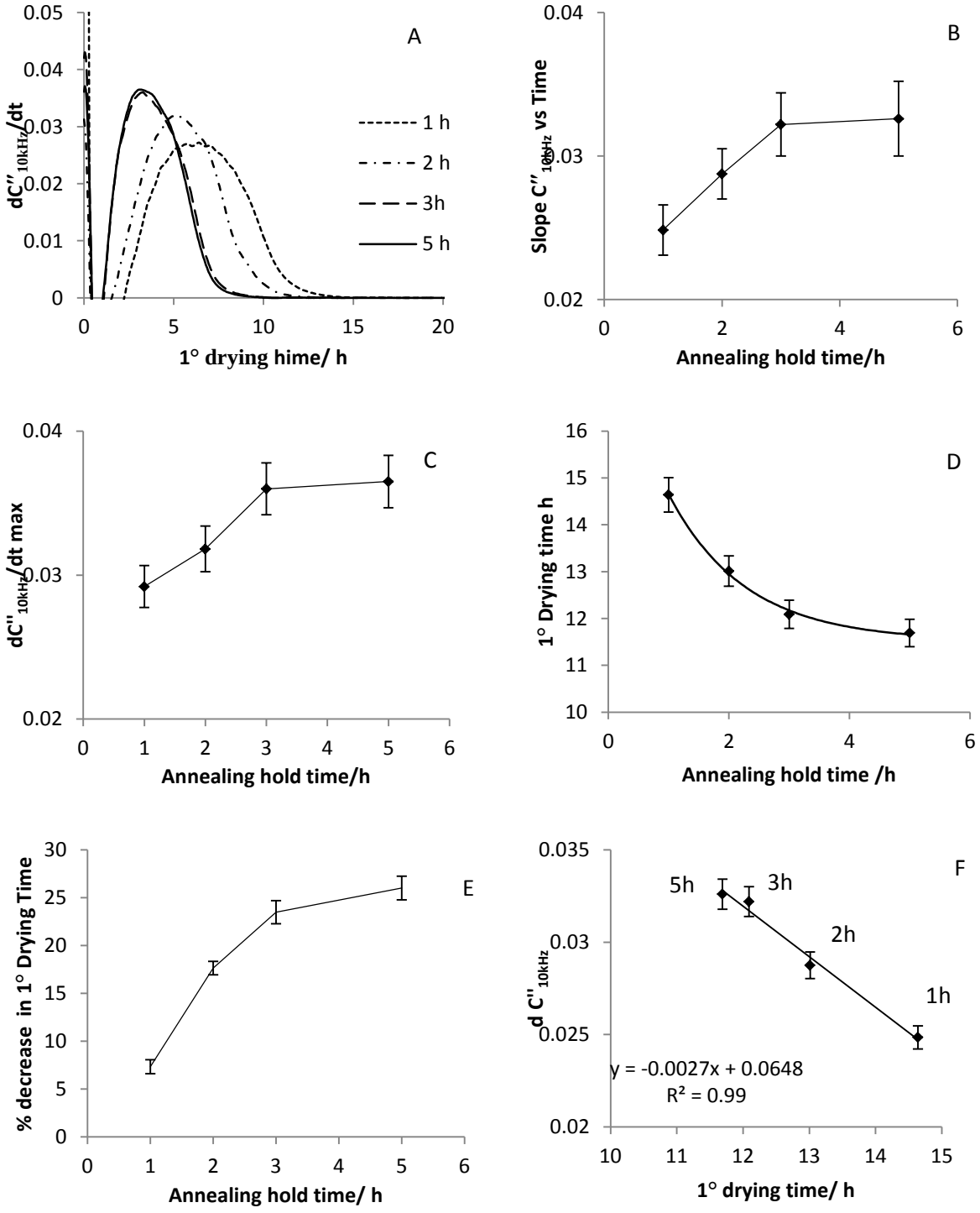

Figure 73 Impact of annealing hold time on the primary drying profiles of maltodextrin 10% w/v. (A) time derivative of the capacitance (C''_{1kHz}) profile; Estimates of the drying rates from (B) the slope of C''_{10kHz} and (C) dC''_{10kHz}/dt (max) ; (D) describes the the duration of primary drying time, (E) % decrease in primary drying time (F) correlation between dC''_{10kHz}/dt (max) (a surrogate for the sublimation rate and primary time. (n=4 error bars ±1SD).

9.3.4 Impact of annealing temperature on the drying time

This section examines the impact of annealing temperature on the subsequent rates of primary drying. The results show the primary drying time decreased from ~15h to ~10 h as the annealing temperature was raised from -15 °C to -5 °C, i.e. 2-10 °C above the glass transition temperature of -17 °C (

Figure 74A, B). The results also indicate a higher gradient of the imaginary capacitance at 10 kHz in the formulations annealed at elevated hold temperatures (data not shown) which is more clearly demonstrated as elevated peak in the time derivative of capacitance (dC''_{10kHz}/dt) profiles (

Figure 74 C).

The increase in the mass transfer rates is a possible outcome of larger ice morphologies which on sublimation generate larger pores and a lower resistance to vapour flow, resulting in the reduced drying times. Both the increase in the drying rate estimated from the maximum of dC_{10kHz}/dt and the reduction in the primary drying times in response to the annealing temperature (

Figure 74B and D respectively) can be modelled by an exponential function (Equation 46).

$$Y = Y0 + Ae\text{^}(T/\tau) \qquad \text{Equation 46}$$

where Y_0 = offset value of the response to the annealing hold temperature, A is the amplitude and τ is decay/growth constant.

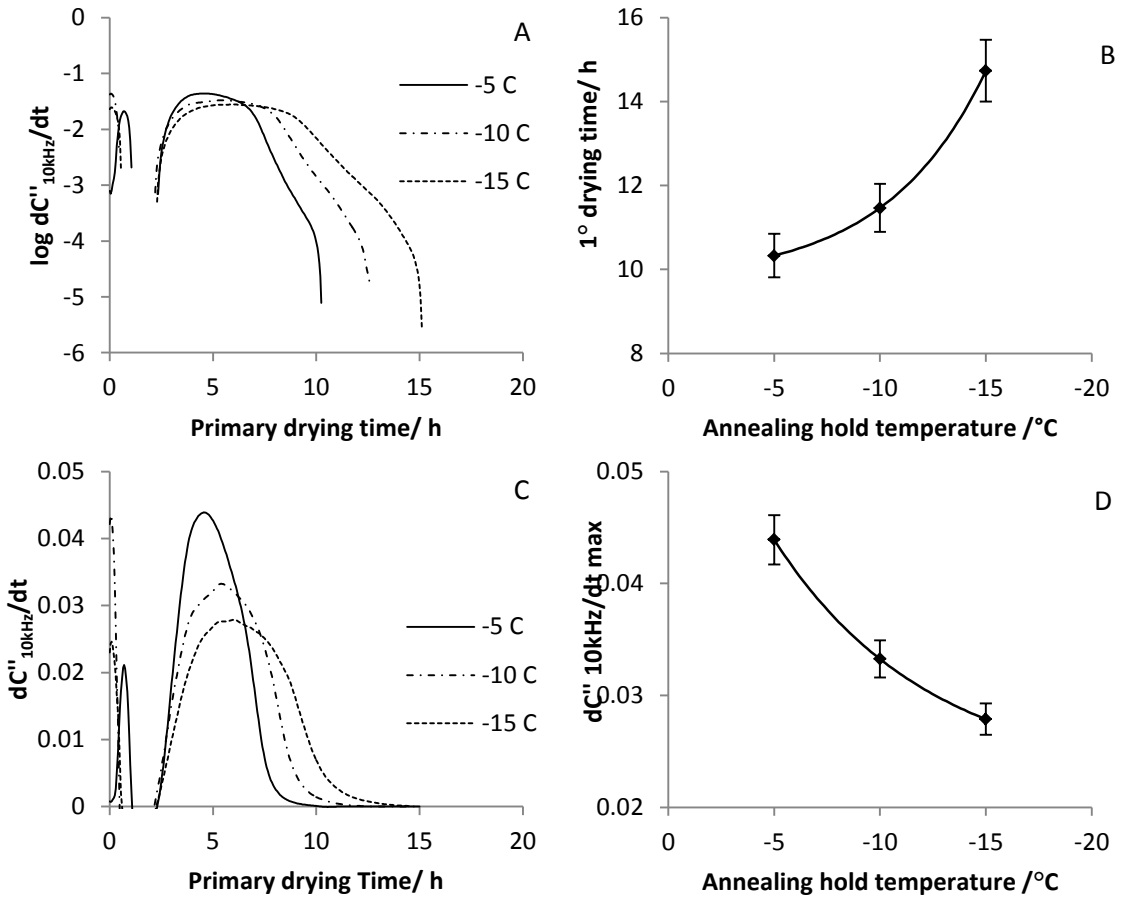

Figure 74 The impact of annealing temperature on the rate and duration of primary drying of frozen solution of 10% w/v maltodextrin. Time profiles of (A) C″ at 10 kHz, (B) time derivative of C″ at 10kHz, (C) log of time derivative of C″ at 10 kHz, (D) primary drying times following annealing at different hold temperatures, (E) changes in dC''_{10kHz}/dt_{max} during primary drying as a function of annealing temperature.

.

9.3.5 Mechanisms of Annealing

The interfacial polarization peak changes, in both the amplitude and frequency, as the product temperature is ramped and maintained during the annealing step (Figure 75). These shifts in the interfacial polarization peak are the possible outcome of changes in the structure of frozen matrix which contribute to the shortened primary drying times that result directly from the annealing steps.

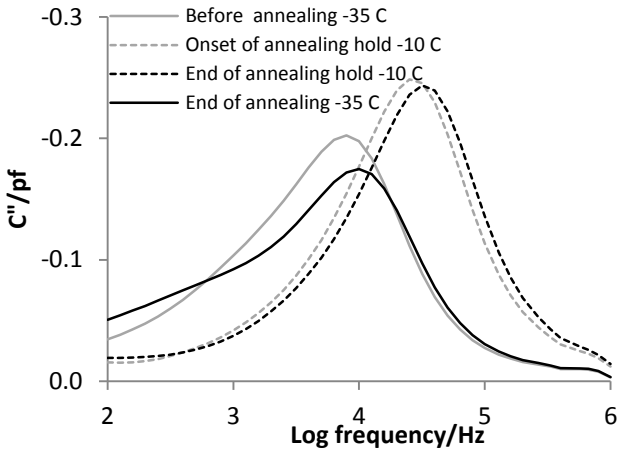

Figure 75 Impedance spectrum of 10% w/v maltodextrin solution during annealing showing the changes in position and amplitude of interfacial polarization peak

In order to understand the physical processes related to the observed changes in the primary drying time, the impedance spectra were then characterized by an equivalent electrical circuit model (Figure 31), comprising the physical elements of a resistor (R), a capacitor (C) and constant phase element (CPE), (Figure 48). The parameters C and R model the bulk electrical properties of the contents of the vial, while CPE models the characteristics of the interface between the internal surface of the glass vial and the contents of the glass vial. The electrical capacitance of the contents of the vial is dependent on the dielectric constant of the matrix, which is a function of the phase state and composition of the matrix (ice fraction to unfrozen fraction). Simple mixture formula (Cosenza et al., 2009) of a two phase system should suffice to estimate the bulk dielectric constant of a frozen solution in which an ice-rich phase coexists with an amorphous water rich phase (the unfrozen fraction). The electrical resistance also reflects the composition and phase state of the matrix. In particular, it depends on the concentration and diffusion coefficients of delocalised charges within the matrix, which are in turn dependent on (I) the viscosity of the unfrozen fraction and (II) the connectivity between the ice crystals and the specific conductance of the individual ice crystal structures.

The time profiles from both the features of interfacial polarization peak height and peak frequency and the impedance modelling parameters (C and R) were compared with the product temperature in order to characterize the impact of the different stages of the annealing cycle (viz. annealing temperature ramp up, annealing hold, and annealing temperature ramp down) (Figure 76) on the physical characteristics of the frozen matrix. In particular, it might be shown how (I) the glass transition of the matrix may be determined from the temperature ramp up and ramp down phases, (II) the kinetics of the ice crystal growth may be extracted from the hold phase of the annealing cycle.

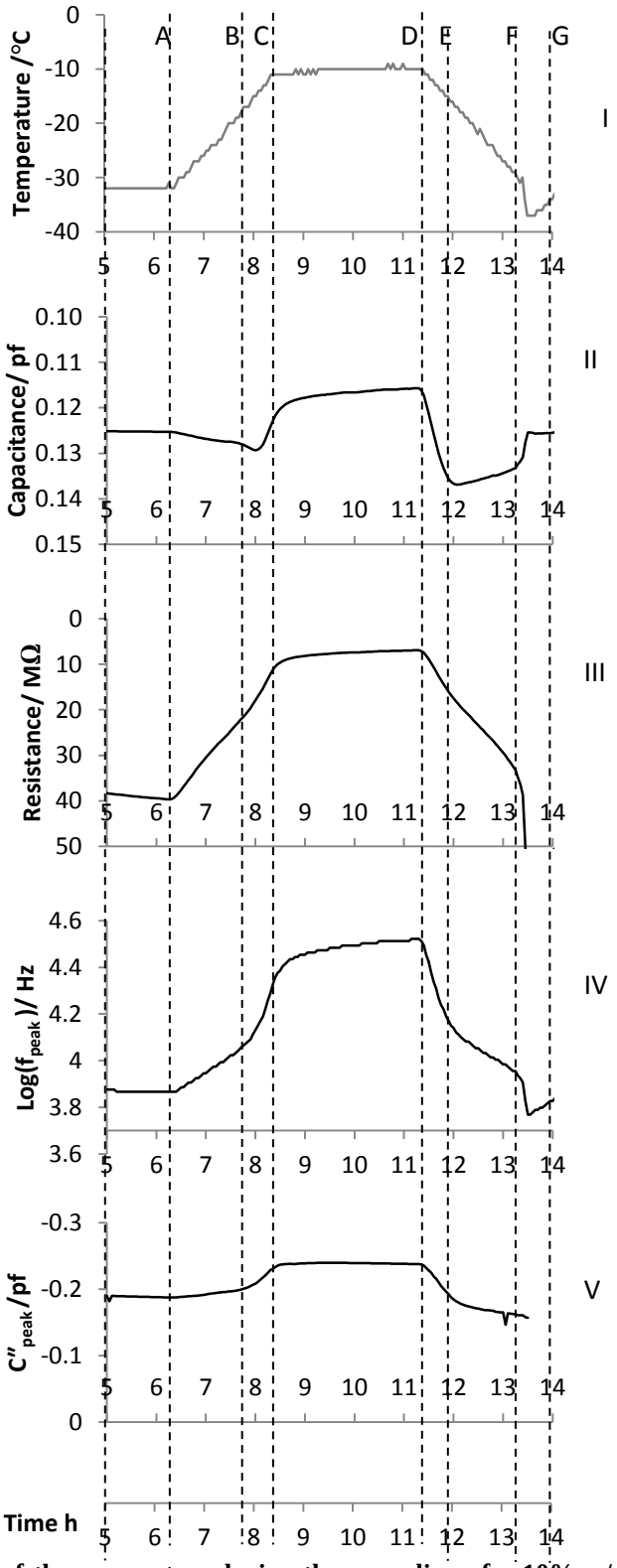

Figure 76 Time profiles of the parameters during the annealing of a 10% w/v maltodextrin solution a) temperature; b) fitting parameter capacitance, C; c) fitting parameter resistance, R; d) f_{peak} in logarithm scale; e) capacitance peak amplitude, C''_{peak}. Vertical lines correspond to the different stages of the annealing step: A-C annealing temperature ramp up; B glass transition during annealing temperature ramp up; C-D annealing temperature hold step; D-F temperature ramp down E the glass transition during temperature ramp down part annealing F vacuum applied to initiate primary drying

Temperature ramp up A-C

In contrast to the linear rise in the temperature, the product impedance parameters changed in a non-linear fashion, with discontinuities at time points in the product temperature profile (Figure 76 point B). These discontinuities in the impedance parameters (F_{peak}, C''_{peak}, R and C) were found to be in agreement with the glass transition temperature measured by DSC (-17 °C). The gradients of f_{peak}, C''_{peak} and R, against time, were smaller at temperatures below T_g than the gradient above this critical temperature. The change in the slope can be explained by the loss of co-operative motion of the molecules following the glass to liquid transition. The fact that the glass transition is clearly observed in the electrical parameters that characterize the frozen solution confirms that these parameters are clearly dependent on the characteristics of the unfrozen phase.

Effect of annealing on the glass transition temperature (B)

Previously, a method for determining the glass transition from the inflection point, the time derivative plots of the bulk capacitance or resistance of the formulation has been described in chapter 7. In this method, two linear functions are plotted to the data above and below the apparent inflection temperature, and the glass transition then estimated from the intersection between the lines of best fit. The root mean squared error for each line was calculated to determine the uncertainty in the estimate for T_g; The upper limit for the uncertainty in T_g was calculated by adding the RMS error to the value of the intercept for the sub T_g line and subtracting it from the line of best fit for the intercept for the supra-T_g line. The lower limit was calculated in an analogous way. This assessment of the degree of uncertainty can be taken as a measure of the precision of the glass transition estimation.

The methodology for analysis of the glass transition temperature was improved in this study. For the annealing ramp-up stage, the experimental temperature data measured by thermocouple were scattered. Nevertheless these data reveal the linear behaviour as a function of time and therefore they were exchanged by the model data estimated from the best fit to the linear function. Then all experimental parameters were analysed as a function of the linearized temperature (Figure 77). This methodology significantly reduced the level of scattering in experimental data and therefore decreased the uncertainty in Tg estimations from 0.3 – 0.5 °C to 0.03 – 0.2 °C.

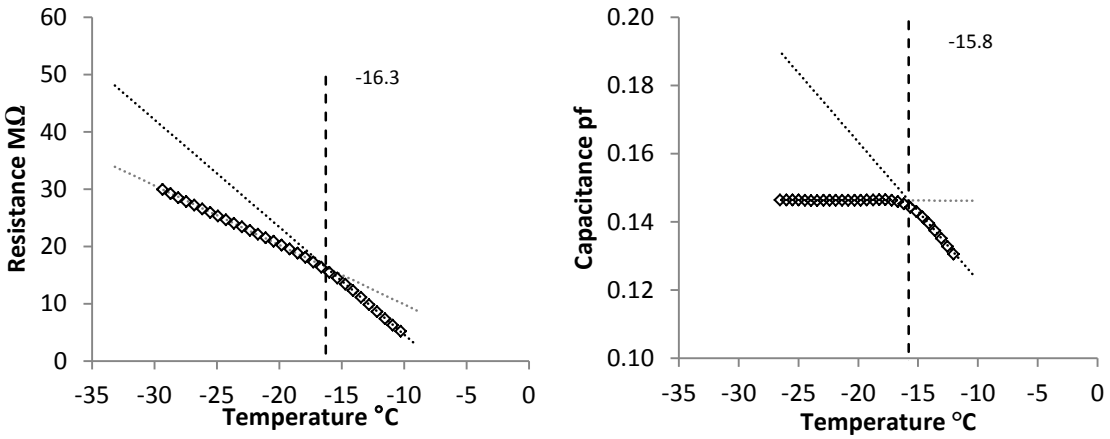

Figure 77 Estimates of glass transition temperature of maltodextrin 10% w/v from different the impedance data

The glass transition temperatures were calculated from both the temperature ramp up and ramp down stages, for each parameter describing the impedance spectrum (C, R). The results are summarized in Table 14.

Table 14 Estimates for the glass transition temperature from the equivalent circuit parameters (C and R).

Hold time h	Step detail	Tg from element C (°C)			Mean	SD	Tg from element R (°C)			Mean	SD
		Vial 1	Vial 2	Vial 3			Vial 1	Vial 2	Vial 3		
5	Ramp Up	-14.4	-17.2	-14.1	-15.23	1.40	-15.6	-16.5	-15.6	-15.9	0.42
	Ramp Down	-15.8	-16.1	-16.2	-16.03	0.17	-16.2	-15.8	-15.7	-15.9	0.22
3	Ramp Up	-14.9	-15.7	-15.6	-15.4	0.36	-15.5	-15.7	-15.4	-15.53	0.12
	Ramp Down	-15.5	-15.4	-16.1	-15.67	0.31	-15.4	-14.8	-14.4	-14.87	0.41
2	Ramp Up	-14.5	-15.1	-14.6	-14.73	0.26	-15.5	-15.3	-15.6	-15.47	0.12
	Ramp Down	-15	-16.1	-15.1	-15.4	0.50	-15.9	-15.8	-15.5	-15.73	0.17
1	Ramp Up	-15.1	-17.7	-16.7	-16.5	1.07	-16		-16.1	-16.05	0.05
	Ramp Down	-15.5	-16.9	-16.3	-16.23	0.57	-16.4	-16.1	-15.4	-15.97	0.42

The glass transition temperatures measured each parameter are lower (by ~ 0.5 °C on average) in the ramp down stage compared with the ramp up stage. A lower T_g in the ramp down stage is counter intuitive given that annealing is likely to increase the amount of ice. Increased ice would result in further concentration of the product and would therefore be expected to increase T_g observed during the ramp down stage rather than lowering it. What may therefore be proposed is that these differences are a systematic 'error' introduced by the nature of the measurement, i.e. whereby there is a delay in the registration of the transition point. This 'delay' would then translate to low estimate for T_g on ramp down and a slightly higher estimate for T_g on ramp up. More importantly these observations suggest that no further ice is formed during the annealing stage, and that the observed reduction in the primary drying temperature must be due primarily to the process of recrystallization.

Structural changes in ice during the holding temperature (phase C-D)

Having passed through T_g on the ramp up phase of the annealing stage (Figure 76) the solution then equilibrates to the shelf temperature. At 8 h (taken as time 0 in the annealing hold) the solution temperature has now stabilised at the target temperature of -10 °C. After this time point, the characteristics of the solution continue to evolve as evidenced by the progressive changes in the electrical capacitance and the electrical resistance of the matrix within the vial (Figure 78). However, on closer examination it appears that the capacitance change is somewhat negligible (< 3%) compared with the resistance change (~ 30%). One can suppose that the maltodextrin solution has reached an equilibrium temperature but there is a continued development of the ice structure during the holding period. Given that the capacitance changes little but the resistance changes dramatically one can suppose that the volume fraction of ice is not changing but that the structure (ice crystal size and connectivity between ice crystals) is changing significantly. Given the earlier inference from the observation of a glass transition (that the electrical parameters are dependent on the unfrozen phase) it might also be inferred that these changes in the electrical resistance during the hold phase are indirect mean of the changes in frozen matrix. Strictly speaking the observed changes in the electrical resistance are the consequence of simplification of the matrix architecture both in term of the ice structure and the interstitial spaces unfrozen phase. From the resistance plot it appears that the rate of change slows significantly after 3h, again pointing towards a saturation of the recrystallization mechanism.

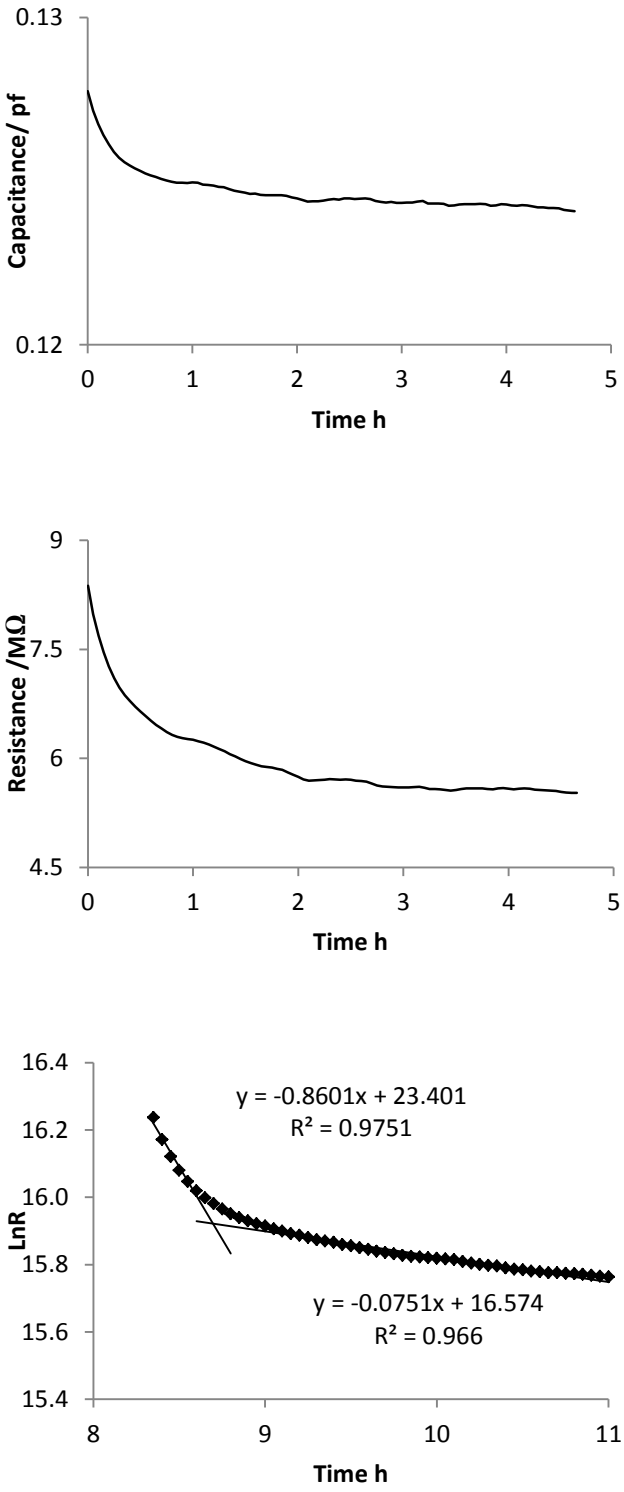

Figure 78 impedance profile of maltodextrin 10% w/v during the annealing hold phase A) Capacitance B) Resistance C) ln R

Given that only the resistance is changing and the capacitance remains approximately constant then it is possible to speculate on the mechanisms of annealing. The invariant capacitance during the annealing hold time shows that ice volume fraction does not increase appreciably during hold period. Partial devitrification is therefore an unlikely explanation for an increased ice crystal size that is inferred from the observed increased in drying rate. However, the fact that resistance changes appreciably is taken to imply that the connectivity between the crystals is increasing during the hold period.

Rate of resistance change during annealing

Taking the logarithm of the resistance and re-plotting against time may provide an opportunity to extract rate constants (Figure 78C). The data might appear to suggest that there are in fact two rates of recrystallization however it is possible that the first fast rate may be an artefact, which does not reflect the recrystallization process, but is rather the tail end of the temperature equilibration phase.

Alternatively, there may indeed be two rates of recrystallization. The process of recrystallization results from the fact that small crystals are thermodynamically unstable and rich source of water molecules to promote the growth of larger crystals. However, the dissolution of a population of small crystals and the growth of larger ones also requires the diffusion of the liberated water molecules form one interface to another. The diffusion path length will then define the rate as much as the diffusion coefficient of the water molecule through the unfrozen fraction.

However, there is another possibility that there may be a population of needle like crystals that have high surface energies at their apex. Water molecules at these locations may detach from the surface and relocate to a more favourable (lower energy) size elsewhere on the crystal. The diffusion path length for these events will be much shorter than those associated with a small crystal dissolving and the constituent molecules relocating to the interface of a separate crystal. Once these have been exhausted then the rate slows down to one which depends on devitrification. The slow rate may results from the low chemical potential of water molecules in the amorphous state compared with those occupying position in the lattice of a small crystal, coupled to the greater diffusion path length between these molecules and the ice crystal interface.

Weight loss on primary drying

The formulation weight was measured before the start of freeze-drying and the end of primary drying (as determined from the impedance measurements). The result from residual weight (%) of the formulation after primary drying suggests an insignificant increase in amount of ice after annealing as the weight of dried mass was recorded to be 9.85±1.35 % compared to the one recorded from non-annealed formulations (10.6±0.3 %). Inaccuracies in these measurements result to some degree from the trailing cables that are difficult to accommodate on the top balance.

9.4 Discussion

In the first part of this chapter the relationships between drying rates (as determined by dC″/dt) and the primary drying time (duration) were explored and it was found that both increasing the annealing hold time and annealing temperature increase the subsequent primary drying rate until an annealing hold time of 3 h (Figure 73D and E). Annealing times greater than 3 h does not any further effect and the drying rate appears to stay constant. Not surprisingly the dependence of drying time vs. drying rate is also linear (Figure 73F).

At first glance this might appear to be an obvious/expected result. However it is one which is based on the assumption that dC″/dt is time measurement of relative drying rate. These results appear to substantiate that assumption. Moreover, the results obtained in the present study are in good agreement with the literature conclusion about correlation between the annealing hold time and elevated sublimation rates resulting from decrease in the dry layer resistance (Abdelwahed et al., 2006). These increments in the sublimation rates are the possible outcome of restructuring of the frozen/unfrozen phases during annealing which can be explained with the changes in the electrical impedance of the formulation.

The behaviour of electrical capacitance and electrical resistance are explored to see if the mechanism of annealing may be elucidated. Results have shown that of these two parameters, the most sensitive parameter to annealing is the resistance, which is directly related to conductivity of the frozen matrix. The possible mechanisms for conductivity in a frozen solution containing an ice phase and a solute rich unfrozen solution phase are: (i) conductivity of the ions in the viscous unfrozen fraction; (ii) proton hopping through and over the surface of ice crystals, and (iii) conductivity through the ice crystals due to defects in the ice structure. Contribution of these mechanisms depends on the temperature range.

The bulk conductivity /resistance can be estimated if the volume fractions of unfrozen water and ice, the connectivity within each fraction, and the specific conductivities of each phase, are first known. At positive temperatures (i.e. above the melting point) only the conductivity of water and dissolved solutes can contribute. However, on freezing (phase separation of water as ice) there is the potential contribution from ice to consider. The efficiency of the proton hopping conduction mechanism through the new ice phase will depend on the geometry (length, width) of the channels which then grow, or change in shape, during annealing. During freezing at low volume fraction of ice, if the connectivity between ice crystals is limited then the resistance will depend on the conductivity of the unfrozen fraction; which will in turn be governed by the concentration of water, ions and other charged species within that phase and the temperature (which defines the viscosity). However, at a critical concentration of ice (which also depends on the shape, size, and orientation of the individual ice crystals) on might expect a significant increase in the connectivity between ice crystals, providing a connected pathway/channel for the protons. Once the ice crystal connectivity reaches a saturation level then the percolation of charge is said to occur. The amount of ice that forms in the 10% maltodextrin solution is close to that theoretical maximum provided by the available water (i.e. ~ 90%) and therefore one might presume that charge percolation through a partially connected network of ice crystal structures will be a feature of this system. However, this does not imply that the resistance of the system is now dominated by the percolation of charge through the ice crystal structures, as it is possible that the specific conductivities of this phase is much less than that of the unfrozen fraction. It remains a distinct possibility that the overall resistance of the mixed phase system remains that due (at least in part) to the connectivity of the channels within the unfrozen fraction. Whereas, at temperatures below glass transition (T_g), it can be assumed that the unfrozen fraction will have a very low specific conductivity, and therefore the proton hopping conductivity mechanism through the ice phase will dominate. In the relatively narrow temperature range between glass transition and annealing temperature both mechanisms may contribute with the exact proportional contributions from each mechanism being affected by annealing process. A transient increase in the gradient of conductivity recorded at temperature exceeding glass transition appears to confirm the emerging dependence of the matrix conductivity on the physical properties unfrozen fraction.

The connections between the ice crystals can be thought of as channels, not only for the routing of protonic charge through the ice phase, but also for the diffusion of water vapour

during the sublimation phase. The architecture of the matrix associated with the unfrozen viscous solution is expected to adapt to the shape which complements the connected ice networks. It is expected that these structures will therefore become less tortuous as the ice structure becomes more regular. Given that the dimensions and architecture of the ice channels are the same that those which define the dry layer mass transfer resistance then one might expect there to be a correlation between the electric resistance of the frozen matrix and the drying rate.

However, one might also argue that the ice crystal size growth is also accompanied by some degree to devitrification which also improves the connectivity between the ice structures by increase in the volume fraction of ice. In that case one might expect that the amount of ice can be estimated by means of gravimetric measurements (freeze drying microbalance and or weighing the formulation by interrupting the cycle (Scorer T et al., 2004)) and/or by assessments of the physical properties of the formulation (changes in the electrical capacitance using mixture formula (Bittelli et al., 2004) and changes in the glass transition temperature via the Gordon Taylor equation (Gordon and Taylor, 1952)). However, there are likely to be differences in the limit of detection of the new ice phase, that could form on devitrification, by each of these techniques (e.g. Freeze drying microbalance ± 5mg (Christ, 2010), analytical balance 50 mg (Scorer T et al., 2004)).

Given the precision of the through-vial impedance method for the measurement of the glass transition temperature, an assessment of the changes in the freeze concentration of the solution from glass transition data was made by using Gordon-Taylor equation. The phase diagram of maltodextrin (calculated from the Gordon-Taylor equation (Gordon and Taylor, 1952)) suggests a significant increase in T_g from -16.9 to -11.5 °C as the concentration of the unfrozen solution (C_g) increased from 85 to 86% w/w. However, the results from the glass transition measurement reported herein, demonstrate an insignificant variation in T_g following annealing (within the margin of error ~0.5°C). This implies that a maximal freeze concentration of the solution (C_g' ~ 86% w/w maltodextrin) is achieved during the initial pre-freezing phase. It can also be assumed that the glass transition, measured at each annealing stage, can be assumed to approximate to T_g' (i.e. T_g Prime) and therefore it may be concluded that annealing does not result in the formation of more ice volume.

The next step was to calculate the impact of a possible 1% shrinkage in the volume of the unfrozen fraction, on the weight of additional ice that might form as a consequence of

devitrification, in order to assess the suitability of gravimetric methods for determining devitrification phenomenon. The additional ice can be approximated by taking the weight of maltodextrin (3g) and then calculating the difference between the weight of water in an 85% solution and an 86% solution of maltodextrin. The net change in water content weighs 0.004g which resides within the error limit of gravimetric techniques as delineated above, thereby making the gravimetric techniques much less applicable in the assessment of devitrification.

9.5 Summary

Possibly the most useful application of impedance measurements, over thermocouple measurements, is the opportunity it provides to assess the impact of annealing on both the structure of ice that forms and the consequent impact on the primary drying rate. It has also been demonstrated from in-vial measurements of the glass transition temperature, that maximum freeze concentration of the maltodextrin solution is accomplished during the initial freezing phase; and that annealing doesn't increase the volume fraction of the ice in sample, but simply increases the connectivity between ice crystals, thereby creating larger pores within the solid matrix which facilitate the diffusion of water vapours from the product and accelerate the drying rate. Impedance measurements may provide information on the optimal condition of the sample (in relation to ice crystal structure and maximal freeze-concentration) at the end of the pre-freezing stage, before the decision is made to initiate the primary drying phase. Once primary drying has started then it would be impossible to reverse the process. However, the pre-freezing stage may be re-cycled as many times as necessary to create the optimal ice-structure prior to initiating the next phase. It follows that in-process impedance measurements might provide the necessary insight into the structural properties of the frozen solution to inform the process development cycle.

10 General Discussion

Characterization of the freeze-drying process

The different parameters, characterising the impedance spectrum from through-vial impedance spectroscopy measurements, have been shown to be more or less sensitive to the features of the process, i.e. product cooling, ice formation, solute crystallization, glass transition and primary drying endpoint.

A good correlation between both f_{peak} and R with temperature can be explained by the fact that the relaxation time constant for a given solution, within the electrode assembly, is primarily a function of temperature (provided that there is no phase change). However, during ice formation the impedance profile is then impacted by the exothermic ice crystallization process, the change in state from solution to partial solid, and the changes in the viscosity of the unfrozen fraction. In brief, the parameter f_{peak} decreases by 1-2 decades during ice formation as a consequence of the solidification process.

Solute crystallization, on the other hand, demonstrates a comparatively smaller decrease in f_{peak} than the ice formation, the decrements of which are further reduced visually if plotted on log scale. As an alternate, a linear scale presentation of R data shows a clearer evidence of solute crystallization.

The gradients of both f_{peak} and R changed following the glass transition as the ion mobility increased due to temperature driven viscosity changes. The gradients of parameter C in contrast changed more significantly, which may in part be explained by a lower values dielectric constant of water (ε_{water} 80) than ice (ε_{ice} 100). Since the gradient of C is steeper, one may argue that other mechanisms are also contributing to this change in capacitance. A correlation between the C with the heat capacity of the unfrozen solution may explain the decrease in former (C) more precisely.

During primary drying, the imaginary part of impedance provide a realistic evidence of primary drying end point as it measures the contribution from the ice whereas the real part of capacitance measures the response of entire mass comprising of both the dried and frozen matrix.

Chapter 10

In the later part of this study, the impedance measurement were employed to explore the mechanistic basis of changes in ice structure/volume fractions during the thermal treatments which results in shorter primary drying times. The reduction in dry layer resistance to vapour flow has been explained by ice crystal size growth; the sublimation of which provides a wider passage for the upcoming vapours. A possibility of increased ice crystal sizes by devitrification was discounted on the basis that the glass transition temperature, a primary determinant of the water-solute composition in the unfrozen fraction, was not changed before or after annealing. The electrical resistance of the frozen matrix decreased during the annealing hold time which suggests that the unfrozen matrix continues to achieve a simplified structure as a consequence of Ostwald ripening.

Perspectives for extended application of the technology

The data reported to date concerns a limited range of solutes/solutions and process conditions (i.e. fixed vacuum pressure). Clearly, in applying the technology in a broader sense one needs to consider a number of features of the system in order to record the interfacial polarization peak within the measurement frequency range. These include; conductivity of the solution, fill volume in relation to the height of electrode, vial size/geometry.

- The **conductivity** of a solution, defined by, ionic species present, their mobility factors and concentrations carries an inverse correlation with the electrical impedance. Due to reason solution with high conductivity (e.g. maltodextrin) did not show an interfacial relaxation peak in the liquid state as it is expected to exist above the measured frequency range. Nevertheless, decreased charge mobility in the frozen state results in an increased resistance which brings the f_{peak} in the measured frequency window.
- The sensitivity of the interfacial relaxation process to the fill height can explained by the fact that the f_{peak} increased significantly as **fill volume** across the electrode walls was increased. However increments in the fill volume above the electrode demonstrate only small increments in the f_{peak}. It may be satisfactory to state that representative product information can be obtained at the fill factor range of 0.5 to 1.5.
- The impedance of a solution within a cell (vial) is described with a cell constant which is explained by a well-known relationship to the geometrical parameters $C \propto A/d$ where d internal diameter of the vial and A is vertical cross sectional area of the

electrode. Due to the fact, the position of interfacial polarization peak may differ in different vial sizes. This was covered in appendix 2.

Process Optimization and Process Control Applications

The applications of impedance spectroscopy in the measurement of phase transition, ice recrystallization, primary drying rates end points provides the basis for its utility as a PAT and the opportunity to apply the quality by design approach in the development, monitoring and control of freeze drying process. A number of aspects to this opportunity are now presented:

In-vial measurement of critical temperatures: Measurement of the post ice-formation phase changes (i.e. glass transition, eutectic crystallization) in the unfrozen fraction of a frozen solution contained in the glass vials placed on the temperature regulated shelf of the freeze drier, by impedance measurement system, provide a rational for the development of an evidence based freeze drying cycle without additional safety temperature margins as practiced with the results from off-line thermo-physical characterizations. Moreover the impact of added excipient (sucrose) on the critical temperatures suggests the application of impedance measurement not only in the freeze drying cycle development for complex formulations but also in the confirmation of the quality of the supplied excipients. Added impurities would result a change in the glass transition or crystallization behaviour of the material.

Characterization of primary drying: characterization of the primary drying by TVIS provides valuable information on the mass transfer rate without perturbing the heat flow as observed in the case of freeze drying microbalance. This is in addition to the benefit of measuring the electrical response from the vial located within the hexagonal array on the shelf. However this application will requires a calibration of impedance profile with the gravimetric responses.

The estimates for sublimation rate are also expected to be more accurate than the MTM as the measurement as mass transfer rate (MTR) are not calculated ‘as averages values’ indirectly from the pressure rise data acquired by isolating the chamber drying chamber which in a way is perturbing the vapour flow. In addition, there is no minimum fill load limit as is required by MTM measurement during the cycle development which adds to the process development cost. The impedance measurement system is expected to complement the pressure rise/ MTM

results by providing the realistic measurement of mass transfer instead of the averaged estimates made from the MTM data which may significantly differ from the real data due to low fill load and a non-planer sublimation front.

Measurement of the end of primary drying enables the timely switching to secondary drying which bear a significant impact on the duration and cost of the process. This methodology would exclude time overage routines generally practiced with the thermocouple measured end point to accommodate the probe related as well spatial variations in the sublimation profiles. Moreover the impact of different process/product parameters, such as controlled nucleation, annealing temperature, annealing hold time; and the concentration of the excipients in a formulation on the sublimation profile, can be evaluated to develop an improved understanding of the process without including product invading probes which perturb the process.

It is evident the impedance measurement system can be employed to measure (i) the critical temperatures which are a pre-requisite for the set up drying temperatures and (ii) the monitoring of the drying process (iii) and the primary drying end point. In so doing the technology benefits the process development scientist with “Right first time” approach in cycle development.

Representative measurement: The non-invasive measurement of a product cooling rate, ice onset and progression by the impedance profiles is advantageous over the thermocouple probes as the latter induce freezing at low degree of super-cooling with a consequence of coarser ice morphologies and faster drying rates than the regular vials without probes. The impedance measurement system, in contrast, measures the responses which are representative of the controls, (regular vials) therefore, provides a more reliable estimate of physical changes in the formulation.

Optimization of freeze drying cycles: in the present study, the impedance measurement system has been applied to optimize the annealing stage of the freeze drying process. Similarly, the technique can also be employed to evaluate the impact of other process parameters such as the impact of degree of super-cooling and controlled nucleation on the primary drying. A recently reported capability of impedance measurement system in the identification of product collapse relative to the shelf temperature and the chamber pressure provide the basis for the set-up of optimum primary drying conditions. Furthermore, in

combination with the MTM-based smart freeze drying technique, the impedance measurement system is expected to consequence better controlled, short duration optimized cycles without compromising the critical quality attributes such as cake structure, reconstitution time.

Limitations

The principal limitation is that the impedance of a frozen solution represents the bulk characteristic of the mass contained within the glass vial. As a consequence it does not provide information about the microstructure of the ice matrix.

Since, the ice crystal growth initiate from the vial base and progress to the top, one may suggest that the crystal habit in the vial follows a vertical arrangement which is least described by this electrode assembly.

It follows that the technology has limited scope for the accurate measurement of the polydispersity of the ice crystals within the frozen matrix. However a possible correlation between the time derivative of capacitance (dC″/dt) with the sublimation rate will extend the application of impedance spectroscopy in the measurement of mass transfer resistance through the dry layer which will provide indirect evidence of the ice crystal habits.

11 Conclusions

It has been demonstrated that the impedance measurement approach registers the manifestation of (i) ice formation and (ii) critical transitions in the frozen state (i.e solute crystallization and glass transition) which confirms that the unfrozen fractions in the frozen matrix are stable enough to support its structure during next stage i.e. primary drying. The technology has been shown to monitor and record the progression and completion of ice sublimation results in realistic measurement of drying times without invading the product.

Amongst the single vial process analytical technologies, the impedance measurement system is the first one described with a valuable role in the optimization of annealing stage. Previously, a batch measurement technique MTM was employed to investigate the optimum annealing hold times. The operation of this PAT requires a higher fill loads which increases the cost of development. In so doing the development costs as well as the scale up issues are expected to be reduced with the impedance spectroscopy. The product profiles from the impedance measurement vials are believed to be representative of the formulations processed in the regular vials which provides the basis of more realistic freeze drying cycle development approach.

In summary, the application of impedance measurement system provides a non-invasive, real time product characterization which benefits with an improved quality risk management and process control.

12 Future Perspectives

Non-invasive measurement of the freezing and primary drying of the surrogate formulations at different position of shelf within the hexagonal array may be employed to investigate the spatial variations in the temperature distribution across the freeze drier shelf. Hot and cold spots are expected to pose challenges like product collapse and protracted drying times respectively. The premier (hot spot) will help to set up ceiling drying temperatures while the latter (cold spot) will provide realistic information of the primary drying end points.

The ice sublimation rates measured from the decrease in imaginary part of the capacitance profile may be calibrated with the gravimetric measurements performed with freeze drying microbalance. Thereby the impact of different process/ product parameters (annealing, solute concentration, ice crystal sizes) may be studied on the sublimation kinetics. The sublimation rate estimated from impedance data will be employed to calculate the thermal co-efficient of the vial more representative of the plain vial as compared to thermocouple data. Variation in the thermal co-efficient of the vials (K_v) with reference to the fill load on the shelf and/ or spatial distribution may provide the basis for the development of a realistic model of the heat and mass flow which will predict the scale up of freeze drying process more faithfully.

Furthermore the technology may be employed to characterize more complex formulations containing different polymeric solutions to identify the phase separation during freeze thawing. In doing so, the techniques can be of value in the screening of excipients.

The technology may also be applied in the development/ optimization of formulations containing biopharmaceutical agents (such as proteins, nucleic acids, hormones) will reduce the cost/time for the development of these pharmaceutical formulations.

Other potential application of TVIS may include the measurement of product shrinkage or collapse during freeze drying cycles. A timely identification of product collapse may provide an opportunity to protect the residual formulation by adjusting the process parameters during primary drying. The technology may also be applied to differentiate between planar or cone shaped ice front during the sublimation stage.

13 References

A.I. LIAPIS, R. B., M.J. PIKAL 1996. Research and development needs and opportunities in freeze drying. *Drying Technology,* 14**,** 1265-1300.

ABDELWAHED, W., DEGOBERT, G. & FESSI, H. 2006. Freeze-drying of nanocapsules: Impact of annealing on the drying process. *International Journal of Pharmaceutics,* 324**,** 74-82.

ABLETT, S., IZZARD, M. J. & LILLFORD, P. J. 1992. Differential scanning calorimetric study of frozen sucrose and glycerol solutions. *Journal of the Chemical Society-Faraday Transactions,* 88**,** 789-794.

ALTMANN, R. 1890. Die Elementarorganismen und ihre Beziehungen zu den Lellen. Leipzig: Veit and Co.

ANGELL, C. A. 2002. Liquid Fragility and the Glass Transition in Water and Aqueous Solutions. *Chemical reviews,* 102**,** 2627-2650.

ARMSTRONG, J. G. 1980. Use Of The Capacitance Manometer Gauge in Vacuum Freeze-Drying. *PDA Journal of Pharmaceutical Science and Technology,* 34**,** 473-483.

AULTON, M. E. 2002. Drying. *In:* AULTON, M. E. (ed.) *Aulton's Pharmaceutics:The Design and Manufacture of Medicines.* 2 ed. London: Elsevier.

BARDAT, A., BIGUET, J., CHATENET, E. & COURTEILLE, F. 1993. Moisture Measurement: A New Method for Monitoring Freeze-drying Cycles. *PDA Journal of Pharmaceutical Science and Technology,* 47**,** 293-299.

BARRESI, A. A., PISANO, R., FISSORE, D., RASETTO, V., VELARDI, S. A., VALLAN, A., PARVIS, M. & GALAN, M. 2009. Monitoring of the primary drying of a lyophilization process in vials. *Chemical Engineering and Processing,* 48**,** 408-423.

BARRESI., A. A., VELARDI., S. A., PISANO., R., RASETTO., V., VALLAN., A. & GALAN., M. 2009. In-line control of the lyophilization process. A gentle PAT approach using software sensors. *international journal of refrigeration,* 32**,** 1003–1014.

BERGMAN, J. 2008. Ernst Chain: Antibiotic poineer. *Acts and facts,* 37**,** 10-12.

BERNTSSON, O., DANIELSSON, L. G., LAGERHOLM, B. & FOLESTAD, S. 2002. Quantitative in-line monitoring of powder blending by near infrared reflection spectroscopy. *Powder Technology,* 123**,** 185-193.

BILIADERIS, C. G., SWAN, R. S. & ARVANITOYANNIS, I. 1999. Physicochemical properties of commercial starch hydrolyzates in the frozen state. *Food Chemistry,* 64**,** 537-546.

BITTELLI, M., FLURY, M. & ROTH, K. 2004. Use of dielectric spectroscopy to estimate ice content in frozen porous media. *Water Resour. Res.,* 40**,** W04212.

BORDE, B., BIZOT, H., VIGIER, G. & BULEON, A. 2002. Calorimetric analysis of the structural relaxation in partially hydrated amorphous polysaccharides. I. Glass transition and fragility. *Carbohydrate Polymers,* 48**,** 83-96.

BRÜLLS, M., FOLESTAD, S., SPARÉN, A. & RASMUSON, A. 2003. Near-Infrared Spectroscopy Monitoring of the Lyophilization Process. *Pharmaceutical Research,* 20**,** 494-499.

BYEONG S. CHANG, S. Y. P. 2004. Freeze drying process development for protein pharmaceuticals. *In:* COSTANTINO, H. R. P., MICHAEL J. (ed.) *Lyophilization of Biopharmaceuticlas.* Arlington: American Association of pharmaceutical scientist.

CARPENTER, J. F., PIKAL, M. J., CHANG, B. S. & RANDOLPH, T. W. 1997. Rational Design of Stable Lyophilized Protein Formulations: Some Practical Advice. *Pharmaceutical Research,* 14**,** 969-975.

CAVATUR, R., VEMURI, N. M., PYNE, A., CHRZAN, Z., TOLEDO-VELASQUEZ, D. & SURYANARAYANAN, R. 2002. Crystallization Behavior of Mannitol in Frozen Aqueous Solutions. *Pharmaceutical Research,* 19**,** 894-900.

CHAMPION, D., LE MESTE, M. & SIMATOS, D. 2000. Towards an improved understanding of glass transition and relaxations in foods: molecular mobility in the glass transition range. *Trends in Food Science and Technology,* 11**,** 41-55.

CHANG, B. S. & PATRO, S. Y. 2004. Freeze-drying Process Development for Protein Pharmaceuticals. *In:* COSTANTINO., H. R. & PIKAL, M. J. (eds.) *Lyophilization of Biopharmaceuticals.* 2 ed. New York: Springer.

CHAPLIN, M. 2007. Water's Hydrogen Bond Strength. *ArXiv e-prints***,** 20.

CHEN, R., SLATER, N. K. H., GATLIN, L. A., KRAMER, T. & SHALAEV, E. Y. 2008. Comparative Rates of Freeze-Drying for Lactose and Sucrose Solutions as Measured by Photographic Recording, Product Temperature, and Heat Flux Transducer. *Pharmaceutical Development and Technology,* 13**,** 367–374.

CHIN, K. B., BUEHLER, M. G., SESHADRI, S., KEYMEULEN, D., ANDERSON, R. C., DUTZ, S. & NARAYANAN, S. R. 2007. Investigation of water and ice by ac impedance using electrochemical properties cup. *Review of Scientific Instruments,* 78**,** 016104-3.

CHOUVENC, P., VESSOT, S. & ANDRIEU, J. 2006. Experimental Study of the Impact of Annealing on Ice Structure and Mass Transfer Parameters during Freeze-Drying of a Pharmaceutical Formulation. *PDA Journal of Pharmaceutical Science and Technology,* 60**,** 95-103.

CHOW, R., BLINDT, R., CHIVERS, R. & POVEY, M. 2003. The sonocrystallisation of ice in sucrose solutions: primary and secondary nucleation. *Ultrasonics,* 41**,** 595-604.

CHRIST, M. 2010. Smart Freeze Drying Basic principles, optimum procedures and applications. Germany: Martin Christ.

CIRKEL, P. A., VAN DER PLOEG, J. P. M. & KOPER, G. J. M. 1997. Electrode effects in dielectric spectroscopy of colloidal suspensions. *Physica A: Statistical Mechanics and its Applications,* 235**,** 269-278.

CONNELLY, J. P. & WELCH, J. V. 1993. Monitor Lyophilization with Mass Spectrometer Gas Analysis. *PDA Journal of Pharmaceutical Science and Technology,* 47**,** 70-75.

CORVELEYN, S. & REMON, J.-P. 1996. Maltodextrins as Lyoprotectants in the Lyophilization of a Model Protein, LDH. *Pharmaceutical Research,* 13**,** 146-150.

COSENZA, P., GHORBANI, A., CAMERLYNCK, C., REJIBA, F., GUERIN, R. & TABBAGH, A. 2009. Effective medium theories for modelling the relationships between electromagnetic properties and hydrological variables in geomaterials: a review. *Near Surface Geophysics,* 7**,** 563-578.

COSLOVICH, D. & PASTORE, G. 2009. Dynamics and energy landscape in a tetrahedral network glass-former: direct comparison with models of fragile liquids. *Journal of Physics: Condensed Matter,* 21**,** 285107.

CRAIG, D. Q. M. (ed.) 2005. *Dielectric analyis of pharmaceutical systems,* London: Taylor and Francis.

CUKIERMAN, S. 2006. Et tu, Grotthuss! and other unfinished stories. *Biochimica et Biophysica Acta (BBA) - Bioenergetics,* 1757**,** 876-885.

DE BEER, T., BURGGRAEVE, A., FONTEYNE, M., SAERENS, L., REMON, J. P. & VERVAET, C. 2010. Near infrared and Raman spectroscopy for the in-process

monitoring of pharmaceutical production processes. *International Journal of Pharmaceutics,* In Press, Corrected Proof.

DE BEER, T. R. M., ALLESO¸, M., GOETHALS, F., COPPENS, A., VANDER HEYDEN, Y., LOPEZ DE DIEGO, H., RANTANEN, J., VERPOORT, F., VERVAET, C., REMON, J. P. & BAEYENS, W. R. G. 2007. Implementation of a Process Analytical Technology System in a Freeze-Drying Process Using Raman Spectroscopy for In-Line Process Monitoring. *Analytical Chemistry,* 79**,** 7992-8003.

DE BEER, T. R. M., VERCRUYSSE, P., BURGGRAEVE, A., QUINTEN, T., OUYANG, J., ZHANG, X., VERVAET, C., REMON, J. P. & BAEYENS, W. R. G. 2009. In-line and real-time process monitoring of a freeze drying process using Raman and NIR spectroscopy as complementary process analytical technology (PAT) tools. *Journal of Pharmaceutical Sciences,* 98**,** 3430-3446.

DEBENEDETTI, P. G. & STILLINGER, F. H. 2001. Supercooled liquids and the glass transition. *Nature,* 410**,** 259-267.

DEBYE, P. 1929. Polar molecules. *Chemical Catalog Co. New York***,** Pp172.

EDINARA ADELAIDE BOSS, R. M. F., EDUARDO COSELLI VASCO DE TOLEDO 2004. Freeze drying process: real time model and optimization. *Chemical Engineering and Processing,* 43**,** 1475–1485.

ELNAGGAR, Y., EL-MASSIK, M., ABDALLAH, O. & EBIAN, A. 2010. Maltodextrin: A Novel Excipient Used in Sugar-Based Orally Disintegrating Tablets and Phase Transition Process. *AAPS PharmSciTech,* 11**,** 645-651.

ELSER, W. J., THOMAS, R. A. & STEFFEN, G. I. 1935. The Desiccation of Sera and Other Biological Products (Including Microörganisms) in the Frozen State with the Preservation of the Original Qualities of Products So Treated. *Journal of Immunology,* 28**,** 433-473.

ERMOLINA, I. & SMITH, G. 2011. Dielectric spectroscopy of low-losses sugar lyophiles: III: The influence of moisture on the dielectric response of freeze-dried lactose. *Journal of Non-Crystalline Solids,* 357**,** 671-76.

F BORDAS & D'ARSONVAL., M. 1906. C R Acad Sci Paris 142:1058 and 1079; 143:567.

FDA 2004. Guidance for Industry PAT — A Framework for Innovative Pharmaceutical Development, Manufacturing, and Quality Assurance. Rockville USA.

FISSORE, D., VELARDI, S. A. & BARRESI, A. A. 2008. In-Line Control of a Freeze-Drying Process in Vials. *Drying Technology,* 26**,** 685 - 694.

FLOSDORF, E. W., AND, L. W. H. & MUDD, S. 1945. Drying by Sublimation. *Journal of Immunology,* 50**,** 21-54.

FLOSDORF, E. W. & MUDD, S. 1935. Procedure and Apparatus for Preservation in "Lyophile" form of Serum and Other Biological Substances. *Journal of Immunology,* 29**,** 389-425.

FLOSDORF., E. & STOKES., S. F. M. 1940. THe desivac process for drying from the frozen state. *Journal of the American Medical Association,* 115**,** 1095-1097.

FRAKE, P., GREENHALGH, D., GRIERSON, S. M., HEMPENSTALL, J. M. & RUDD, D. R. 1997. Process control and end-point determination of a fluid bed granulation by application of near infra-red spectroscopy. *International Journal of Pharmaceutics,* 151**,** 75-80.

FRANKS, F. 2007. *Freeze-drying of Pharmaceuticals and Biopharmaceuticals,* Cambridge, The Royal Society of Chemistry,.

GAN., K. H., BRUTTINI., R., CROSSER., O. K. & LIAPIS., A. I. 2005. Freeze-drying of pharmaceuticals in vials on trays: effects of drying chamber wall temperature and tray

side on lyophilization performance. *International Journal of Heat and Mass Transfer,* 48**,** 1675–1687.

GENIN, N., RENE, F. & CORRIEU, G. 1996. A method for on-line determination of residual water content and sublimation end-point during freeze-drying. *Chemical Engineering and Processing,* 35**,** 255-263.

GIESELER, H., KESSLER, W. J., FINSON, M., DAVIS, S. J., MULHALL, P. A., BONS, V., DEBO, D. J. & PIKAL, M. J. 2007a. Evaluation of tunable diode laser absorption spectroscopy for in-process water vapor mass flux measurements during freeze drying. *Journal of Pharmaceutical Sciences,* 96**,** 1776-1793.

GIESELER, H., KRAMER, T. & PIKAL, M. 2007b. Use of Manometric Temperature Measurement (MTM) and SMARTTM Freeze Dryer Technology for Development of an Optimized Freeze-Drying Cycle. *Journal of Pharmaceutical Sciences,* 96**,** 3402-3418.

GIORDANO, A., BARRESI, A. A. & FISSORE, D. 2011. On the use of mathematical models to build the design space for the primary drying phase of a pharmaceutical lyophilization process. *Journal of Pharmaceutical Sciences,* 100**,** 311-324.

GORDON, M. & TAYLOR, J. S. 1952. Ideal copolymers and the second-order transitions of synthetic rubbers. i. non-crystalline copolymers. *Journal of Applied Chemistry,* 2**,** 493-500.

GREAVES, R. I. N. 1946. *The Preservation of Proteins By Drying With Special Reference to the Production of Dried Human Serum and Plasma for Transfusion,* London, HMSO.

GROHGANZ, H., FONTEYNE, M., SKIBSTED, E., FALCK, T., PALMQVIST, B. & RANTANEN, J. 2009. Role of excipients in the quantification of water in lyophilised mixtures using NIR spectroscopy. *Journal of Pharmaceutical and Biomedical Analysis,* 49**,** 901-907.

HAUSMAN, D. S., CAMBRON, R. T. & SAKR, A. 2005. Application of on-line Raman spectroscopy for characterizing relationships between drug hydration state and tablet physical stability. *International Journal of Pharmaceutics,* 299**,** 19-33.

HAWE, A. & FRIEß, W. 2006. Impact of freezing procedure and annealing on the physico-chemical properties and the formation of mannitol hydrate in mannitol-sucrose-NaCl formulations. *European Journal of Pharmaceutics and Biopharmaceutics,* 64**,** 316-325.

HAWE, A. & FRIESS, W. 2006. Physicohemical characterization of the freezing behavior of mannitol-human serum albumin formulations. *AAPS PharmSciTech,* 7**,** E85-E94.

HER, L.-M. & NAIL, S. L. 1994. Measurement of Glass Transition Temperatures of Freeze-Concentrated Solutes by Differential Scanning Calorimetry. *Pharmaceutical Research,* 11**,** 54-59.

HEWES, J. 2011. *Capacitance and Uses of Capacitors* [Online]. The electronics club. Available: http://www.kpsec.freeuk.com/capacit.htm [Accessed 5-01-12 2012].

HOTTOT, A., ANDRIEU, J., HOANG, V., SHALAEV, E. Y., GATLIN, L. A. & RICKETTS, S. 2009. Experimental Study and Modeling of Freeze-Drying in Syringe Configuration. Part II: Mass and Heat Transfer Parameters and Sublimation End-Points. *Drying Technology,* 27**,** 49 - 58.

HSU, C. L., HELDMAN, D. R., TAYLOR, T. A. & KRAMER, H. L. 2003. Influence of Cooling Rate on Glass Transition Temperature of Sucrose Solutions and Rice Starch Gel. *Journal of Food Science,* 68**,** 1970-1975.

ICH 2005. International Conference on Harmonisation (ICH) Harmonised tripartite guidelines: Q9 Quality risk management.

ICH 2009. International Conference on Harmonisation (ICH) Harmonised tripartite guidelines: Q8(R2) Pharmaceutical development.

ICH 2010. International Conference on Harmonisation (ICH) harmonised tripartite guidelines: Q10 pharmaceutical quality system.

ICH 2011. International Conference on Harmonisation (ICH) Guidelines on the Development and manufacture of drug substances (chemical entities and biotechnological/biological entities: Q11 step 2.

INSTRUMENTS, G. 2010. *Basics of Electrochemical Impedance Spectroscopy* [Online]. warminster: Gamry Instruments. Available: http://www.gamry.com/assets/Application-Notes/Basics-of-EIS.pdf [Accessed 08-01-2011 2012].

IZUTSU, K.-I. & KOJIMA, S. 2002. Excipient crystallinity and its protein-structure-stabilizing effect during freeze-drying. *Journal of Pharmacy and Pharmacology,* 54**,** 1033-1039.

JAMES A. SEARLES, J. F. C., THEODORE W. RANDOLPH 2000. Annealing to Optimize the Primary Drying Rate, Reduce Freezing-Induced Drying Rate Heterogeneity, and Determine Tg in Pharmaceutical Lyophilization. *Journal of Pharmaceutical Sciences,* 90**,** 872-887.

JAMES A. SEARLES, J. F. C., THEODORE W. RANDOLPH 2001. The Ice Nucleation Temperature Determines the Primary Drying Rate of Lyophilization for Samples Frozen on a Temperature-Controlled Shelf. *Journal of Pharmaceutical Sciences,* 90**,** 860-871.

JOHNSON, R. E., OLDROYD, M. E., AHMED, S. S., GIESELER, H. & LEWIS, L. M. 2009. Use of manometric temperature measurements (MTM) to characterize the freeze-drying behavior of amorphous protein formulations. *Journal of Pharmaceutical Sciences,* 99**,** 2863-2873.

KAMAT, M. S., LODDER, R. A. & DELUCA, P. P. 1989. Near-Infrared Spectroscopic Determination of Residual Moisture in Lyophilized Sucrose Through Intact Glass Vials. *Pharmaceutical Research,* 6**,** 961-965.

KASPER, J. C. & FRIESS, W. 2011. The freezing step in lyophilization: Physico-chemical fundamentals, freezing methods and consequences on process performance and quality attributes of biopharmaceuticals. *European Journal of Pharmaceutics and Biopharmaceutics,* 78**,** 248-263.

KAUZMANN, W. 1948. The Nature of the Glassy State and the Behavior of Liquids at Low Temperatures. *Chemical Reviews,* 43**,** 219-256.

KETT., V. 2010. Development of Freeze-dried Formulations Using Thermal Analysis and Microscopy. *American Pharmaceutical Review***,** 10.

KILMARTIN, P. A., REID, D. S. & SAMSON, I. 2000. The measurement of the glass transition temperature of sucrose and maltose solutions with added NaCl. *Journal of the Science of Food and Agriculture,* 80**,** 2196-2202.

KIRSCH, J. D. & DRENNEN, J. K. 1996. Near-Infrared Spectroscopic Monitoring of the Film Coating Process. *Pharmaceutical Research,* 13**,** 234-237.

KNOPP, S., CHONGPRASERT, S. & NAIL, S. 1998. The Relationship Between the TMDSC Curve of Frozen Sucrose Solutions and Collapse During Freeze-Drying. *Journal of Thermal Analysis and Calorimetry,* 54**,** 659-672.

KOCHS, M., KÖRBER, C., HESCHEL, I. & NUNNER, B. 1993. The influence of the freezing process on vapour transport during sublimation in vacuum-freeze-drying of macroscopic samples. *International Journal of Heat and Mass Transfer,* 36**,** 1727-1738.

KRAMER, M., SENNHENN, B. & LEE, G. 2002. Freeze-drying using vacuum-induced surface freezing. *Journal of Pharmaceutical Sciences,* 91**,** 433-443.

KUU, W. Y., O' BRYAN, K. R., HARDWICK, L. M. & PAUL, T. W. 2010. Product mass transfer resistance directly determined during freeze-drying cycle runs using tunable diode laser absorption spectroscopy (TDLAS) and pore diffusion model. *Pharmaceutical Development and Technology,* 16**,** 343-357.

KYUYA NAKAGAWA, A. E. H., S´EVERINE VESSOT, JULIEN ANDRIEU 2006. Influence of controlled nucleation by ultrasounds on ice morphology of frozen formulations for pharmaceutical proteins freeze-drying. *Chemical Engineering and Processing,* 45**,** 783–791.

LESKER, K. J. 1996. Global Vacuum product guide, section 7: Pressure measurement. 9 ed. USA.

LESLIE, J. 1813. *A Short Account of Experiments and Instruments, Depending on the Relations of Air to Heat and Moisture,* Edinburgh, William Blackwood and J Ballantyne.

LI, X. & NAIL, S. L. 2006. Nuclear magnetic resonance imaging of freeze-drying. *Journal of Pharmaceutical Sciences,* 95**,** 2516-2525.

LIAO, X., KRISHNAMURTHY, R. & SURYANARAYANAN, R. 2005. Influence of the Active Pharmaceutical Ingredient Concentration on the Physical State of Mannitol—Implications in Freeze-Drying. *Pharmaceutical Research,* 22**,** 1978-1985.

LIAO, X., KRISHNAMURTHY, R. & SURYANARAYANAN, R. 2007. Influence of Processing Conditions on the Physical State of Mannitol—Implications in Freeze-Drying. *Pharmaceutical Research,* 24**,** 370-376.

LIU, J., VIVERETTE, T., VIRGIN, M., ANDERSON, M. & DALAL, P. 2005. A Study of the Impact of Freezing on the Lyophilization of a Concentrated Formulation with a High Fill Depth. *Pharmaceutical Development and Technology,* 10**,** 261-272.

LIU, Y., BHANDARI, B. & ZHOU, W. 2006. Glass Transition and Enthalpy Relaxation of Amorphous Food Saccharides: A Review. *Journal of Agricultural and Food Chemistry,* 54**,** 5701-5717.

LOTLIKAR, M. 2013. Quality risk management: A Review. *Journal of Drug Delivery and Therapeutics,* 3**,** 149-154.

LOUIS REY, J. C. M. 2004. *Freeze-Drying/lyophilization of Pharmaceutical and Biological Products,* New York, Marcel Dekker, Inc.,.

LU, X. & PIKAL, M. J. 2004. Freeze Drying of Mannitol Trehalose Sodium Chloride Based Formulations: The Impact of Annealing on Dry Layer Resistance to Mass Transfer and Cake Structure. *Pharmaceutical Development and Technology,* 9**,** 85-95.

LUECKEL, B., BODMER, D., HELK, B. & LEUENBERGER, H. 1998. Formulations of Sugars with Amino Acids or Mannitol Influence of Concentration Ratio on the Properties of the Freeze-Concentrate and the Lyophilizate. *Pharmaceutical Development and Technology,* 3**,** 325-336.

LUYET, B. & RASMUSSEN, D. 1968. Study by differential thermal analysis of the temperatures of instability of rapidly cooled solutions of glycerol, ethylene glycol, sucrose and glucose. *Biodynamica,* 10**,** 167-91.

MACDONALD., J. R. & JOHNSON, W. B. 2005. Fundamentals of Impedance Spectroscopy. *In:* EVGENIJ BARSOUKOV & MACDONALD, J. R. (eds.) *Impedance spectroscopy Theory, experiment and applications.* 2 ed. New Jersey: Wiley interscience.

MACKENZIE, A. P. 1964. Apparatus for microscopic observations during freeze-drying (AFBR FREEZE-DRYING MICROSCOPE MODEL 2). *Biodynamica,* 9**,** 213-22.

MACKENZIE, A. P. 1976. The physico-chemical basis for the freeze-drying process. *Developments in biological standardization,* 36**,** 51-67.

MACKENZIE, A. P., DERBYSHIRE, W. & REID, D. S. 1977. Non-Equilibrium Freezing Behaviour of Aqueous Systems [and Discussion]. *Philosophical Transactions of the Royal Society of London. Series B, Biological Sciences,* 278**,** 167-189.

MAYERESSE, Y., VEILLON, R., SIBILLE, P. & NOMINE, C. 2007. Freeze-drying Process Monitoring Using A Cold Plasma Ionization Device. *PDA Journal of Pharmaceutical Science and Technology,* 61**,** 160-174.

MEISTER, E. & GIESELER, H. 2009. Freeze-dry microscopy of protein/sugar mixtures: Drying behavior, interpretation of collapse temperatures and a comparison to corresponding glass transition Data. *Journal of Pharmaceutical Sciences,* 98**,** 3072-3087.

MEREDITH, P., DONALD, A. M. & PAYNE, R. S. 1996. Freeze-drying: In situ observations using cryoenvironmental scanning electron microscopy and differential scanning calorimetry. *Journal of Pharmaceutical Sciences,* 85**,** 631-637.

MEYER, J. D., NAYAR, R. & MANNING, M. C. 2009. Impact of bulking agents on the stability of a lyophilized monoclonal antibody. *european journal of pharmaceutical sciences,* 38**,** 29-38.

MICHAEL WIGGENHORN, I. P., GERHARD WINTER 2005. The Current State of PAT in Freeze-Drying. *American Pharmaceutical Review,* 8**,** 38-44.

MILTON N, PIKAL MJ, ROY ML & NAIL SL 1997. Evaluation of manometric temperature measurement as a method of monitoring product temperature during lyophilization. *PDA J Pharm Sci Technol,* 51**,** 7-16.

MORRIS, K. R., EVANS, S. A., MACKENZIE, A. P., SCHEULE, D. & LORDI, N. G. 1994. Prediction of lyophile collapse temperature by dielectric analysis. *PDA J Pharm Sci Technol,* 48**,** 318-29.

MOUSAVI, R., MIRI, T., COX, P. W. & FRYER, P. J. 2005. A Novel Technique for Ice Crystal Visualization in Frozen Solids Using X-Ray Micro-Computed Tomography. *Journal of Food Science,* 70**,** e437-e442.

MUJAT, M., GRECO, K., GALBALLY-KINNEY, K. L., HAMMER, D. X., FERGUSON, R. D., IFTIMIA, N., MULHALL, P., SHARMA, P., PIKAL, M. J. & KESSLER, W. J. 2012. Optical coherence tomography-based freeze-drying microscopy. *Biomed. Opt. Express,* 3**,** 55-63.

NAIL, S. L. 1980. The Effect of Chamber Pressure on Heat Transfer in the Freeze Drying of Parenteral Solutions. *PDA Journal of Pharmaceutical Science and Technology,* 34**,** 358-368.

NAKAGAWA, K., HOTTOT, A., VESSOT, S. & ANDRIEU, J. 2007. Modeling of freezing step during freeze-drying of drugs in vials. *AIChE Journal,* 53**,** 1362-1372.

NAZARI, K. 2012. *Some studies using LyoDEA™ as an in-line process analytical technology for freeze-drying.* M Phil, De Montfort University.

OETJEN, G.-W. 2007. Foundations and Process Engineering. *Freeze-Drying.* Weinheim: Wiley-VCH Verlag GmbH.

OLMI, R., MERIAKRI, V. V., IGNESTI, A., PRIORI, S. & RIMINESI, C. 2007. Monitoring alcoholic fermentation by microwave dielectric spectroscopy. *Journal of Microwave Power and Electromagnetic Energy,* 41**,** 37-49.

ORLIEN, V., ANDERSEN, M. L., JOUHTIMÄKI, S., RISBO, J. & SKIBSTED, L. H. 2004. Effect of Temperature and Glassy States on the Molecular Mobility of Solutes in Frozen Tuna Muscle As Studied by Electron Spin Resonance Spectroscopy with Spin Probe Detection. *Journal of Agricultural and Food Chemistry,* 52**,** 2269-2276.

PATEL, R. M. & HURWITZ, A. 1972. Eutectic temperature determination of preformulation systems and evaluation by controlled freeze drying. *Journal of Pharmaceutical Sciences,* 61**,** 1806-1810.

PATEL, S., BHUGRA, C. & PIKAL, M. 2009. Reduced Pressure Ice Fog Technique for Controlled Ice Nucleation during Freeze-Drying. *AAPS PharmSciTech,* 10**,** 1406-1411.

PATEL, S., DOEN, T. & PIKAL, M. 2004. Determination of End Point of Primary Drying in Freeze-Drying Process Control. *AAPS PharmSciTech,* 11**,** 73-84.

PATEL, S., DOEN, T. & PIKAL, M. 2010. Determination of End Point of Primary Drying in Freeze-Drying Process Control. *AAPS PharmSciTech,* 11**,** 73-84.

PATEL, S. M. & PIKAL, M. 2009. Process Analytical Technologies (PAT) in freeze-drying of parenteral products. *Pharmaceutical Development and Technology,* 14**,** 567-587.

PETERSEN, A., SCHNEIDER, H., RAU, G. & GLASMACHER, B. 2006. A new approach for freezing of aqueous solutions under active control of the nucleation temperature. *Cryobiology,* 53**,** 248-257.

PETROVSKY, V., JASINSKI, P. & DOGAN, F. 2012. Effective dielectric constant of two phase systems: Application to mixed conducting systems. *Journal of Applied Physics,* 112**,** 034107.

PIKAL, M. 1990. Freeze-drying of proteins, part 2: formulation selection. *BioPharm* 3**,** 26.

PIKAL, M. J. 1985. Use of Laboratory Data in Freeze Drying Process Design: Heat and Mass Transfer Coefficients and the Computer Simulation of Freeze Drying. *PDA Journal of Pharmaceutical Science and Technology,* 39**,** 115-139.

PIKAL, M. J., ROY, M. L. & SHAH, S. 1984. Mass and heat transfer in vial freeze-drying of pharmaceuticals: Role of the vial. *Journal of Pharmaceutical Sciences,* 73**,** 1224-1237.

PIKAL, M. J., SHAH, S., ROY, M. L. & PUTMAN, R. 1990. The secondary drying stage of freeze drying: drying kinetics as a function of temperature and chamber pressure. *International Journal of Pharmaceutics,* 60**,** 203-207.

PIKAL, M. J., SHAH, S., SENIOR, D. & LANG, J. E. 1983. Physical chemistry of freeze-drying: Measurement of sublimation rates for frozen aqueous solutions by a microbalance technique. *Journal of Pharmaceutical Sciences,* 72**,** 635-650.

PISANO, R., FISSORE, D., VELARDI, S. A. & BARRESI, A. A. 2010. In-line optimization and control of an industrial freeze-drying process for pharmaceuticals. *Journal of Pharmaceutical Sciences,* 99**,** 4691-4709.

PYNE, A., SURANA, R. & SURYANARAYANAN, R. 2002. Crystallization of Mannitol below Tg′ during Freeze-Drying in Binary and Ternary Aqueous Systems. *Pharmaceutical Research,* 19**,** 901-908.

PYNE, A. & SURYANARAYANAN, R. 2001. Phase Transitions of Glycine in Frozen Aqueous Solutions and During Freeze-Drying. *Pharmaceutical Research,* 18**,** 1448-1454.

PYNE, A. & SURYANARAYANAN, R. 2003. The Effect of Additives on the Crystallization of Cefazolin Sodium During Freeze-Drying. *Pharmaceutical Research,* 20**,** 283-291.

RAHMAN, M. S., GUIZANI, N., AL-KHASEIBI, M., ALI AL-HINAI, S., AL-MASKRI, S. S. & AL-HAMHAMI, K. 2002. Analysis of cooling curve to determine the end point of freezing. *Food Hydrocolloids,* 16**,** 653-659.

RAMBHATLA, S. & PIKAL, M. 2003. Heat and mass transfer scale-up issues during freeze-drying, I: Atypical radiation and the edge vial effect. *AAPS PharmSciTech,* 4**,** 22-31.

RAMBHATLA, S., RAMOT, R., BHUGRA, C. & PIKAL, M. 2004. Heat and mass transfer scale-up issues during freeze drying: II. Control and characterization of the degree of supercooling. *AAPS PharmSciTech,* 5**,** 54-62.

RAMBHATLA, S., TCHESSALOV, S. & PIKAL, M. 2006. Heat and mass transfer scale-up issues during freeze-drying, III: Control and characterization of dryer differences via operational qualification tests. *AAPS PharmSciTech,* 7**,** E61-E70.

RATHORE, A. S. 2009. Roadmap for implementation of quality by design (QbD) for biotechnology products. *Trends in biotechnology,* 27**,** 546-553.

RATHORE, A. S. & WINKLE, H. 2009. Quality by design for biopharmaceuticals. *Nature Biotechnology,* 27**,** 26-34.

RAULT, J. 2000. Origin of the Vogel–Fulcher–Tammann law in glass-forming materials: the α–β bifurcation. *Journal of Non-Crystalline Solids,* 271**,** 177-217.

RESEARCH, P. A. Basics of Electrochemical Impedance Spectroscopy. *In:* REASEARCH, P. A. (ed.).

REY, L. R. 1960. Thermal analysis of eutectics in freezing solutions. *Annals of the New York Academy of Sciences,* 85**,** 510-534.

REYES, A., BUBNOVICH, V., BUSTOS, R., VÃ¡SQUEZ, M., VEGA, R. & SCHEUERMANN, E. 2010. Comparative Study of Different Process Conditions of Freeze Drying of Murtilla™ Berry. *Drying Technology,* 28**,** 1416 - 1425.

ROMERO-TORRES, S., WIKSTROM, H., GRANT, E. R. & TAYLOR, L. S. 2007. Monitoring of Mannitol Phase Behavior during Freeze-Drying Using Non-Invasive Raman Spectroscopy. *PDA Journal of Pharmaceutical Science and Technology,* 61**,** 131-145.

ROTH, C., WINTER, G. & LEE, G. 2001. Continuous measurement of drying rate of crystalline and amorphous systems during freeze-drying using an in situ microbalance technique. *Journal of Pharmaceutical Sciences,* 90**,** 1345-1355.

ROY, M. L. & PIKAL, M. J. 1989. Process Control in Freeze Drying: Determination of the End Point of Sublimation Drying by an Electronic Moisture Sensor. *PDA Journal of Pharmaceutical Science and Technology,* 43**,** 60-66.

ROY ML, P. M. 1989. Process control in freeze drying: determination of the end point of sublimation drying by an electronic moisture sensor. *J Parenter Sci Technol,* 43**,** 60-6.

RYDER, A. G., O'CONNOR, G. M. & GLYNN, T. J. 2000. Quantitative analysis of cocaine in solid mixtures using Raman spectroscopy and chemometric methods. *Journal of Raman Spectroscopy,* 31**,** 221-227.

S. ZHAI, R., TAYLOR, R., SANCHES & SLATER, N. K. H. 2003. Measurement of lyophilisation primary drying rates by freeze-drying microscopy. *Chemical Engineering Science***,** 2313 – 2323.

SALVATORE A. VELARDI, A. A. B. 2008. Development of simplified models for the freeze-drying process and investigation of the optimal operating conditions. *chemical engineering research and design,* 86**,** 9–22.

SALVATORE A. VELARDI, H. H., ANTONELLO A. BARRESI 2009. In-line monitoring of the primary drying phase of the freeze-drying process in vial by means of a Kalman filter based observer. *Chemical Engineering Research and Design,* 8 7**,** 1409–1419.

SCHNEID, S. 2009. Process analytical tools (PAT) for use in freeze drying processes. *SP Industries webinar*.

SCHNEID, S. & GIESELER, H. 2008. Evaluation of a New Wireless Temperature Remote Interrogation System (TEMPRIS) to Measure Product Temperature During Freeze Drying. *AAPS PharmSciTech,* 9**,** 729-739.

SCHNEID, S. C., GIESELER, H., KESSLER, W. J. & PIKAL, M. J. 2009. Non-invasive product temperature determination during primary drying using tunable diode laser absorption spectroscopy. *Journal of Pharmaceutical Sciences,* 98**,** 3406-3418.

SCHWAN, H. P. 1968. Electrode polarization impedance and measurements in biological materials. *Annals of the New York Academy of Sciences,* 148**,** 191-209.

SCORER T, PERKIN M & BUCKLEY M 2004. *Measurement good practice guide: Weighing in Pharmaceutical Industry,* UK, National Physical Laboratory.

SHACKELL, L. F. 1909. An improved method of desiccation, with some applications to biological problems. *American Journal of Physiology,* 24**,** 325-340.

SMITH, G., POLYGALOV, E., ARSHAD, M. S., PAGE, T., TAYLOR, J. & ERMOLINA, I. 2013. An impedance-based process analytical technology for monitoring the lyophilisation process. *International Journal of Pharmaceutics,* 449**,** 72-83.

SOLEY, A., LECINA, M., GAMEZ, X., CAIRO, J. J., RIU, P., ROSELL, X., BRAGAS, R. & GADIA, F. 2005. On-line monitoring of yeast cell growth by impedance spectroscopy. *Journal of Biotechnology,* 118**,** 398-405.

SONG, C. S., NAM, J. H., KIM, C. J. & RO, S. T. 2005. Temperature distribution in a vial during freeze-drying of skim milk. *Journal of Food Engineering,* 67**,** 467-475.

STEVEN L. NAIL, J. A. S. 2008. Elements of quality by design in development and sacle up of freeze-dried parenterals. *BioPharm International,* 21**,** 44-49.

SUHERMAN, P. M. & SMITH, G. 2003. A percolation cluster model of the temperature dependent dielectric properties of hydrated proteins. *Journal of Physics D-Applied Physics,* 36**,** 336-342.

SUNDARAMURTHI, P., PATAPOFF, T. & SURYANARAYANAN, R. 2010. Crystallization of Trehalose in Frozen Solutions and its Phase Behavior during Drying. *Pharmaceutical Research,* 27**,** 2374-2383.

TANG, X., NAIL, S. & PIKAL, M. 2006a. Evaluation of manometric temperature measurement (MTM), a process analytical technology tool in freeze drying, part III: Heat and mass transfer measurement. *AAPS PharmSciTech,* 7**,** E105-E111.

TANG, X., NAIL, S. & PIKAL, M. 2006b. Evaluation of manometric temperature measurement, a process analytical technology tool for freeze-drying: Part I, product temperature measurement. *AAPS PharmSciTech,* 7**,** E95-E103.

TANG, X., NAIL, S. & PIKAL, M. 2006c. Evaluation of manometric temperature measurement, a process analytical technology tool for freeze-drying: Part II measurement of dry-layer resistance. *AAPS PharmSciTech,* 7**,** E77-E84.

TANG, X., NAIL, S. L. & PIKAL, M. J. 2005. Freeze-Drying Process Design by Manometric Temperature Measurement: Design of a Smart Freeze-Dryer. *Pharmaceutical Research,* 22**,** 685-700.

TANG, X. & PIKAL, M. 2004. Design of Freeze-Drying Processes for Pharmaceuticals: Practical Advice. *Pharmaceutical Research,* 21**,** 191-200.

VALLAN, A. A Measurement System for Lyophilization Process Monitoring. Instrumentation and Measurement Technology Conference Proceedings, 2007. IMTC 2007. IEEE, 1-3 May 2007 2007. 1-5.

VANSTEENBERGE.M.P. 1903. Precede de conservation a l'etat sec. *Cr. Seanc. Soc. BioI,* 55**,** 1646-47.

VARSHNEY, D., KUMAR, S., SHALAEV, E., SUNDARAMURTHI, P., KANG, S.-W., GATLIN, L. & SURYANARAYANAN, R. 2007. Glycine Crystallization in Frozen and Freeze-dried Systems: Effect of pH and Buffer Concentration. *Pharmaceutical Research,* 24**,** 593-604.

VELARDI, S. A., HAMMOURI, H. & BARRESI, A. A. 2010. Development of a High Gain Observer for In-Line Monitoring of Sublimation in Vial Freeze Drying. *Drying Technology,* 28**,** 256 - 268.

WANG, W. 2000. Lyophilization and development of solid protein pharmaceuticals. *International Journal of Pharmaceutics,* 203**,** 1-60.

WARD, K. R. & MATEJTSCHUK, P. 2010. The Use of Microscopy, Thermal Analysis, and Impedance Measurements to Establish Critical Formulation Parameters for Freeze-Drying Cycle Development. *In:* REY, L. & MAY, J. C. (eds.) *Freeze Drying/Lyophilization of Pharmaceutical and Biological Products.* New york: Marcel Dekker.

WEI, W. 2000. Lyophilization and development of solid protein pharmaceuticals. *International Journal of Pharmaceutics,* 203**,** 1-60.

WINKLE, H. N. Implementing Quality by Design. PDA/FDA Joint Regulatory Conference, 2007. FDA.

WOLLASTON, W. H. 1813. On a Method of Freezing at a Distance. *Philosophical Transactions Royal society of London,* 103**,** 71-74.

XIANG, J., HEY, J. M., LIEDTKE, V. & WANG, D. Q. 2004. Investigation of freeze-drying sublimation rates using a freeze-drying microbalance technique. *International Journal of Pharmaceutics,* 279**,** 95-105.

YUNSONG, Q., LEI, Z. & YUFENG, J. A novel micro pirani gauge with mono-wire sensing unit for microsystem application. Electronic Packaging Technology & High Density Packaging, 2009. ICEPT-HDP '09. International Conference on, 10-13 Aug. 2009 2009. 467-470.

ZHAI, S., SU, H., TAYLOR, R. & SLATER, N. K. H. 2005. Pure ice sublimation within vials in a laboratory lyophiliser; comparison of theory with experiment. *Chemical Engineering Science,* 60**,** 1167-1176.

ZHAO, Y., WANG, M. & HAMMOND, R. B. 2011. Characterization of crystallisation processes with electrical impedance spectroscopy. *Nuclear Engineering and Design,* 241**,** 1938-1944.

ZHOU, G.-Y., WANG, W.-Y., ZHANG, J., XU, F., LIU, B., CAO, B.-H. & HUA, T.-C. 2009. Detection of the sublimation end-point of a freeze-drying process by the dew-point method. *Cryobiology,* 59**,** 400-400.

Appendix 1: **Estimation of the peak frequencies of liquid and frozen sucrose solution (3% w/v) within tubing vial of different vial geometries**

In a simple approximation, the impedance of the object under test can be described as a combination of resistor and capacitor; the resistance of which is defined by following equation

$$R = K_1 d/A_{CS}\sigma \quad (1)$$

where K_1 is a geometrical coefficient, d is the internal diameter of the vial, A_{CS} is an area of effective vertical cross section of the sample (i.e. the solution within the vial) and σ is specific conductivity of the sample. The capacitance can be defined by the following equation.

$$C = \varepsilon_0\varepsilon\ A/l \quad (2)$$

Where ε_0 is the permittivity of a vacuum, ε is the dielectric constant of glass, A is the area of the electrodes and l is thickness of the glass wall. For the purpose of these calculations, the wall thickness is assumed to be constant for all sizes of vial.

Multiplying R by C results in

$$\tau = RC = K_1\varepsilon_0\varepsilon dA/\sigma l A_{CS} \quad (3)$$

where τ is the known as the time constant of the serial RC circuit. It is this time constant which defines the position of the interfacial relaxation peak in the experimental frequency window (where $f_{peak} = 1/2\pi\tau$).

In a first approximation A_{CS} can be presented as $A_{CS} = AK_2$ where K_2 is a constant coefficient (associated with the fixed cylindrical shape of the sample volume). Then (3) can be rewritten as

$$\tau = RC = K_1\varepsilon_0\varepsilon dA/\sigma l A K_2 \quad (4)$$

A in the numerator and denominator can be cancelled thus giving

$$\tau = RC = K_1\varepsilon_0\varepsilon d/\sigma l\ K_2 \quad (5)$$

For simplicity let us denote

$$K_p = K_1\varepsilon_0\varepsilon/l\sigma\ K_2 \quad (6)$$

Since all members in the right side of (6) are constants then K_p (the proportionality coefficient) is also a constant, and expression 5 can be simplified to

$$\tau = K_p d \quad (7)$$

and respectively

$$F_{peak} = 1/2\pi\tau = 1/2\pi K_p d \quad (8)$$

Expression 8 shows that the frequency position of the peak has an approximately inverse dependence on the internal diameter of the vial.

Having measured the experimental value of f_{peak} for a 10 ml ($f_{peak10ml}$) it is then straight forward to estimate $F_{peak(xml)}$ for different sized vials from the ratio of the diameters, according to the formula below.

$$f_{peakx} = f_{peak(10ml)} \times d_{10ml}/d_{xml} \quad (9)$$

Table 1 gives theoretical estimates for the peak frequency for different sized vials, for both the liquid state and the frozen state.

Table1 estimated position of interfacial relaxation peak for a 10% solution of sucrose in distilled water within glass tubing vials of varying diameter (but constant wall thickness: 2 mm). * Values of f_{peak} for a 10% sucrose solution in the 10 ml tubing vial (Schott) have been determined experimentally

Vial size (ml) Schott	**internal diameter (mm)**	**F_{peak} liq (kHz)**	**F_{peak} Frozen (kHz)**
10	21.95	64.021	1.390
2	13.91	101.056	2.194
4	13.92	100.959	2.192
6	19.92	70.579	1.532
8	19.90	70.626	1.533

Appendix 2: Thermal Mass Contributions from the External Electrodes

The basis for these calculations is to first determine the position of the top of the guard electrode from the base of the vial (Fig. 1, dimension A) for a fill volume that provides a constant ratio of the liquid cross sectional area to the liquid fill height, for all sizes of vial and which is equal to that for a 3 ml fill volume in a 10 ml vial.

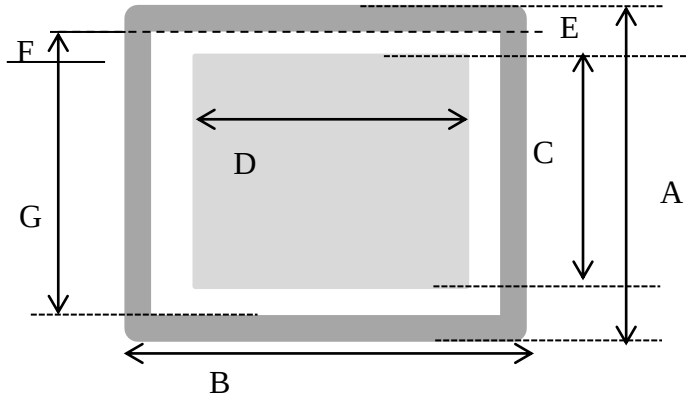

Figure 1 Schematic of the electrode assembly. A: electrode height, B length of guard electrode, C height of stimulating/sensing electrode, D width of stimulating/sensing electrode, E width of guard electrode, F spacing between guard electrode and sensing electrode, G is the height of the side segment of the guard electrode

Once the position of the top of the guard electrode is defined then the next step is to estimate the length of the sensing/stimulating electrode (dimension D, Fig. 1). This dimension is defined by the ratio of the electrode length to the circumference of the vial, which is fixed at 0.4 for all vials. All other dimensions, i.e. the separation/gap between the guard and the sensing/stimulating electrodes and the width of the guard electrode are fixed at 1 and 1.5 respectively. Knowing the dimensions A, D, E, and F permits the calculation of all other dimensions, from which the total area of the electrode assembly can then be calculated (Table 1). The mass of the electrode assembly is then determined from the specific weight of the electrode material (0.4 mg/mm^2 for the copper foil used on the 10 ml vial) and the % increase in vial weight from attaching the copper foil is then determined from the weight of the vial. Table 2 shows the dimensions of the electrode assemblies and the results of these calculations of % increase in mass.

Table 1 Calculation of liquid cross sectional area (a) and liquid fill height (h) corresponding to a fixed ratio of a/h=45 mm

vial size	Mean Wt (g)	± SD (Wt)	Mean diameter (mm)	±SD (Diameter)	a:Mean area of liquid (mm^2)	± SD (Area)	h:Mean liquid Fill height (mm)	± SD (fill height)
2	4.420	0.014	15.950	0.010	199.833	0.251	4.433	0.006
4	5.584	0.034	15.983	0.042	200.669	1.046	4.451	0.023
6	7.999	0.085	21.937	0.006	377.996	0.199	8.385	0.004
8	8.639	0.084	21.923	0.076	377.537	2.629	8.375	0.058
10	9.283	0.068	23.957	0.061	450.816	2.299	10.000	0.051

Table 2 Theoretical calculations of the % increase in thermal mass on fixing an electrode pair (with guard electrodes) to different volumes of tubing vial

Vial Size ml	Vial wt (mg)	electrode height mm	sensing electrode			Top and bottom guard electrode			2 side guard electrodes			total area of electrode assembly mm^2	wt of electrode assembly	thermal mass as % of vial wt
			height (mm)	width (mm)	Area mm^2	height (mm)	width (mm)	Area mm^2	height (mm)	width (mm)	Area mm^2			
2	4419	4.4	2.22	11	24.37	1.11	15.9	17.64	4.7	1.11	5.22	94.48	37.793	0.86
4	5584	4.5	2.23	16.3	36.34	1.11	15.9	17.64	4.7	1.11	5.22	118.43	47.37	0.85
6	7998	8.4	4.19	16.3	68.29	2.09	21.75	45.58	6.5	2.08	13.52	254.81	101.92	1.27
8	8639	8.4	4.19	16.3	68.29	2.09	21.79	45.67	6.5	2.09	13.59	255.11	102.04	1.18
10	9282	10	5	18	90	2.5	24	60	7	3	21	342.00	136.8	1.47

The application of electrodes was practicable by the current method (manually) for vial sizes 6ml, 8ml and 10ml as the dimensions of different electrode components were greater than 1mm thickness. On contrary for smaller sized glass vials i.e. 2ml and 4ml, dimension electrodes and its spacing fractionate between 1mm which may require an alternate methodology (sputtering) to apply thermal mass of the electrode.

Appendix III: Standard operating procedure TVIS data acquisition software LyoDEA

Aim: The aim of this section is to provide instructions on the use of the LyoDEA measurement system

Procedure:

1. Check that the measurement vial (Figure 1) is clean from dust, discolouration of the electrode and not containing any residual volume of cleaning solvent (water).

Figure 1 Impedance measurement vial

2. Introduce a liquid formulation (e.g. 3ml) to the measurement vial and place the rubber closure half open as it will provide an effective path for the water vapour during primary drying.

3. Place the measurement vial on the shelf and attach the connectors to the junction box located in the drying chamber (Figure 2). (‘click’ sound confirms that the connector is properly connected to junction box)

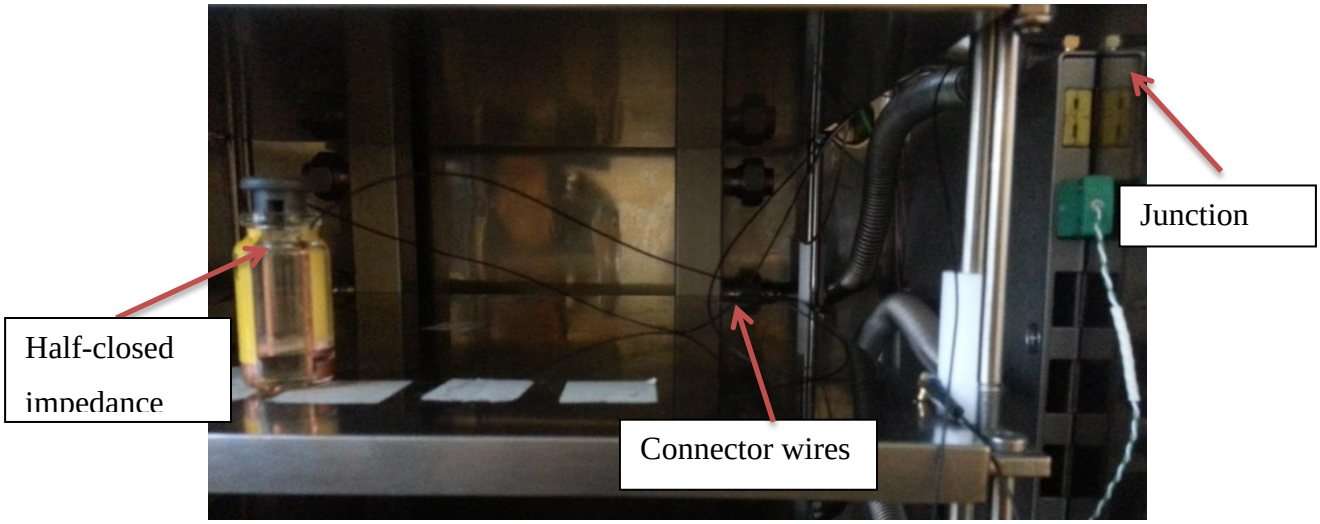

Figure 2 Measurement vial connected to Junction box

4. Click on the LyoDEA software exe. 

5. You will observe the main window (Figure 3) of the software.

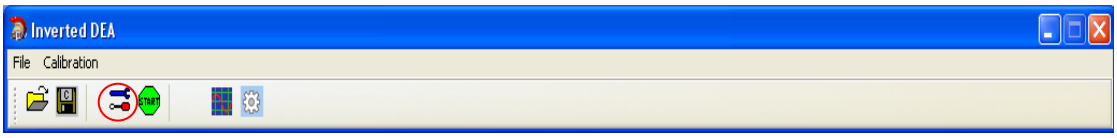

Figure 3 Lyosense main windows

6. Click the settings key  . This will open the experiment setup window (Figure 4). Within this module one can select the following experimental conditions.

- Frequency
- AC Amplitude
- Selection of Channels
- Scan interval
- Number of scan
- Integration period
- Comments

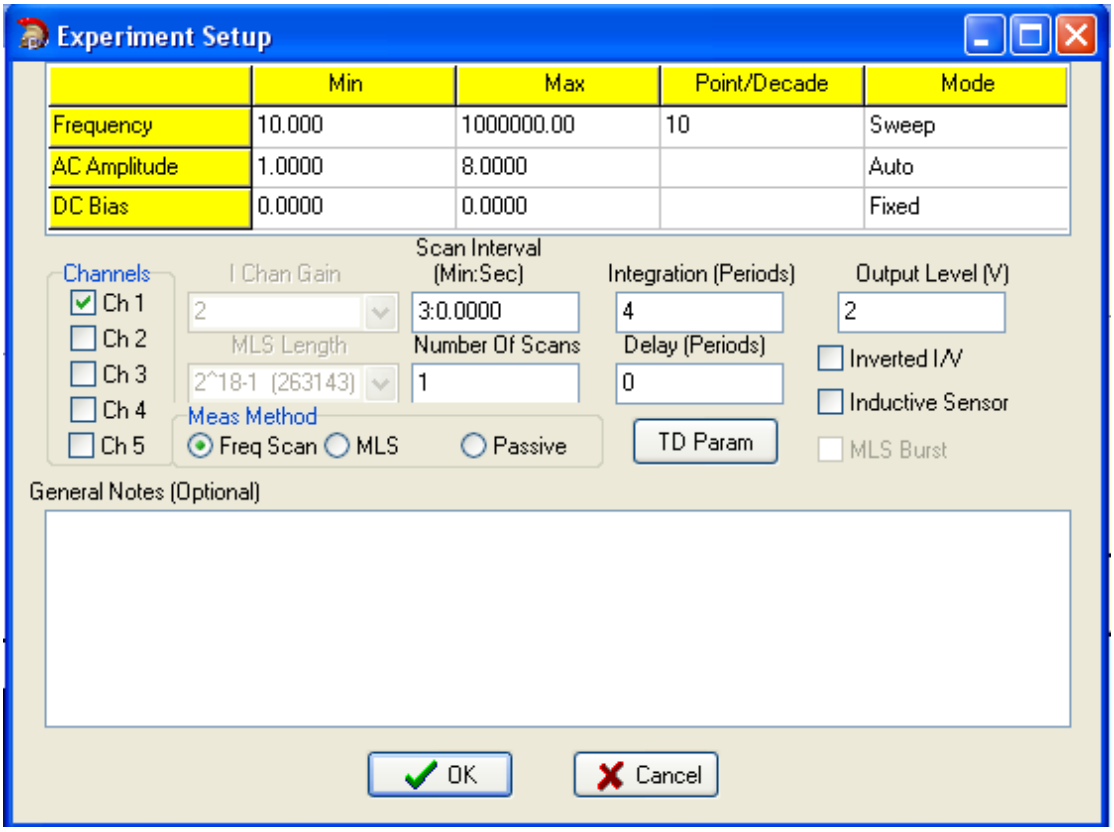

Figure 4 Experiment setup

- Frequency range for dielectric analysis may range from 1 hertz to 1 megahertz. In usual operation, the frequency range is set from 10 Hz to 1,000,000 Hz.
- The points per decade represent the no. of data points per one decade of frequency. This value can be set at 5, 10 or 20. Here 10 is the intermediate value for points per decade.
- AC amplitude represents the value of the applied voltage. The recommended value is between 0.2 to 8.0.Volts
- The DC bias and Mode options are currently inactive in this version of the software.
- Channel represents the measurement channel on the instrument. Any channel can be selected and de-selected.
- The Scan Interval (Min) defines the time (Minutes) between subsequent measurements of individual spectra.

- Number of scans defines the length of the data acquisition period and should be set so that spectra are recorded during the whole length of the freeze-drying cycle. Calculate the number of scan which should be taken during the whole experiment by dividing the length of the freeze-drying cycle (in minutes) by the scan interval (in minutes). Put this value in the box requiring the Number of scans. This value should not exceed 1200 (Maximum limit for the software). This value is independent of the total number of channels/vials included the freeze drying cycle.

- The Integration period defines both the time duration to record a single spectrum and the accuracy of the measurement. Keep the integration period high (4) in order to reduce the noise in data recording.

- The Output Level is recommended to be set to 2V.

- Always select measure vs time option.

- Any comments regarding the sample name, method of experiment can be added to the comment box.

- Once you have finished defining the experimental setup then press OK

7. Once again the main window Figure 3 will open up

8. Now click on the green hexagonal button 

on your screen. This action will result save data interface.

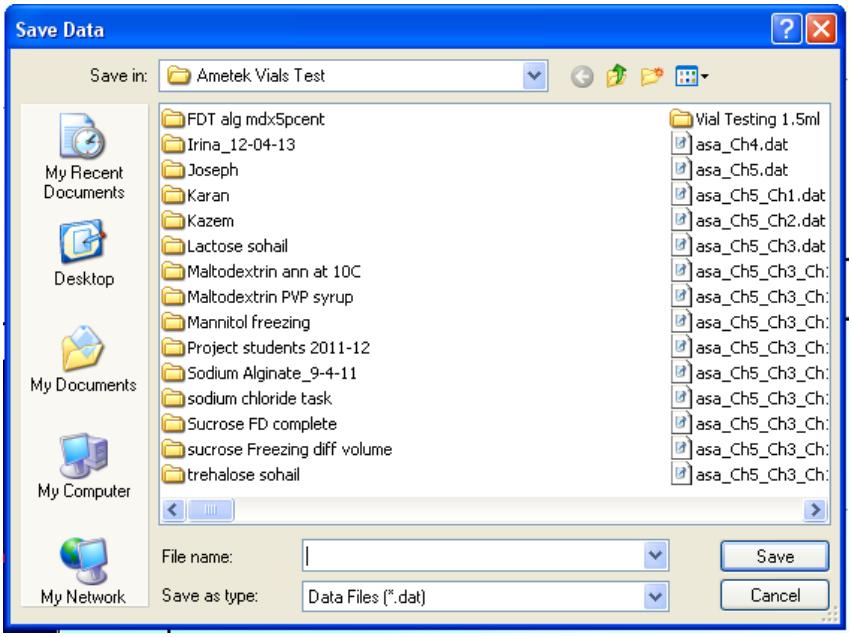

Figure 5 Save data option

9. Select the folder where you are intending to save data of the experiment. After selection of folder for storage of data, put some group name in the field requiring file name. Click on the save button. This action will start the measurement cycle.

10. When the measurement vial containing formulation is connected to the data acquisition system, following plots will be observed (Figure 6).

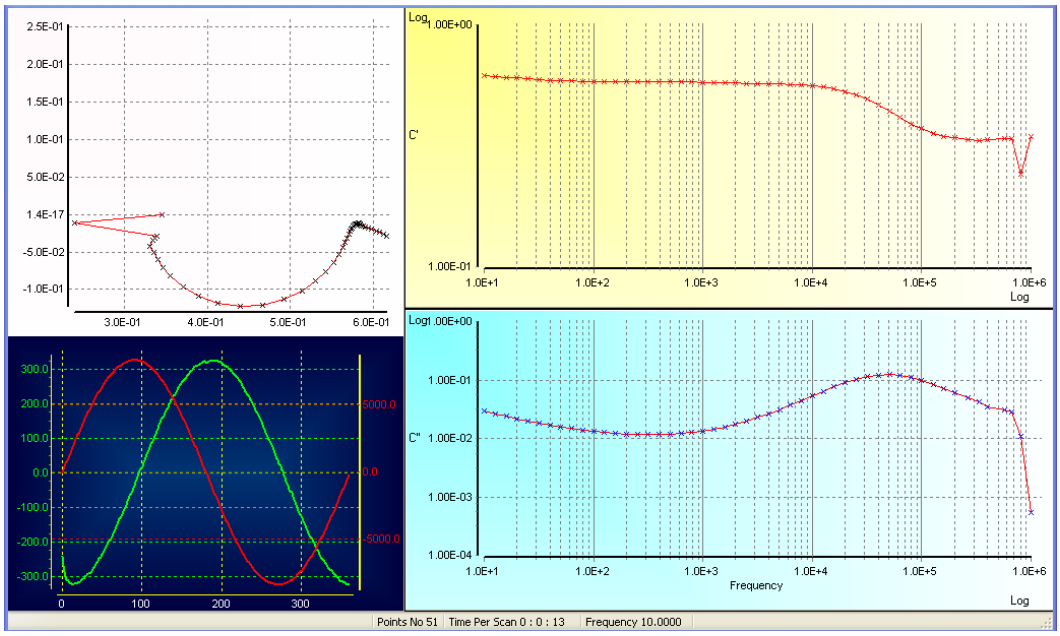

Figure 6 data acquisition interface

11. The Upper left graph shows the Cole plot of **imaginary capacitance** against **real capacitance**; the upper right graph shows **real part of the capacitance** C′ vs **frequency** on the logarithmic scale; the lower right graph gives the values of **imaginary part of the capacitance** C″ vs frequency on the logarithmic scale. The graph on the Lower left side of the screen is more related to the engineering aspects of the process. The red line provides information about stimulating signals while the green shows the current flow through the sample. Smooth wave forms for each signal are indicators of appropriate signal flow from the electrode containing vials (hence assisting the operator in checking that the connections between vial and measurement system are good.

12. Inappropriate connection between the measurement vial and the impedance analyser (lost connection, no vial attached to the system, short circuit due to accumulation of dirt on the external surface of vial) results in irregular abnormal spectral plots (Figure 7).

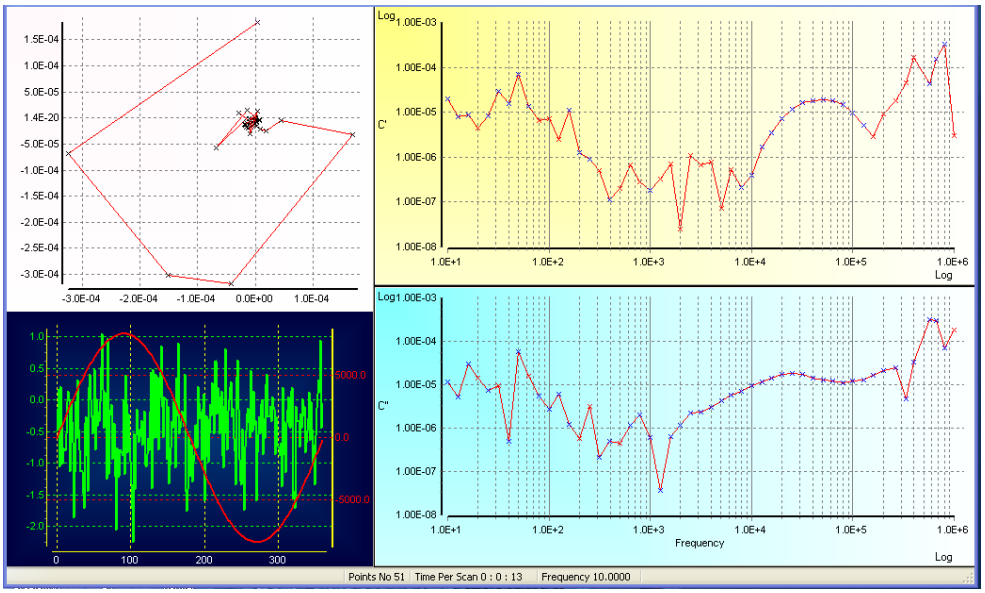

Figure 7 data acquisition during failed interrupted conection

Neither the cole-cole plot is semicircle nor is the imaginary capacitance plot showing distinct peak. Also the real part of the capacitance is also not step like increase capacitance.

13. During data acquisition, the hexagonal button 

is changed to 

.

14. Start both the Freeze drying cycle and the LyoDEA data acquisition at the same time point to obtain real time process information.

15. At the end of freeze drying cycle, once the pre-set time is passed, the system will stop automatically. Alternatively if you intend to interrupt the measurement cycle, then press the stop key 

.

16. Switch the Amplifier OFF.

Note: Before starting the lyophilisation cycle recording with LyoDEA, it may be appropriate to perform single scan to establish the integrity of the connections and signal flow.

Appendix IV: Vial Cleaning

1) Rinse vials thoroughly five times with distilled water.
2) Ensure the internal vial is visually clean.
3) Place the vials in an oven at temperature 45^{o}C for 2 hours in order to ensure vial is sufficiently dried.
4) Once dried, clean the external electrode system and the glass walls of the vial with alcohol dipped cotton swabs (figure 1).

Figure 1 Cleaning external vial with alcohol

5) Dry the external surface of the vial with another cotton swab not dipped in alcohol.
6) Leave for 2 minutes to allow the alcohol to evaporate off.
7) The dried cleaned vials are ready to use
8) Avoid contact with the electrode system during the transferring of liquid, connection to the junction box.

Note: Avoid contact with the electrode system during the transferring of liquid, connection to the junction box.

Appendix V: Standard Operating procedure Lyoview

Aim: The aim of this guide is to provide instructions on the use of the LyoView software for the analysis of data generated by the LyoDEA measurement control software.

Procedure

1. To run the application, click the icon  , and the software's main window (figure 1) will open up

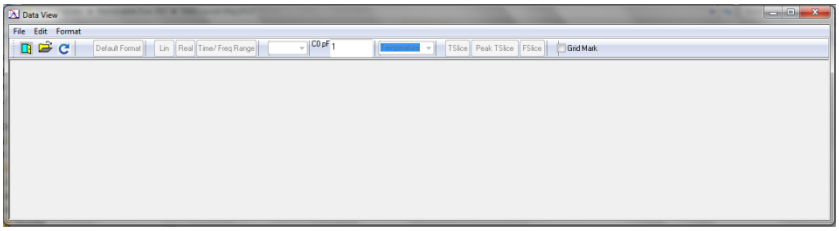

Figure 1 LyoDEA view main window

2. Click the open folder option  in the main window (Figure 1). This action will result in the opening of another window: **Select Data File** (Figure 2)

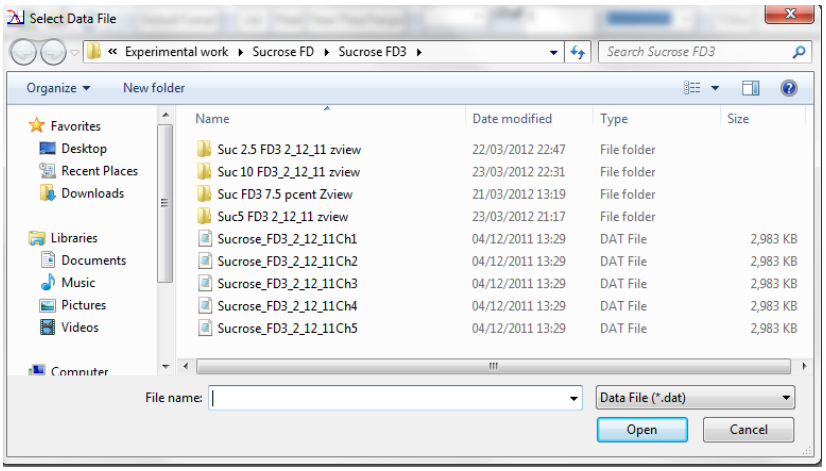

Figure 2 Select Data file window file type Data file (*.dat)

Note The data files from the LyoDEA measurement and control software are saved as text files with a name assigned by the operator and followed by a number which gives the channel number from the LyoDEA instrument. Either one, or all files, can be selected for analysis. These file are in the format given in Figure 1

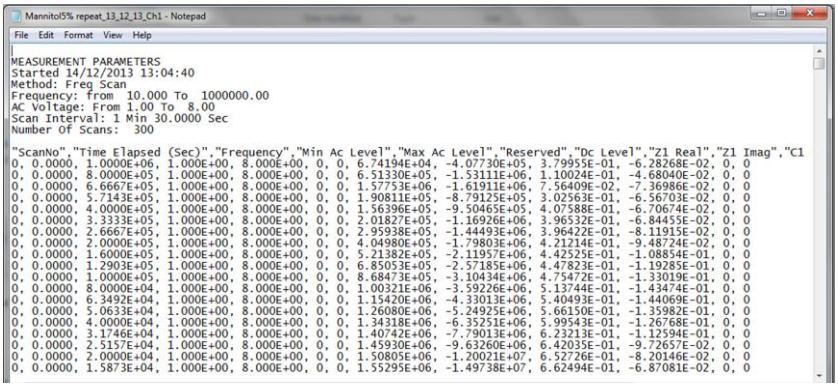

3. After the selection of files, click the button 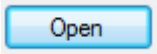

(Figure 2). All the files will be displayed in a 3 Dimensional graph of imaginary capacitance (dielectric loss) as the function of frequency and time (Figure 3).

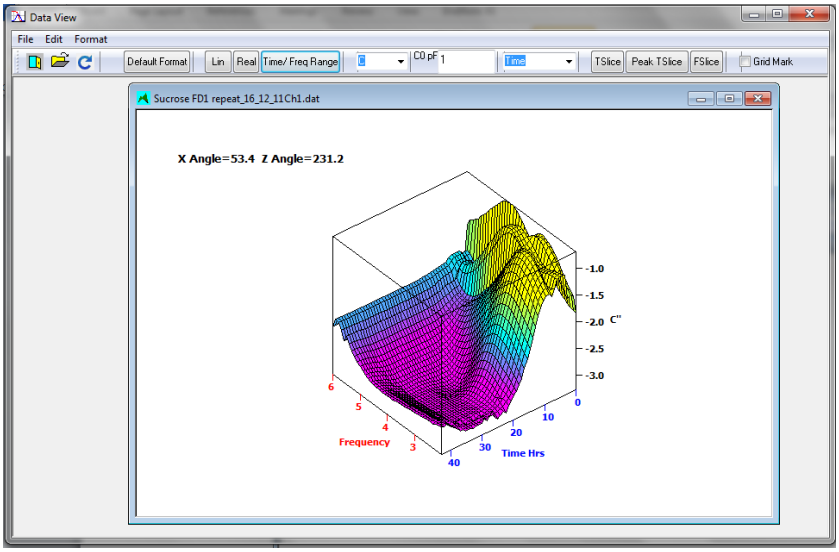

Figure 3 Three dimensional response surface plot of the selected data. The example shown here is the imaginary capacitance

All the options for data analysis are listed in the top bar of the window. See Fig. 4 for a magnified view.

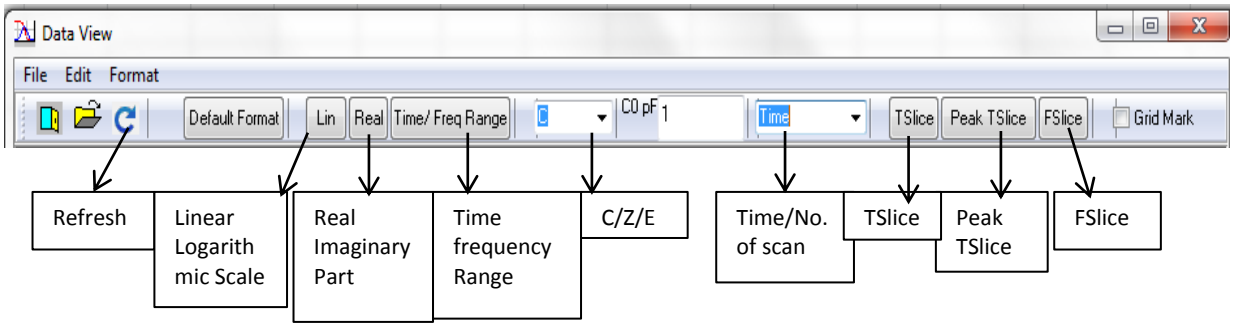

Figure 4 Description of buttons on the tool bar

- Refresh
- Default format
- Linear/Logarithmic Scale
- Imaginary/Real Image
- Time/Frequency range
- C1/Z1/E1
- Tslice (this option is not so informative compared with Peal T slice)
- Peak T slice
- Fslice

4. The refresh button  will update the plot if the data files are opened during data acquisition process.
5. The default format button 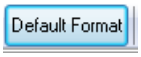 displays the response graph is on the logarithmic scale. Selection of the linear scale  displays linear values of capacitance accordingly.
6. The imaginary part of the complex capacitance is observed as the default. Selection of Real  on the toolbar displays the real part capacitance (Fig. 5)

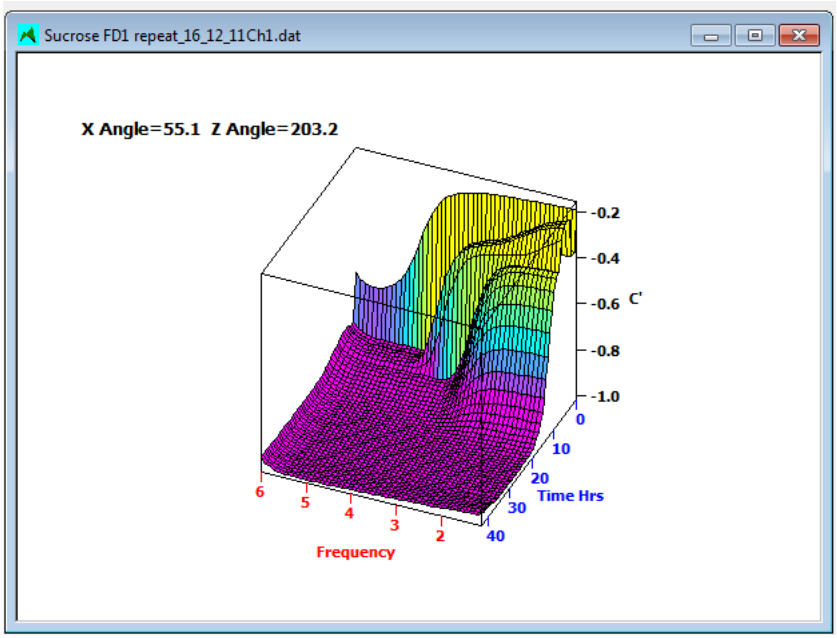

Fig. 5 real part of the capacitance

7. Time and frequency range can be selected to observe data for a particular time period over a particular frequency range. By clicking Time/ Freq Range option in Figure 4, a time and frequency selection dialogue will be observed (Figure 6). Different phases of the freeze drying process can be selectively analysed by varying the time period of the data displayed in the graphs.

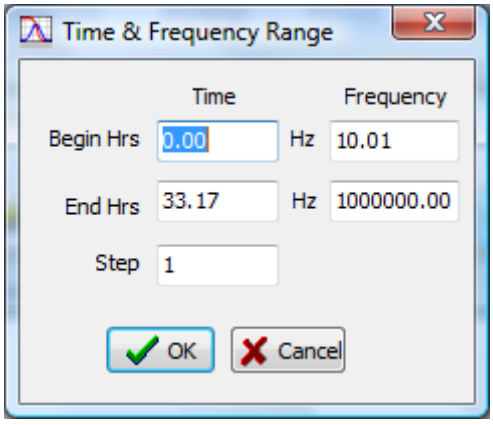

Figure 6 Time and frequency range selection

8. The time window selected at Step 7 can then be viewed by clicking the Peak Tslice Peak TSlice in button (Figure 4). This action will generate a 2-dimensional view of the peak frequency vs time (Fig 7 bottom graph) and the magnitude of the peak capacitance vs time (Figure 7 top graph).

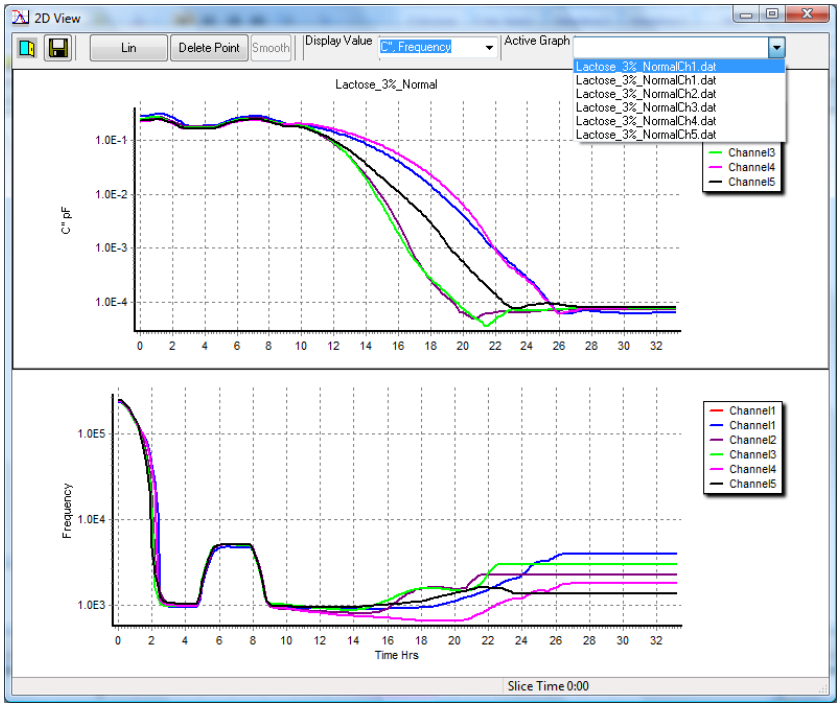

Figure 7 Graphs of Imaginary (peak) capacitance vs Time (Top) and Peak Frequency Vs Time (Bottom)

9. The figure above shows the capacitance and frequency values on Logarithmic scale. These parameters can be viewed on a linear scale by clicking the button  (Figure 7).

10. In addition, the derivative of the capacitance can be viewed over time by selecting the Display Value option 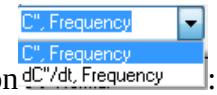 : dC"/dt, Frequency (Figure 8)

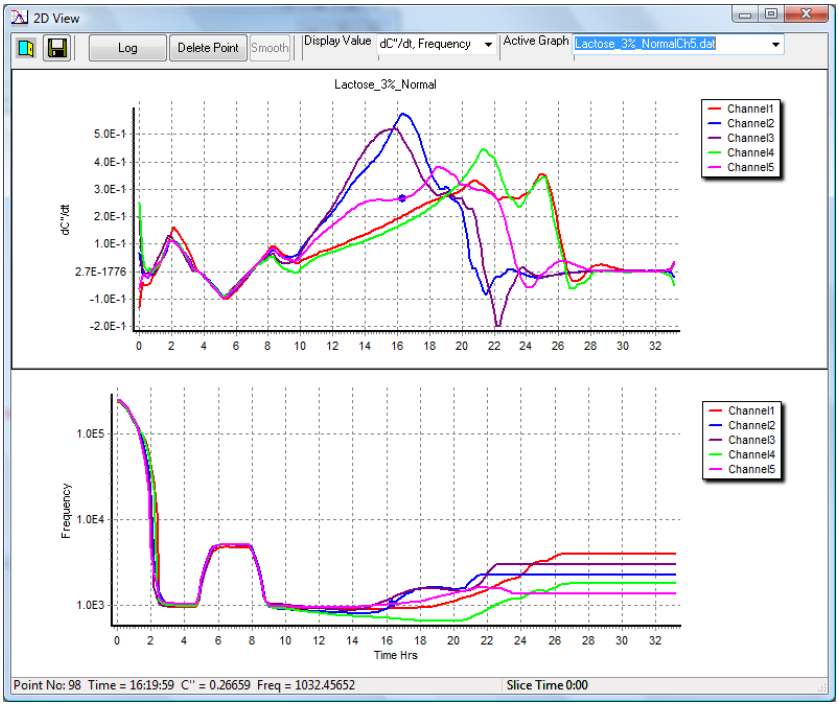

Figure 8 Graphs of derivative of capacitance vs time (top) and Frequency vs time (Bottom)

11. The active graph options provide an opportunity to select a data line from the set of data lines under study, a subsequent clicking at some point of activated data line will provide value of the time, values of Capacitance or derivative of the capacitance and frequency. For instance channel 5 is selected in active graph option, making right click on the graph line representing channel 5 will add a blue dot on both the capacitance derivative vs time graph and frequency vs time graph. Moreover the values of scan number, capacitance derivative or the capacitance as the case may be, time and frequency are also shown at the bottom of the graph.
12. The Peak Tslice option also provides an opportunity to export and save the peak amplitude and peak position data in text format. Click save button on the toolbar

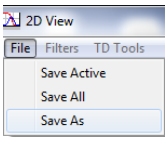

in figure 6 and/or figure 8 .This action will lead to another window requiring save as options for the text data.

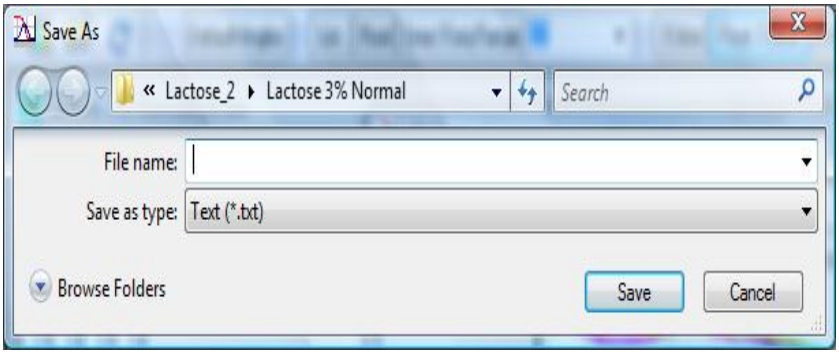

Figure 9 Save as text files Peak TSlice data.

Click on save key 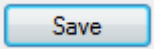

in figure 9 after file name and folder are entered. This action will result in export and save of the text files.

Caution: Text files can be generated using Capacitance vs time graph or derivative of capacitance vs time graph. It is suggested that while saving the text file, specify in the text file name whether the text file is generated from capacitance data or derivative of capacitance. Once the text file is made both the capacitance and derivative of capacitance appear as C'' in the data columns.

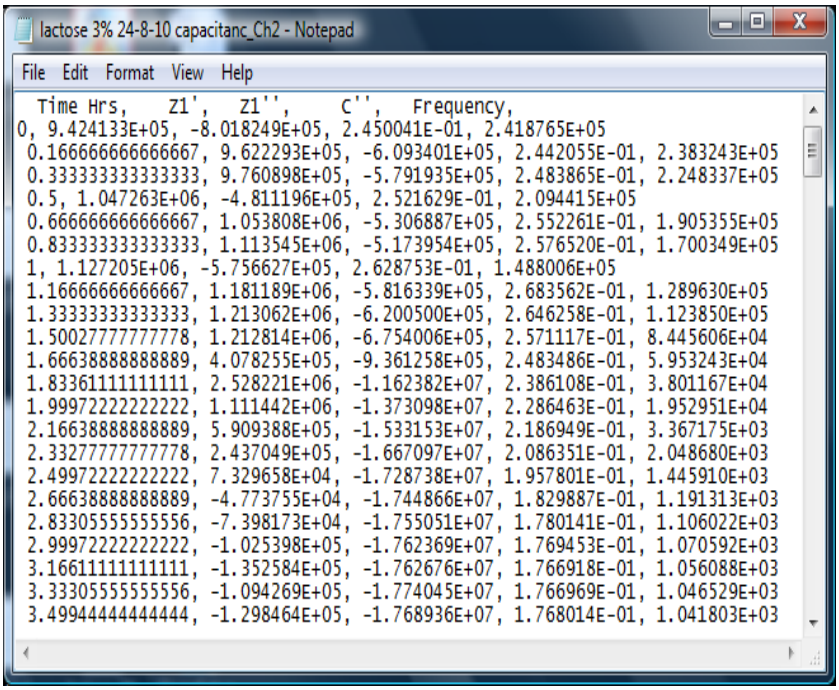

Figure 10 Text data file exported from Peak TSlice window

13. TSlice option provides an opportunity to observe data over a discrete frequency value.

Click the Tslice 

in figure 4. This action will result in select frequency option window (fig 11), providing a range of frequency over which the data was collected.

Selection of a frequency value will result in a graph displaying both the real and imaginary part of capacitance vs time values.

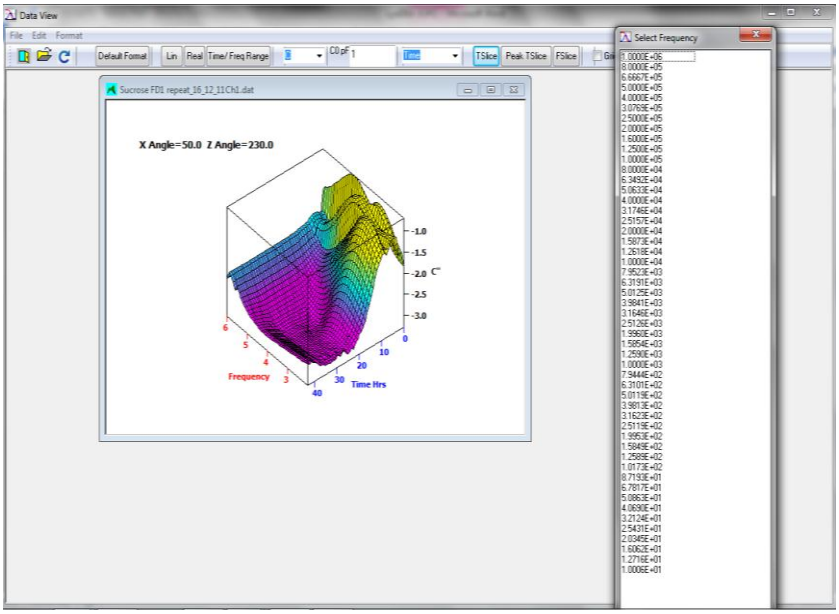

Figure 11 TSlice button opens select frequency option window

14. Selection of a frequency value relating to the position of peak during primary drying stage (e.g. 1000 Hz) in the 'frequency selection pan' will display the capacitance profile which can be employed to define the end of e primary drying (Fig 12).

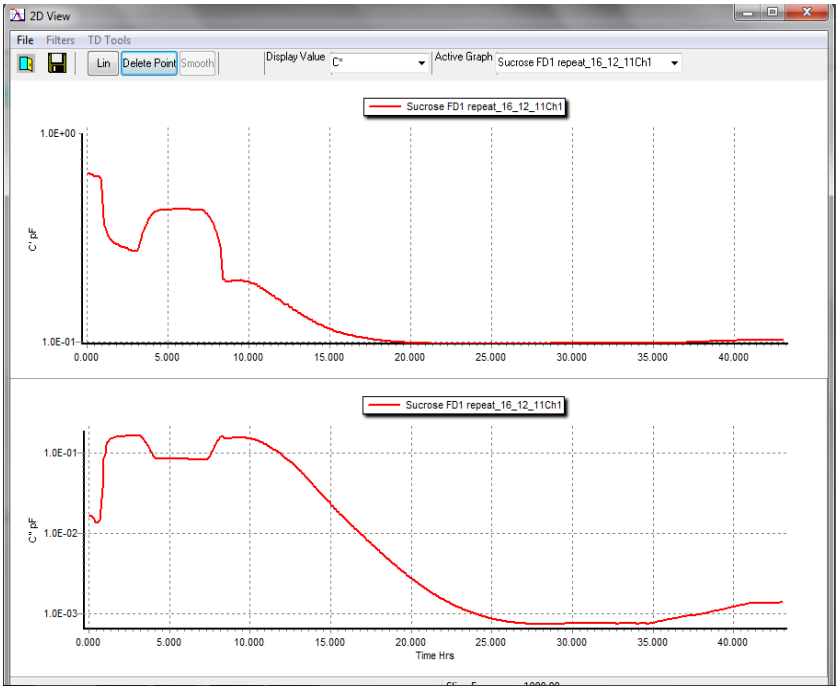

Figure 12 Tslic of capacitance at 1 KHz

15. The Tslice option also provides an opportunity to export and save the peak amplitude and peak position data in text format. Click "file → save as" button on the toolbar 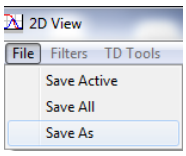

in figure 12.
16. This action will lead to another window requiring the user to enter the name of the file to hold the data in text format.

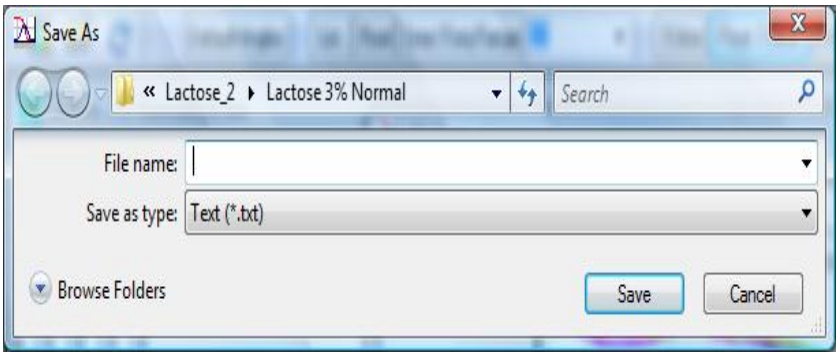

Figure 13 Save as text files Peak TSlice data.

Click on save key 

in figure 13 after file name and folder are entered. This action will result in export and save of the text files.

17. Fslice provide values of the frequency range over a particular point of time. Click the option in the toolbar of figure 4 

, this action will lead to a select time option wherein whole duration of experiment is provided (Figure 14).

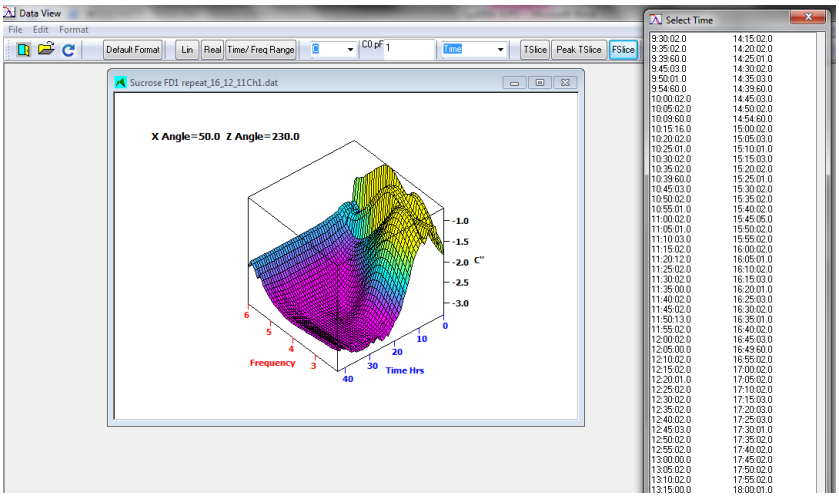

Figure 14 select time window for fslice

18. Selection of a particular time value will provide a graphical presentation of capacitance plots at the entire frequency range (an example spectrum is given in Figure 15).

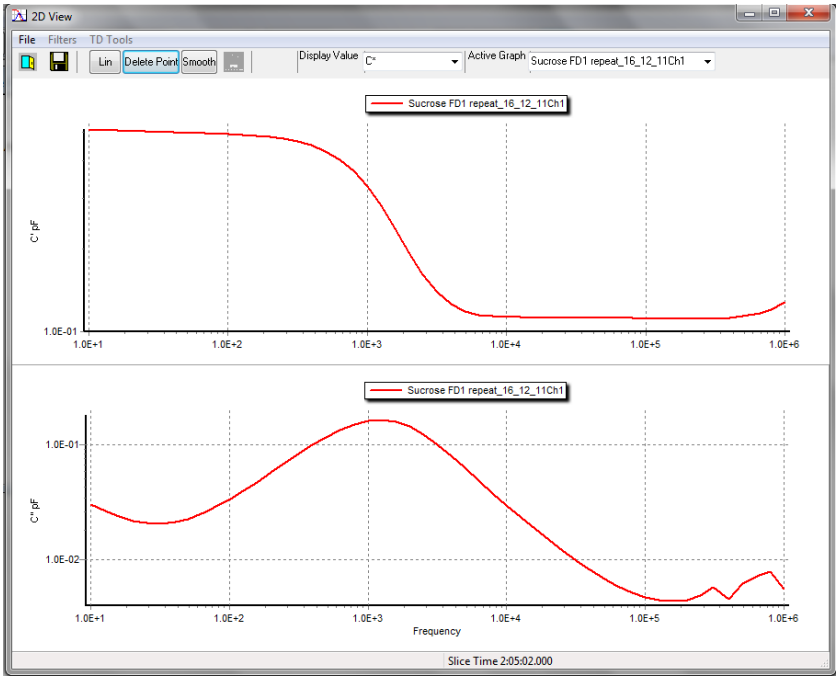

Figure 15 Fslice of a sucrose solution at 2 h

19. The impedance data file from a freeze drying cycle can also be fragmented into individual spectral files compatible with the Z-View software using LyoDEA data analysis software. Click on file and then unpack to Z format option as shown in the figure 16. This action will unpack all the spectra into individual text files that can be analysis further by the Z-View software.

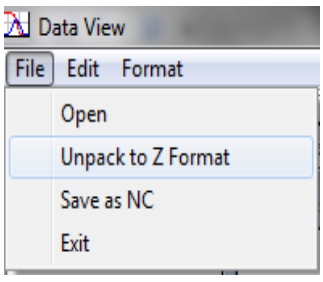

Figure 16 Unpack to Z format

Note: The Z View files are saved in the destination folder containing the text file acquired from the LyoDEA control software.

Appendix IV: Development of equivalent electric circuit model for the characterization of the interfacial polarization process, of a solution within a glass freeze-drying vial

The impedance spectrum of the test object i.e. glass vial with external electrode system containing 3 ml of sucrose 3% w/v (fig 1) was recorded over a frequency range 10^1-10^6 Hz.

Figure 1 A schematic view of an impedance measurement vial with external electrodes containing sucrose 3% w/v.

Basic theory of impedance

The impedance refers to the opposition to the flow of current through a circuit following the application of a defined voltage. For a particular circuit, the total impedance is a vector sum of in phase resistance and out of phase reactance, inductance contribution from the resistor, capacitor and inductors respectively in the circuit.

The symbol used for impedance is $Z(i\omega)$, where i indicates the complex nature of this parameter and the symbol ω indicates that the impedance of the object may vary as a function of the applied frequency. An impedance response can be described in terms of magnitutde ($|Z|$) and phase angle (Θ) or (Z' and Z'' projections on the complex plane of $Z(i\omega)$ (Figure 2).

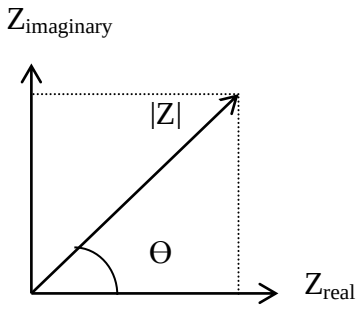

Figure 2 Argand diagram showing complex impedance in terms of magnitude of impedance |Z| and phase angle (Θ).

Changes in the magnitude of impedance and the phase angle recorded over the scanning frequency are described in (Fig 3 Top). The spectral data can also be displayed in terms of real and imaginary impedance and/or capacitance (Fig 3 centre and bottom). The real part of capacitance shows a step like decrease in the capacitance while the imaginary part show a peak within the scanning frequency range (Fig 3 Bottom).

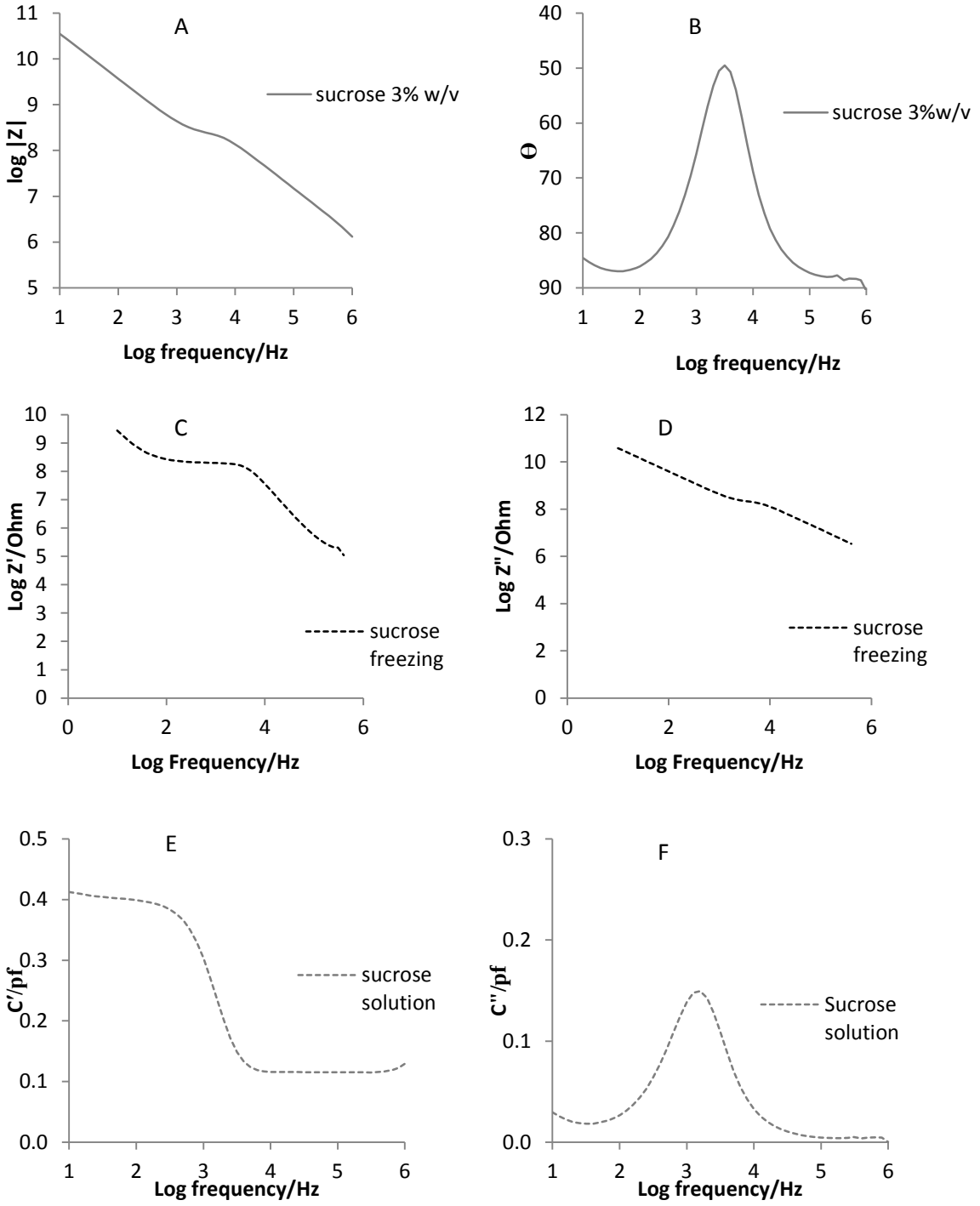

Figure 3 Impedance spectrum a 3% w/v solution of sucrose (A) Magnitude of Impedance; (B) phase angle plots (C) real part of Impedance (D) imaginary part of Impedance (E) real part of capacitance (F) imaginary part of capacitance.

Discussion of basic elements

The characteristics of each of the circuit elements in the model for the glass vial-solution assembly are now described in order to demonstrate how each parameter is manifest in the impedance spectrum.

Resistor (R) 

The symbol for this element is a zig-zag line

The capacitance of a resistor element lacks the real part while the response in the imaginary part is described as linear decrease exponentially with the frequency. The same can be described as negative linear slope on the logarithmic scale (Fig 4).

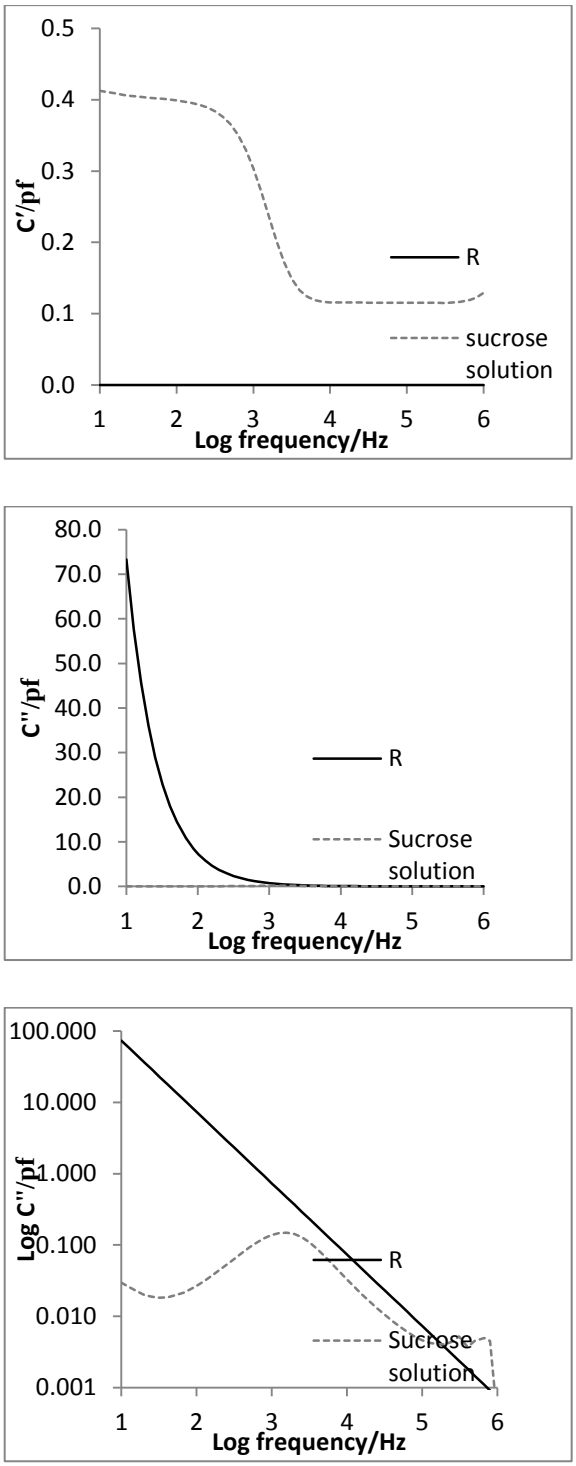

Figure 4 Capacitance plot for a resistor element R; (A) capacitance plot real part at linear scale (B) imaginary capacitance at linear scale (C) imaginary plot at logarithmic scale.

Capacitor (C) 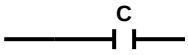

The symbol for this element is two vertical lines parallel to each other.

Frequency response of a capacitor element is described with, a value of capacitance in the real part which is independent of the scanning frequency. The imaginary part on the other hand does not show any contribution from the capacitor element.

The capacitance plot (real part) of sucrose solution in the low frequency range resemble to the capacitor 0.413 pF (Fig 5 Top), while at high frequency responses can be characterized with a 0.137 pF (Fig 5 Bottom).

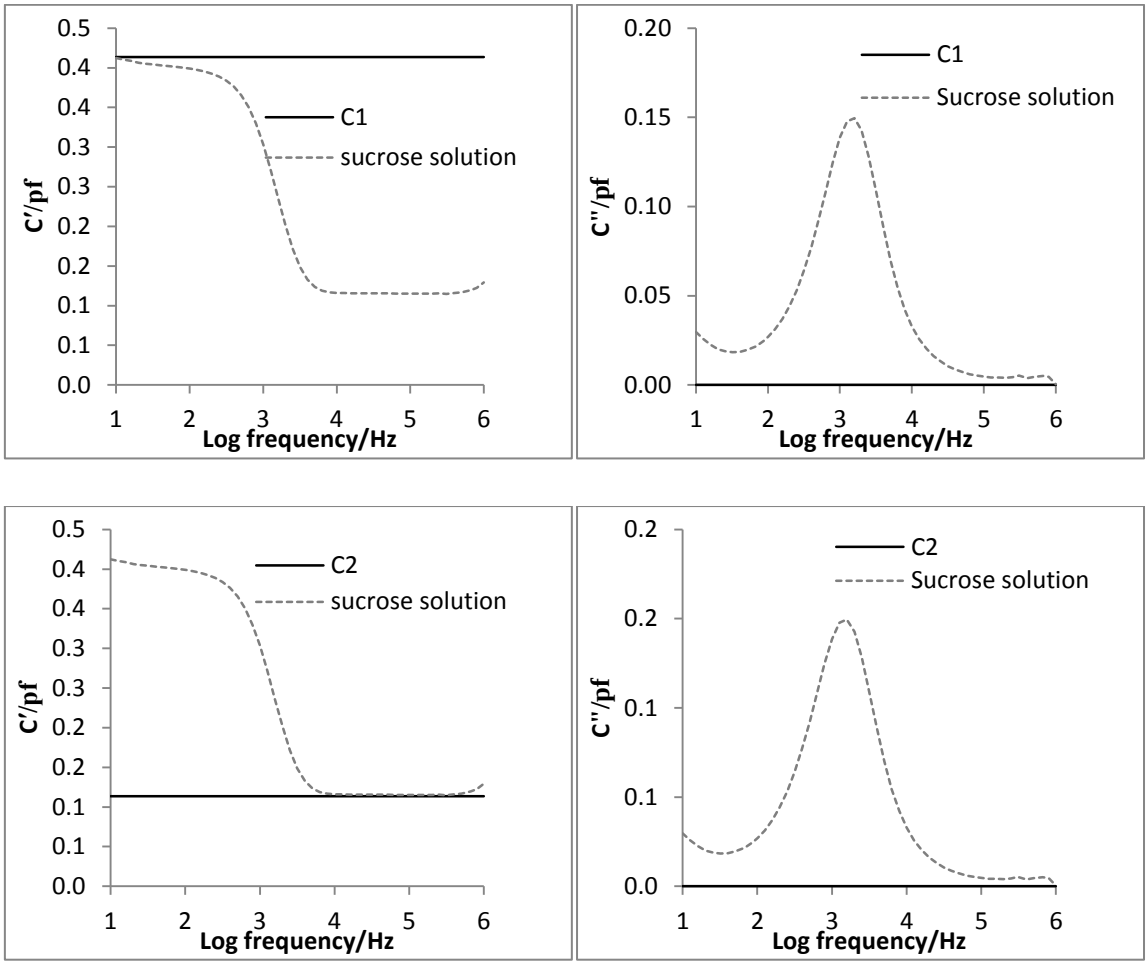

Figure 5 Capacitance plot for capacitor elements values C1= 0.413 and C2=0.137 pF

Constant Phase element (CPE) 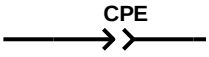

The symbol for this element is an arrow head and an arrow tail.

Frequently, CPE is included in a model to compensate for non-homogeneity in the system arising from rough or porous surface which result in a double-layer capacitance. Such impedance responses (double layer capacitance) can be characterized by a CPE which depends on two components T and P equation. P value of 1 results in a pure capacitor.

The low frequency capacitance responses from sucrose solution are appropriately modelled by CPE as the glass vial and formulation interface behaves like a non-ideal capacitor (Fig 6).

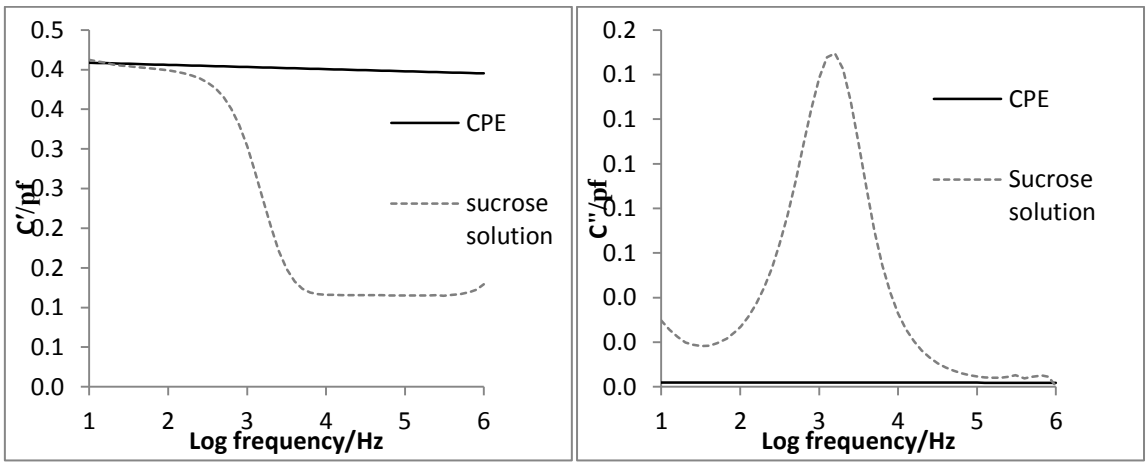

Figure 6 Capacitance plot for CPE element.

Circuit element in series

As the individual elements characterize the impedance response at only small frequency range combinations of different circuit elements may characterize the complete impedance spectrum of sucrose solution. Different combinations are discussed below

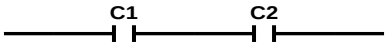

Capacitor (C1) in series with another capacitor (C2)

Total capacitance of a circuit model comprising of two capacitor elements arranged in series is explained by

$$\frac{1}{Ct} = \frac{1}{C1} + \frac{1}{C2}$$

As follows from the equation above, the capacitor C2 is smaller in value but as denominator it will be more contributing to the total impedance of the circuit. Only a small decrement is observed after the addition of a capacitor with a comparatively higher capacitance (Fig 7).

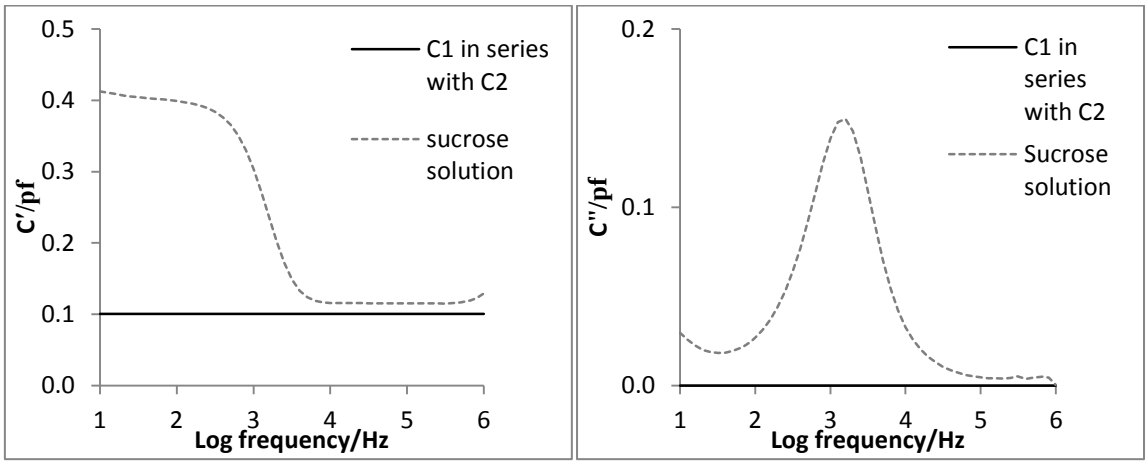

Figure 7 Capacitance plot for capacitor elements C1 (0.413) in series with C2 (0.137 pF).

C in series with R 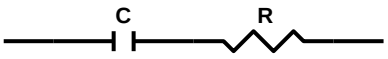

The inclusion of a resistor element in series with the capacitor results in a capacitance response with a relaxation process which empirically models capacitance from electrode-glass vial wall-solution assembly at low and intermediate frequency range.

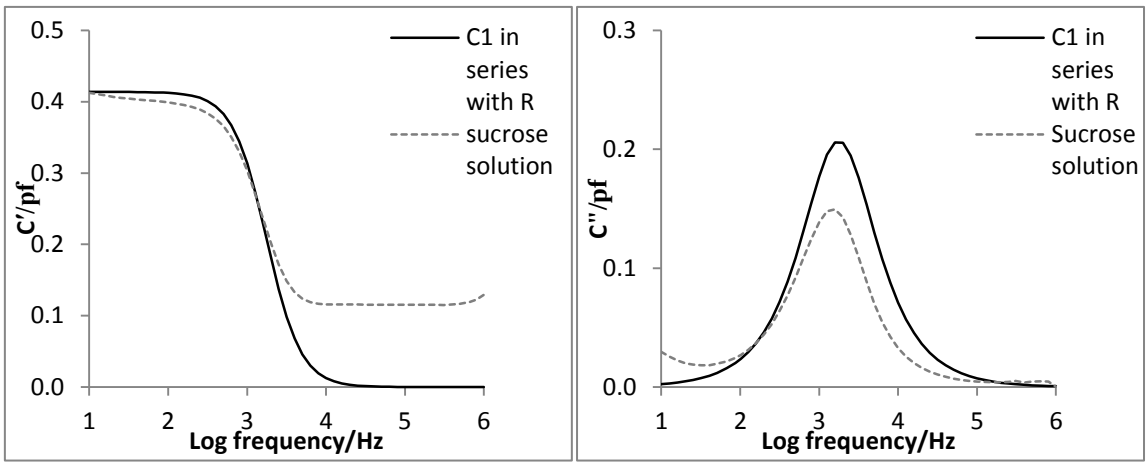

Figure 8 Capacitance plot for capacitor elements C1 in series with a resistor.

It appears that high capacitance recorded at low frequency is due to the charging of electrodes while the intermediate relaxation process is due to both the resistor and capacitor. Nevertheless high frequency low capacitance is poorly characterized by this model (Fig 8). Due to the reason amplitude of the imaginary capacitance peak is higher in the modelled spectrum.

CPE in series with R

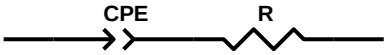

Substitution of capacitor in the C-R equivalent circuit model with the CPE results in capacitance profile which precisely models the low frequency polarization phenomenon while the relaxation peak in imaginary part broadly resembles to the one measured from the electrode formulation interface (Fig 9).

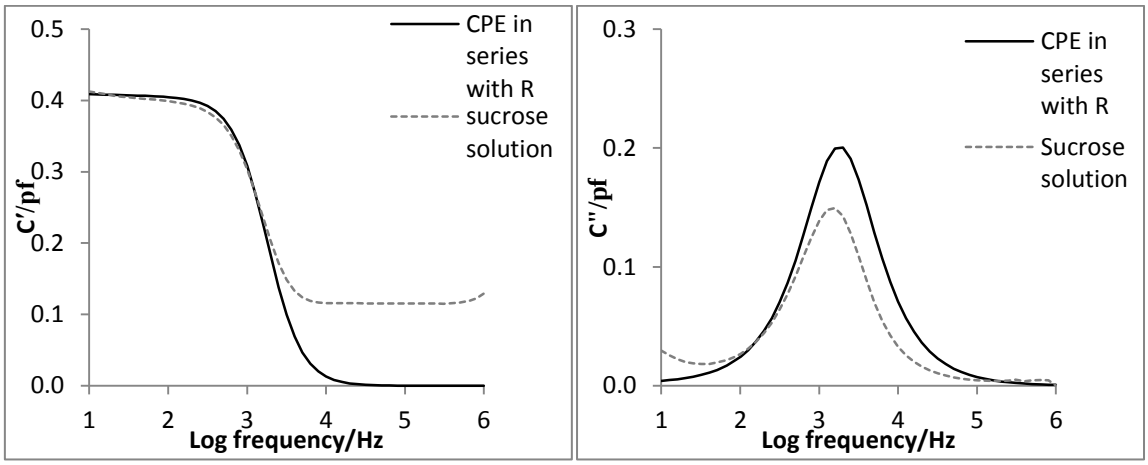

Figure 9 Capacitance plot for capacitor elements CPE in series with a resistor.

The capacitance profile at high frequency is inaccurately explained with this circuit model which may suggest the inclusion of additional element in the model.

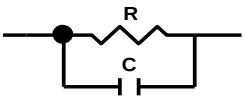

R in parallel to C (RC)

The capacitance profiles of a circuit element containing a resistor in parallel to the capacitor are similar to the spectrums recorded with a resistor and a capacitor separately; the contribution from a capacitor is observed in the real part of capacitance plot while the imaginary part describes the output from the resistors (Fig 10).

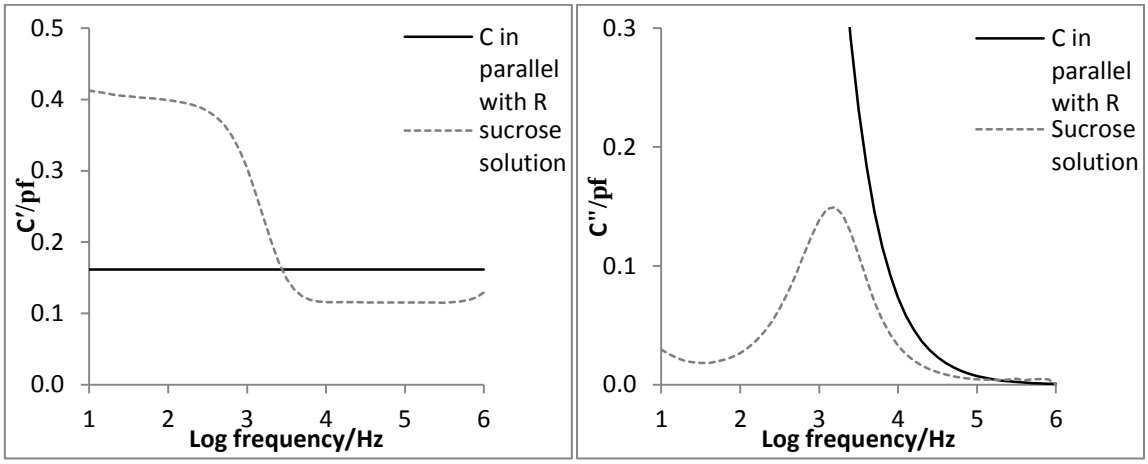

Figure 10 Capacitance plot for an equivalent circuit model containing capacitor elements C2 in parallel with a resistor.

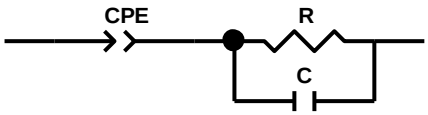

CPE-RC Circuit

The capacitance spectrum of an equivalent circuit model comprising of a CPE in series with RC (i.e. a resistor in parallel with a capacitor) models the real part of complete spectrum arising from the relaxation of the electrode-glass vial-solution assembly. At low frequency the CPE have sufficient time for charging which result in a high capacitance. At intermediate frequency the electrode charging is decreased and charge flow through the CPE and resistor demonstrates the decrease in capacitance. At higher frequencies the capacitance of the system is described by a charge flow through the CPE in series with capacitor (Fig 11).

The interfacial polarization peak in the imaginary capacitance plot is also modelled appropriately by this equivalent circuit model except the low frequency increase in the capacitance which appears to be the onset of another process the characterization of which is beyond the scope of present study.

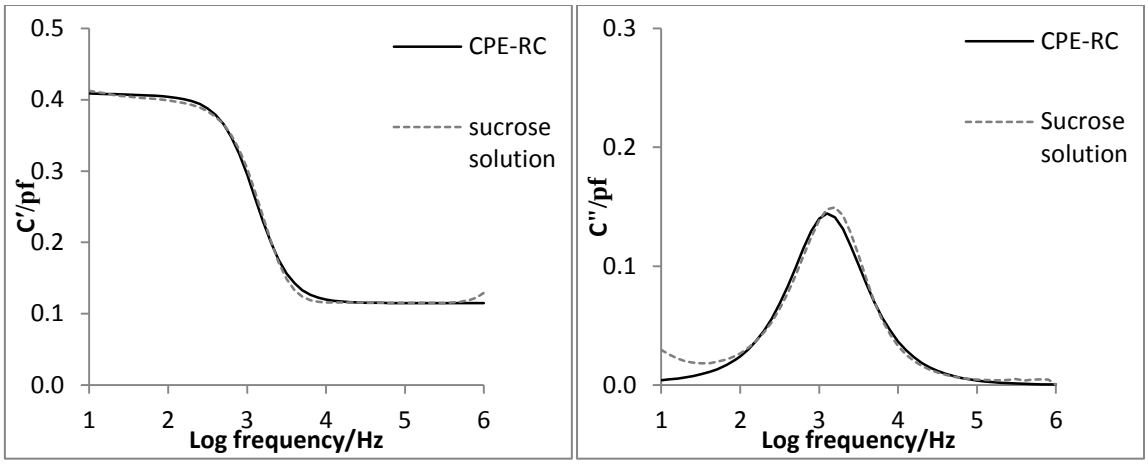

Figure 11 Capacitance plot for an equivalent circuit model containing CPE-RC.

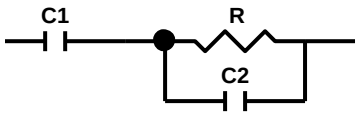

C-RC circuit model

As values of parameter P in the CPE RC circuit model was recorded close to 1 (0.98), the element CPE may be replaced to pure capacitor C which result in the low frequency capacitance changes in the real part are not appropriately characterized with this equivalent circuit model. Nevertheless the relaxation process and the imaginary capacitance are modelled appropriately (Fig 12).

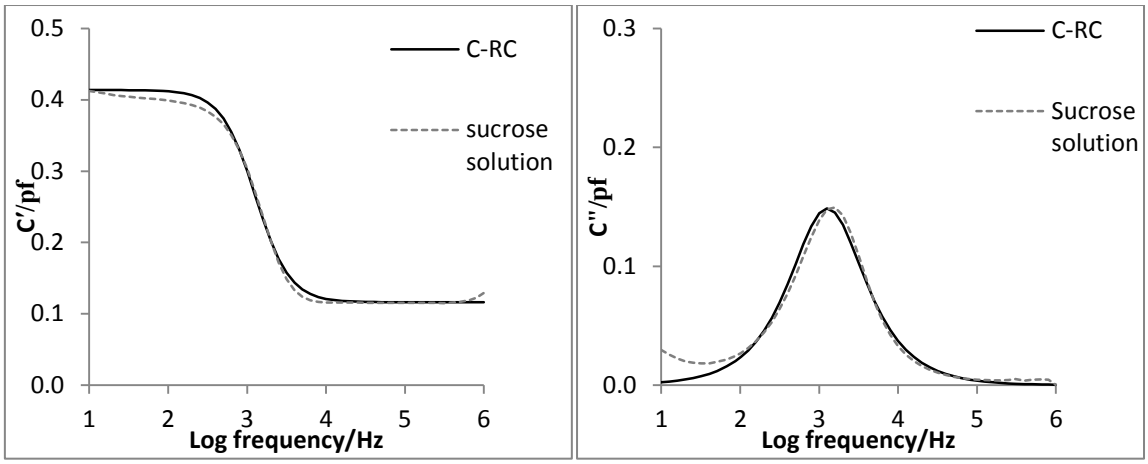

Figure 12 Impedance spectrum of C in series with RC circuit.

Mathematical basis for the measurement of real and imaginary capacitance

The impedance of model C-CR (Fig 12) can be calculated from the following equation

$$Z^* = \frac{1}{i\omega C*} = \frac{1}{i\omega C0} + \frac{1}{\frac{1}{R} + i\omega C1}$$

From the complex impedance formula, the expressions for real and imaginary capacitance can be calculated to explain the origin of interfacial polarization peak

$$Z^* = \frac{1}{i\omega C_0} + \frac{R}{1 + i\omega RC_1} = \frac{1 + i\omega R(C_1 + C_0)}{i\omega C_0 - \omega^2 RC_0C_1}$$

$$C^* = \frac{1}{i\omega Z^*} = \frac{C_0 + i\omega RC_0C_1}{1 + i\omega R(C_1 + C_0)}$$

By multiplying nominator and denominator by complex conjugate of denominator and grouping real and imaginary members decompose C* into real C' and imaginary parts

$$C^* = \frac{1}{i\omega Z^*} = \frac{(C_0 + i\omega R C_0 C_1)(1 - i\omega R(C_1 + C_0))}{(1 + i\omega R(C_1 + C_0))(1 - i\omega R(C_1 + C_0))}$$

$$C^* = \frac{C_0 + \omega^2 R^2 C_0 C_1 (C_1 + C_0) - i\omega R C_0^2}{1 + (\omega R((C_1 + C_0))^2}$$

Thus obtain

$$C' = \frac{C_0 + \omega^2 R^2 C_0 C_1 (C_1 + C_0)}{1 + (\omega R((C_1 + C_0))^2}$$

and

$$C'' = -\frac{\omega R C_0^2}{1 + (\omega R((C_1 + C_0))^2}$$

For an example spectrum, at $\omega \rightarrow 0$, $C'' = 0$ which increases to a maximum value with the frequency and then decreases to 0 as the $\omega \rightarrow \infty$reaching maximum $C''_{MAX}=C_0^2/2(C_0+C_1)$ at $\omega=1/R\ (C_0+C_1)$ Fig 13.

The values of real part of capacitance at $\omega \rightarrow 0$ $C' \rightarrow C_0$ and with $\omega \rightarrow \infty$ $C' \rightarrow C_0C_1/\ (C_0+C_1)$ therefore $\Delta C= C_0-C_0C_1/(C_0+C_1)= C_0^2/(C_0+C_1)$.

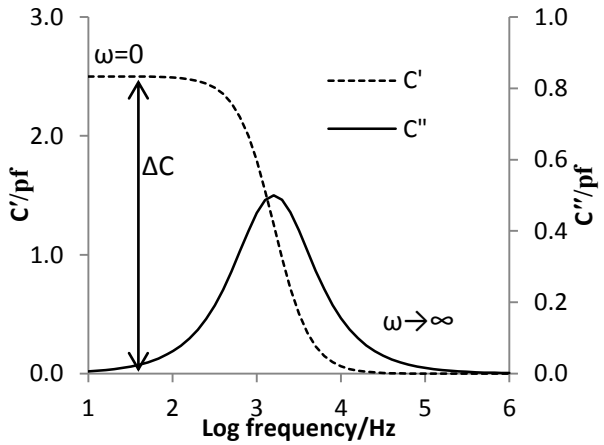

Figure 13 Example Capacitance spectrum calculated from equation.

Impedance Model for the solution-glass vial assembly

In order to explain the observed impedance spectrum of the object under test and relate it to the physical properties or changes that may happen during the freeze-drying process, it is necessary to create an appropriate equivalent circuit model. The impedance response from the solution-vial object can be characterized by equivalent circuit comprising of three discrete elements.

Figure 14 Equivalent circuit model to characterize the through vial impedance spectrum of sucrose solution (A) CPE-RC model (B) C-RC model.

The circuit models (Fig 14) were found to provide an approximate fit to the measured impedance spectrum, where CPE or C1 signifies the interfacial capacitance formed between the glass walls of a vial and the solution, which is charged through the resistance (R) representing the conductivity of the sample, and capacitor C represents the electrical capacitance of the material within the internal volume of a vial.

This imparts a frequency-dependence to the measured dielectric properties, such that the interfacial capacitance (CPE) will have sufficient time to charge completely at low frequency, but at high frequency, it will not have time to accumulate any of the electrical charge that could otherwise be accommodated.

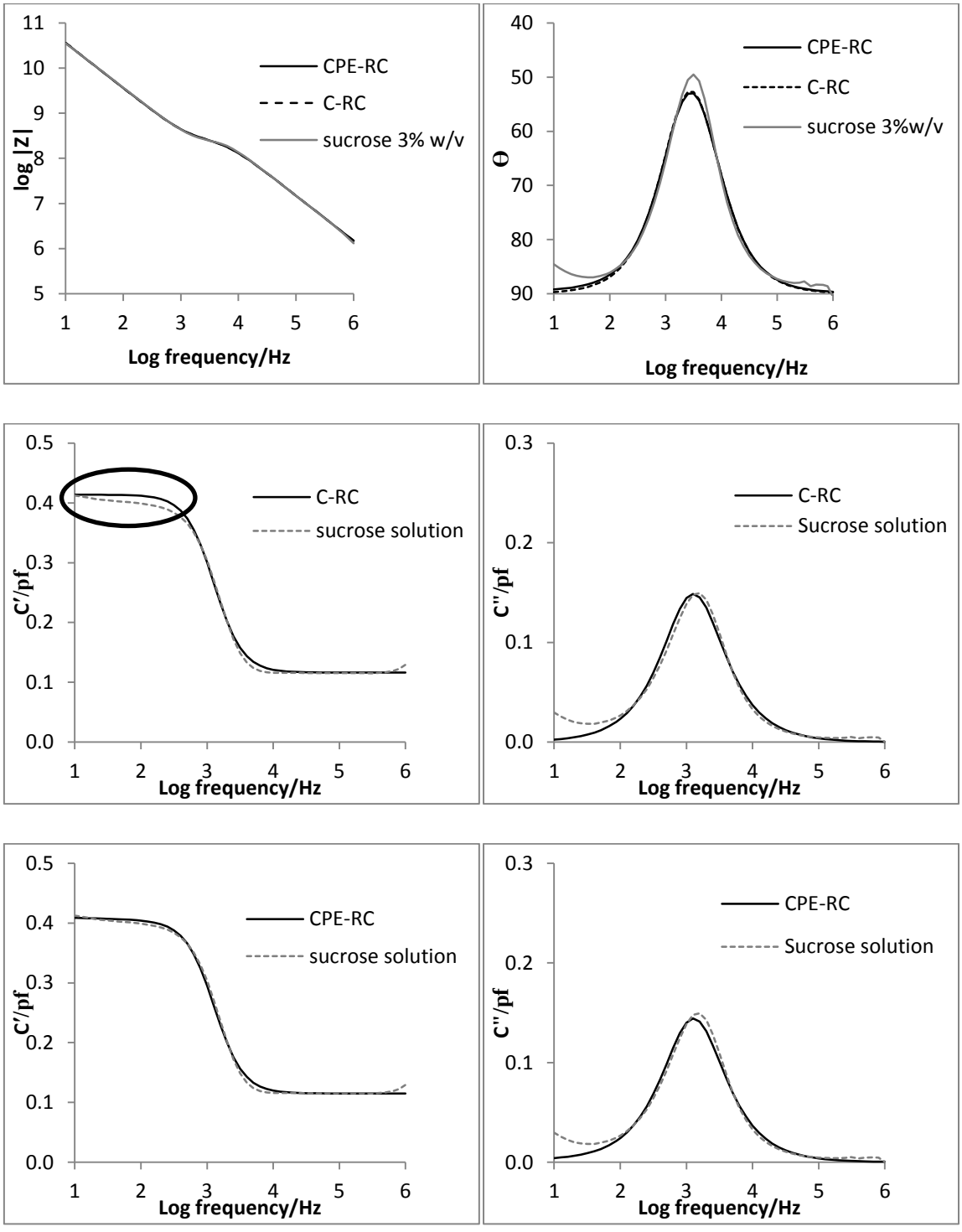

Figure 15 Impedance fit results for 3% w/v sucrose solution using CPE-RC and C-RC circuit model.

The results from the CPE-RC circuit model demonstrate an improved fit in the low frequency range Fig 15 (Bottom); due to the reason CPE-RC model was used for the characterization of interfacial polarization process.